


UNIVERSITY OF POITIERS

&

NATIONAL TECHNICAL UNIVERSITY OF ATHENS

DOCTORAL THESIS

Computational Fluid Dynamics study of heavily loaded fixed-pad thrust bearings operating under thermoelastohydrodynamic regime

Author:
Anastasios Charitopoulos

Supervisors:
Michel Fillon **CNRS Director of Research**
Christos Papadopoulos **Associate Professor**

Jury members:

Ilmar Ferreira Santos	**Professor**, Technical University of Denmark	*Reviewer*
Michał Wodtke	**Associate Professor**, Gdansk University of Technology	*Reviewer*
Lidia Galda	**Assistant Professor**, Rzeszow University of Technology	*Examiner*
Noël Brunetière	**CNRS Director of research**, Pprime Institute	*Examiner*
Lambros Kaiktsis	**Professor**, National Technical University of Athens	*Examiner*
Michel Fillon	**CNRS Director of Research**, Pprime Institute	*Examiner*
Christos Papadopoulos	**Associate Professor**, National Technical University of Athens	*Examiner*

A thesis submitted in fulfilment of the requirements
for the degree of Doctor of Philosophy

in the:
Doctoral School of Materials, Mechanics and Energetics Science and Engineering
and the:
School of Naval Architecture and Marine Engineering of NTUA

15 December 2020

"Και για τον κόσμο που μισείς δεν είμαι άλλος
Και για τον κόσμο που αγαπάς δεν είμαι αυτός
άλλοι νομίζανε πως ήμουνα μεγάλος
κι από σπουργίτι θα γινόμουνα αετός."

Μάνος Ελευθερίου

THESE

POUR L'OBTENTION DU GRADE DE
DOCTEUR DE L'UNIVERSITE DE POITIERS
(FACULTÉ DES SCIENCES FONDAMENTALES ET APPLIQUÉES)
(DIPLÔME NATIONAL - ARRÊTÉ DU 25 MAI 2016)

ECOLE DOCTORALE : SIMME
SECTEUR DE RECHERCHE : TRIBOLOGIE

PRÉSENTÉE PAR :
ANASTASIOS CHARITOPOULOS

Etude numérique (CFD) de butées à patins fixes fortement chargés fonctionnant en régime thermoélastohydrodynamique

---

DIRECTUERS DE THESE :
Michel FILLON **Directeur de Recherche CNRS**
Christos PAPADOPOULOS **Professeur Associé**

SOUTENUE LE 15 DÉCEMBRE 2020
DEVANT LA COMMISSION D'EXAMEN

JURY :

Ilmar Ferreira SANTOS	**Professeur**, Technical University of Denmark	*Rapporteur*
Michał WODTKE	**Professeur Associé**, Gdansk University of Technology	*Rapporteur*
Lidia GALDA	**Professeure Assistante**, Rzeszow University of Technology	*Examinatrice*
Noël BRUNETIERE	**Directeur de Recherche CNRS**, Institut Pprime	*Examinateur*
Lambros KAIKTSIS	**Professeur**, National Technical University of Athens	*Examinateur*
Michel FILLON	**Directeur de Recherche CNRS**, Institut Pprime	*Examinateur*
Christos PAPADOPOULOS	**Professeur Associé**, National Technical University of Athens	*Examinateur*

ΕΘΝΙΚΟ ΜΕΤΣΟΒΙΟ ΠΟΛΥΤΕΧΝΕΙΟ
ΣΧΟΛΗ ΝΑΥΠΗΓΩΝ ΜΗΧΑΝΟΛΟΓΩΝ ΜΗΧΑΝΙΚΩΝ
ΤΟΜΕΑΣ ΝΑΥΤΙΚΗΣ ΜΗΧΑΝΟΛΟΓΙΑΣ

Θερμοελαστοϋδροδυναμική μελέτη υψηλά φορτισμένων ωστικών εδράνων σταθερού πέλματος, με χρήση υπολογιστικής ρευστομηχανικής.

ΔΙΔΑΚΤΟΡΙΚΗ ΔΙΑΤΡΙΒΗ
του
ΑΝΑΣΤΑΣΙΟΥ ΧΑΡΙΤΟΠΟΥΛΟΥ
Διπλωματούχου Ναυπηγού
Μηχανολόγου Μηχανικού Ε.Μ.Π (2015)

Συμβουλευτική επιτροπή:	Χρήστος Παπαδόπουλος	Αναπληρωτής Καθηγητής
	Michel Fillon	Διευθυντής Έρευνας
	Λάμπρος Καϊκτσής	Καθηγητής

Εγκρίθηκε από την επταμελή εξεταστική επιτροπή την 15 Δεκεμβρίου 2020.

Ilmar Ferreira Santos	Καθηγητής, Technical University of Denmark
Michał Wodtke	Αναπληρωτής Καθηγητής,Gdansk University of Technology
Lidia Galda	Επίκουρη Καθηγήτρια, Rzeszow University of Technology
Noël Brunetière	Διευθυντής Έρευνας, Institute Pprime
Λάμπρος Καϊκτσης	Καθηγητής, Εθνικό Μετσόβιο Πολυτεχνείο
Michel Fillon	Διευθυντής Έρευνας, Institute Pprime
Χρήστος Παπαδόπουλος	Αναπληρωτής Καθηγητής, Εθνικό Μετσόβιο Πολυτεχνείο

Abstract

The present Thesis investigates the effects of thermal deformations on the performance of fixed-pad thrust bearings operating under high loads and temperatures. The presented work consists of two main parts. First, in order to identify the mechanisms of pressure build-up in parallel surface thrust bearings, the different theories proposed in the scientific literature have been evaluated. To this end, a CFD-based thermoelastohydrodynamic (TEHD) model has been generated, accounting for all the physical phenomena of the lubricant, of the solid domains and their interaction, which have been suggested in the literature as phenomena contributing to the pressure build-up mechanism of the parallel thrust bearing. The importance of each theory has been quantified and a final modelling approach has been proposed, for accurately evaluating the performance of a parallel surface thrust bearing. Furthermore, the generated model has been validated against experimental results of the literature. The second part of the Thesis utilises the previously proposed modelling approach to evaluate contemporary designs of thrust bearings, such as textured, coated, pocket and tapered-land bearings. In conclusion, the thermal deformations of the bearing pad are established as the main pressure build-up mechanism in parallel thrust bearings. Moreover, they contribute significantly to the performance of textured and coated bearings. Contrariwise, on pocket and tapered-land bearings, the thermal deformations are of negligible importance, even at high loads and operating temperatures.

Resumé

Dans la présente thèse sont étudiés les effets des déformations thermiques sur les performances des butées à patin fixe fonctionnant sous des charges et des températures élevées. Le travail présenté se compose de deux parties principales. Dans une première étape, afin d'identifier les mécanismes de génération de pression dans les butées à surfaces parallèles, les différentes théories proposées dans la littérature scientifique ont été évaluées. À cette fin, un modèle thermoélastohydrodynamique (TEHD) basé sur la Dynamique de Fluides Numérique (CFD) a été généré, en tenant compte tous les phénomènes physiques du lubrifiant, des solides et de leur interaction, qui ont été suggérés dans la littérature comme des phénomènes contribuant au mécanisme de génération de pression des butées à faces parallèles. L'importance de chaque théorie a été quantifiée et une modélisation finale a été proposée afin d'évaluer avec précision les performances d'une butée à faces parallèles. De plus, le modèle généré a été validé par rapport aux résultats expérimentaux de la littérature. La deuxième partie de la thèse utilise l'approche de modélisation proposée précédemment pour évaluer les conceptions contemporaines de butées, telles que les butées à surfaces texturées, revêtus, à poche et à plan incliné. En conclusion, les déformations thermiques des patins de la butée ou de la glissière sont établies comme le principal mécanisme de création de pression dans les butées à surfaces parallèles. En outre, elles contribuent de manière significative aux performances TEHD des butées texturées et revêtues. Au contraire, sur les butées à poche et à plan incliné, les déformations thermiques sont d'une importance négligeable, même à des charges et des températures de fonctionnement élevées.

Σύνοψη

Η παρούσα διδακτορική διατριβή διερευνά τις επιπτώσεις των θερμικών παραμορφώσεων στις επιδόσεις των ωστικών εδράνων σταθερής έδρασης τα οποία λειτουργούν σε υψηλά φορτία και θερμοκρασίες. Η παρούσα εργασία αποτελείται από δύο κύρια μέρη. Πρώτον, για τον προσδιορισμό του μηχανισμού παραγωγής υδροδυναμικής πίεσης σε παράλληλα ωστικά έδρανα, αξιολογήθηκαν οι διάφορες θεωρίες που προτείνονται στη βιβλιογραφία. Για το σκοπό αυτό, δημιουργήθηκε ένα θερμοελαστοϋδροδυναμικό μοντέλο το οποίο βασίζεται σε κώδικα υπολογιστικής υδροδυναμικής, και αντιστοιχεί σε όλες τις φυσικές ιδιότητες του λιπαντικού, των μεταλλικών μερών, και της αλληλεπίδρασής τους, οι οποίες έχουν προταθεί στη βιβλιογραφία ως ιδιότητες που συμβάλλουν στον μηχανισμό παραγωγής υδροδυναμικής πίεσης του παραλλήλου ωστικού εδράνου. Η σημασία κάθε θεωρίας έχει ποσοτικοποιηθεί και έχει προταθεί μια τελική προσέγγιση μοντελοποίησης, για την ακριβή αξιολόγηση της επίδοσης του παραλλήλου ωστικού εδράνου. Επιπλέον, το παραγόμενο μοντέλο έχει συγκριθεί έναντι πειραματικών αποτελεσμάτων της βιβλιογραφίας, και παρατηρήθηκε πολύ καλή συσχέτιση. Το δεύτερο μέρος της διατριβής χρησιμοποιεί την προηγουμένως προτεινόμενη προσέγγιση μοντελοποίησης για την αξιολόγηση σύγχρονων σχεδίων ωστικών εδράνων, όπως ωστικά έδρανα με τεχνητή επιφανειακή τραχύτητα, με επικάλυψη πολυμερών υλικών, ορθογωνικής κοιλότητας και έδρανα με κεκλιμένο και παράλληλο τμήμα. Συμπερασματικά, οι θερμικές παραμορφώσεις του εδράνου είναι ο κύριος μηχανισμός παραγωγής υδροδυναμικής πίεσης σε παράλληλα ωστικά έδρανα. Επίσης, συμβάλλουν σημαντικά στις επιδόσεις των ωστικών εδράνων με επιστρώσεις και τεχνητής τραχύτητας. Αντίθετα, σε ωστικά έδρανα ορθογωνικής κοιλότητας και και έδρανα με κεκλιμένο και παράλληλο τμήμα, οι θερμικές παραμορφώσεις είναι αμελητέας σημασίας, ακόμη και σε υψηλά φορτία και θερμοκρασίες λειτουργίας.

Acknowledgements

Firstly, I would like to express my sincere gratitude to the **France Education Ministry** for funding my Doctoral studies, and the **A.G. Leventis Foundation** for their financial support.

I am deeply grateful to my supervisors, CNRS Director of Research **Michel Fillon** and Associate Professor **Christos Papadopoulos** for their continuous support in the course of my Ph.D. study and related research, for their patience, motivation, and immense knowledge. Their guidance helped me in all the time of research and writing of this Thesis. I could not have imagined having better supervisors and mentors for my Ph.D study.

Besides my supervisors, I would like to thank Professor **Lambros Kaiktsis** for his attention to detail, his valuable corrections, and his endless patience.

My sincere thanks also goes to Associate Professor **Michał Wodtke** for his interest in the progression of my work, his insightful conversations, and for agreeing to review my Thesis.

I am also very grateful for the feedback offered by the reviewer Professor **Ilmar Ferreira Santos**.

I wish to thank the members of my dissertation committee: CNRS Director of research **Noël Brunetière** and Assistant Professor **Lidia Galda** for generously offering their time and review of this document.

On a more personal note, I would like to express my gratitude:

To **Jean Bouyer**, **Noël Brunetière**, **Pascal Jolly** for making me feel accepted (even if I barely spoke any French), for their everyday help, and for teaching me Belote.

To **Mathieu Maillet** and **Laurence Artus** for going out of their way to help me, whenever I asked them.

To **Erwan** and **Samia** for all the phone-calls to the plumber, the bank, etc...

To **Thibaut** and **Louis** for their persistence to teach me the Poitiers' night life.

To **Prasanth** and **Cory** for all the Sunday lunches and the long talks.

To **Omar** for his friendship and positive attitude.

To **George R.** for taking up the slack, when I was not there.

Moreover, I would like to thank my family: my parents, to my sister and my grandmothers for supporting me throughout writing this thesis and in my life in general.

Finally I would like to thank **Kallirroe** for everything.

Contents

List of Figures

List of Tables

List of Abbreviations

TEHD	**T**hermo **E**lasto **H**ydro **D**ynamic
THD	**T**hermo **H**ydro **D**ynamic
FSI	**F**luid **S**tructure **I**nteraction
CFD	**C**omputational **F**luid **D**ynamics
RPM	**R**evolutions **p**er **M**inute
DOF	**D**egree **O**f **F**reedom
AST	**A**rtificial **S**urface **T**exturing
CHT	**C**onjugate **H**eat **T**ransfer

List of Symbols

p	*Pressure*	Pa
ν_f	*Kinematic viscosity*	m^2/s
μ	*Dynamic viscosity*	$Pa \cdot s$
$\vec{u}$	*Velocity vector*	m/s
ρ	*Density*	kg/m^3
τ	*Deviatoric stress tensor*	kg/m^3
λ_S	*Solid thermal conductivity*	$W/(m \cdot K)$
λ_f	*Lubricant thermal conductivity*	$W/(m \cdot K)$
c_{pf}	*Lubricant specific heat capacity*	$J/K/kg$
U_x	*X displacement DOF*	m
U_y	*Y displacement DOF*	m
U_z	*Z displacement DOF*	m
T	*Temperature*	C
R_B	*Bubble diameter*	C
p_v	*Pressure in the bubble*	m
p_c	*Cavitation pressure*	Pa
σ_B	*Surface tension coefficient*	Pa
σ_{ij}	*Stress tensor*	Pa
ϵ_{ij}	*Strain tensor*	ul
E	*Young's modulus*	Pa
α_{se}	*Thermal expansion coefficient*	K^{-1}
ν	*Poisson ratio*	ul
H_{min}	Minimum film thickness	¯m

Thesis Outline

Chapter 1: Introduction

In this chapter, the evolution of the literature, from the Tower [1] experiments in 1883, to the current state-of-the-art, is presented, and the goals of the present study are stated.

A detailed review of the publications on the parallel thrust bearing pressure build-up mechanism has been conducted. The more prevalent theories have been identified and listed. Moreover, a brief review on artificial surface texturing on tribological contacts is presented. Finally, published work on the evolution of bearing coating materials, and their effect on the performance characteristics of different tribological contacts is cited.

Chapter 2: Modelling

In this chapter the governing equations that have been used for the modelling are presented. The different geometries studied in the course of the Thesis are demonstrated. The chosen lubricant and solid material properties are listed. Finally the boundary conditions (BC) for the Full TEHD and the simpler models are explained.

For the different geometries presented in Section 2.2, three basic categories of models have been generated. The isothermal, where the temperature the computational domain, and the lubricant properties are considered constant. The ThermoHydroDynamic (THD), where the energy equation is solved in the lubricant domain, the conjugate heat transfer (CHT) is calculated for the solid domains, and the lubricant properties are temperature dependent. Finally the TEHD, where the solid domains can deform due to thermal expansion and elastic deformation.

Chapter 3: Pressure build-up mechanism investigation

In this chapter the effects of the thermal properties of the lubricant and solid domains are evaluated. The thermal dependent viscosity, density, heat capacity, and thermal conductivity, as well as the thermal deformation of the solid domains, are suggested by the literature, as the main contributing factors of the load carrying capacity of the parallel surface thrust bearing. Thus, a detailed analysis has been performed for each suggested contributing factor, in order to identify their importance in the pressure build-up mechanism.

Chapter 4: Thermal deformation effects on highly loaded contemporary designs

This chapter deals with thermal effects on highly loaded contemporary designs, especially that of thermal deformation of the pad domain. Four different kinds of

the most commonly used contemporary bearing designs are presented below. The tapered-land, pocket, and textured bearings have been evaluated with TEHD and THD models, and a model is proposed for future design evaluation for each one of them. Also, parallel surface bearings with coatings have been studied, considering the thermal and mechanical deformations, and compared with the bronze thrust bearing.

Operational parameters that make bearings considered as heavily loaded are the maximum load, the start-up load, the temperature, and the minimum film thickness H_{min}. Each one of the above parameters, if is close to the operational limit constitutes a bearing as heavily loaded. For example, bearings of the size and rotational speed of the presented models, the safe specific load limit is 3 MPa, the design maximum temperature 100°C, and the minimum permissible film thickness is $H_{lim} = 14\ \mu m$ [2].

Chapter 5: Conclusion

Many different physical phenomena take place in the parallel thrust bearing in order to generate a load carrying capacity. The most pronounce is the effect of the thermal deformation, witch generates a converging wedge that can support a considerable load.

To evaluate the performance of such bearing a 3D TEHD CFD model is needed, and the groove geometry must be modelled. The temperature evaluation and boundary conditions are of utmost importance. Attention must be given to the structural boundary condition, because preliminary investigation suggested that different location and/or number of fixation points can give different deformation profiles.

The imperfection of individual sector pads can introduce different loading conditions on the thrust bearing. Thus measuring a single pad probably would not describe the real working conditions of the whole bearing.

The tapered-land and pocket configurations do not need the computationally expensive TEHD modelling approach.

Textured bearings, especially from moderately to highly loaded need to be studied taking into account the thermal deformation of the pad geometry.

Finally, the effect of coatings on parallel thrust bearings needs to be investigated. A hybrid two coating design might enhance considerably the parallel thrust bearings performance.

Chapter 1

Introduction

Overcoming friction is one of the main objectives of everyday life. Holmberg and Erdemir [3], evaluated that 23% of the total energy consumption today originates from energy losses in tribological contacts. In the direction of reducing the total energy waste and designing more efficient engineering contraptions, the understanding of friction mechanism is the key. Since the beginning of the industrial era, a lot of effort has been made in optimising the efficiency of mechanical designs. Analytical and computational models have been generated through the years, to predict and optimise the performance of such designs. In the past decades, the computational power was scarce, thus driving to simplifications of the physical models in order to acquire meaningful result with limited computational resources. However, in the last 20 years, the available computational power has increased dramatically allowing the scientific and engineering community to utilise more complex and accurate computational models.

The present study focuses on the detailed modelling of the parallel thrust bearing using a CFD-based ThermoElastoHydrodynamic (TEHD) computation approach. The goals of the present study are (a) to evaluate the pressure build-up mechanisms of parallel thrust bearings proposed in the literature over the years, and (b) to evaluate how this complex modelling approach can be used to assess contemporary designs that have been evaluated by simpler computational methods.

In the present chapter, the evolution of the literature, from the Tower [1] experiments in 1883, to the current state-of-the-art, is presented, and the goals of the present study are stated.

1.1 Literature review

1.1.1 Hydrodynamic lubrication of the parallel thrust bearing

After the experiments of Tower [1] in 1883, where the hydrodynamic bearings were formally introduced to the literature, and in 1886 Reynolds [4] simplifying the Navier-Stokes equations with the assumptions of constant viscosity, thin film geometry, no-slip wall boundary conditions, and negligible body forces. Reynolds equation with its many variations through the years and contributions of many researchers still remains a powerful tool for quantifying the performance parameters of tribological contacts.

In 1946, Fogg [5] presented the results of his experiment with parallel thrust bearings. He concluded that parallel thrust bearings can support load of the same order of magnitude as tilting pad thrust bearings. These results contradict the classic lubrication theory, due to the absence of a converging zone. Thus, he suggested that the pressure build-up is the result of the thermal expansion of the lubricant as it passes through the loaded regions of the bearing. The fluid expansion could distort

the velocity profile of the bearing, resembling this of a converging constant volume flow bearing. This theory was later identified as the "thermal-wedge effect" theory. In the discussion of this paper [5], Swift suggested that the pressure generated on the parallel bearing was the result of the thermal deformation of the pad geometry. In the same discussion, Bower suggested that the leading edge chamfer was mainly responsible for the observed load carrying capacity.

Salama [6] studied the effect of macro-roughness on the performance of parallel thrust bearings. He concluded that the explanation of Fogg [5] neglects the compressibility and side leakage effects, while Swift's theory could only be applied to bimetallic bearings. After experimenting with bearings with artificial macro-roughness, he concluded that the pressure build-up mechanism of parallel bearings is the existence of converging and diverging regions generated by the machining of the parallel bearing surface.

In 1958, Cameron and Wood [7] formalised Fogg's thermal wedge effect. They calculated thermal expansion of the lubricant domain assuming negligible heat dissipation through the solid domains, and constant temperature across the fluid depth. They quantified the theoretical load carrying capacity per unit length of a parallel bearing.

Later, Cameron [8] formulated and applied the theory of the viscosity-wedge for the parallel surface thrust bearings. He assumed a constant surface temperature on the pad, and a linear increase of the temperature on the rotor. He considered two scenarios, one with high (hot) and and one with low (cold) pad temperature. For both scenarios the rotor temperature is linearly varying from low (cold) to high (hot). He explained, in the first scenario, that the lubricant in the vicinity of the pad has lower viscosity than that in the vicinity of the rotor, resulting in a convex velocity profile, in the absence of any pressure gradient. At the end (streamwise) of the contact zone, where the pad and rotor are equally hot, the velocity profile should be linear. That contradicts the mass conservation law; thus, a positive pressure gradient at the entry and a negative at the exit should exist. In the same manner he explained the second scenario. Concluding with a comparison with the thermal-wedge effect, he supported that the viscosity wedge can produce an equal magnitude to the hydrodynamic wedge load carrying capacity, which is considerably higher than that predicted by the thermal wedge.

In 1955, Lewicki [9] proposed that the pressure in a parallel surface thrust bearing is generated due to the viscous ram pressure effect. He concluded that the lift is generated in the leading edge area of the bearing. In his calculations he neglected the inertia effects. More analytical work has been performed on the subject. In particular, Pan [10] included the inertial component in his model and successfully predicted the inlet channel pressure. Moreover, Tipei [11] modelled the phenomenon with potential flow, thus neglecting the viscous ram effect. In 1988, Heckelman and Ettles [12] performed extensive experiments to identify the importance of ram pressure. They established that when the film thickness is large, the temperature within the bearing is almost constant. That resulted to an effectively parallel film geometry, on which the bearing performs as dictated by Lewicki's theory. They suggested that, when the film thickness decreases, the viscosity-wedge initiates the edge ram pressure effect. They finally concluded that both viscous and inertia effect must be taken into consideration for the modelling and evaluation of a parallel surface thrust bearing. Moreover, in 1990, Taniguchi et al. [13] manage to experimentally identify the ram pressure effect in tilting-pad journal bearings.

Dowson and Hudson [14] and Hunter and Zienkiewicz [15] proved that variation of temperature and, therefore, viscosity across the film, play a significant role on

load carrying capacity of a thrust bearing. They also noted that the density variation is not as important as the temperature variation on the lubricant domain. Ettles and Cameron [16] added that thermal distortion of the solid domains has greater effect on the pressure build-up mechanism of the parallel surface thrust bearing, supporting Swift's theory as the explanation of Fogg's results. Neal [17] determined that the main pressure build-up mechanism is the thermal distortion of the pad. Furthermore, Ettles and Cameron [16] supported that the viscosity-wedge and the edge ram pressure effect are the main components of the initial load carrying capacity, while the thermal distortion is small. Once the thermal distortion is large enough, the viscosity wedge effect becomes negligible. Currie, Brockley, and Dvorak [18], after performing a series of experiments, also concluded that the the main component of the load carrying capacity of the parallel bearing is the thermal distortion that generates a converging geometry responsible for the pressure build-up. In his dissertation, Ettles [19] supported Currie's conclusions for thermal distortions. He also added that from the above-mentioned theories or effects, thermal-wedge has very small contribution to pressure build-up, and that the viscosity-edge, the ram pressure, and the macro-roughness give additional load carrying capacity to the parallel bearing.

In 1970, Ettles [20] investigated experimentally the hot oil carry-over phenomenon. He underlined the importance of this phenomenon to the thermal flow in the lubricant domain. As he explained, the majority of the lubricant entering the leading edge of a bearing pad is hot oil coming from the outflow region of the previous pad. In order to address this issue, most of the relevant studies have used simplified mixing models to evaluate the exact temperature at pad entrance. Recently, Zouzoulas and Papadopoulos [21] modelled one feeding oil groove half fore and half aft of the pad and imposed periodic conditions, thus managing to evaluate the hot oil carry-over without mixing model approximations.

Robinson and Cameron [22] managed to approximate the order of magnitude of the effect of thermal distortion. They concluded that (a) a two-dimensional approach is not accurate enough to precisely predict the bearing performance characteristics, (b) the three-dimensional energy equation in all domains is needed for accurate results, and (c) even at very low rotational speeds, the thermal distortions generate load carrying capacity for the bearing.

In 1985, Lebeck [23, 24], revising all the contemporary theories, he supported that the only possible explanation for the magnitude of the load carrying capacity of the parallel thrust bearing lies in the deviations from the parallel geometry. He suggested further investigation in the direction of a better understanding of how favourable macrogeometries might be developed, and for the identification of other sources of pressure generation in parallel surface thrust bearings.

Since then, many additional computational studies have been published in order to quantify the effects of each expressed theory. The majority of the studies use the Reynolds equations on the two- or three- dimensional lubricant domain, coupled with the energy equation on the solid domains [25], as the thermal effects seem to be the main reason of the load carrying capacity of parallel surface thrust bearings. Rohde and Oh [26] utilised the Reynolds equation and generated a thermoelastohydrodynamic model. They concluded that the effect of temperature on viscosity is more important than the thermal and mechanical distortions for the incline slider bearing. Brockett, Barrett, and Allaire [27] supported the above results with a finite volume approach of the TEHD Reynolds model. They concluded that the TEHD approach exhibited minor differences from the simple THD model. El-Saie and Fenner [28, 29] studied in detail the heat transfer on pivoted thrust bearing, and suggested

mixing approximation techniques for the temperature profiles at the inlet, in order to take into account the hot oil carry-over. They used those approximations for a TEHD comparison with experimental results for a eight pad pivoted thrust bearing configuration, with a good temperature correlation. Monmousseau, Fillon, and Frene [30] utilised a TEHD model of a tilting pad journal bearings and concluded that realistic thermal modelling is of utmost importance, and that the thermoelastic deformation evaluation, increases significantly the accuracy of the model results. The same approach and results have been published for different applications [31–33]. Their main objectives are the investigation of the thermal boundary conditions, the thermal and mechanical deformation of the pad and rotor, and the thermal properties of the lubricant. The last few years, following the increased availability of computational power, several studies have been published that solve the Navier-Stokes equations [34–37], mainly on tilting pad bearing configurations.

In summary, the literature results have demonstrated that parallel surface thrust bearings have the ability to support load, something that is not obvious by the classic lubrication theory. The most important pressure build-up mechanism theories suggested in the literature are summarised below:

1. The thermal wedge effect.
2. The viscosity wedge effect.
3. The effect of macro-roughness.
4. The effect of thermal distortion.
5. The leading edge ram pressure effect.
6. The effect of leading edge chamfer geometry.

The suggested most prominent theory is that of thermal distortion of the bearing pad, however smaller effects to the load carrying capacity of parallel surface thrust bearings can be attributed to combinations of the other theories/effects.

1.1.2 Artificial Surface Texturing (AST)

In the direction of the drastic efforts that have been made the last decades in order to reduce power losses in mechanical systems, the utilisation of artificial surface texturing (AST) on tribological contacts has been extensively examined by many researchers. The AST has been studied in a variety of application such as piston rings, journal bearings, thrust bearings, and mechanical seals. Many different texturing shapes and sizes have been studied, from simple micro-channels [38] to more complex patterns such as rectangular dimples[39, 40], hexagonal positive asperities [40], and hemispherical dimples [41], resulting to a range of different optimal geometrical designs, even for small alteration on the operating conditions of the mechanical system. Regarding thrust bearings, the use of texturing on the pad surface has been applied, in the majority of the studies, to parallel surface thrust bearings.

For the engine piston ring texturing, Etsion and Sher [42] managed to reduce the engine fuel consumption, by optimising the texture, up to 4%, but with hight repeatability fluctuations. Grabon et al. [43] presented experimentally that the wear in such applications mitigate fast their performance advantages. Lu et al. [44] also presented a friction reduction on reciprocating motion utilising square texture dimples, but with no mention on the wear resistance of the contact.

The texturing in journal bearings has been extensively studied. Brizmer and Kligerman [45] founded that fully textured journal bearings are meaningless, because of the load carrying capacity reduction, and almost identical attitude angles in

comparison with the plain journal. They also observed that partially textured bearings, have improved the dynamic characteristics, but also lowered the load carrying capacity of the bearing. Vlădescu et al. [46] experimentally supported the friction reduction of such designs, but they highlighted the importance of full hydrodynamic lubrication. Yamada, Taura, and Kaneko [47] suggested that texturing on journal bearings, has a negative effect on the static characteristics from the viewpoint of reduction of the load carrying capacity of the journal bearing, and that the texturing may contribute to the improvement of stability margin of the rotor supported by the textured journal bearings. Finally, Fillon [48] concluded, that partially texturing can improve the static performance of loaded journal bearings, only if the textured zone is located out of the active zone of the bearing (at the beginning of film rupture zone). Moreover he supported that fully texturing can improve the dynamic behaviour of loaded journal bearings (due to higher eccentricity and lower attitude angle), but the same can be achieved by simply increasing the clearance of the untextured bearing.

Etsion and Halperin [49] experimentally tested optimised textures on mechanical seals. The partial textured seals manage to increase considerably the hydrodynamic pressure generation, and in parallel to reduce up to 50% the friction losses of the tribological contact. Brunetiere, Tournerie, and Frene [50] underlined the importance of the thermal deformation evaluation on the mechanical seals, and in 2012 Brunetière and Tournerie [51], utilising a THD approach managed to identify that textures reduce the friction dependency on the roughness of the initial surface. Moreover they linked the seal side leakage to the density of the texturing.

In 2003, Brizmer, Kligerman, and Etsion [52] managed to computationally evaluate the pressure build-up mechanism on a textured parallel surface thrust bearing. They identified two physical mechanisms, the micro-dimple "individual effect" and the micro-dimple "collective effect". The individual effect corresponds to a fully textured pad, but is not useful for developing high specific loads. The collective effect refers to the partially textured bearing, that is capable of generating loads of equivalent magnitude as the optimal conventional bearings. Marian et al. [39] and Marian, Kilian, and Scholz [53], supported numerically and experimentally that optimal texturing extend for parallel surface thrust bearing is 50% on the circumferential direction and 90%-100% on the radial direction. Previous and later studies have identified different optimal texture extends, depths and shapes, depending on the operating conditions. As in the previous reported studies, and because the validity of the Reynolds equations for the modelling of such applications has been demonstrated [54–56], most of the published work utilises the Reynolds equation. Nevertheless, due to numerous inconsistencies on the correlation between numerical simulations and experimental measurements [57–59], Ibatan, Uddin, and Chowdhury [60] suggested that the current models should be developed further. They suggested that mechanical properties such as deformation and viscoelastic creep might play a role in the accurate evaluation of textured designs. Moreover, Bai, Meng, and Zhang [61] emphasised the importance of cavitation modelling due to various experimental observations of persistence cavitating regions, usually inside the texture geometry.

Chalkiopoulos et al. [62] proposed that in order to properly identify the tribological characteristics of textured thrust bearings, especially in moderate to highly loaded applications, a 3D CFD thermoelastohydrodynamic (TEHD) modelling approach should be followed. They suggested that the main reason of the inconstancies between the experimental and computational results is the neglection of the thermal deformation of the pad domain.

1.1.3 Coatings

Since the era of wooden, water-lubricated bearings, the material technology of the bearings has advanced considerably. The first studied bearings of Tower [1] were made of steel, but as the range of application and the understanding of the tribological contacts have grown, new materials have been utilised. Copper and steel alloys with better tribological characteristics are the main materials utilised today. Nevertheless, the use of lead and later tin based (Babbitt) alloys have been systematically used as coatings on bearings. The use of such coatings has entered the industrial use in bearings, due to the advantages they offer in comparison with common materials. Firstly, the Babbitt coating acts as safety if the lubrication fails. When the temperature increases, and the hydrodynamic capacity of the bearing is not enough for the applied load, the Babbitt coating melts and behaves as a lubricant until bearing operation is safely stopped. This protects the rotor and the whole rotational system, and with a re-coating the bearing is functional again. The coating also captures wear particles; thus, reduces the extensive abrasive wear. Nevertheless, Babbitt coatings are not always adequately reliable. Biswas, Chander, and Gole [63] studied failed bearings and determined four reasons for those failures, namely: electric discharges, cavitation, thermal fatigue, and local melting in the high pressure regions of the bearing.

Since the 1970's, the Babbitt coatings have, in some cases, been gradually replaced by new synthetic polymers. The first polymer used was Polytetrafluoroethylene (PTFE), which due to its very low static friction property, decreased the start-up friction enough to allow the elimination of the hydrostatic lifting pocket in highly loaded applications. In turn, this led to reduction of the size of the required bearing pad area, which led to bearings of smaller principle dimensions for given operational profile, resulting in lower friction losses, and less costly bearing designs. Moreover, PTFE's normal operation temperature range is considerably higher, with a maximum safe operation temperature above 180°C. The main problem of those coatings is their creeping properties. Moreover, PTFE cannot sustain constant high loads while on thermal cycling. Ettles et al. [64] compared the operation of Babbitt and PTFE coatings, and found that due to the low elastic modulus of PTFE, the tolerances on thickness and flatness can be more relaxed, and that thermal crowning is reduced considerably.

Schubert and Brescianini [65] presented the effect of carbon fibre PEEK composite coating in large hydro power plant thrust bearing refurbishment. He reported higher load carrying capacity, and safe operation. Many hydro power plant operators have introduced, for those reasons, polymer linings on their thrust bearing configuration, constituting the use of such materials a common choice in critical applications. Their ability for working in the mixed lubrication regime, eliminates the need for hydrostatic operation in start-up conditions. This reduces the points of failure, namely the high pressure pump that is needed for the start-up procedure and all its appendages. This also permits reducing the overall design and manufacturing complexity, as well as increasing the safety margin in such critical operations.

Wodtke and Wasilczuk [66] emphasised the effect of the bonding intermediate layer on the mechanical properties of polymer coatings, and that different bonding methods could considerably change the mechanical properties of the coating.

Glavatskih, Wasilczuk, and Fillon [67] supported that new PTFE composites managed to increase its creep endurance considerably, and after the successful industrial use of such materials, as Simmons, Knox, and Moss [68] stated, the PTFE composites seem to be a great alternative to Babbitt. Furthermore, many recent studies have been published presenting the improved properties of new synthetic composite polymers such as PEEK, PAI, etc. Satyanarayana, Sinha, and Ong [69] used a UHMWPE film layer over the PTFE coating introducing hydrophobic properties to the coating. Jahanmir, Hunsberger, and Heshmat [70] studied a heparin treated H-DLC coating for cardiovascular pump bearings, and found that it can survive start/stop cycles and sudden loading. Lan et al. [71] studied the durability and friction coefficient of ATSP coatings in comparison with PEEK and PTFE. They arrived in the conclusion that ATSP coating exhibited the lowest friction and higher wear resistance, with PEEK preforming the worst, and PTFE in between the other two. Katsaros et al. [72] compared DLC and PTFE coatings with the Babbitt reference. They concluded, that the DLC coating disturbs less than PTFE the thermal and flow fields due to its higher thermal conductivity, driving to a more efficient coating for bearing applications. Gheisari, Lan, and Polycarpou [73] expressed the importance of thin coating layers, due to the high insulating properties, low stiffness, and high thermal expansion of thick layers of polymer coatings . Wang and Gao [74] managed to experiment with new ABS resin, CFR-PAI and CFR-PEEK composite coatings under natural seawater lubrication, with minimal wear. However, due to their thermal properties, polymer coatings act as insulators between the lubricant and the pad base. In addition, due to their larger thermal expansivity, Fillon and Glavatskih [75] concluded that the TEHD approach is needed in order to accurate evaluate computationally their performance.

1.2 Goals of the present study

Summarising, past research has concluded that the neglection of certain phenomena in the fluid and solid domains of a bearing, especially with respect to the thermal effects, leads to discrepancies in the computational evaluation of the parallel surface thrust bearing. Thus, in the present Thesis, a detailed study of the phenomena suggested in the Literature has been analysed, evaluated and presented.

In particular, a detailed CFD-based ThermoElastoHydroDynamic (TEHD) model of a thrust bearing has been developed, accounting for the thermal and mechanical deformations of the stator and the rotor. A typical VG46 lubricating oil has been modelled, with thermal dependant properties. This detailed model, capturing all of the required physics of the problem, will be referred to as the "Full TEHD" model. The developed model has the capability of switching on and off the effect of certain physics of the problem. Therefore, by varying the "Full TEHD model", several simpler models have been produced, which have been used to quantify the effect of each studied phenomenon.

On a slightly different path, the performance of parallel surface bearings, with artificial surface texturing at part of the bearing surface has also been considered. As the effect of the thermal deformation of the pad geometry is considered to be one of the main pressure build up mechanisms for a parallel surface thrust bearing, and the experimental results of textured thrust bearings are in general not following the predictions of numerical simulations, a similar CFD-based TEHD model has been generated for the parallel surface textured bearing geometry, with the goal of identifying the effect of thermal deformation on bearing performance. Furthermore,

as coatings on thrust bearings are very commonly utilised in engineering solutions, and their insulation properties can affect considerably the thermal profile of the bearing, a basic single coating CFD-based TEHD model has been generated to study the effect of coatings on parallel surface thrust bearing performance.

Finally, in the last section of this study, an evaluation of the contemporary designs has been performed, with all the material properties that have been deemed necessary for the parallel surface bearing evaluation. The obtained results have been compared against results obtained by simpler THD models and against experimental measurements.

Chapter 2

Modelling Approach

In the present chapter, the governing equations that have been used are presented. The different geometry studied in the course of the Thesis are demonstrated. The chosen lubricant and solid material properties are shown. Finally, the boundary conditions (BC) for the Full TEHD and the simpler models are explained.

For the different geometrical configurations presented in Section 2.2, three basic categories of models have been generated. The isothermal, where the temperature the computational domain, and the lubricant properties are considered constant. The ThermoHydroDynamic (THD), where the energy equation is solved in the lubricant domain taking into account viscous dissipation, the conjugate heat transfer (CHT) is calculated for the solid domains, and the lubricant properties are temperature dependent. Finally, the TEHD modelling, for which the solid domains are able to deform due to thermal expansion and elastic deformation, is presented.

For all geometries presented below, the oil feeding groove is included, because of its importance for the oil mixing (hot oil carry-over), the pad cooling, and the structural boundary conditions.

Regarding the need for good temperature approximation and flow evaluation in deep cavities (grooves and textures), the Navier-Stokes (N-S) equations have been utilised. The importance of the N-S modelling will be demonstrated in the evaluation of the leading edge pressure ram effect, and in the evaluation of the textured geometry. Moreover, no imposed heat transfer coefficient between the lubricant and the solid is need, as the heat flux is calculated at each surface element of the lubricant. This allows the placement of the temperature boundary condition as far as possible from the lubricant domain, which will minimise local inaccuracies.

2.1 Governing equations

The Full TEHD model is a coupled model between a CFD solver (ANSYS CFX) and a FE solver (ANSYS Mechanical). The N-S momentum equation (2.1) coupled with the mass conservation equation (2.2) are used for the lubricant flow, in addition with the energy equation on the lubricant domain (2.3). The lubricant viscosity, density, thermal conductivity, and specific heat capacity are considered temperature dependent. The viscosity is described by the the Walther and McCoull equation (2.7) for the ISO VG 46 oil, the rest properties are approximated by linear equations from interpolating manufacturing data from Idemitsu Kosan Co. Ltd. The equations of the lubricant properties for the ISO VG 46 oil are presented in the model parameters section 2.3. The cavitation model chosen, is the Rayleigh-Plesset described by the equation (2.6).

For solid domains, namely the rotor and pad, the Conjugate Heat Transfer (CHT) is calculated by the equation (2.4). The elastic and mechanical deformations on the solid domains, are described by the equation (2.5).

Momentum equations for incompressible flow:

$$\rho \frac{D\vec{u}}{Dt} = -\nabla p + \mu \nabla^2 \vec{u} \tag{2.1}$$

Mass conservation:

$$\nabla \cdot \vec{u} = 0 \tag{2.2}$$

Lubricant domain energy equation:

$$\rho \cdot c_{pf} \cdot \vec{u} \cdot \nabla T = \nabla \cdot (\lambda_f \cdot \nabla T) - \tau : \nabla \cdot \vec{u} \tag{2.3}$$

Solid domain energy equation:

$$\nabla \cdot (\lambda_s \cdot \nabla T) = 0 \tag{2.4}$$

The stress equation for the mechanical and thermal deformations of the solid domains:

$$\begin{bmatrix} \sigma_{xx} \\ \sigma_{yy} \\ \sigma_{zz} \\ \sigma_{yz} \\ \sigma_{xz} \\ \sigma_{xy} \end{bmatrix} = \frac{E}{(1+\nu)(1-2\nu)} \begin{bmatrix} 1-\nu & \nu & \nu & 0 & 0 & 0 \\ \nu & 1-\nu & \nu & 0 & 0 & 0 \\ \nu & \nu & 1-\nu & 0 & 0 & 0 \\ 0 & 0 & 0 & \frac{(1-2\nu)}{2} & 0 & 0 \\ 0 & 0 & 0 & 0 & \frac{(1-2\nu)}{2} & 0 \\ 0 & 0 & 0 & 0 & 0 & \frac{(1-2\nu)}{2} \end{bmatrix} \begin{bmatrix} \epsilon_{xx} \\ \epsilon_{yy} \\ \epsilon_{zz} \\ \epsilon_{yz} \\ \epsilon_{xz} \\ \epsilon_{xy} \end{bmatrix} - \frac{E\alpha_{se}\nu T}{1-2\nu} \begin{bmatrix} 1 \\ 1 \\ 1 \\ 0 \\ 0 \\ 0 \end{bmatrix} \tag{2.5}$$

and where ν is the Poisson ratio, E the Young's modulus, T the temperature, and α^{se} the coefficient of thermal expansion.

Rayleigh-Plesset cavitation equation:

$$R_B \frac{d^2 R_B}{dt^2} + \frac{3}{2}(\frac{dR_B}{dt})^2 + \frac{2\sigma_B}{\rho R_B} = \frac{p_v - p}{\rho} \tag{2.6}$$

2.2 Geometry

For the model generation for the different stages of the present Thesis three basic geometrical configurations have been used, a thrust slider 2.2.1, a single sector pad of an eight pad thrust bearing 2.2.2, and a full eight pad thrust bearing 2.2.3. In order to be able to compare the computational results with experimental data, the bearings

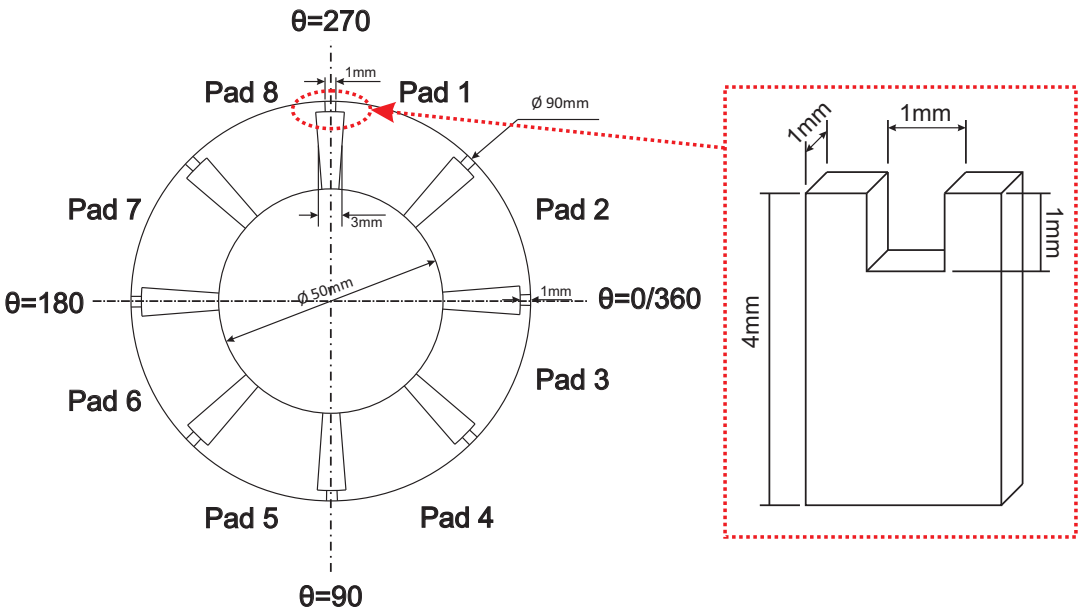

FIGURE 2.1 – Thrust bearing top view and gouge design details.

geometry is based on the bearing utilised by Henry, Bouyer, and Fillon [57] for their experiments, with a simplification on the groove and gouge features. As seen in Fig. 2.1 the walls of the oil feeding groove have radial direction; thus, not parallel as in [57], but the distance between the sides at the mid-diameter of the bearing is equal to the reference geometry. Moreover, the gouge feature in the reference geometry has a triangular section, yet in the present work the gouge section is considered rectangular in order to allow a fully hexahedral mesh in the lubricant domain.

TABLE 2.1 – Basic geometrical data for the reference thrust bearing.

Parameter	Description	Value	Units
NOP	Number of pads	8	*ul*
$\mathbf{D_{Inner}}$	Pad Inner Diameter	50	*mm*
$\mathbf{D_{Outer}}$	Pad Outer Diameter	90	*mm*
$\mathbf{L_{GO}}$	Gouge Length	1	*mm*
$\mathbf{D_{GO}}$	Gouge Depth	1	*mm*
$\mathbf{L_{GR}}$	Groove Width	3	*mm*
$\mathbf{D_{GR}}$	Groove Depth	4	*mm*
$\mathbf{D_P}$	Stator Thickness	10	*mm*
$\mathbf{D_S}$	Rotor Thickness	20	*mm*

TABLE 2.2 – Basic geometrical data for the reference thrust slider.

Parameter	Description	Value	Units
L	Stator Length	24.49	*mm*
B	Stator Breadth	20	*mm*
$\mathbf{L_{GO}}$	Gouge Length	1	*mm*
$\mathbf{D_{GO}}$	Gouge Depth	1	*mm*
$\mathbf{L_{GR}}$	Groove Width	3	*mm*
$\mathbf{D_{GR}}$	Groove Depth	4	*mm*
$\mathbf{D_P}$	Stator Thickness	10	*mm*
$\mathbf{D_S}$	Slider Thickness	20	*mm*

2.2.1 Slider

Due to the large computational cost of a 3D CFD, and the complexity of sector pad thrust bearing, a simplification of the geometry in some cases has been made in order to be able to assess the modelling parameters, and then apply them to a more complex geometry. In some cases, because of computational limitations only slider models have been evaluated and presented.

The main geometrical details for the slider are presented in Table 2.2. The slider is designed as close as possible to the thrust bearing dimensions. The stator, runner, and lubricant domain are depicted in Fig. 2.2. The naming scheme of the slider model surfaces is given in Fig. 2.3.

To account for the feeding oil grooves for the slider, half groove is modelled preceding the pad and half succeeding it. Thus, applying periodic boundary conditions on the end of the computational domains, an infinite slider with oil feeding grooves is represented. By modelling the groove an oil mixing model is not necessary, and with the correct meshing on the lubricant domain the model will be able to account for the hot oil carry-over phenomenon [20, 21].

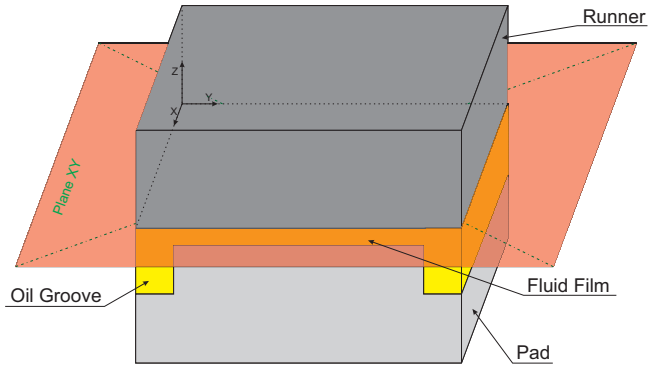

FIGURE 2.2 – Slider domains

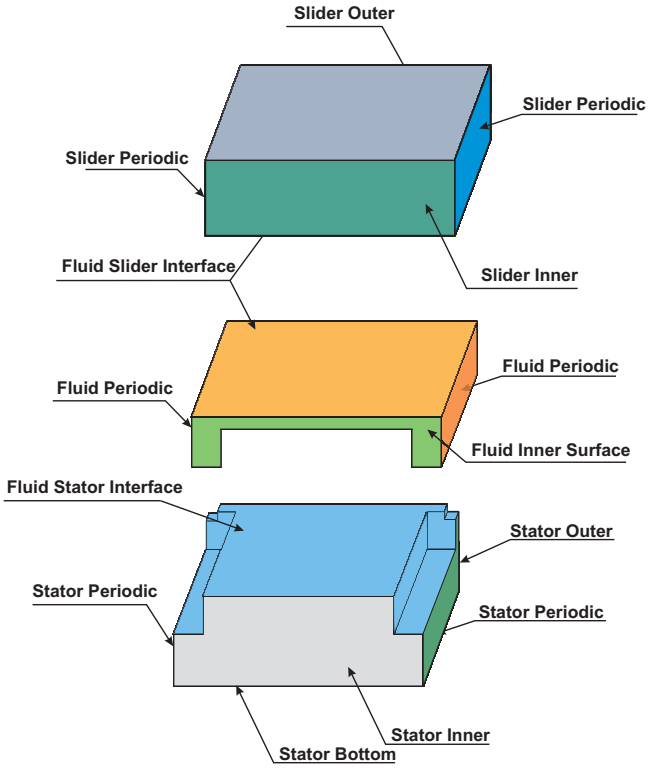

FIGURE 2.3 – Slider naming scheme and basic geometrical representation of the computational domains.

2.2.2 Sector Pad

An eight pad thrust bearing with identical pads, due to rotational periodicity of the geometry, can be computationally approached by the simplified one pad model with rotational periodic conditions on its two sides. Half oil feeding groove is modelled preceding and half succeeding the single sector pad geometry.

The main geometrical details for the eight sector pad thrust bearing are presented in Table 2.1. The stator, rotor, and lubricant domain are depicted in Fig. 2.4. The naming scheme of the sector pad model surfaces is given in Fig. 2.5.

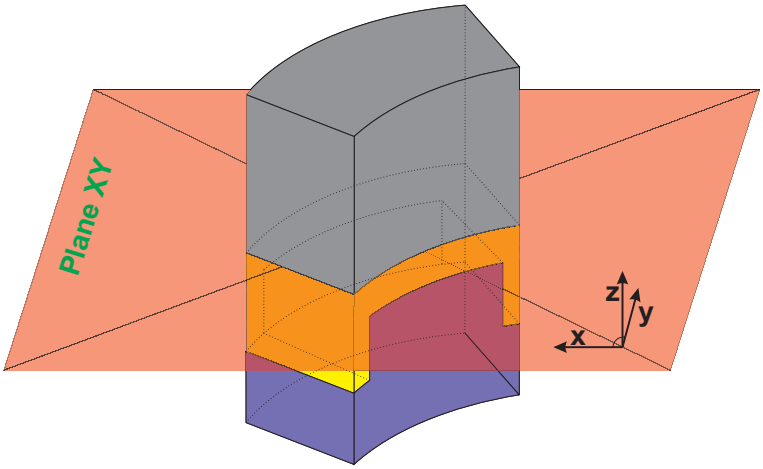

FIGURE 2.4 – Sector pad domains

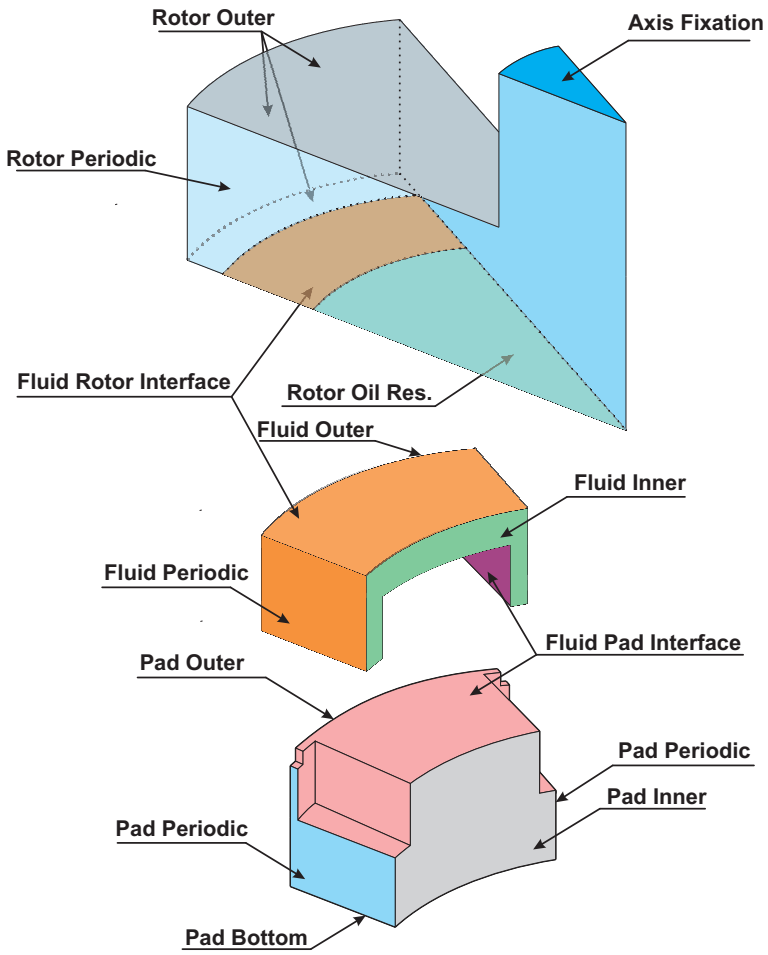

FIGURE 2.5 – Sector pad naming scheme and basic geometrical representation of the computational domains.

2.2.3 Full thrust bearing

When features of the bearing's geometry remove the rotational periodicity of the domain a full eight pad thrust bearing model is needed. In the present Thesis, the full thrust bearing is used to evaluate the effects of the pad fixation and to compare the modelling approach with experimental data of a precisely measured geometry.

The main geometrical details of the eight pad thrust bearing model are the same with the sector pad model and are presented in Table 2.1. The stator, rotor, and lubricant domain are depicted in Fig. 2.6. The naming scheme of the sector pad model surfaces is given in Fig. 2.7.

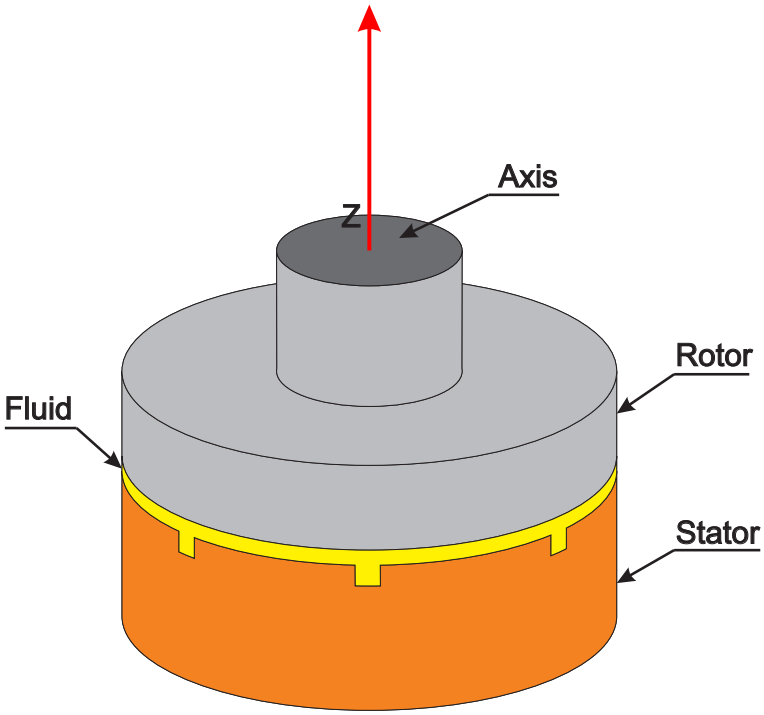

FIGURE 2.6 – Full eight sector pad thrust bearing domains

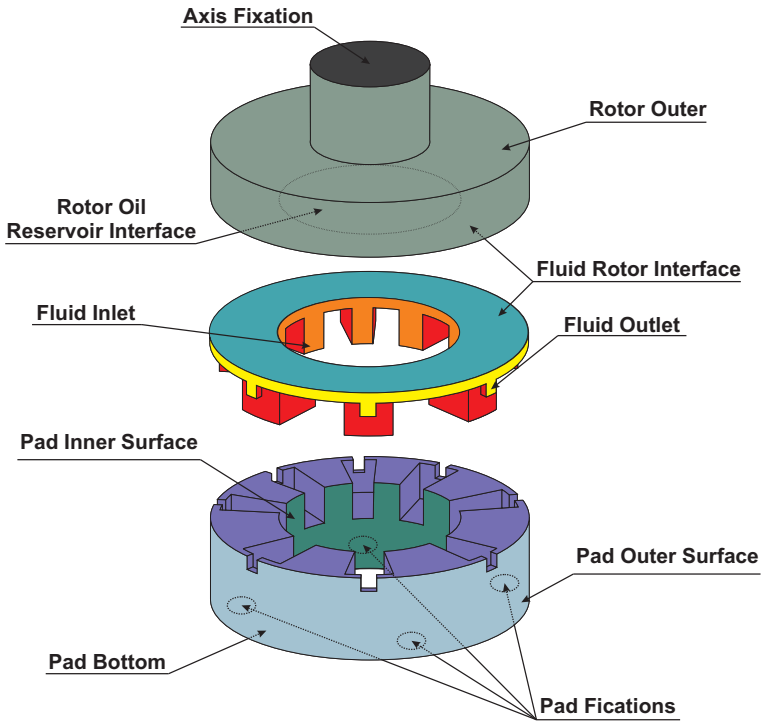

FIGURE 2.7 – Full eight sector pad thrust bearing naming scheme and basic geometrical representation of the computational domains.

2.2.4 Initial geometric imperfections

As it was suggested by Salama [6], macro-roughness might play a significant role on the pressure build-up mechanism of the parallel thrust bearing. Charitopoulos et al. [76] suggested five typical manufacturing defects that could affect the performance

of thrust bearings. Therefore all three modelled configurations account for five different manufacturing imperfections for the parallel surface thrust bearing, namely concave, convex, converging, diverging, and sinusoidal. The geometric imperfections are named from the resulting shape of the lubricant domain. A section of each defect at the longitudinal mid-plane of the bearing is depicted in Fig 2.8.

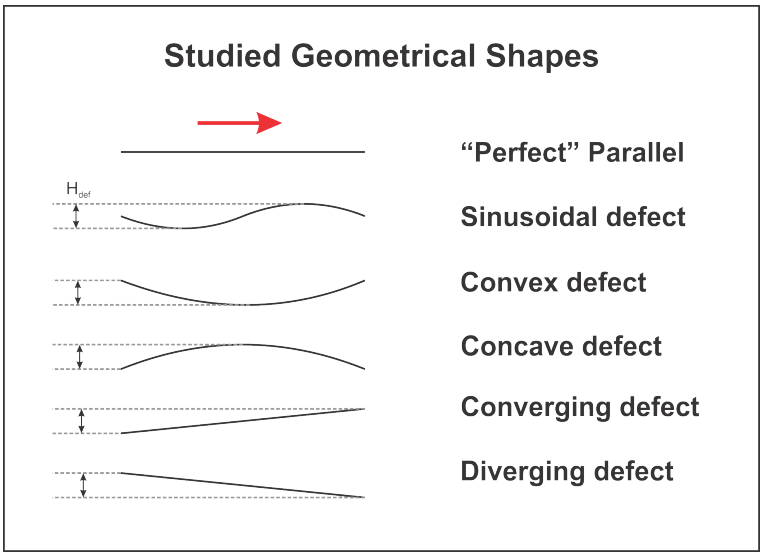

FIGURE 2.8 – Section at the longitudinal mid-plane section of the imperfect bearing.

2.2.5 Surface Texturing

In Introduction, the importance of AST on thrust bearings has been demonstrated along with the inconsistency of calculations and experimental results. In the present work, the selected texturing design is that of a 8×8 grid of orthogonal dimples with depth of 20 μm. The textured area is set as the 60% of the pad length by the 80% of the pad width. The textured area is composed of 64 cells. Each cell has a dimple in its centre, with length and width equal to 80% of the cell length and width respectively, concluding in a texture density of 64%. The texturing pattern is sawn in Fig 2.9 for the slider bearing and in Fig 2.10 for the sector pad.

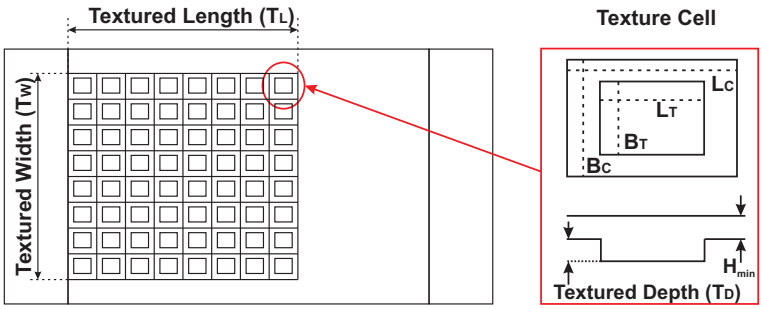

FIGURE 2.9 – Texturing pattern for the slider geometry

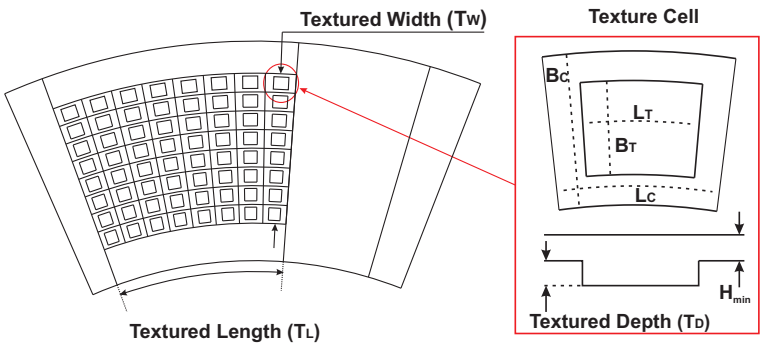

FIGURE 2.10 – Texturing pattern for the sector pad geometry

2.2.6 Coatings

In order to identify the thermal effects of coatings on parallel thrust bearings a single sector pad geometry is generated with a layer of coating with the mechanical and thermal properties of Babbitt, PEEK, or PTFE. Two geometrical configurations have been produced, one for a single coating and one for a dual coating approach as shown in Fig. 2.11.

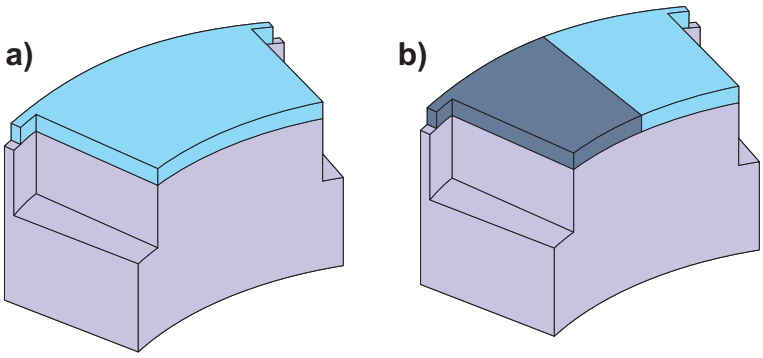

FIGURE 2.11 – Coating geometry a) single coating, b) dual coating.

2.2.7 Measured experimental geometry

To be able to compare the TEHD modelling approach with experimental data, the exact experimental geometry needs to be generated. As mentioned above, the geometry has been measured by Henry, Bouyer, and Fillon [57]. The approximation values utilised are listed in Table 2.3, and a circumferential section at the mid diameter of the full thrust bearing is depicted in Fig. 2.12.

TABLE 2.3 – Characteristics of the imperfections on each pad of Henry's thrust bearing.

Pad	**Imperfection**	**Amplitude** $[\mu m]$	H_{min} **discrepancy in** $[\mu m]$
1	convex	1	-1
2	diverging	1.25	-1
3	converging	1.25	-0.5
4	diverging	0.5	-0.5
5	convex	1	-0.75
6	convex	0.5	-1
7	convex	0.5	-1
8	convex	0.5	-0.5

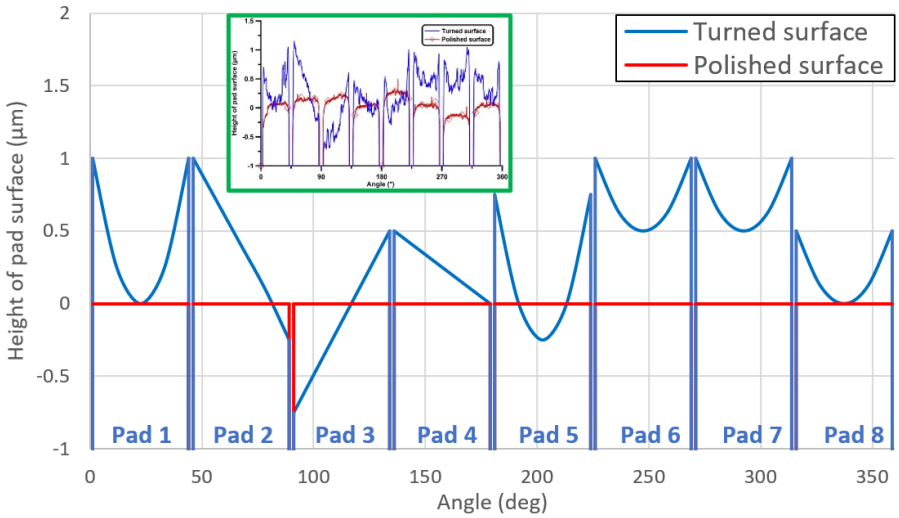

FIGURE 2.12 – Experimentally measured defected geometry by Henry [77] for each pad.

2.2.8 Fixations

In the experiments [77] the thrust bearing has been fastened on the pad support by four screws, as it is shown in Fig. 2.13. This feature has been modelled for the evaluation of the bearing fixation on the thermal and mechanical deformations.

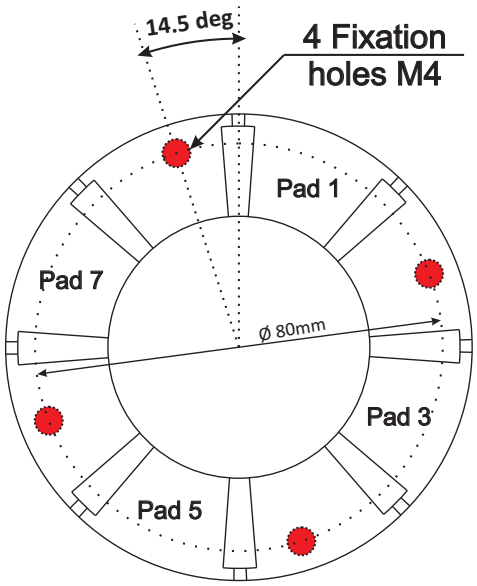

FIGURE 2.13 – Fixation location for the full thrust bearing.

2.2.9 Contemporary designs

The contemporary designs selected in the present study are those experimentally evaluated by Henry, Bouyer, and Fillon [57]. A classic tapered-land bearing depicted in Fig 2.14, and a pocket bearing depicted in Fig 2.15. The design parameters for both bearings are listed in Table 2.4. A 3D representation of the stator computational domain is shown in Fig. 2.16 for both designs.

TABLE 2.4 – Basic geometrical data for the pocket and tapered-land selected configurations.

Parameter	Description	Value	Units
$\mathbf{L_{Taper}}$	Taper Length	15	mm
$\mathbf{H_1}$	Taper Depth	20	μm
$\mathbf{L_{Pocket}}$	Pocket Length	80	%
$\mathbf{B_{Pocket}}$	Pocket Width	80	%
$\mathbf{H_{Pocket}}$	Pocket Depth	20	μm

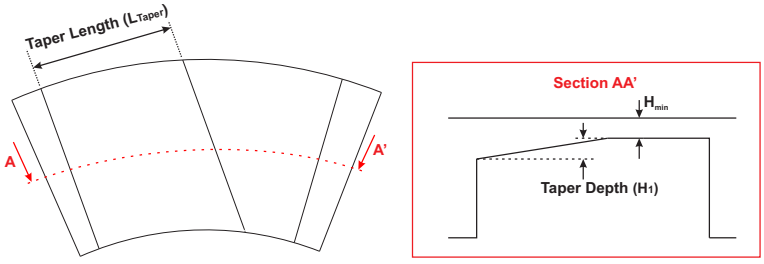

FIGURE 2.14 – Tapered-land bearing configuration sketch.

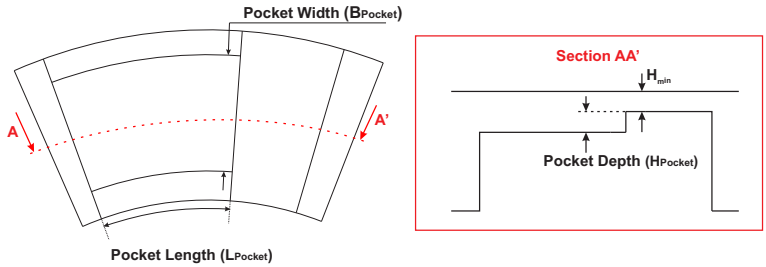

FIGURE 2.15 – Pocket bearing configuration sketch.

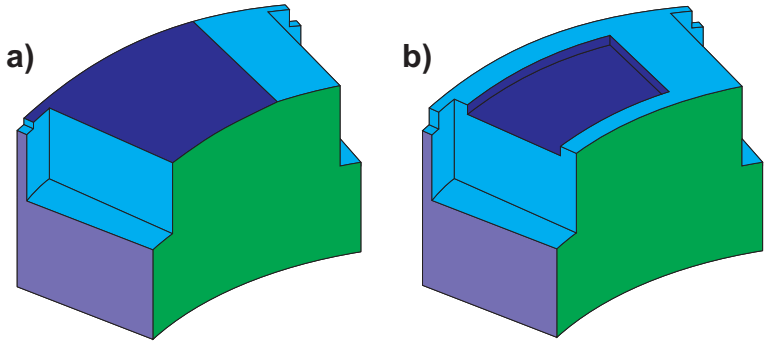

FIGURE 2.16 – 3D representation of the a) tapered-land and b) pocket bearing configurations.

2.3 Modelling Parameters

2.3.1 Lubricant

The lubricant used in all simulations is the ISO VG 46. As stated in section 2.1 for the more complex models the lubricant properties are temperature dependent and are evaluated from the following equations.

The viscosity is described by Walther and McCoull equation (2.7).

$$\log_{10}\left(\log_{10}\left(\nu_f + \alpha\right)\right) = b - n\log_{10}\left(T\right) \tag{2.7}$$

where: ν_f is the kinematic viscosity of the fluid in cSt, and the parameters:

α=0.6,
b=9.02865,
n=3.52681

The density is described by the linear equation (2.8):

$$\rho(T) = -0.6877 \cdot (T - 273.15) + 891.04)[kg/m^3] \tag{2.8}$$

The specific heat capacity is described by the linear equation (2.9):

$$C_p(T) = 3.6 * (T - 273.15) + 1810)[J/(kg^{-1} \cdot K^{-1})] \tag{2.9}$$

The thermal conductivity is described by the linear equation (2.10):

$$\lambda_f(T) = -7 \cdot 10^{-05} \cdot (T - 273.15) + 0.134)[W/(m \cdot K)] \tag{2.10}$$

For the simpler models where constant values of the above properties are used. Those values are listed in Table 2.5.

TABLE 2.5 – Constant values of the ISO VG 46 lubricant parameters.

Symbol	Parameter	Value	Units
ν_{f40}	Viscosity at 40°C	0.04160	$Pa \cdot s$
ν_{f90}	Viscosity at 90°C	0.00816	$Pa \cdot s$
ρ	Density	864	kg/m^3
C_p	Specific heat capacity	1954	$J/(kg^{-1} \cdot K^{-1})$
λ_f	Thermal conductivity	0.1312	$W/(m \cdot K)$
p_c	Cavitation pressure	50	kPa

2.3.2 Solids

For all the calculation the rotor/slider material is steel, and the pad material is bronze. In the case of coatings, an additional material is added on top of the bronze pad base as depicted in Fig 2.11.For the Babbitt, PEEK, PTFE materials, the properties in the literature differ from publication to publication; thus, the most commonly used values have been selected. All material properties displayed in Table 2.6

TABLE 2.6 – Material properties for the solid domains.

Parameter	Steel	Bronze	PTFE	PEEK	Babbitt
Density $[Kg/m^3]$	7850	8300	2200	1320	7300
Thermal expansion $[K^-1]$	$1.2E^{-05}$	$1.85E^{-05}$	$1.35E^{-04}$	$5.00E^{-05}$	$2.10E^{-05}$
Thermal conductivity $[W/(mK)]$	60.5	120	0.4	0.25	40
Young's modulus, E $[GPa]$	200	110	0.34	3.56	53
Poisson's ratio, ν	0.3	0.34	0.46	0.4	0.35
Tensile Yield strength $[MPa]$	250	125	40	100	69

2.4 Boundary conditions

In the following tables the boundary conditions (BCs) for the single sector pad models are presented. The BCs for the slider and full sector pad thrust bearing are listed in Appendix A.

In Table 2.7 and Table 2.8, the BCs of two TEHD models are listed. The first table refers to the modelling of a deformable stator and a rigid rotor. The second table refers on the TEHD model with deformable both solid domains. The BCs for the THD model are presented in Table 2.9, and for the isothermal in Table 2.10.

TABLE 2.7 – Thermal and structural boundary conditions for the single sector pad TEHD model with rigid rotor.

Location	Temperature BC's	Structural BC's
	Stator	
Sides	Periodic conditions	Frictionless support
Pad Bottom	HTC: 1000 $W/(m^2K)$, T = 40°C	Uz=0
Pad Inner	HTC: 300 $W/(m^2K)$, T = 40°C	Free
Pad Outer	HTC: 25 $W/(m^2K)$, T = 40°C	Free
Fluid Stator Interface	2-way FSI: Continuity of heat flux and temperature	Free
	Rotor	
Sides	Periodic conditions	Fixed
Rotor Outer	HTC: 25 $W/(m^2K)$, T = 20°C	Fixed
Axis Fixation	HTC: 1000 $W/(m^2K)$, T = 20°C	Fixed
Rotor Oil Res.	HTC: 300 $W/(m^2K)$, T = 40°C	Fixed
Fluid Rotor Interface	Continuity of heat flux and temperature, Rotating velocity 6000 RPM	Fixed
	Lubricant	
Sides	Periodic conditions	Frictionless support
Fluid Inner	Opening with F.P. 0.1MPa, Temperature 40°C	Ux=0, Uy=0
Fluid Outer	Outlet with static pres. of 0 and Temp. 20°C	Ux=0, Uy=0

*Heat Transfer coefficient (HTC)

**Feeding Pressure (F.P.)

TABLE 2.8 – Thermal and structural boundary conditions for the single sector pad TEHD model with deformable pad and rotor.

Location	Temperature BC's	Structural BC's
	Stator	
Sides	Periodic conditions	Frictionless support
Pad Bottom	HTC: 1000 $W/(m^2K)$, T = 40°C	Uz=0
Pad Inner	HTC: 300 $W/(m^2K)$, T = 40°C	Free
Pad Outer	HTC: 25 $W/(m^2K)$, T = 40°C	Free
Fluid Stator Interface	2-way FSI: Continuity of heat flux and temperature	Free
	Rotor	
Sides	Periodic conditions	Frictionless support
Rotor Outer	HTC: 25 $W/(m^2K)$, T = 20°C	Free
Axis Fixation	HTC: 1000 $W/(m^2K)$, T = 20°C	Fixed
Rotor Oil Res.	HTC: 300 $W/(m^2K)$, T = 40°C	Free
Fluid Rotor Interface	2-way FSI: Continuity of heat flux and temperature, Rotating velocity 6000 RPM	Free
	Lubricant	
Sides	Periodic conditions	Frictionless support
Fluid Inner	Opening with F.P. 0.1MPa, Temperature 40°C	Ux=0, Uy=0
Fluid Outer	Outlet with static pres. of 0 and Temp. 20°C	Ux=0, Uy=0

*Heat Transfer coefficient (HTC)

**Feeding Pressure (F.P.)

TABLE 2.9 – Thermal and structural boundary conditions for the single sector pad THD model.

Location	Temperature BC's	Structural BC's
	Stator	
Sides	Periodic conditions	Fixed
Pad Bottom	HTC: 1000 $W/(m^2K)$, T = 40°C	Fixed
Pad Inner	HTC: 300 $W/(m^2K)$, T = 40°C	Fixed
Pad Outer	HTC: 25 $W/(m^2K)$, T = 40°C	Fixed
Fluid Stator Interface	Continuity of heat flux and temperature	Fixed
	Rotor	
Sides	Periodic conditions	Fixed
Rotor Outer	HTC: 25 $W/(m^2K)$, T = 20°C	Fixed
Axis Fixation	HTC: 1000 $W/(m^2K)$, T = 20°C	Fixed
Rotor Oil Res.	HTC: 300 $W/(m^2K)$, T = 40°C	Fixed
Fluid Rotor Interface	Continuity of heat flux and temperature, Rotating velocity 6000 RPM	Fixed
	Lubricant	
Sides	Periodic conditions	Fixed
Fluid Inner	Opening with F.P. 0.1MPa, Temperature 40°C	Fixed
Fluid Outer	Outlet with static pres. of 0 and Temp. 20°C	Fixed

*Heat Transfer coefficient (HTC)

**Feeding Pressure (F.P.)

TABLE 2.10 – Boundary conditions for the single sector pad Isothermal model.

	Lubricant	
Sides	Periodic conditions	Fixed
Fluid Inner	Opening with F.P. 0.1MPa	Fixed
Fluid Outer	Outlet with static pressure of 0MPa	Fixed
Fluid Pad Interface	No sliding wall	Fixed
Fluid Rotor Interface	Rotating velocity 6000 RPM	Fixed

*Feeding Pressure (F.P.)

2.5 Computational procedure

2.5.1 TEHD

In order to compute the final fluid and pad geometry due to temperature and mechanical deformation, a 2-way fluid solid interaction (FSI) model has been generated. A flow chart of the TEHD model calculation can be seen in Fig. 2.17. At the beginning of the calculation, after the mesh and input files for the three domains and the two solvers have been generated, the domain interface between the fluid domain and the pad, is mapped. The first calculation step is the evaluation of the thermal deformation of the stator in the FE solver, from a cold temperature of 20°C to the feeding oil temperature of 40°C. Then the displaced interface node locations are passed to the CFD solver, and the mesh displacement of the fluid domain is applied. The CFD solver calculates until convergence the hydrodynamic flow, the heat generation in the fluid, and the CHT on the rotor domain. The pressure and temperature values of the domain interface is passed to the FE solver and the CHT, and the mechanical and thermal deformation of the stator is re-evaluated. Finally, the last two steps will be executed until the maximum mesh displacement between two consecutive calculations is less than 0.01 μm, and the CFD solver is converged. When this iterative procedure is completed, the tribological characteristics are calculated, and the pressure, temperature, and deformation values of all the domains are exported. The aforementioned model is computationally very intensive. The time needed until convergence, for a single calculation of a sector pad thrust bearing, is approximately a little more than 3 days, with a 64-core and 96 Gb RAM compute unit. The time for a textured bearing geometry on the same compute unit exceeds the 5 days, due to the finer mesh needed for the dimple features.

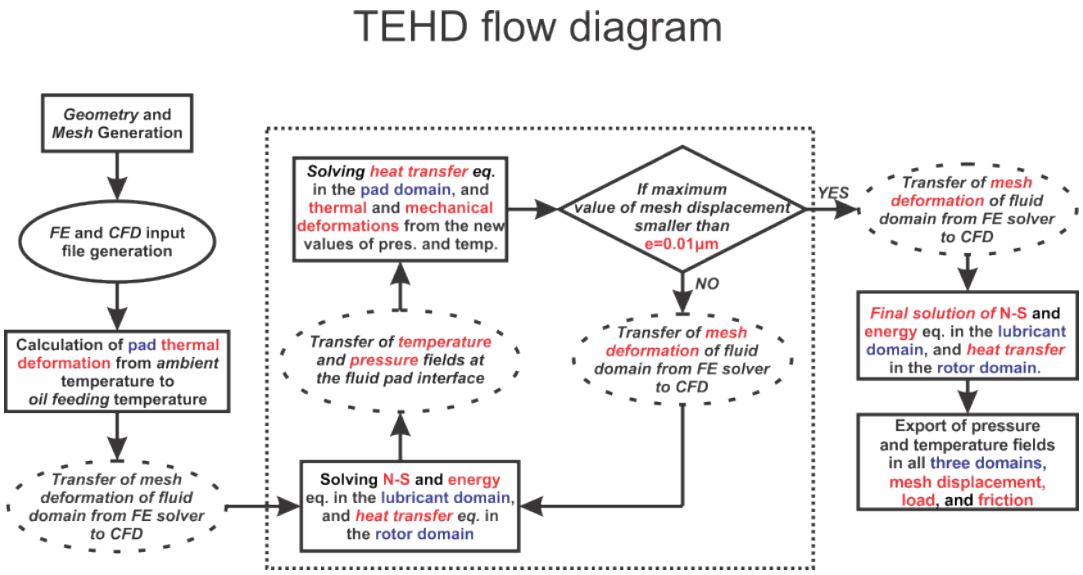

FIGURE 2.17 – TEHD model flow chart.

2.5.2 THD

For the THD model, all three domains have been modelled and calculated with the CFD solver. For a fully converged calculation, approximately 3.5 hours are needed for a highly loaded case.

2.5.3 Isothermal

For the Isothermal model only the fluid domain has been modelled, and the temperature is considered constant and equal to 40°C. Thus, all the temperature dependent properties of the fluid are considered constant. All the boundary faces in this model have been considered fixed. The time needed for a single isothermal calculation does not exceed 1.5 hours for a full convergence.

2.6 Mesh study

Mesh studies have been conducted for all the different modelling approaches. In the Thesis only the mesh study for the TEHD model for the parallel slider is presented. Two separate mesh studies have been conducted for the lubricant domain mesh. One for varying number of elements in the longitudinal direction, and one for varying the element number in the cross-flow direction (film thickness). In all presented cases the number of elements in the transverse direction is the half of the elements in the circumferential direction.

Taking into consideration Fig. 2.18 and Fig. 2.19, the number of elements selected for the circumferential direction is 120, and for the fluid thickness 16. Comparing the results of the models with those values, with the models with the higher number of elements, the accuracy is very good in terms of the goals of the present study.

For the slider model, the pad consists of approximately 50.000 hexahedral elements, the rotor of 50.000 hexahedral and tetrahedral elements, and finally the lubricant of 150.000 elements for the parallel configuration.

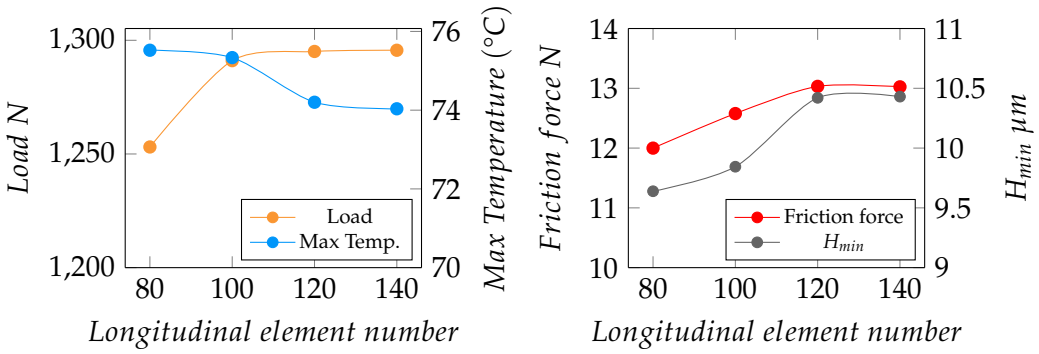

FIGURE 2.18 – Mesh study for varying number of elements in the circumferential direction.

A typical mesh for the sector pad geometry is depicted in Fig 2.20 for the parallel single sector pad geometry. Figures depicting the mesh of the other configurations can be found in Appendix B.

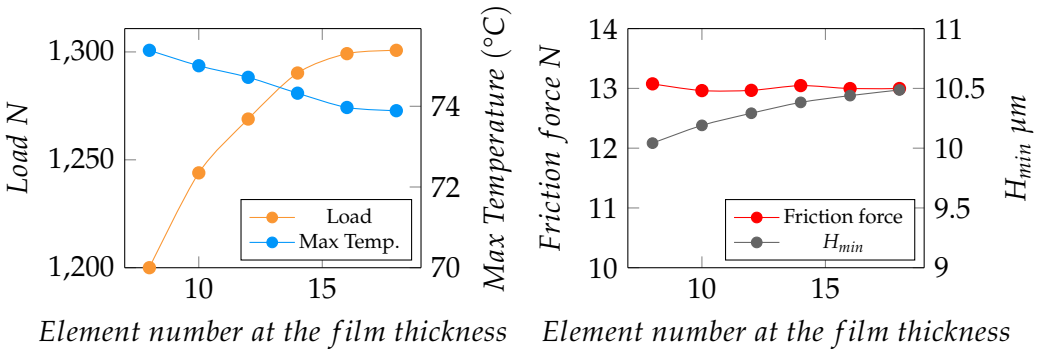

FIGURE 2.19 – Mesh study for varying number of elements in the cross-flow direction (across the fluid thickness).

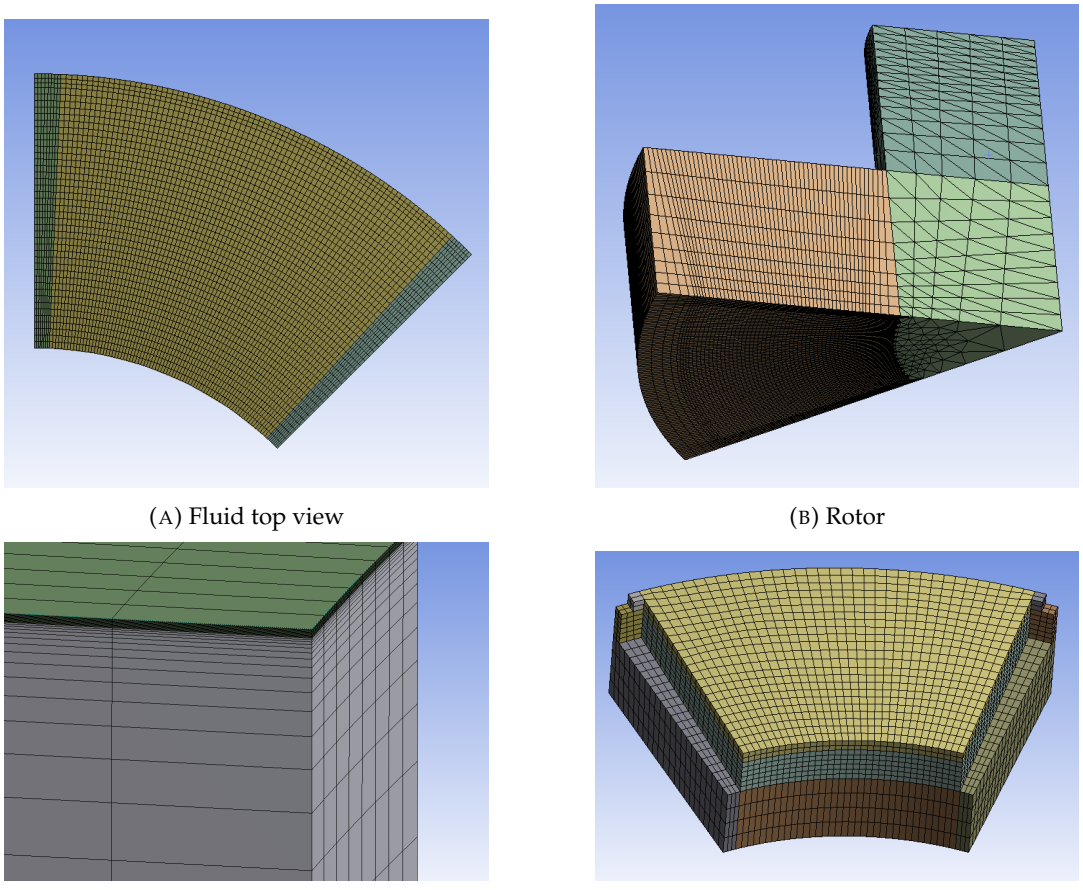

(A) Fluid top view

(B) Rotor

(C) Fluid groove iso-view

(D) Pad

FIGURE 2.20 – Mesh details of the single sector pad parallel surface model.

2.7 Convergence study

In order to calculate the TEHD model, an iterative procedure is needed, alternating the calculations between the FE and the CFD solvers, as explained in subsection 2.5.1. The amount of iterations needed to fully converge to the solution was not known. In order to investigate the required number of iterations needed, a convergence study has been conducted. The needed iteration number vary a lot from application to application; thus, for each model a different convergence study has been conducted. In the Thesis only the convergence study for the TEHD model for the parallel surface slider is presented.

Regarding the maximum number of iterations, in Fig. 2.21 calculations of the main slider performance indices are presented, namely thrust load, maximum lubricant temperature, friction force, minimum film thickness, as a function of iteration number. Based on the results, an iteration number value of 15 has been selected. For reference, for the simple TEHD sector pad model 60 iterations have been selected, and for the sector pad coated parallel surface thrust bearing 200.

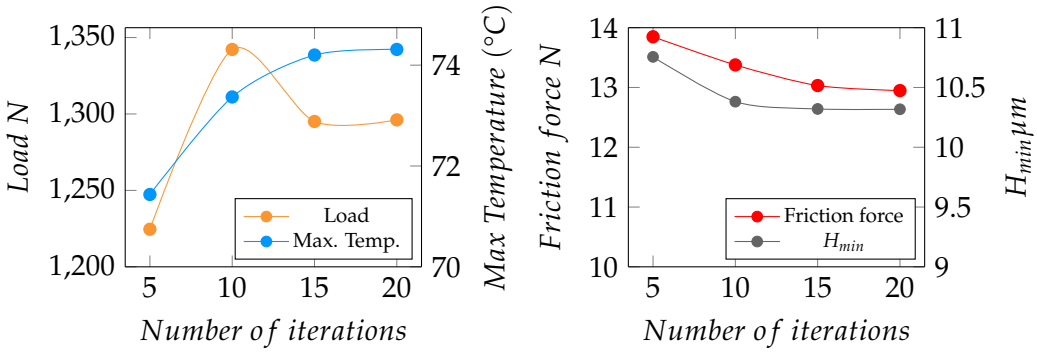

FIGURE 2.21 – Converging study, for varying number FE-CFD iterations.

2.8 List of presented models

To summarise, the generated models for the present study are divided into three categories: the thrust slider, the single sector pad thrust bearing, and the whole eight pad thrust bearing.

For all three configurations isothermal, THD, and TEHD models have been generated. For the slider geometry two configurations have been presented in the next chapters the textured and untextured parallel surface slider. For both configurations isothermal, THD, and TEHD results have been presented.

For the single sector pad configuration, the following models have been presented for the pressure build-up investigation with the parallel surface thrust bearing geometry:

1. **Isothermal no cavitation:** with no cavitation and constant temperature.
2. **Isothermal:** enabled cavitation and constant temperature.
3. **THD:** viscous dissipation, temperature dependent lubricant viscosity, and heat transfer on all domains with enabled cavitation.

4. **THD no cavitation:** As THD with no cavitation evaluation .
5. **THD with mechanical deformation:** as THD but with deformable stator only by the pressure generated by the flow.
6. **THD with temperature dependent density:** As THD with temperature dependent density.
7. **THD with temperature dependent density and constant viscosity:** Viscous dissipation with temperature dependent density and constant viscosity.
8. **simple TEHD:** Mechanical and thermal deformation of the pad, temperature dependent viscosity, constant density, and enabled cavitation.
9. **Full TEHD:** As Simple TEHD with temperature dependent density,thermal conductivity, and heat capacity.
10. **TEHD with deformable rotor:** As Full TEHD with mechanical deformation, with thermal and mechanical deformation of the stator and rotor domains.

Moreover, the single coating, tapered-land, and pocket bearing configurations for the single sector pad geometry utilising the Full TEHD, and the THD models have been evaluated, in order to identify the proper modelling approach for such designs. Specifically, the effects of thermal deformations on the contemporary design evaluation accuracy is assessed.

Finally, for the full thrust bearing geometry only two TEHD evaluations are presented. The full parallel thrust bearing with mechanical and thermal deformations of the pad domain, temperature dependent viscosity, density, thermal conductivity and heat capacity, with four fixation points on the pad bottom surface as displayed in subsection. 2.2.8, the rest of the bottom pad surface is supported by a compression only spring.

The second full thrust bearing geometry utilises the previous modelling approach, but with the whole pad bottom surface considered fixed, and the bearing geometry is replaced with the measured experimental geometry presented in subsection 2.2.7.

Chapter 3

Pressure build-up mechanism investigation

Experimental results for the parallel surface thrust bearing report that specific loads over 1.5 MPa can be supported. This contradicts with the classic lubrication theory. In that direction, in the present Thesis the pressure build-up mechanism of the parallel surface thrust bearing is investigated. In this chapter, the effects of the thermal properties of the lubricant and solid domains are evaluated. The thermal dependent viscosity and density as well as the thermal and mechanical deformations of the solid domains, are suggested by the literature as the main contributing factors of the load carrying capacity of the parallel surface surface thrust bearing. Thus, a detailed analysis has been performed for each suggested contributing factor, in order to identify their importance in the pressure build-up mechanism.

In this, and in the next chapter, the evaluated models have been compared with experimental results from the literature. All presented experimental results have been published in [57, 58, 77]. All results plotted in the figures of the present Thesis, represent values at the fluid-pad interface, unless differently stated in the caption.

3.1 Non thermal pressure build-up mechanisms in the lubricant domain (Ram pressure, hydrostatic lift, and cavitation)

For most bearing applications in literature and in industry, the isothermal approach is used. This approach assumes constant temperature in the whole lubricant domain. On a parallel surface thrust bearing, such modelling can only account for the leading edge ram pressure effect, and the hydrostatic lift generated by the oil feeding pressure. In Fig. 3.1 the load versus the H_{min} are plotted for the two isothermal models, one with and one without cavitation, alongside with the results of the isothermal model with no cavitation for no rotational speed. The viscosity on the lubricant is imposed to the value of the ISO VG 46 viscosity at 40°C ($\nu_{f40} = 0.0416034\ Pa \cdot s$).

The first pressure effect that we can identify is that of the hydrostatic lift from the feeding oil pressure. A constant hydrostatic load of approximately 34.5 N can be supported in the range of studied H_{min} values. So, if we subtract the hydrostatic lift pressure from the isothermal with no cavitation the ram pressure effect is isolated, and if we subtract the ram pressure and the hydrodynamic lift from the isothermal with cavitation model results, the effect of cavitation in the load carrying capacity can be identified.

As seen in Fig. 3.2, the ram pressure increases as the H_{min} decreases, and after a threshold H_{min} value, in the specific case $15\mu m$, the effect deteriorates. The amplitude of this effect is almost negligible, as it accounts for a maximum specific

load of 0.16 MPa. Moreover, comparing the isothermal with and without cavitation pressure profiles for the same H_{min} in Fig. 3.3, it is observed, that due to the high pressure zone generated by the ram pressure effect, radial leakage occurs near the leading edge region. Thus, local oil starvation conditions are present in the mid-section of the pad. For low values of viscosity this is countered by the flow from the inner surface, where the lubricant is supplied. For high values of viscosity, this flow is not large enough to supply the mid region with oil, driving to a pressure drop (see Fig. 3.4). This decreases considerably the load carrying capacity. The cavitation modelling allows to a more accurate description of those phenomena. Yet, in manner of the pressure build-up mechanism for the parallel surface thrust bearing, cavitation only accounts, in this case, for a maximum of 0.2 MPa specific load.

The viscosity utilised on the above-mentioned results was the viscosity value of the ISO VG 46 oil at the feeding oil temperature. This temperature is not close enough to the working temperature of a parallel surface thrust bearing operating in small H_{min} values. In order to see if the effect of ram pressure and cavitation change as the temperature increases, a second set of computations has been made, and presented for the ISO VG 46 viscosity at the temperature of 90°C. This temperature is selected as the maximum average temperature of a THD model operating at the same range of H_{min}.

In Fig. 3.5 the Load vs H_{min} for the two models operating at the higher temperature are presented. There are two main differences that can be pointed out. First, both the hydrostatic lift and the ram pressure effect produce a considerably lower load together than before, resulting to a specific pressure of 0.14 MPa for a $H_{min} = 15\ \mu m$. The pressure almost never passes the cavitation limit (see Fig. 3.6); therefore, both models exhibit almost the same behaviour.

Concluding, neither the pressure ram effect, nor the cavitation are proven able to support the observed load of the parallel surface thrust bearing. Both phenomena affect the bearing performance, but their effect decreases as the temperature increases. Moreover, contradicting Heckelman and Ettles [12] the ram pressure is not initiated due to the viscosity wedge, but is an independent flow phenomenon.

TABLE 3.1 – Isothermal results comparison with and without cavitation modelling for $H_{min} = 5\ \mu m$ and reference temperature of 40°C.

Parameter	No cavitation	Cavitation
Load $[N]$	51.93	151.79
Friction $[N \cdot m]$	3.46	3.41
Max. Pressure $[MPa]$	1.259	1.303
Oil flow rate $[l/min]$	1.196	1.197

TABLE 3.2 – Isothermal results comparison with and without cavitation modelling for $H_{min} = 5\ \mu m$ and reference temperature of 90°C.

Parameter	No cavitation	Cavitation
Load $[N]$	54.04	54.12
Friction $[N \cdot m]$	0.65	0.64
Max. Pressure $[MPa]$	0.59	0.59
Oil flow rate $[l/min]$	1.421	1.406

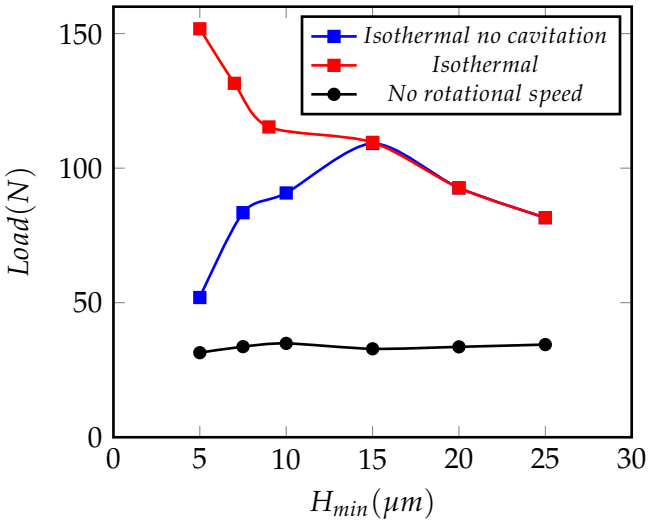

FIGURE 3.1 – Isothermal results: H_{min} *vs Load at* 40°C

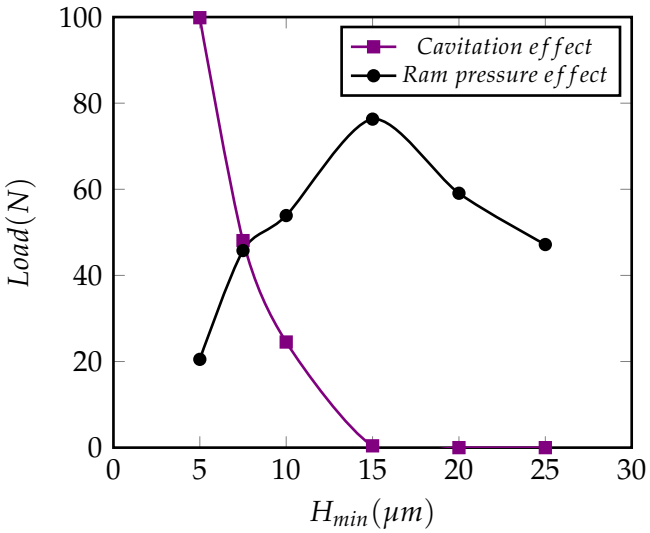

FIGURE 3.2 – Isothermal results: Ram pressure and cavitation effects

3.2 Thermal effects on the lubricant domain (thermal and viscosity wedge)

As the non-thermal suggested by the literature effects are not enough to explain the load carrying capacity of the parallel surface thrust bearing, different temperature dependant physical properties of the lubricant have been modelled, and compared

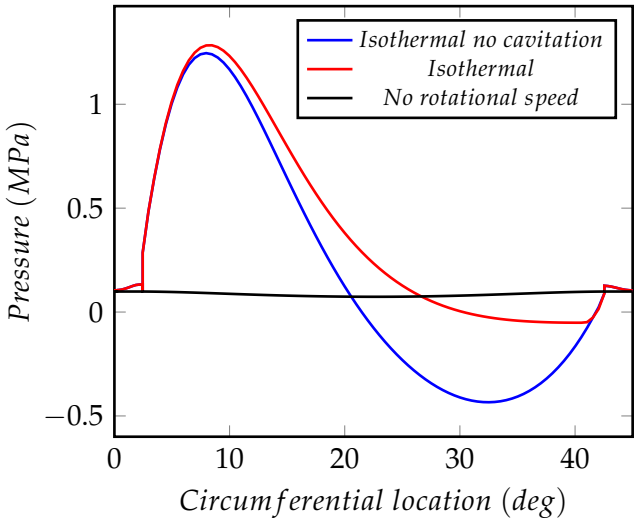

FIGURE 3.3 – Isothermal results: Pressure profiles for $H_{min} = 5\mu m$ at 40°C

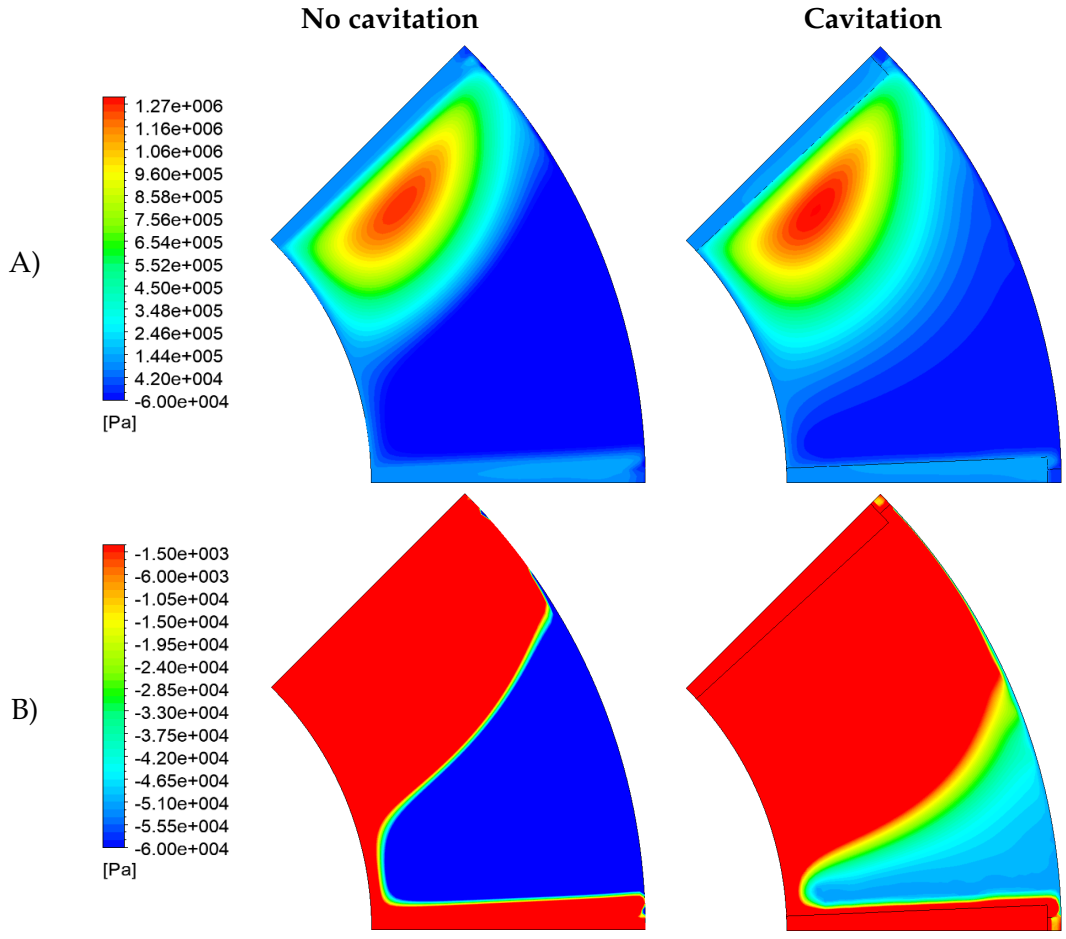

FIGURE 3.4 – A) Pressure distribution and B) Low pressure regions for the isothermal model results with and without cavitation at 40°C.

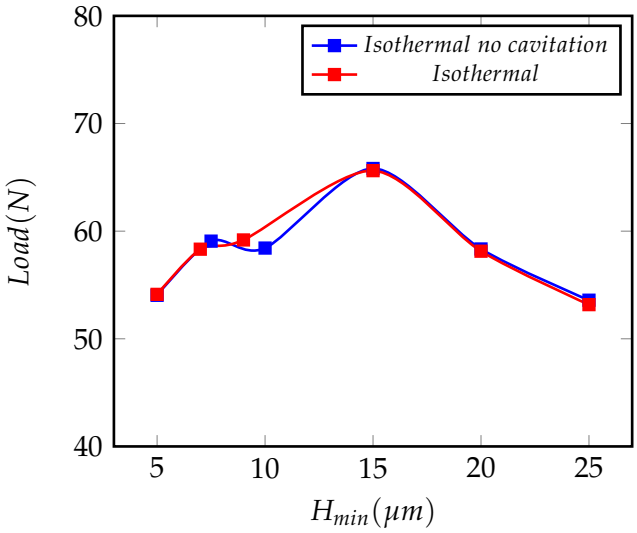

FIGURE 3.5 – Isothermal: H_{min} *vs Load at* 90°C

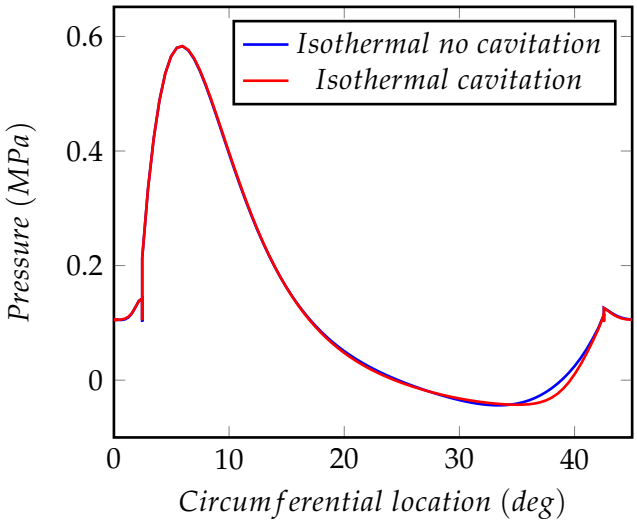

FIGURE 3.6 – Isothermal results: Pressure profiles for $H_{min} = 5\mu m$ *at* 90°C

in order to identify the importance of each property and finally help in the understanding of the pressure build-up mechanism.

3.2.1 Temperature dependent density (thermal wedge effect)

The first published theory explaining the load carrying capacity of the parallel surface bearing, was the thermal wedge effect by Fogg [5]. He suggested that the thermal expansion of the lubricant inside the thrust bearing would change the velocity profiles of the flow. A schematic of this theory is depicted in Fig. 3.7. The lubricant enters the film region with a temperature T_1, and its velocity profile can be considered linear. As the lubricant advances in the film region, due to viscous dissipation, its temperature increases to T_2. This temperature difference drives to a thermal expansion of the oil, considering an incompressible flow and constant film thickness, the average speed of the flow needs to increase in order to respect the mass conservation. When the flow is accelerated, the pressure decreases. Because the pressure in the two feeding oil grooves is the same, a possible pressure decrease needs the same pressure increase amplitude. This pressure increase is the reason that the thermal wedge can help with the load carrying capacity of the parallel surface thrust bearing.

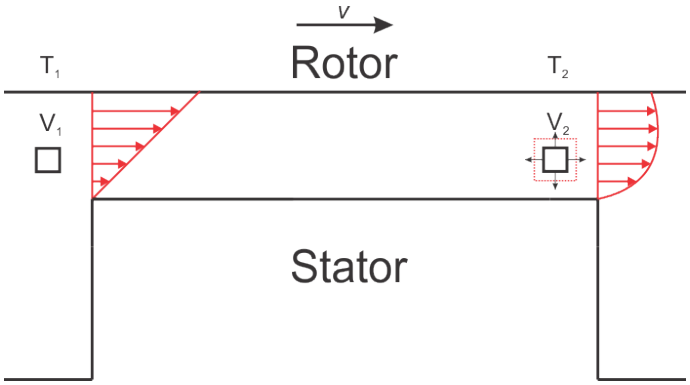

FIGURE 3.7 – Thermal wedge effect theory, velocity streamlines.

In order to identify the validity of this theory, two models have been generated and compared. The isothermal model presented above, and a THD model with temperature dependent density. For both models, the viscosity is considered constant and equal to 0.00816 $Pa \cdot s$, the viscosity value of the ISO VG 46 for a temperature of 90°C. One pressure distribution evaluation of each model is presented in Fig. 3.8 for the same H_{min} value. The generated pressure for both evaluations has similar shape, but the THD model exhibits higher values of pressure. This is a very strong indication that the thermal wedge is a contributing factor of the load carrying capacity of the parallel surface thrust bearing. Plotting the pressure profile on a circumferential section at the mid-radius of the bearing for the two models in Fig. 3.9, alongside with their pressure differences, the magnitude of the thermal wedge effect can be evaluated. Subtracting the pressure of the isothermal model from the THD, more specific the hydrostatic lift and the pressure ram effect, the black dashed curve represents the pressure generated by the thermal wedge. The magnitude of the specific pressure of the thermal wedge is approximately 0.076 MPa.

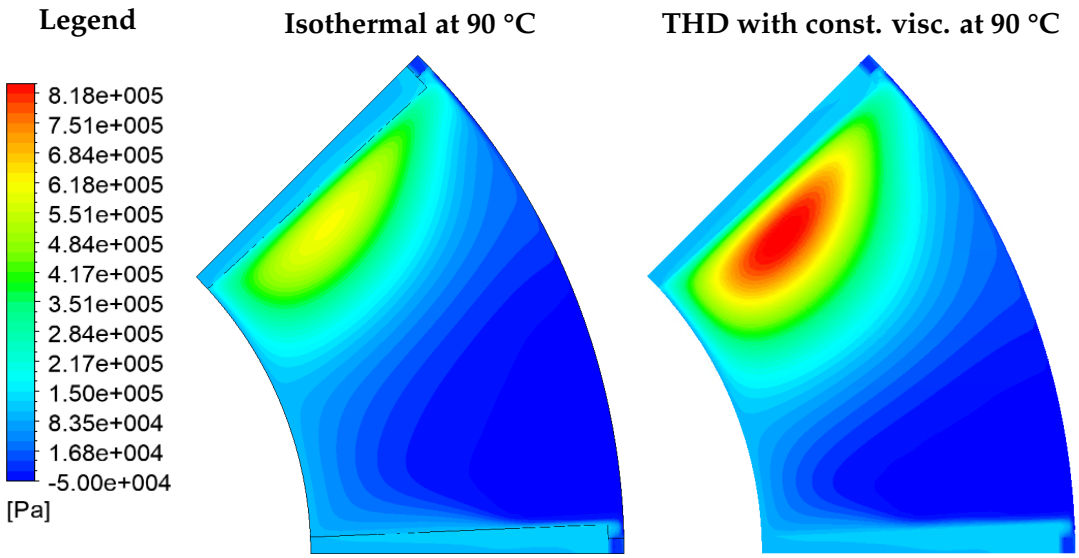

FIGURE 3.8 – Pressure distribution for the isothermal and the THD with temperature dependant density and constant viscosity models at 90°C.

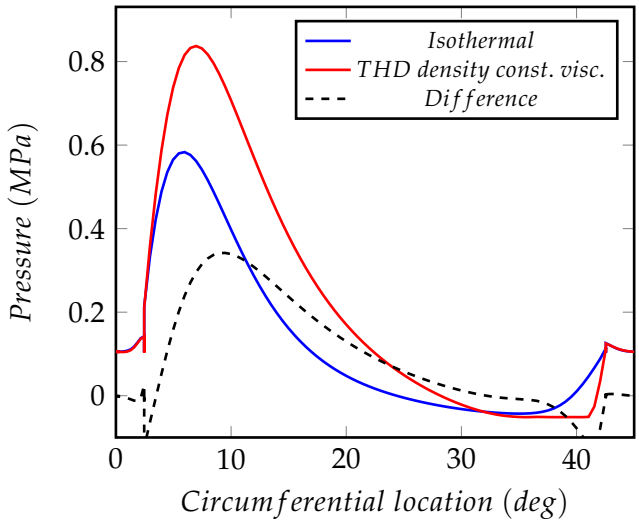

FIGURE 3.9 – Pressure circumferential mid-section profile comparison for the isothermal model at 90°C, with the THD model with constant viscosity at the same temperature, with temperature dependant density.

Even if the thermal wedge effect contributes to the pressure build-up mechanism, its effect is very small. The main reason is that the temperature gradient in the circumferential direction of the lubricant is not large enough for such effect to affect the overall load carrying capacity. The effect is present mainly close to the leading edge region, as it can be observed by the pressure circumferential profile in Fig, 3.9.

3.2.2 Temperature dependent viscosity (viscosity wedge effect)

In 1958 Cameron [8], formalised a second theory for the pressure build-up mechanism of the parallel surface thrust bearing, the viscosity wedge. This theory suggest that the pressure is generated due to differences in viscosity in the streamwise direction and in the thickness of the film.

In the calculations of the present Thesis, the viscosity wedge effect can be identified near the trailing edge of the bearing (see Fig. 3.10). The effect of the viscosity wedge cannot be isolated, due to the ram pressure constant presence. A simple explanation of the viscosity wedge is the following. As the temperature increases in the streamwise direction, the average viscosity decreases, and instantly increases at the trailing edge were the pad is cooled by the feeding oil. If we assume that the velocity profile before the trailing edge has a linear distribution, at the trailing edge the velocity profile will be concave, because of the larger shear near the pad. For this, a pressure gradient is needed, to overcome the increased shear forces. This pressure gradient is the viscosity wedge. A simple schematic representation can be seen in Fig. 3.11.

The presence of the viscosity wedge has been identified in all THD models with temperature dependent viscosity, as is seen in Fig. 3.12 and Fig. 3.13. Yet, the magnitude of the viscosity wedge in all simulations exhibited lesser values than that of the thermal wedge, meaning that its significance in the pressure build-up mechanism of the parallel surface bearing, is almost negligible.

Comparison of the load carrying capacity of all THD models is presented in Fig. 3.14, and the equivalent pressure distribution at the circumferential mid-radius section for the $H_{min} = 5\ \mu m$ instance is plotted in Fig. 3.15.

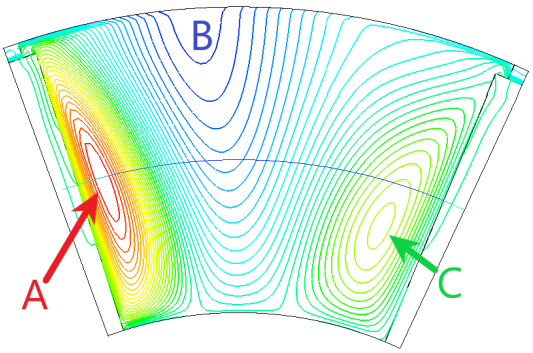

FIGURE 3.10 – Pressure regions and effect correlation, A) Ram pressure region B) Low pressure region C) Viscosity wedge region.

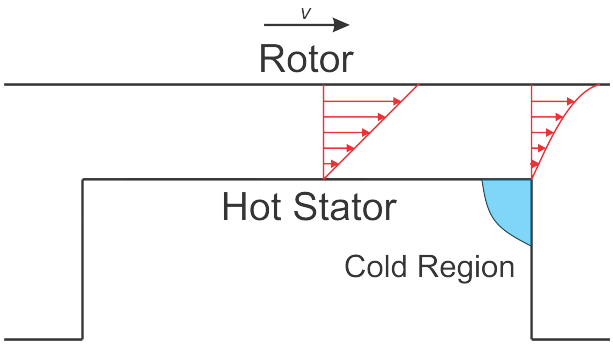

FIGURE 3.11 – Viscosity wedge effect theory, velocity streamlines.

TABLE 3.3 – Performance parameters for the selected cases from the five THD models for $H_{min} = 5\ \mu m$.

Parameter	No cav.	THD	Density	Density const. visc.	Mech. def.
Load $[N]$	49	38	81	40	133
Friction torque $[N \cdot m]$	0.576	0.559	0.515	0.568	0.609
Max. Temperature $[°C]$	109.3	108.3	110	128	103
Max. Pressure $[MPa]$	0.526	0.538	0.645	0.540	1.08
Oil flow rate $[l/min]$	1.2145	1.2155	1.2100	1.2149	1.2151

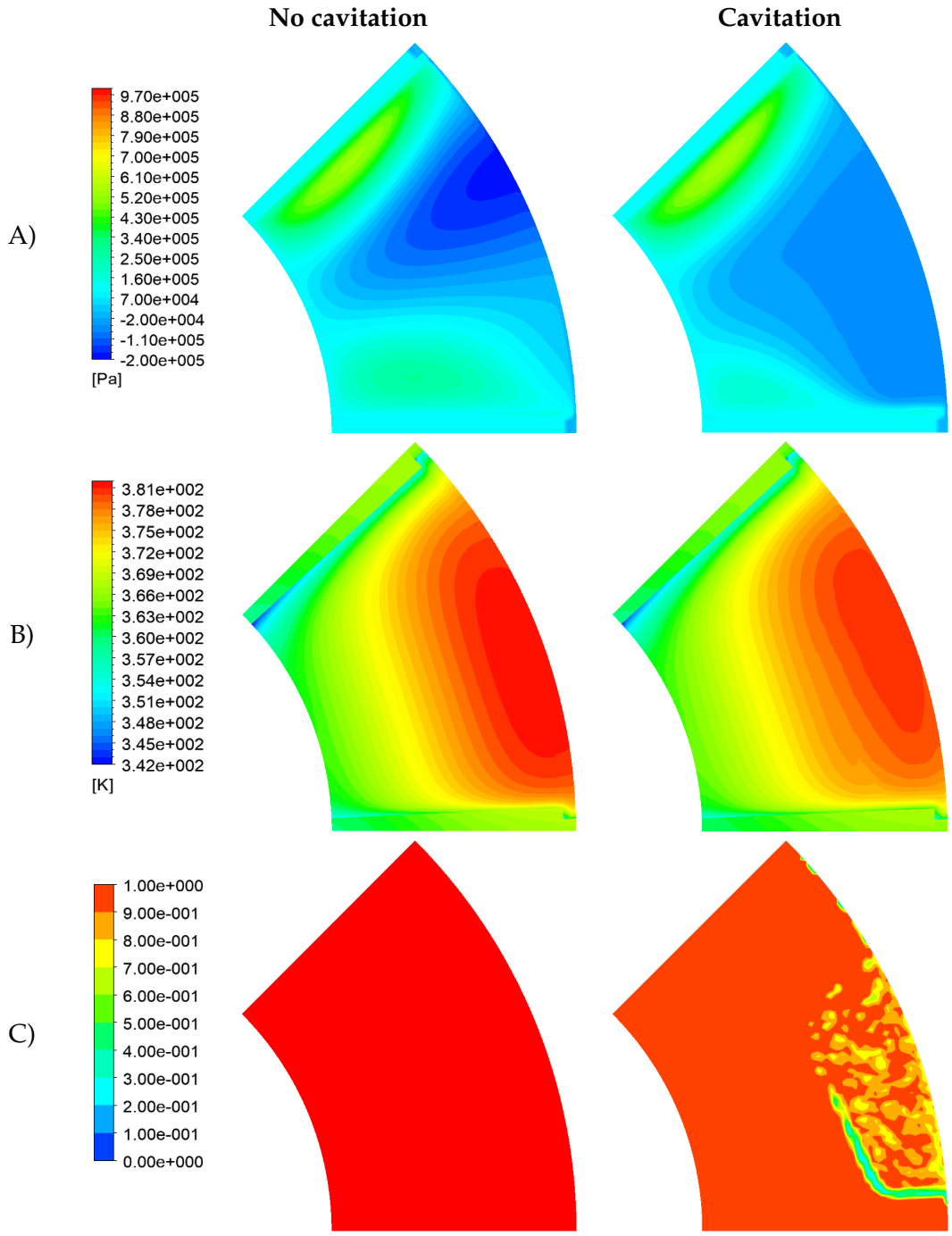

FIGURE 3.12 – Distribution of A) Pressure, B) Temperature, and C) Volume fraction for the THD with and without cavitation models.

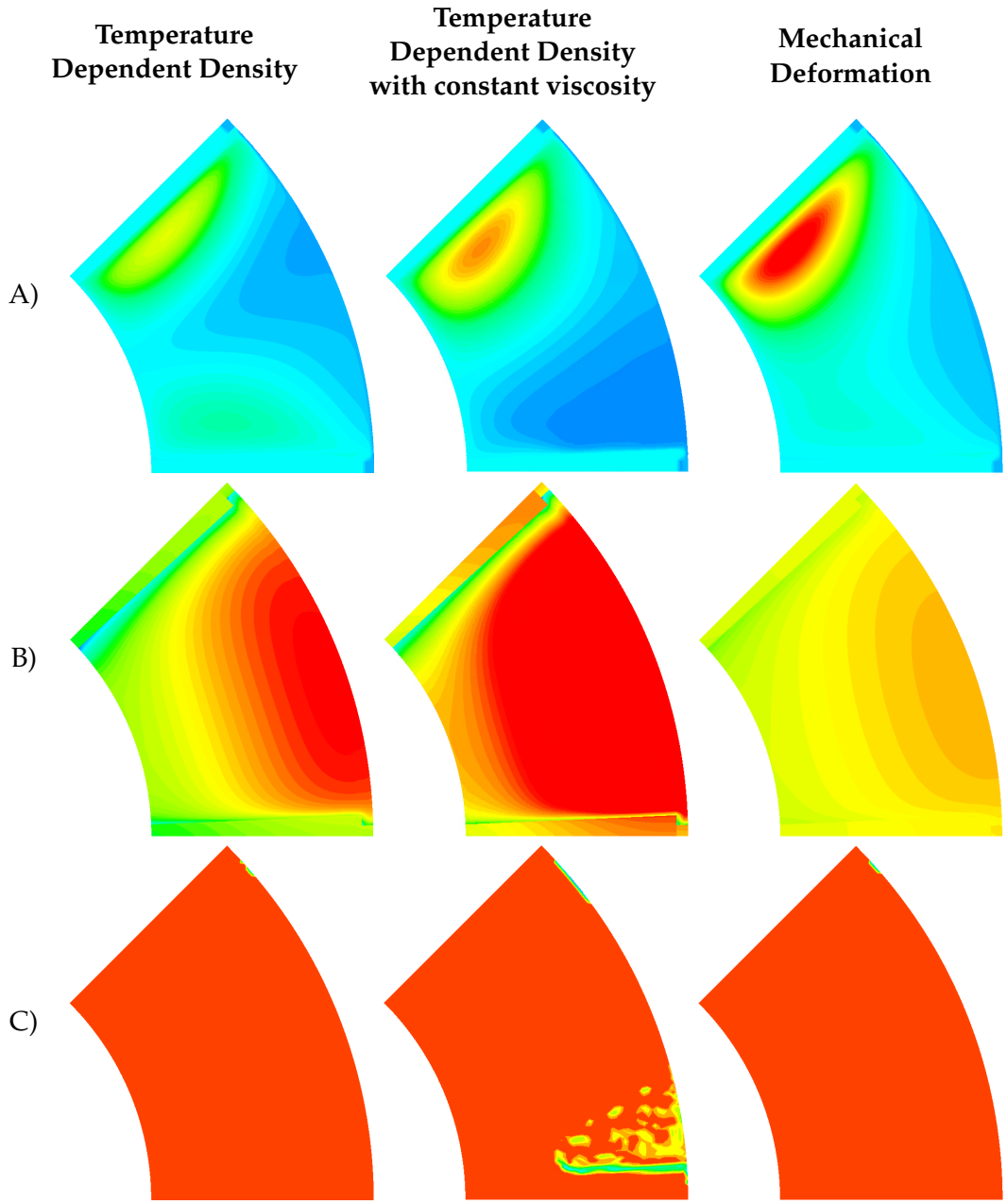

FIGURE 3.13 – Distribution of A) Pressure, B) Temperature, and C) Volume fraction for the THD with temperature dependent viscosity and density, the THD with temperature dependent density and constant viscosity, and THD with mechanical deformations.

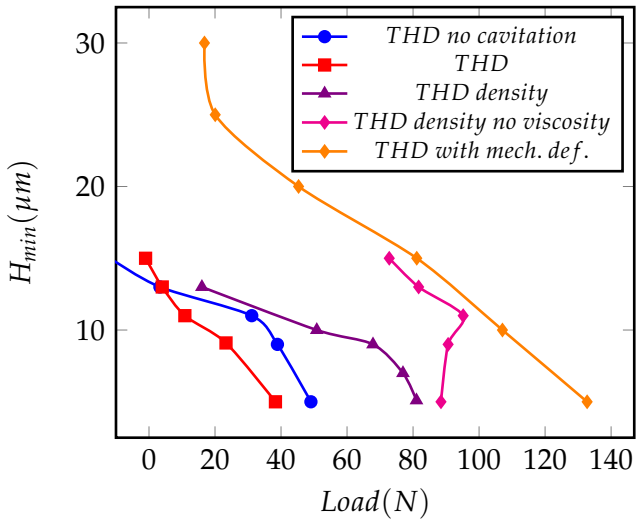

FIGURE 3.14 – THD results: H_{min} *vs Load*

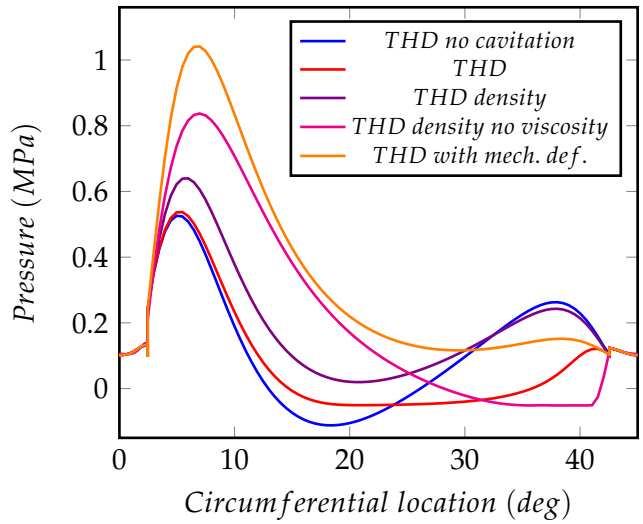

FIGURE 3.15 – THD results: Pressure profile comparison

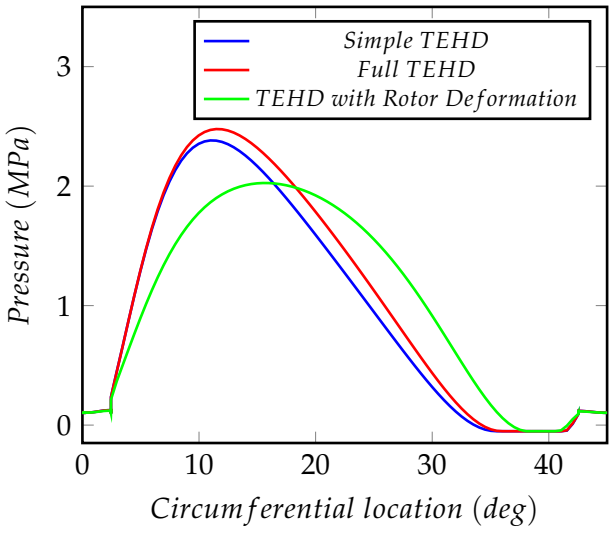

FIGURE 3.16 – TEHD results: Pressure profile comparison at the circumferential section at the mid radius for the three TEHD models.

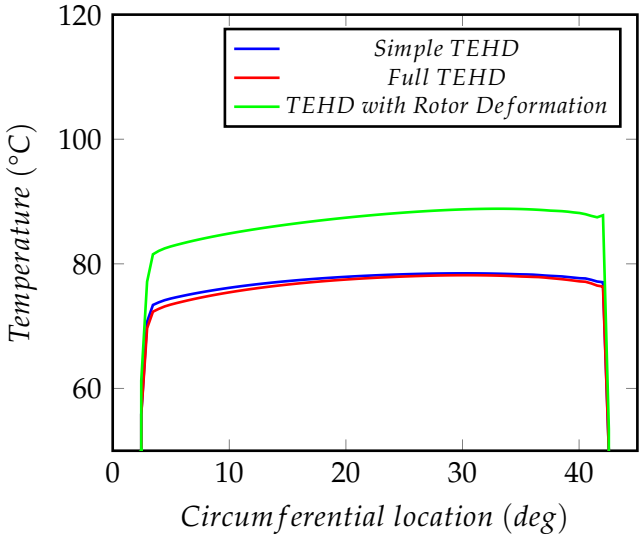

FIGURE 3.17 – TEHD results: Temperature profile comparison at the circumferential section at the mid radius for the three TEHD models.

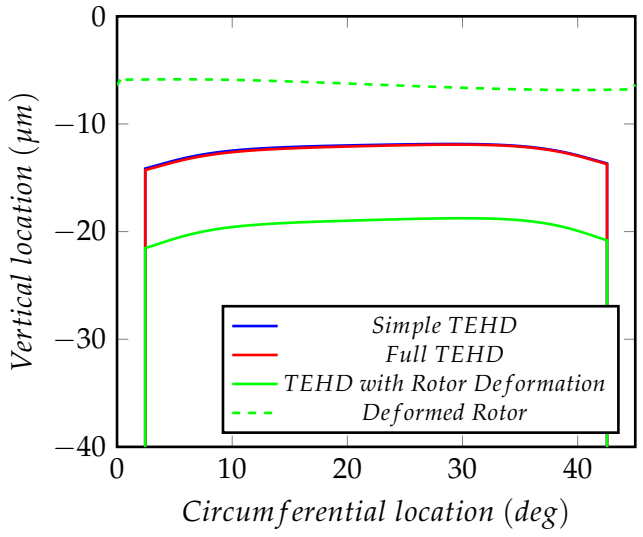

FIGURE 3.18 – TEHD results: Final film profile comparison at the circumferential section at the mid radius for the three TEHD models.

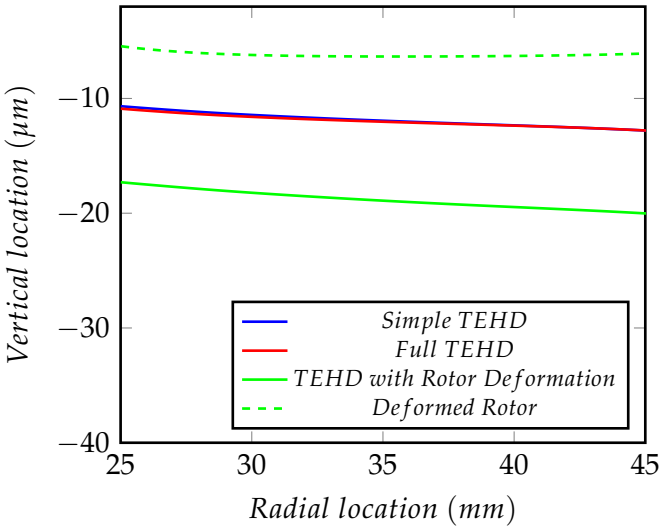

FIGURE 3.19 – TEHD results: Final film radial profiles for the three TEHD models

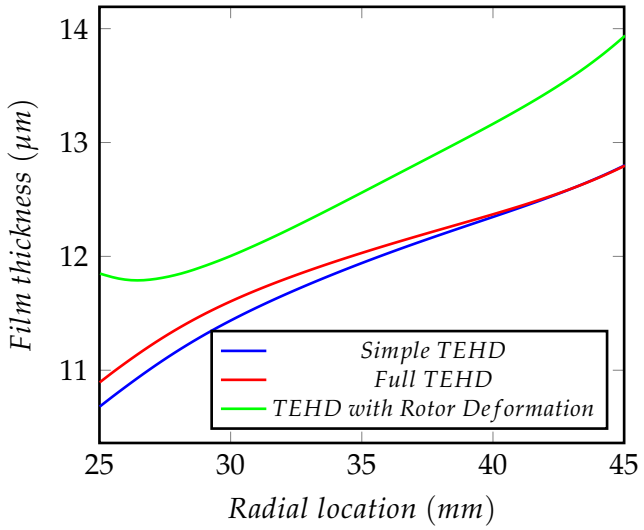

FIGURE 3.20 – TEHD results: Radial film thickness distribution for the three TEHD models

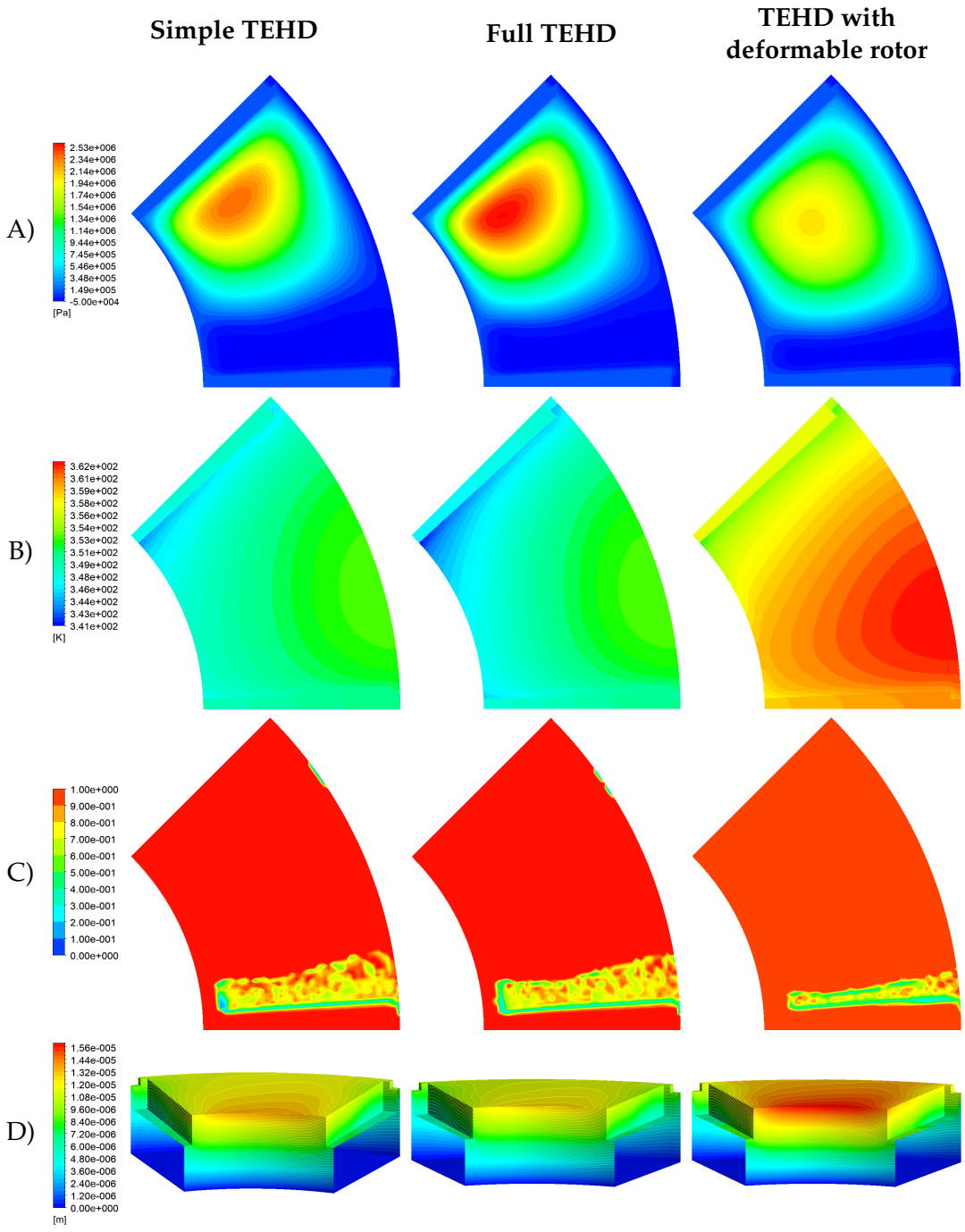

FIGURE 3.21 – Distribution of A) Pressure, B) Temperature, C) Oil volume fraction and D) mesh displacement for the three TEHD models.

3.3 Solid domain deformations

As Swift suggested, deformations of the pad and rotor domain, have the most pronounced effects on the pressure build-up mechanism of the parallel surface thrust bearing. To evaluate the effect of the deformations four different models have been generated and are presented below. The first is a THD model with mechanical deformation on the pad domain, in order to evaluate the effect of mechanical deformation. The second is the Simple TEHD model, which accounts for thermal and mechanical deformations of the pad domain with temperature dependent viscosity, but with constant density, for the evaluation of the effect of thermal deformation. The third is the Full TEHD model with temperature dependent viscosity, density, thermal conductivity and heat capacity, in addition to the mechanical and thermal deformation of the pad domain. This model incorporates all previously studied mechanisms that add to the load carrying capacity of the parallel surface thrust bearing, with the addition of a better approximation of the temperature distribution in the lubricant domain. Finally, the TEHD with rotor deformations model is presented, an extension of the Full TEHD that also accounts for the mechanical and thermal deformations of the rotor domain, seeking to estimate the effect of rotor deformations on the performance of the parallel surface thrust bearing. Three instances, one for each TEHD model have been selected, and presented in this subsection. The selected instances operate in similar loads for a better comparison, and all the performance characteristics are listed in Table 3.4. The THD model with mechanical deformations cannot evaluate specific loads of the magnitude of the TEHD models; thus it is presented in comparison with the other THD models previously reported in Table 3.3 and Fig. 3.14. A circumferential section of the pressure, temperature, and final pad profile at the mid radius section of the TEHD models are depicted in Fig. 3.16, Fig. 3.17, and Fig. 3.18 respectively. Also the radial final pad profiles at the 12.5 deg radial section for the three instances are presented in Fig. 3.19, and the final radial film shapes at the same location are presented in Fig. 3.20. Finally, for all the TEHD models the pressure, temperature, oil volume fraction, and pad mesh deformation are depicted in Fig. 3.21.

3.3.1 Mechanical deformations

In pivoted thrust bearings, the mechanical deformations of the pad alter considerably the film geometry. In order to identify if the mechanical deformations affect also the performance of the fixed parallel surface thrust bearing, a THD model accounting for the mechanical deformations has been generated, utilising the FE solver for the evaluation of CHT and mechanical deformations in the pad domain. For the whole studied range of H_{min} the mechanical deformations seem to affect the most the load carrying capacity, in comparison with the previously studied mechanisms, with a maximum increase of the specific load of 0.2 MPa over the THD approach (were the ram pressure, the viscosity wedge, and the hydrostatic lift are evaluated) as it can be observed in Fig. 3.14 and Fig. 3.15.

The reason that the mechanical deformation consideration, generates a pressure gradient is the alteration of the parallel geometry of thrust bearing. Initial pressure generated near the leading edge of the pad, due to the ram pressure effect slightly deforms the pad generating a small geometrical wedge as seen in Fig. 3.22. This geometrical wedge generates an extra amount of pressure. The amplitude of the geometrical wedge is in the order of magnitude of 0.04 μm at the maximum calculated load, not large enough to support loads of the experimentally observed order

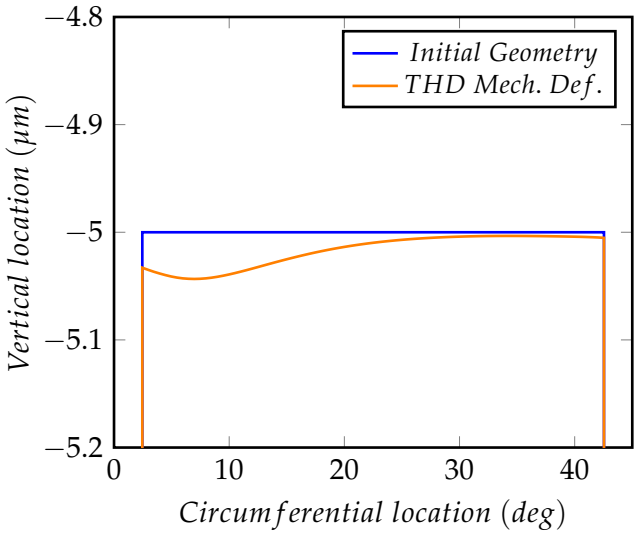

FIGURE 3.22 – THD results: Circumferential section of the film profile at the mid radius for the THD with mechanical deformations model.

of magnitude, but even with small loads the mechanical deformations alter the film shape. This supports the claims of Salama [6], that small amplitude imperfections of the pad could help support a portion of load on a parallel surface thrust bearing.

The final shape of the mechanically deformed bearing is diverging from the leading edge for 5 deg with a diverging amplitude of 0.01 μm and then converging until the 30 deg mark, with an amplitude of 0.04 μm. As described in Fig. 3.15, the maximum pressure point is approximately at 9 deg from the groove mid plane, and it exhibits a small pressure increase near the trailing edge due the viscosity wedge. No cavitation is present in the lubricant domain (3.12), and the temperatures of the fluid domain are considerably lower than those calculated by the other THD models.

Finally, a mechanical deformation wedge is created, but its amplitude is so insignificant that the load it can support, with the contributing effect of hydrodynamic lift, viscosity wedge, and the ram pressure effect, cannot exceed specific loads over 0.3 MPa, for a $H_{min} = 5\ \mu m$.

3.3.2 Pad thermal deformations

As previously discussed, the suggested by the literature main pressure build-up mechanism of the parallel surface thrust bearing is the thermal deformation/distortion of the pad domain; Thus, the Simple TEHD model has been generated, taking into account the thermal and mechanical deformation of the pad, the CHT in the solid domains, and temperature dependent viscosity.

Instantly the calculated performance of the thrust bearing with the TEHD model resemble better the experimental results [57]. The parallel surface thrust bearing seems to be able to support specific loads of 1.5 MPa with values of H_{min} higher than 8.5 μm (see Fig. 3.23).

In Fig. 3.24 the pressure and final film longitudinal profiles are presented. For the increasing load, the location of maximum pressure moves forward, from 10 deg in low load to 15 deg for the maximum evaluated load. A cavitation zone is present in all evaluations and extends to the last 8 deg of the pad. Both pressure attributes can be explained by the shape of the deformed pad. For all the evaluations a converging

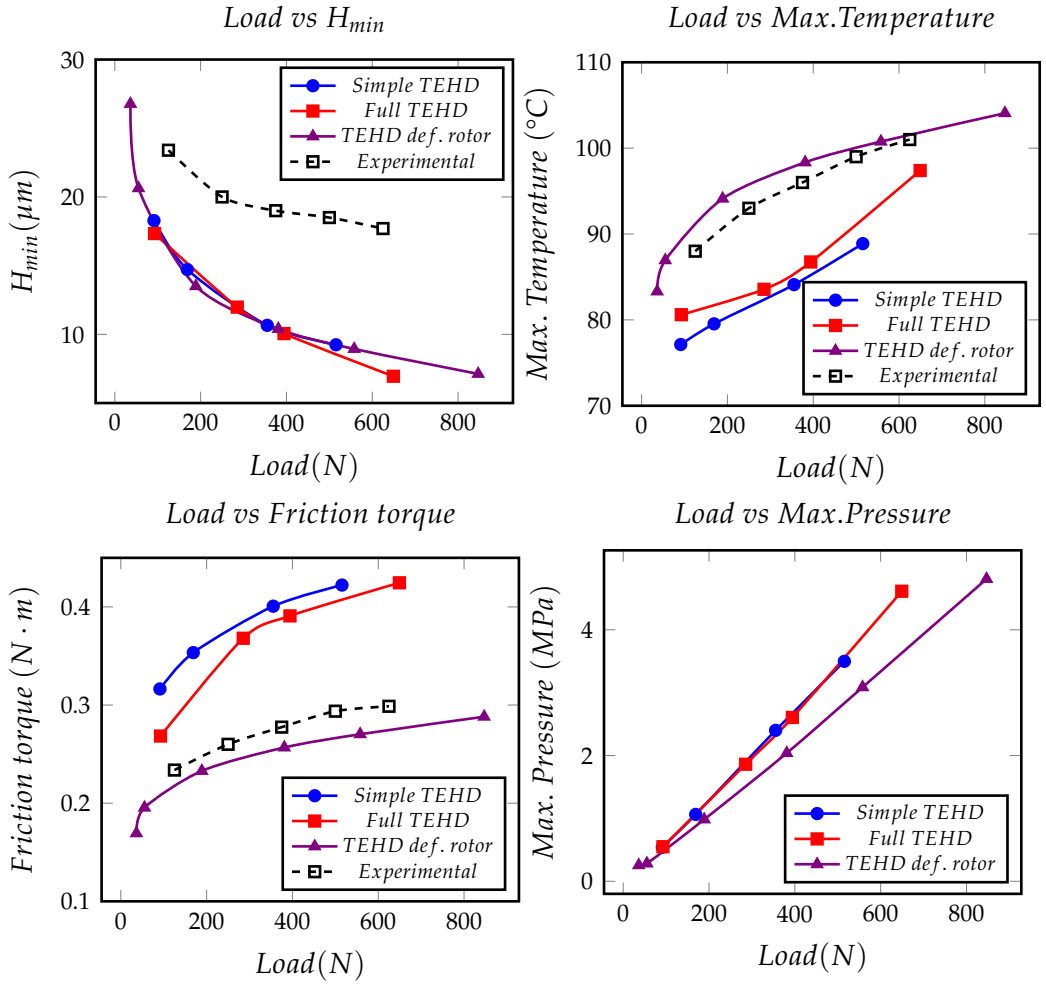

FIGURE 3.23 – TEHD results: Performance characteristics evaluated with the three TEHD models, and experimentally measured [77].

and diverging shape is generated due to the thermal deformations. The converging part starts from the leading edge and extends to the 33 deg mark, with a steeper slope from the leading edge to the hight pressure point, and a linear increase from the high pressure point to the H_{min} point. The diverging shape starts from the H_{min} point and ends at the trailing edge.

The reason for such deformation profile is the temperature distribution on the pad domain. As seen in Fig. 3.25, the temperature in the groove regions, is considerably lower, because of the cooling effect of the feeding oil. After a steep increase at the leading edge, a smoother increase of the temperature is exhibited from the maximum pressure point to the H_{min} location, where a steep decrease of the temperature is present until the trailing edge. The large temperature gradients are responsible for the steep converging and diverging regions.

Moreover, the viscosity wedge effect, that has been identified previously to generate pressure near the trailing edge, is eliminated from the diverging wedge generation. This means that load carrying capacity of the parallel surface slider is not enhanced from the viscosity wedge effect when thermal deformations occur.

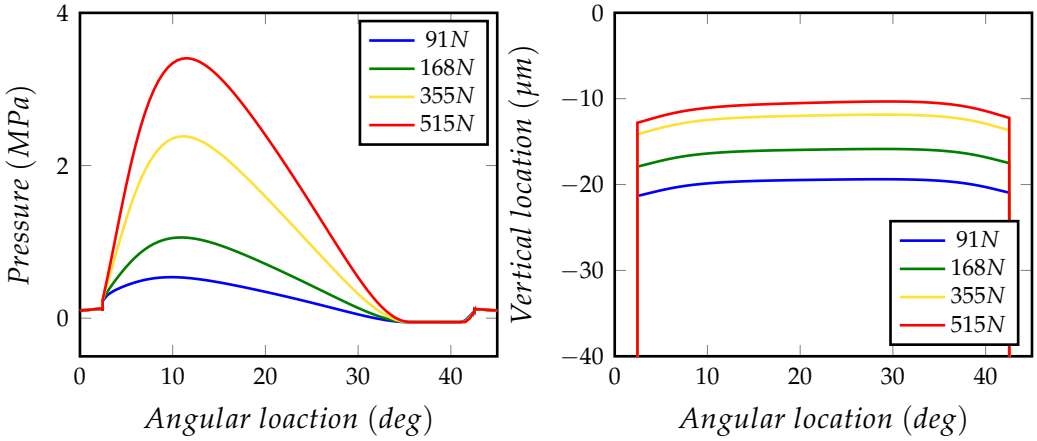

FIGURE 3.24 – Simple TEHD results: Pressure and film profiles for different load evaluations.

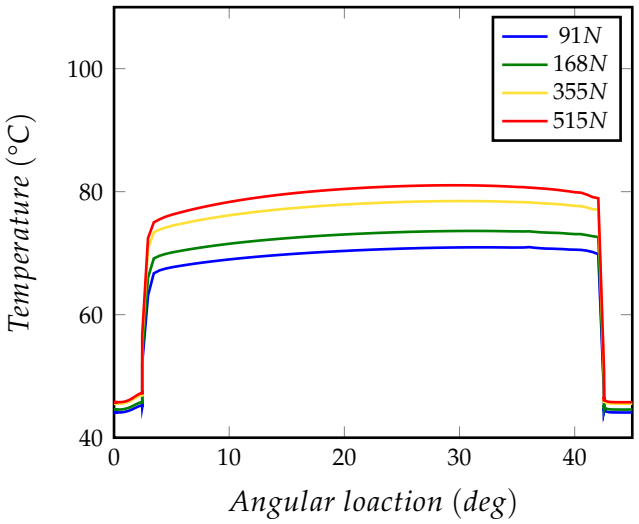

FIGURE 3.25 – Simple TEHD results: Temperature profile for different load evaluations.

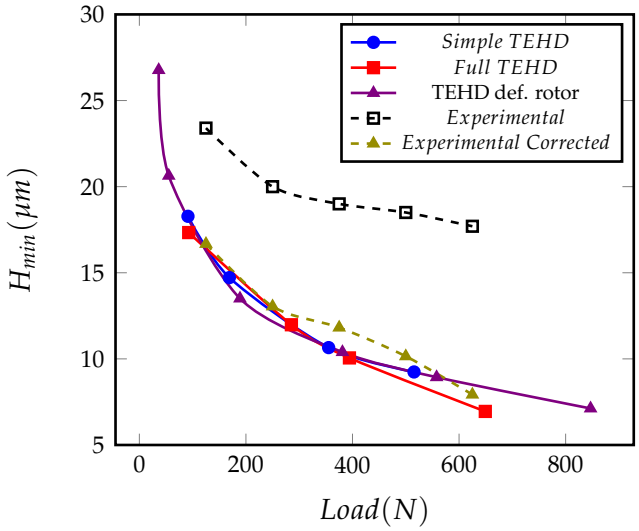

FIGURE 3.26 – TEHD results: Experimental H_{min} correction [57].

The next step is to incorporate to the Simple TEHD model the temperature dependent density of the lubricant to better evaluate the effect of the density wedge, as well as the temperature dependent heat capacity and thermal conductivity. The tribological characteristics of the parallel surface thrust bearing have been evaluated with both models, and can be seen in Fig. 3.23. The main differences on those evaluations are the underestimation of temperature and overestimation of the friction torque of the Simple TEHD model in the whole studied range. The maximum pressure for both models is almost identical, as the H_{min} vs Load curve.

Comparing with the experimental results of Henry [77], both models seem to overestimate the friction torque and underestimate the maximum temperature. Moreover, there is no correlation between the models and experiments for H_{min} values.

The main reason for the large discrepancies in the H_{min} values, is the way the measurements have been conducted in the experiments. Henry names this value as "Displacement between runner and pads (μm)", and makes these measurements outside of the bearing; thus, not accounting for the thermal expansion from the probe fixation to the fluid pad surface. With a correction for the thermal expansion of the pad geometry the resulting H_{min} vs Load curve seen in Fig. 3.26 has not only the same trend with the evaluated results for the TEHD models, but is almost identical especially for low loads.

Finally, even with the temperature and friction torque differences, the TEHD modelling approach manages to estimate with a great accuracy the H_{min} values resulting to the best tool for approximating the performances of the parallel surface thrust bearing, in terms of load carrying capacity.

Taking the comparison a step further, in Fig. 3.27 the measured pressure profile for the Full TEHD model and the measured data are presented. The pressure distribution of the calculation resembles a lot the measured results, but there are some identifiable differences. The model estimates a larger maximum pressure, and its location is closer to the leading edge. The opposite is true for the temperature distribution, which is depicted in Fig. 3.28. The model estimates particularly good the

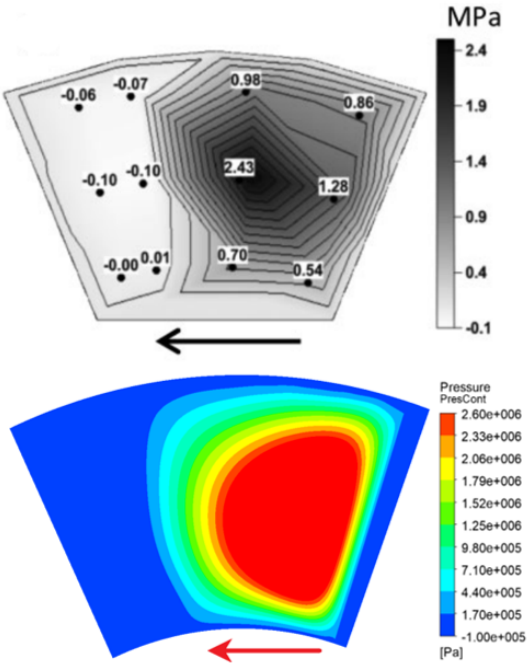

FIGURE 3.27 – Full TEHD results: Pressure comparison with experimental data from [57].

temperature distribution, yet all the temperature values are lower than the measured ones.

The above can be explained by two important parameters, that are going to be addressed below. First, the neglection of the rotor deformations in the modelling approach, and second, the manufacturing imperfections of the thrust bearing geometry.

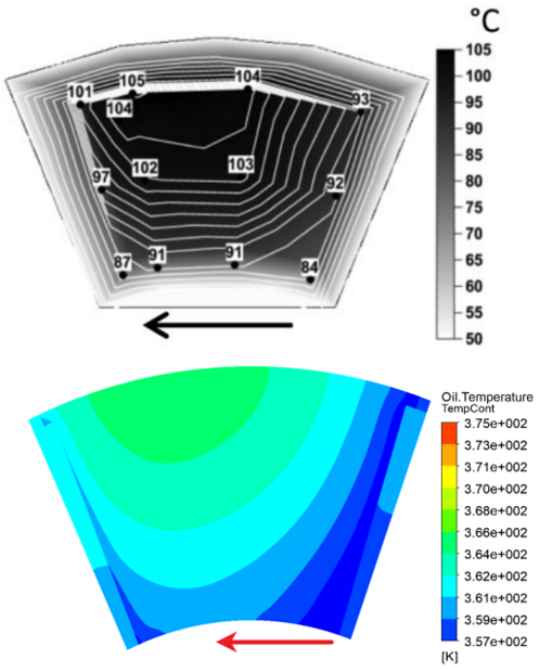

FIGURE 3.28 – Full TEHD results: Temperature comparison with experimental data from [57].

3.3.3 Rotor thermal deformations

In the direction of increasing the correlation of the model with the experimental results, a new TEHD has been introduced. The new model adds the mechanical and thermal deformations of the rotor to the Full TEHD model evaluation. This model manages to evaluate with a better correlation all the tribological characteristics of the parallel surface thrust bearing, as it can be seen in Fig. 3.23. The temperature estimations are a couple degrees higher, and the friction torque evaluations are slightly lower than the experiments. Furthermore, the H_{min} correlation is the same with the previous TEHD model, but the evaluation of maximum pressure is lower. Considering mechanical and thermal deformation for both the pad and the rotor geometry, is the modelling approach that can better estimate the performance characteristics of a parallel surface thrust bearing. Minor modification to the thermal and structural boundary conditions of the model should manage to eliminate the small deviations from the experimental data.

To understand the effect of the rotor deformations on the performance of the bearing, a side to side comparison with the TEHD models with rigid rotor is needed. In Fig. 3.16 the pressure profile at the circumferential mid-section is plotted for the three TEHD models for the similarly loaded cases presented in Table: 3.4. The rigid rotor cases exhibit higher values of pressure, but in a smaller high-pressure area. Moreover the cavitation region is larger on those cases, this is also illustrated in Fig. 3.21. The reason for such behaviour can be identified in circumferential mid section film profile in Fig. 3.18. Due to lower temperatures in the groove region, the rotor expansion is minimised over the leading edge region and maximised over the high-temperature section of the pad. This in addition to the deformation shape of the pad, generates a converging film geometry with a more pronounced convergence in the middle part of the bearing than the model evaluation with the rigid rotor. Taking also into account the slightly higher temperature differential between

the leading and trailing edge on the TEHD model with the deformable rotor (see Fig. 3.25), which drives to a slightly steeper converging geometry on the pad, the ability of the rotor to deform allows to a larger high-pressure region, with lower maximum pressure for the same load estimated by the other two models. Furthermore, this extension of the high-pressure zone reduces considerably the cavitation region, as it is depicted in Fig. 3.21.

In the radial direction, the pad deformation is almost identical for all three models (see Fig. 3.19), but because of the rotor thermal deformation the final radial film shape is different, as it can be seen in Fig. 3.20. This slightly moves the maximum pressure point closer to the centre of the bearing in comparison to the Full TEHD model that does not account for the rotor deformation.

TABLE 3.4 – Performance parameters for the selected cases from the Simple TEHD, Full TEHD, and TEHD with deform rotor models.

Parameter	Simple TEHD	Full TEHD	TEHD with rotor def.
Load $[N]$	355	394	381
Friction torque $[N \cdot m]$	0.401	0.391	0.257
H_{min} $[\mu m]$	10.65	10.86	10.39
Max. Temperature $[°C]$	84.1	86.7	98.3
Max. Pressure $[MPa]$	2.40	2.61	2.01
Oil flow rate $[l/min]$	1.2137	1.2155	1.2192

3.4 Pad manufacturing imperfections

As previously mentioned, one reason for deviation from the experimental results could be the imperfect geometry construction. In the present section, the measured geometry of an eight pad thrust bearing has been modelled and calculated with the Full TEHD model, in order to evaluate the performance of a geometry as close as possible to the one measured by Henry, Bouyer, and Fillon [57]. In general, there are two main imperfections in comparison with the perfect parallel surface thrust bearing. First, the shape of each pad surface, that due to the manufacturing process are not perfectly parallel, and can be approximated by sinusoidal, converging, diverging, concave, or convex shapes. Second, if the rotor is considered parallel to the pad bottom surface, the minimum distance of each pad of the rotor differs for each pad. This imperfection, will result in different loading of each bearing; thus, experimental results could differ from pad to pad not only from the surface imperfections.

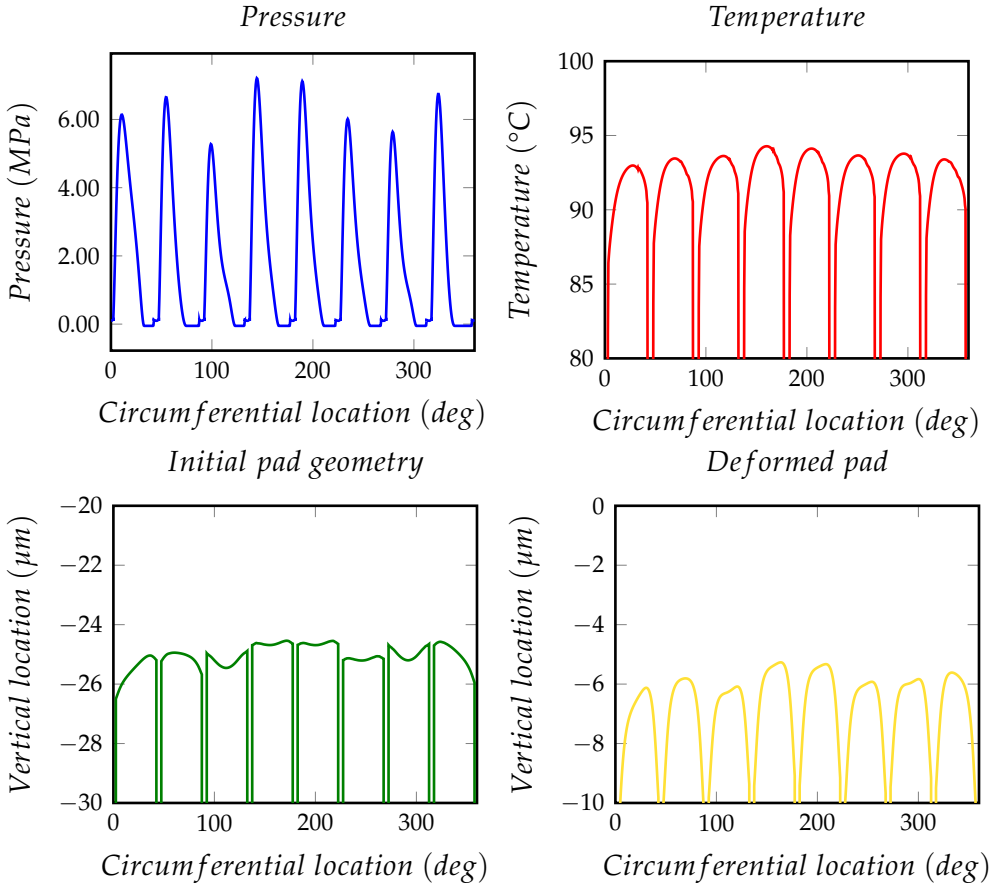

FIGURE 3.29 – Pressure, temperature, initial pad geometry, and final pad geometry profiles at the circumferential section at the mid radius for the full thrust bearing with the measured by Henry, Bouyer, and Fillon [57] geometry.

The experimentally measured geometry and the modelling approximations are presented in Fig. 2.12. Three defect shapes have been identified, namely converging, diverging, and convex, with an amplitude varying from 0.5 μm to 1.25 μm, and deviation from the maximum pad point to the minimum of 1.75 μm. In order to evaluate the full thrust bearing, the Full TEHD model has been utilised, and the rotor has been considered rigid.

In Fig. 3.29 the pressure, temperature, final, and initial pad geometry profiles at the circumferential section at the mid radius are plotted. The individual pad pressure profiles vary considerably, even with those small initial geometry variations. The shape of the temperature profiles is almost identical for all pads, with a small shift of the maximum temperature. The temperature shift for each pad depends on two parameters, namely the load of the individual pad and the temperature of the previous one. As it can be seen in Fig. 3.30, the higher values of the temperature do not occur on the more loaded pads only, but also to the pads following them. For example, pads 8 and 1 that follow the pads 6 and 7 which are the most highly loaded pads, have larger temperatures than pad 3 which is loaded higher than pads 8 and 1. Moreover, due to the deformation profile of all the pads, cavitation regions can be identified near the trailing edge of each pad. A larger cavitation area can be identified in pad 2, due to its large diverging initial defect. This initial divergence amplified the diverging region generated by the thermal deformation; therefore, altering the most the cavitation profile from the observed by the "perfect" parallel

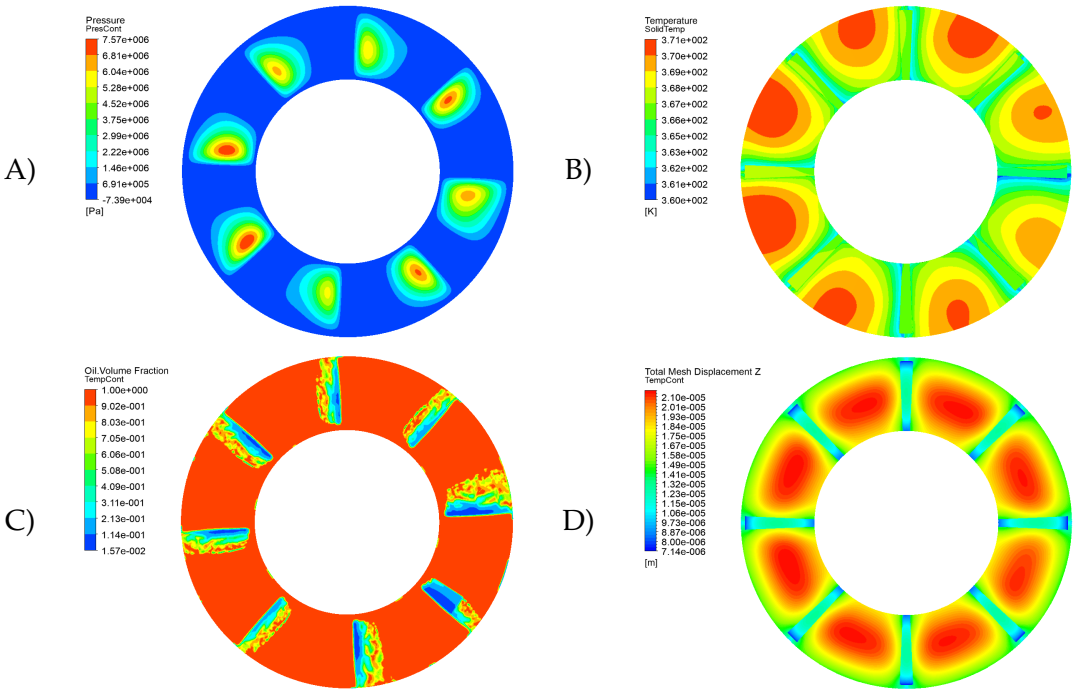

FIGURE 3.30 – Distributions of the A) Pressure B) Temperature C) Volume fraction, and D) Mesh displacement for the full thrust bearing with the measured by Henry, Bouyer, and Fillon [57] geometry.

surface thrust bearing. Furthermore, the main parameter that can predict if a pad will be highly loaded is not the shape of the imperfection, but the initial average film thickness.

Finally, in Fig. 3.31, the temperature distribution of the rotor bottom surface is presented. The temperature is almost constant at the fluid rotor interface and lower at the rotor's outer surfaces. The slightly colder regions between the pads are the result of the cooling effect of the feeding oil to the rotor domain.

A direct comparison of this model with the experimental results is not possible. The computational time of the TEHD full thrust bearing model even with rigid rotor domain was approximately one month until full convergence for one load instance. Due to the computational algorithm, nor the final H_{min}, neither the final load are imposed. For that reason, at least four calculations are needed in order to be able to interpolate the initial model parameters for a specific load evaluation. The only available calculated instance is outside of the range studied in the experiments.

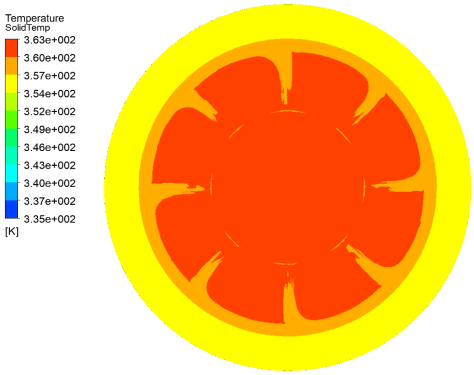

FIGURE 3.31 – Temperature distribution at the rotor bottom surface for the full thrust bearing with the measured by Henry, Bouyer, and Fillon [57] geometry.

3.5 Pad fixations

Some consideration has been given on the validity of the structural boundary conditions utilised on the modelling. All the presented results in the Thesis consider the bottom pad surface fixed in the Z direction. Some initial evaluations of models with different structural boundary conditions have been done, considering the position of the bolt fixation on the experimental apparatus. The four fixations have been considered fixed in all directions (U_X, U_Y, U_Z) as also the inner bottom diameter of the bearing. The rest of the bearing pad bottom surface is supported by a compression only spring of large stiffness value (equivalent of a thick steel plate).

Not conclusive results have been acquired, because of the model complexity and computational cost. The inner diameter fixation has been placed in order to mitigate folding mesh problems during the solution process, and it does not represent any physical constraint. The presented figures depict a **not converged evaluation** for the parallel surface eight sector pad thrust bearing.

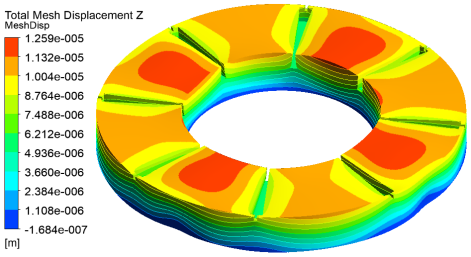

FIGURE 3.32 – Mesh displacement in the Z direction for the four fixation parallel surface full bearing model.

In Fig. 3.32 the mesh displacement of the model is presented, and exhibits a non-periodic behaviour. The same can be identified in Fig. 3.33 for the pressure distribution. Even with those non converged results, a simple conclusion can be made. For a solid fixed pad parallel surface thrust bearing, the location and number of fixation points can alter its performance and impose a load imbalance between the individual pads.

The modelling of the fixation of such bearings should be investigated further.

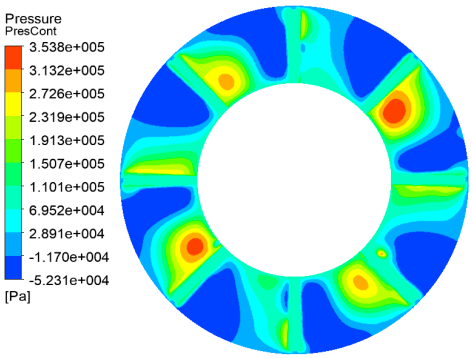

FIGURE 3.33 – Pressure distribution for the four fixation parallel surface full bearing model.

3.6 Conclusions

In the present chapter, most of supported by the literature pressure build-up mechanisms of the parallel surface thrust bearing have been evaluated. For this evaluation, three modelling approaches have been utilised, in order to disengage specific phenomena and asses them separately.

With the isothermal modelling, three mechanisms have been assessed. First, the calculation of the hydrostatic lift, from the feeding oil pressure was evaluated by the isothermal model without imposed rotational speed of the rotor. The magnitude of the hydrostatic lift was insignificant, but important to subtract its value from the total load carrying capacity for the evaluation of the other effects.

The second flow effect that has been studied is the ram pressure effect. Subtracting the hydrostatic lift from the simple isothermal results with rotating rotor, the leading edge ram pressure effect was observed. With a maximum of 0.16 MPa specific load, its significance as pressure build-up mechanism is very small.

Moreover, cavitation has been modelled with the Rayleigh-Plesset equation. The isothermal model has been evaluated with two values of viscosity with and without cavitation. It is observed, that due to the high pressure zone generated by the ram pressure effect, radial leakage occurs near the leading edge region. Thus, local oil starvation conditions are present in the mid-section of the pad. For low values of viscosity this is countered by the flow from the inner surface, where the lubricant is supplied. For high values of viscosity, this flow is not large enough to supply the mid region with oil, driving to a pressure drop. This decreases considerably the load carrying capacity. The cavitation modelling allows to a more accurate description of those phenomena.

In a second step of the analysis, the proposed mechanisms that derive from temperature dependent properties of the lubricant have been evaluated, in means of THD modelling. A THD model with temperature dependent density and constant viscosity has been generated and compared with the isothermal results for the same viscosity value. The pressure build-up was more pronounced in the THD model, driving to the conclusion that the thermal wedge takes part in the load carrying capacity of the parallel surface thrust bearing. Yet, the specific pressure generated by the thermal wedge is of the magnitude of 0.076 MPa, not large enough to account for the experimentally observed loads.

Furthermore, a THD model with temperature dependent viscosity and constant density has been generated and evaluated, in order to identify the viscosity wedge

effect. All the THD evaluations with temperature dependent viscosity exhibit a pressure increase near the trailing edge. This increase can be attributed to the high viscosity gradient near the groove region. The cooling from the feeding oil of the pad, increases the viscosity near the fluid pad interface, driving to higher shear forces in that area. This would drive to a flow deceleration; thus, a pressure gradient is generated. Even if the effect is observable in all the above-mentioned models, its magnitude is even smaller than the thermal wedge effect.

The pressure build-up mechanisms concerning the fluid domain seem to be of small importance to the load carrying capacity of the parallel surface thrust bearing. Moving to the mechanical and thermal properties of the solid domains seems the next logical step. First a THD model that takes into account the mechanical deformations of the pad geometry is introduced. The mechanical deformations generated a small converging geometry. The converging amplitude of 0.04 μm managed to increase the specific load from the previous THD models an additional 0.16 MPa.

Moving forward, the thermal deformations of the pad have been introduced to the previous model, generating the Simple TEHD model. Evaluating the bearing performance with this model, resulted in specific loads over the 1.5 MPa limit, suggesting that the main pressure build-up mechanism of the parallel surface thrust bearing is the converging wedge geometry generated by the thermal deformations on the pad domain. Additionally, the Simple TEHD model has been expanded to account for the temperature dependent density and heat capacity. The new model is referred as the Full TEHD model and being able to evaluate the load carrying capacity taking into account all the identified pressure build-up mechanisms, plus a better approximation of the domain temperatures. The difference of the two models are minimal. The Full TEHD evaluates lower values of friction torque and higher values of temperature.

Comparing both models with published experimental results, gave a fairly good correlation, with the Full TEHD being a closer approximation.

Because the thermal deformations of the pad plays such a big role in the load carrying capacity, the Full TEHD model was extended to account also for the thermal and mechanical deformations of the rotor domain. The new model managed to correlate with the experimental measurements almost completely, with a slight overestimation of the temperature and underestimation of the friction torque.

Summarising, after a detailed analysis of all the possible pressure build-up mechanisms for the parallel surface thrust bearing, the findings of this chapter are that the thermal and mechanical deformations of both the pad and the rotor are the reason of the observed load carrying capacity of such bearings.

In order to eliminate any possible deviation from the physical phenomenon, two more points have been made. The first is, that due to manufacturing imperfections of the parallel surface bearing, deviation on the pressure, temperature, and film thickness distributions occur between the individual pads of the thrust bearing. This makes some pads more heavily loaded than others, and experimentally measured data might differ from pad to pad. Thus, it is strongly advised a careful evaluation of the bearing geometry before experimental measurements, and the measurement of at least more than one pad in order to acquire valid results. The second is, that it strongly believed that the structural constrains (fixations) of the parallel surface bearing affect the thermal deformations, resulting in different final shape for the individual pads.

Chapter 4

Thermal effects on highly loaded contemporary designs

The present chapter deals with thermal effects on highly loaded contemporary designs, especially that of thermal deformation of the pad domain. Four different kinds of the most commonly used contemporary bearing designs are presented below. The tapered-land, pocket, and textured bearings have been evaluated with TEHD and THD models, and a model is proposed for future design evaluation for each one of them. Also, parallel surface bearings with coatings have been studied, considering the thermal and mechanical deformations, and compared with the bronze thrust bearing.

Operational parameters that make bearings considered as heavily loaded are the maximum load, the start-up load, the temperature, and the H_{min}. Each one of the above parameters, if is close to the operational limit constitutes a bearing as heavily loaded. For example, bearings of the size and rotational speed of the presented models, the safe specific load limit is 3 MPa, the design maximum temperature 100°C, and the minimum permissible film thickness is $H_{lim} = 14\ \mu m$ [2].

4.1 Tapered-land bearings

Tapered-land bearings are one of the most commonly used fixed-pad thrust bearing configuration. Most of the published studies utilise the isothermal approach, but also many THD studies have been published. In Fig. 4.1, the performance characteristics of the tapered-land bearing described in subsection 2.2.9 are presented for the TEHD and THD models alongside with the experimental results from the Ph.D. Thesis of Henry [77].

Comparing the numerical results of the two models with the experimental data for the tapered-land bearing we can conclude the following. Both models manage to estimate the friction torque close to the experimental results, but both underestimate the pressure at the the 70%-50% point. This could be attributed to the manufacturing imperfections of the specific pad that the measurements have been conducted, or to the exclusion of the rotor deformation from the TEHD model, as stated in the previous chapter. Small variation on individual pad elevation can produce different pressure profiles on each pad. The rotor deformation could change the maximum pressure location and value. Moreover, the TEHD model managed to estimate almost perfectly the temperature at the 75%-75% point, in contrast with the THD model, which overestimated the temperatures in the whole studied range.

The TEHD and THD model also agree in the H_{min} evaluation for a given load. Trying to compare this value with the experimental results is not straightforward,

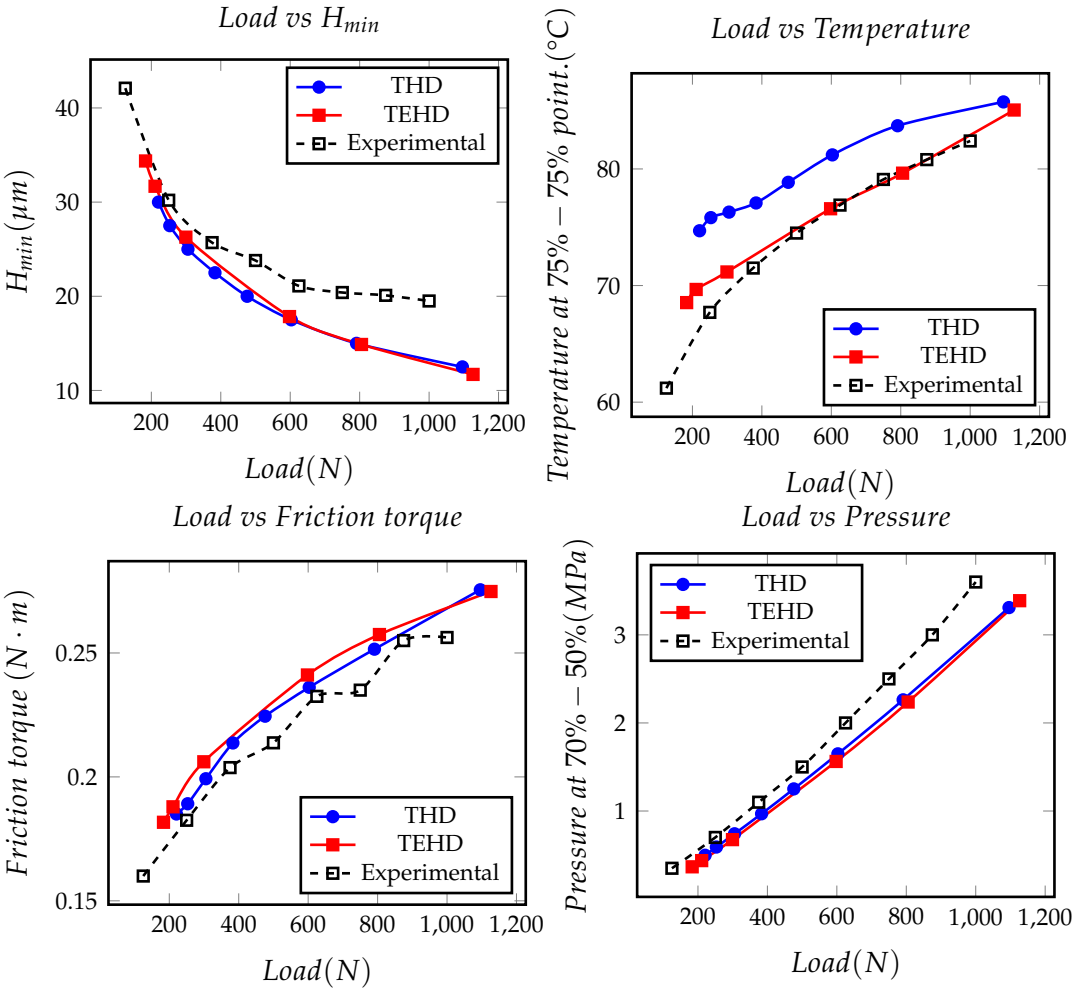

FIGURE 4.1 – Tapered-land thrust bearing: Performance characteristics comparison for the THD, and TEHD models, and experimental results.

due to the measuring procedure during the experiment. Henry [77] names this values as "Displacement between runner and pads (μm)", and makes these measurements outside of the bearing; thus, not accounting for the thermal expansion from the probe fixation to the fluid pad surface. With a correction for the thermal expansion of the pad geometry the resulting H_{min} vs Load curve seen in Fig. 4.2 has the same trend with the evaluated results for the TEHD model, with a small shift to lower values of H_{min}. This small shift is highly possible a result of the rotor deformation in the experiments, that the TEHD model utilised does not account for.

Concluding, the computational evaluation of the tapered-land bearing correlates in most ways with the experimental results, except an overestimation on the pressure on the 70%-50% point. The TEHD model approximates better the temperature at the 75%-75% point, but overall, both models adequately evaluate the bearing's performance characteristics. A better approximation could be possible with a deformable rotor TEHD model, but the achieved accuracy of both models makes the extra complexity and computational cost not required.

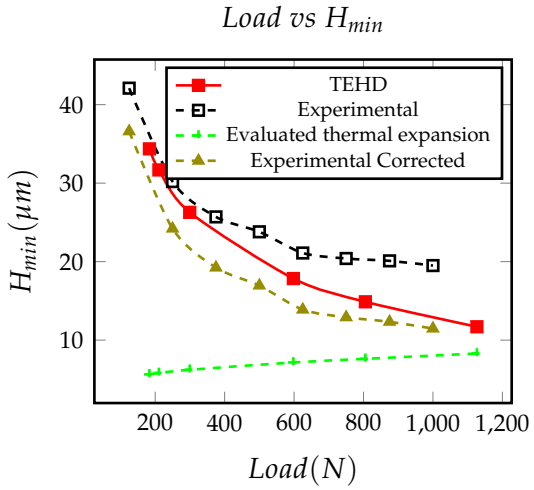

FIGURE 4.2 – Tapered-land thrust bearing: Corrected H_{min} vs the Load accounting for the thermal deformation of the pad.

In order to evaluate the differences of the two models, similarly loaded instances have been chosen for both of them. The performance characteristics of the chosen cases are presented in the Table 4.1. The circumferential mid-section profiles for pressure and temperature distribution are presented in Fig. 4.3 and Fig. 4.4 respectively. Moreover, the film profile circumferential mid-section is presented in Fig. 4.5. Finally, the pressure and temperature profiles for both cases are depicted in Fig. 4.6

Comparing the pressure profiles of the two models, we can identify some small differences. Taking into account that the TEHD evaluation supports 3% larger load, the TEHD exhibits higher pressure values, and has a smaller high-pressure zone. This is attributed to the small diverging fluid geometry near the trailing edge, due to the thermal deformation, where the pressure drop is faster. The final geometrical shape of the pad is better illustrated in Fig. 4.7, where the total mesh displacement in the Z direction is presented. Furthermore, the slope from the leading edge to the parallel part is steeper, and the parallel part of the bearing is slightly deformed, also generating a converging region. This shape change is the reason that the maximum pressure point is moved somewhat forward. Moreover, the THD model evaluates higher temperatures at the whole lubricant domain. Again, the steeper taper allows somewhat more cold lubricant to enter the converging part of the pad, driving the average temperature to lower values.

Concluding, both models approach well the experimental results. Although, the THD model fails to correctly evaluate the temperature profile. The TEHD model for the tapered-land bearing was computationally 3 times more expensive, for the studied range of loads. In general, the THD modelling approach is recommended for this design, because of the small benefits of the TEHD over its computational cost. Although if a precise evaluation is needed, especially in terms of temperature distribution, the TEHD modelling approach is suggested, but the need to model the rotor deformations is considered unnecessary.

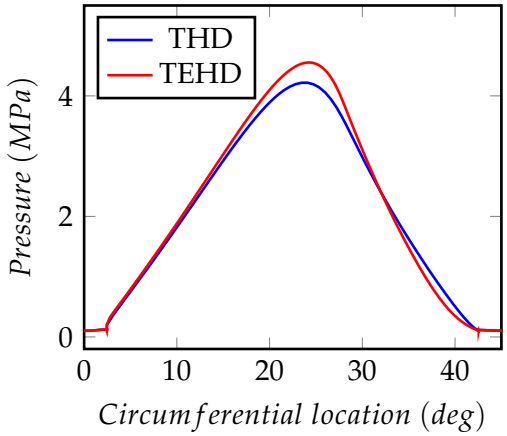

FIGURE 4.3 – Tapered-land thrust bearing: Pressure profiles for the THD and TEHD models at a circumferential section at the mid radius.

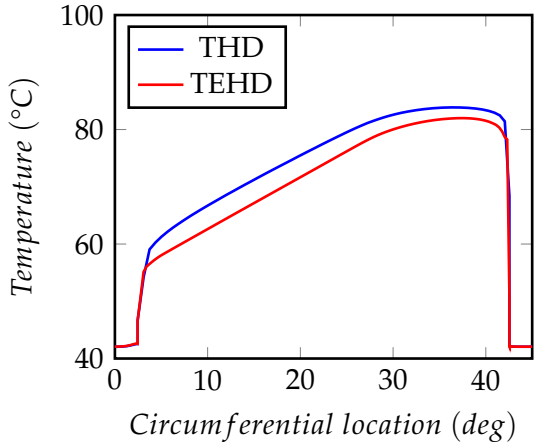

FIGURE 4.4 – Tapered-land thrust bearing: Temperature profiles for the THD and TEHD models at a circumferential section at the mid radius.

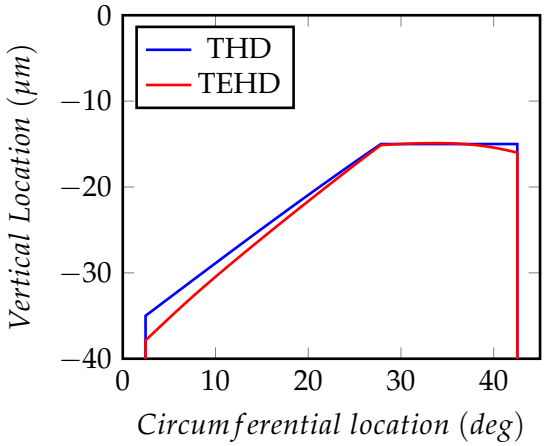

FIGURE 4.5 – Tapered-land thrust bearing: Final film geometry profiles for the THD and TEHD models at a circumferential section at the mid radius.

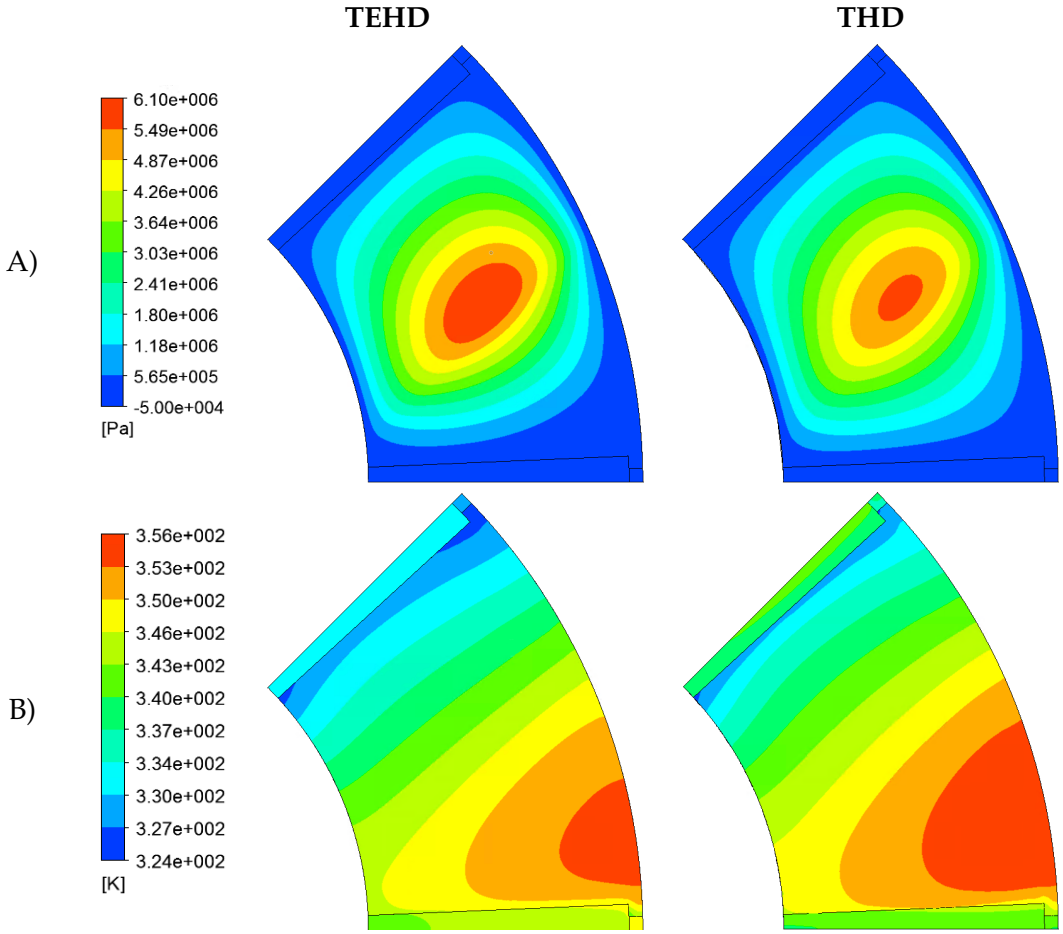

FIGURE 4.6 – Tapered-land thrust bearing: A) Pressure and B) Temperature profile comparison of the TEHD and THD models.

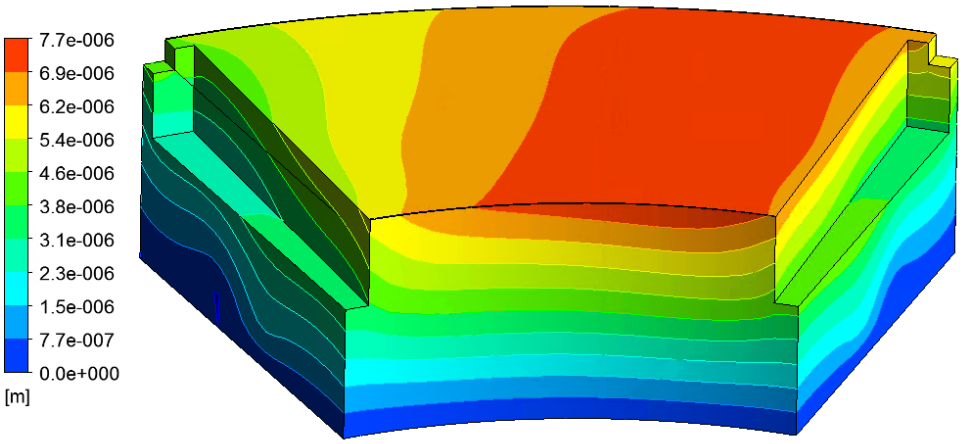

FIGURE 4.7 – Tapered-land thrust bearing: Pad domain total mesh displacement on the Z direction

TABLE 4.1 – Tapered-land thrust bearing: Performance parameters for the selected cases from the TEHD and THD models.

Parameter	TEHD	THD
Load $[N]$	1126	1096
Friction torque $[N \cdot m]$	0.275	0.275
H_{min} $[\mu m]$	11.70	12.5
Max. Temperature $[°C]$	94.9	94.8
Max. Pressure $[MPa]$	6.75	6.05
Oil flow rate $[l/min]$	1.2739	1.2656

4.2 Pocket bearings

Another less commonly utilised fixed pad thrust bearing configuration is the pocket bearing. It is a step bearing, shrouded at both the inner and outer sides. The inner and outer shrouding lips, allow for a minimisation of a side leakage; thus, higher loads can be achieved, in comparison with the step bearing.

The pocket results are presented in similar fashion as in the tapered-land section. The geometrical configuration of the pocket bearing has been described in subsection 2.2.9. Its performance characteristics are presented in Fig. 4.8 for the TEHD and THD models alongside with the experimental results from the Ph.D. Thesis of Henry [77].

Both THD and TEHD are in a good agreement for the H_{min} and pressure at the 70%-50% point, but the THD presents higher values of temperature and lower values of torque for a given load.

Comparing them with the experimental results, both models overestimate the pressure prediction at the 70%-50% point. The TEHD model estimates very accurately the friction torque, compared to the measured by the experiment values. Nevertheless, the measured temperatures are between the THD and TEHD predictions, exhibiting the same trend with a minor shift.

The main difference is the H_{min} evaluation for a given load. In Fig.4.9 a correction of the experimental values have been made, in order to account for the thermal expansion of the pad domain. But again, there is not a very good correlation between

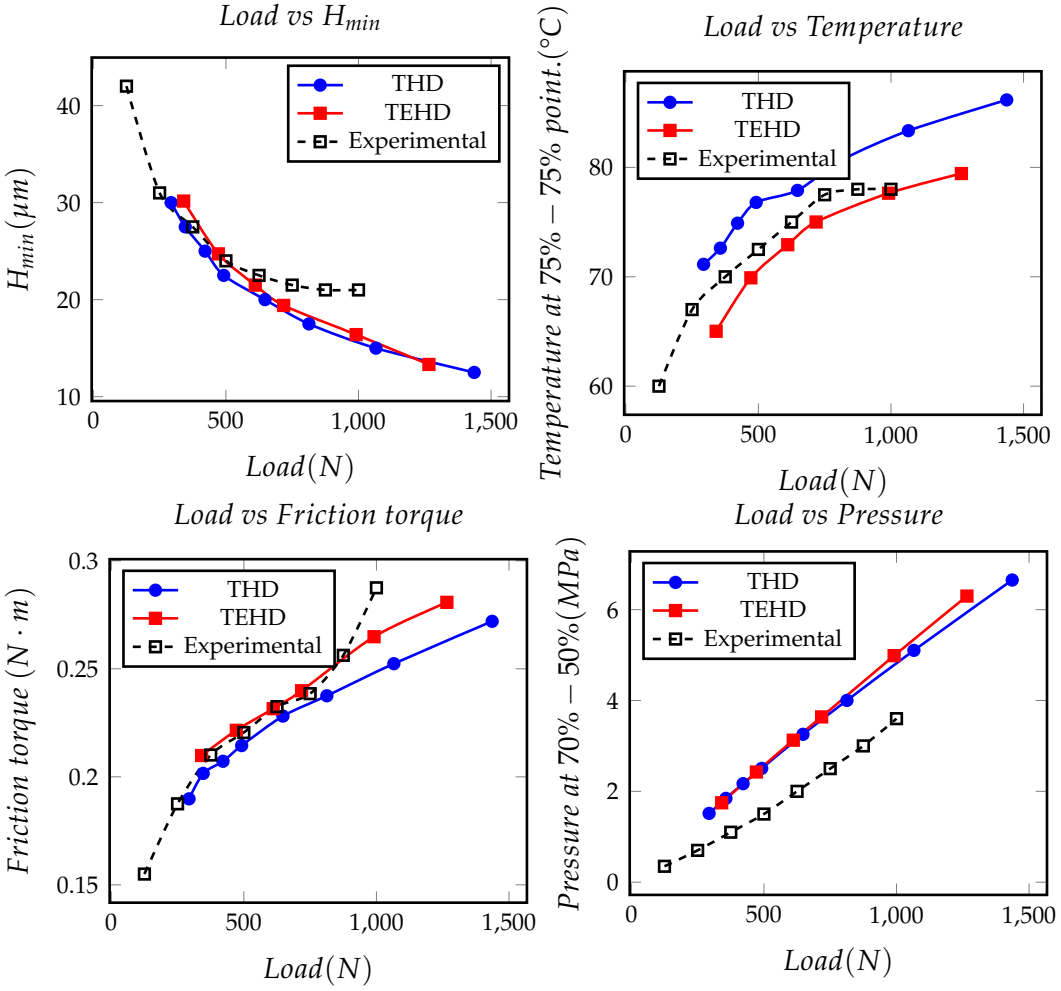

FIGURE 4.8 – Pocket thrust bearing: Performance characteristics comparison for the THD, and TEHD models, and experimental results.

the corrected experimental values and the TEHD model evaluations.

Something that could mitigate this discrepancy could be the inclusion of rotor thermal and mechanical deformation calculations in the TEHD model. In Fig. 4.10 the total mesh displacement at the Z direction is illustrated, and the maximum mesh displacement is located at the outer diameter of the pocket bearing close to the trailing edge. If we take into account the shape of the rotor deformation of the parallel surface thrust bearing, as seen in Fig. 3.18, we can conclude with a moderate amount of confidence that the final H_{min} location would be slightly closer to the centre of the bearing, with a larger value.

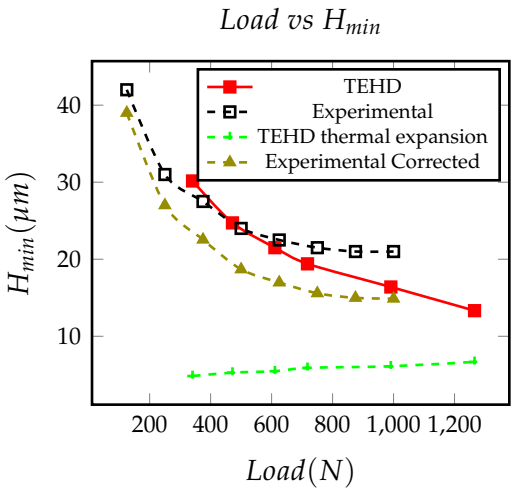

FIGURE 4.9 – Pocket thrust bearing: Corrected H_{min} vs the Load accounting for the thermal deformation of the pad.

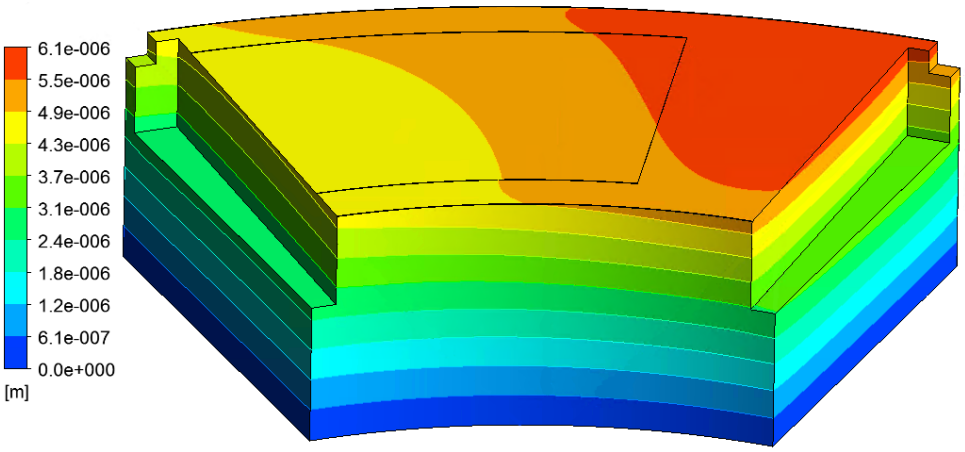

FIGURE 4.10 – Pocket thrust bearing: Pad total mesh displacement on the Z direction.

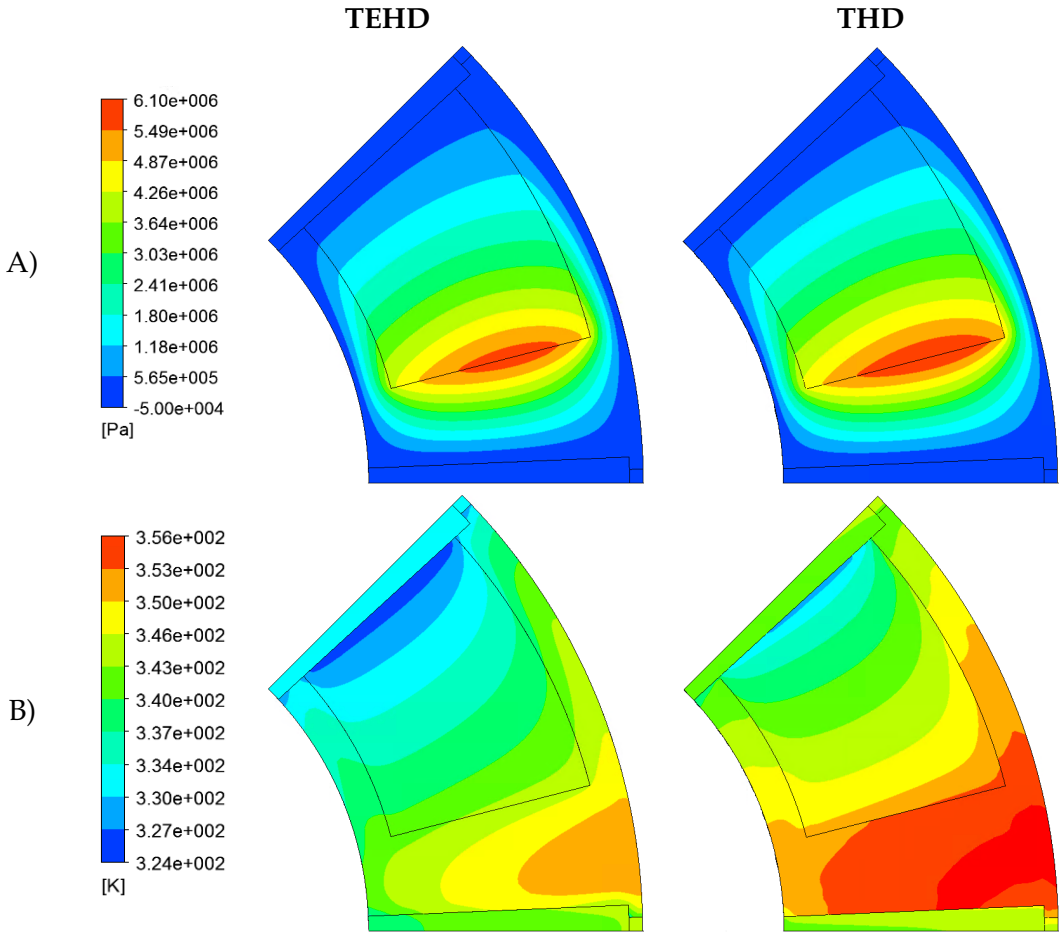

FIGURE 4.11 – A) Pressure, and B) Temperature, profile comparison of the TEHD and THD approach for the pocket thrust bearing.

In order to evaluate closer, the differences of the two models, similarly loaded instances have been chosen for both of them. The performance characteristics of the chosen cases are presented in the Table 4.2. Also the pressure and temperature profiles for both cases are depicted in Fig. 4.11, and circumferential section profiles for pressure and temperature distribution are presented in Fig. 4.12 and Fig. 4.13 respectively. Finally, the film profile circumferential mid-section is presented in Fig. 4.14.

The load difference between the two selected cases is 7.2%; thus, the very small difference observed in the pressure profile in Fig. 4.12. Moreover, the temperature in the whole lubricant domain is overestimated by the THD model. The reason for this discrepancy is probably the wedge generated inside the pocket from the thermal deformation, allowing for a larger amount of cold lubricant to flow from the oil feeding groove, reducing the average temperature inside the pocket for the TEHD model.

Summarising, in the pocket bearing case, the THD model can predict with some confidence the tribological characteristics of the bearing. It overestimates the temperature, and slightly underestimates the friction torque. On the other hand, the TEHD model manages to evaluate better both the temperature and the friction torque, but there are some H_{min} evaluation discrepancies. Those differences can be attributed to the lack of thermal deformation on the rotor, but also to the imperfection of the experimental measurements, or the calculated corrections done in the present study.

For designing a new pocket bearing, the THD approach can be considered accurate enough. If the evaluation accuracy needed is higher, it is suggested to evaluate

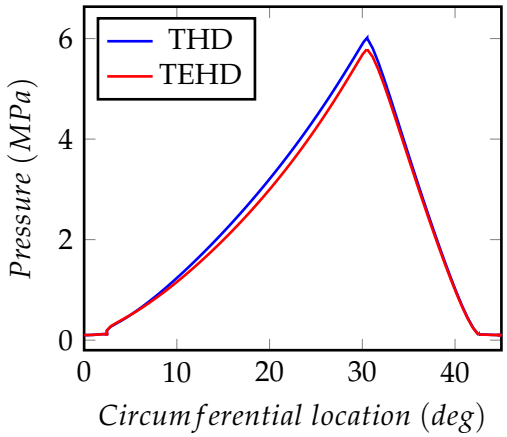

FIGURE 4.12 – Pocket thrust bearing: Pressure comparison for the THD and TEHD models at a circumferential section at the mid radius.

the new geometry considering the thermal and mechanical deformations for both the pad and the rotor geometry.

TABLE 4.2 – Pocket thrust bearing: Performance parameters for the selected cases from the TEHD and THD models.

Parameter	**TEHD**	**THD**
Load $[N]$	992	1066
Friction torque $[N \cdot m]$	0.271	0.252
H_{min} $[\mu m]$	16.397	15
Max. Temperature $[°C]$	83.2	89.7
Max. Pressure $[MPa]$	5.85	6.10
Oil flow rate $[l/min]$	1.2136	1.2013

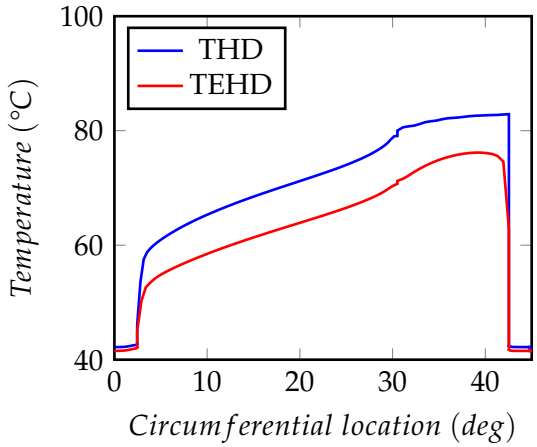

FIGURE 4.13 – Pocket thrust bearing: Temperature comparison for the THD and TEHD models at a circumferential section at the mid radius.

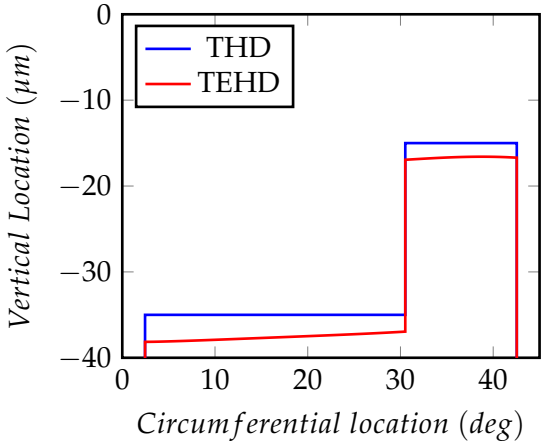

FIGURE 4.14 – Pocket thrust bearing: Final film geometry profile comparison for the THD and TEHD models at a circumferential section at the mid radius.

4.3 Textured bearings

This section has two main objectives. The first one is to compare the different modelling approaches and understand the importance of thermal deformations on textured parallel surface thrust bearings. The second objective is to evaluate the performance of a textured parallel surface thrust slider with an untextured one, in order to understand the effect of texturing on the parallel surface thrust bearing's performance.

Due to time limitations, the evaluation of the single sector pad geometry was not possible. Thus, the slider geometry solution is presented, for the texturing evaluation. A simple texture design of an 8 by 8 array of orthogonal dimples has been generated. The chosen texture density is 64%, and the texture width and length have been set to 80% and 60% respectively.

4.3.1 Thermal effects on AST

As it is stated in the literature, the experimental and computational evaluations of texture designs are not in very good agreement, especially on high loads. As it is demonstrated in Chapter 3, the thermal deformations and thermal properties of the fluid domain, play a significant role on the performance of the parallel surface thrust bearing. Thus, in order to understand the behaviour of textured parallel surface thrust bearings, and why traditional isothermal modelling overestimates its performance, the selected design has been evaluated in means of isothermal, THD, and TEHD models in a range of loads.

The considered load limit for the following calculation is considered that of 1500 N, which corresponds to specific load of 3 MPa. Typical operating range for such bearings would be between 0.5 MPa and 2.5 MPa, which corresponds to approximately 250 N and 1250 N respectively.

In Fig. 4.15 the bearing performance characteristics evaluated with the three different models are presented. The isothermal model exhibits considerably larger values of H_{min} and friction force for the same values of load. The main reason of such behaviour is the constant viscosity, that is set as the viscosity of ISO VG 46 at the feeding oil temperature of 40°C. For the THD and TEHD models the viscosity is evaluated at at each element, from the local temperature value, resulting to a considerably lower value of average viscosity. A better isothermal approach would be, if the the power loss and lubricant flow rate were estimated from an initial isothermal calculation and then the average temperature was calculated. With this average temperature approximation, the corresponding viscosity value would be applied to the whole lubricant domain. This approximation would be considerably closer to the one evaluated by the THD model, but requires temperature estimations for each load instance, as the temperature varies considerably in the studied load range.

A comparison between THD and TEHD models, concludes that the two modelling approaches are remarkably similar in low load operating conditions. Nevertheless, as the load increases, the two models diverge. When the thermal deformations were evaluated, the bearing can support considerably higher loads for the same value of H_{min}, but not as high as compared with the isothermal model.

In Fig, 4.16 the maximum temperature at the fluid domain is presented versus the load for the TEHD model. The maximum temperature exhibits an unusual behaviour. As the load increases, the maximum temperature increase, until the 1000 N load mark. From 1000 N to 1500 N the maximum temperature decreases, and then increase again.

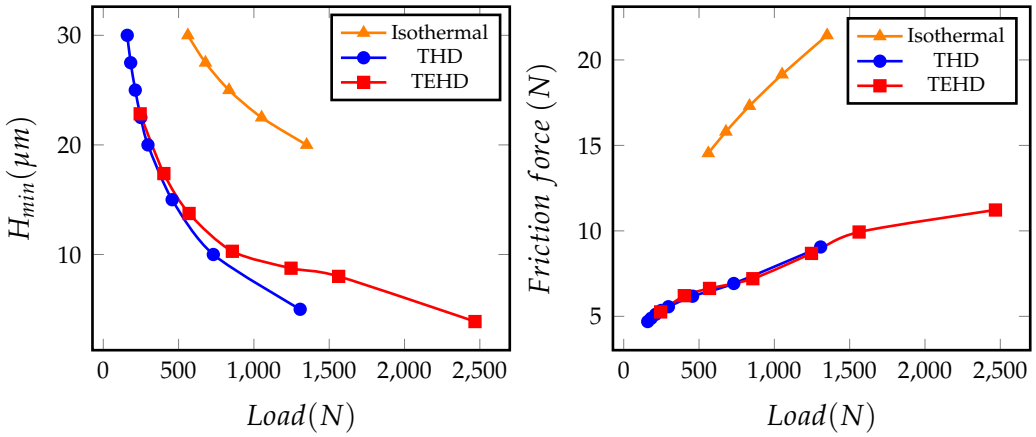

FIGURE 4.15 – Performance characteristics comparison for the Isothermal, THD, and TEHD models for the textured parallel surface slider.

In order to understand this unintuitive behaviour, three instances with different loads have been studied further. The mesh displacement at the Z axis, pressure, temperature, volume fraction, and heat flux profiles for the selected cases are depicted in Fig 4.17, and their performance parameters are listed in Table 4.3. The pressure, temperature, and final film profiles at the mid-plane longitudinal section are presented in Figs. 4.18,4.19,4.20.

TABLE 4.3 – Performance parameters for the selected textured cases.

Parameter	Case 1	Case 2	Case 3
Load $[N]$	402	856	1562
Friction $[N]$	6.21	7.20	9.93
Max. Temperature $[°C]$	80.6	88.4	84.4
Max. Pressure $[MPa]$	2.48	5.09	9.34
Oil flow rate $[l/min]$	0.6289	0.6223	0.6164

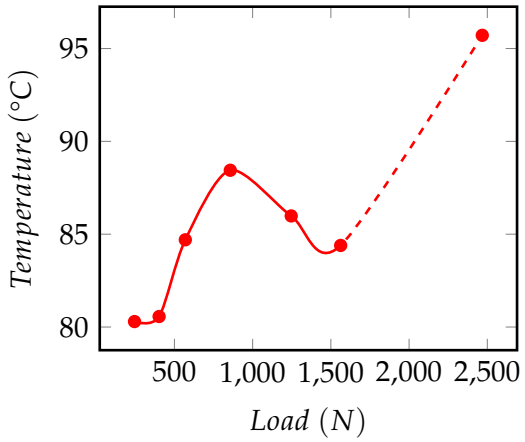

FIGURE 4.16 – Maximum temperature at the fluid domain for the textured TEHD model.

Two main reasons have been identified for the temperature behaviour of the parallel surface textured thrust slider. First, as the load and temperature increase the thermal deformations generate a diverging zone near the trailing edge of the slider. As a consequence of the diverging zone's pressure drop a cavitation zone is generated. As the H_{min} decreases the volume fraction of the gas phase of the lubricant increases, driving to larger transverse flow from the lubricant inlet surface. The increased mass flow at the cavitation zone is mixed with the hot lubricant, reducing the average temperature of the lubricant exiting the pad. While the hot oil carry over phenomenon is present at all load instances, the larger the cavitation region the higher the temperature differential from the start of the cavitation region to the leading edge of the next pad is. This can be also contributed to the disturbance of the thermal boundary layer on the fluid rotor surface from the cavitation.

Moreover, the second and probably more important flow phenomenon is presented inside the individual dimples. In Fig 4.21, a graphical representation of the flow inside the a dimple is depicted for the three cases. In Case 1, where the H_{min} and the texture depth are almost the same, and the Reynolds number is 4 (calculated with the average viscosity in the texture region), the flow can be characterised as creeping. No recirculation zones are present at the bottom of the dimple, and the flow speed near the texture fluid pad surface is very low, almost eliminating the convection between the fluid and stator. In Case 2, the Reynolds number, increases to approximately 10, and the dimple depth over the H_{min} ratio increases to 2. Due to the high ratio and Reynolds number a recirculation zone appears at the bottom of the dimple. The recirculation zone speed near the fluid pad surface is still very low, perpetuating the very low values of convection between the fluid and the stator. However, in Case 3 the higher Reynolds number (approximately 16) and the larger texture depth over the H_{min} ratio lead to a larger recirculation zone with larger speed near the boundary, which increases considerably the convection heat flux, driving to lower operating temperatures.

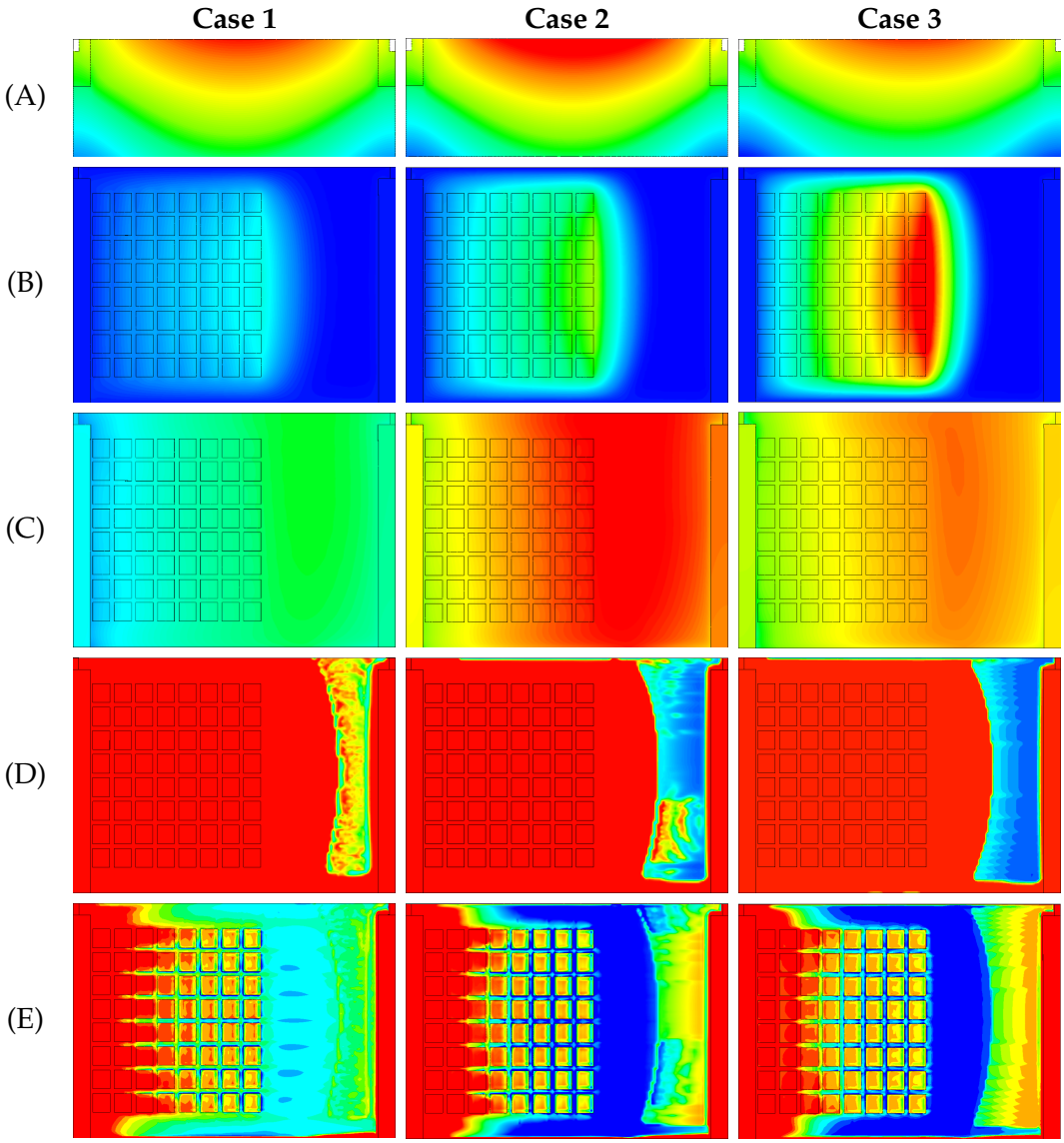

FIGURE 4.17 – Comparison of the 3 different load instances of the parallel surface textured thrust slider A) Mesh displacement in the Z direction on the pad inner side, B) Pressure, C) Temperature, D) Lubricant volume fraction, E) Heat flux

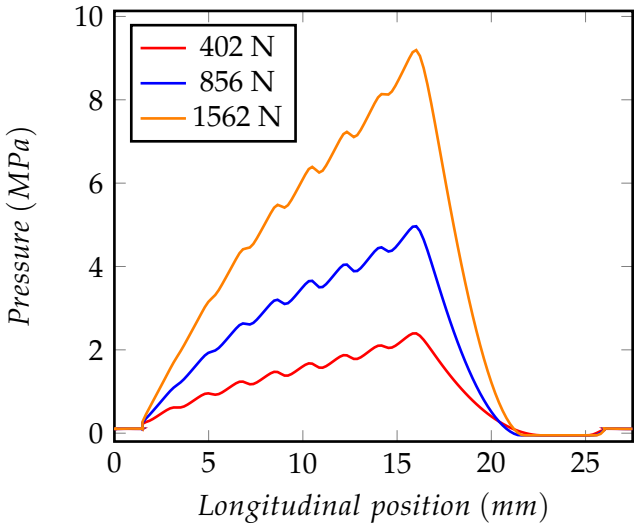

FIGURE 4.18 – Pressure comparison of textured slider in different loads at the mid-plane section

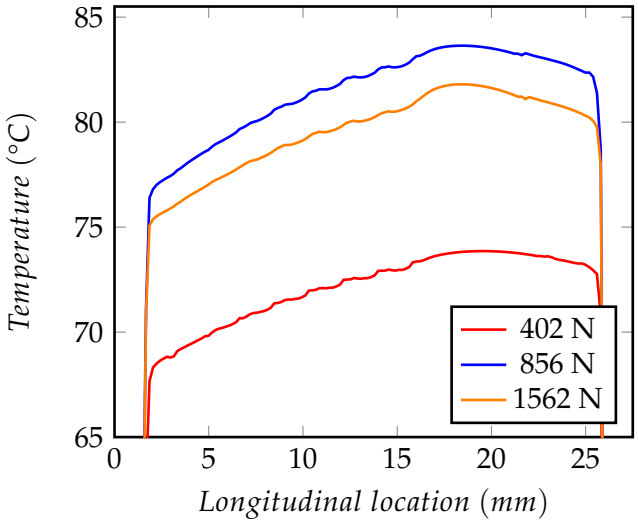

FIGURE 4.19 – Temperature comparison of textured slider in different loads at the mid-plane section

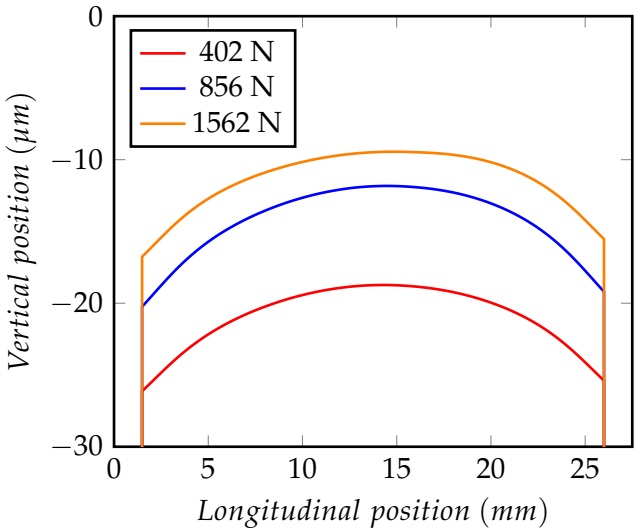

FIGURE 4.20 – Final film geometry comparison of textured slider in different loads at the mid-plane section

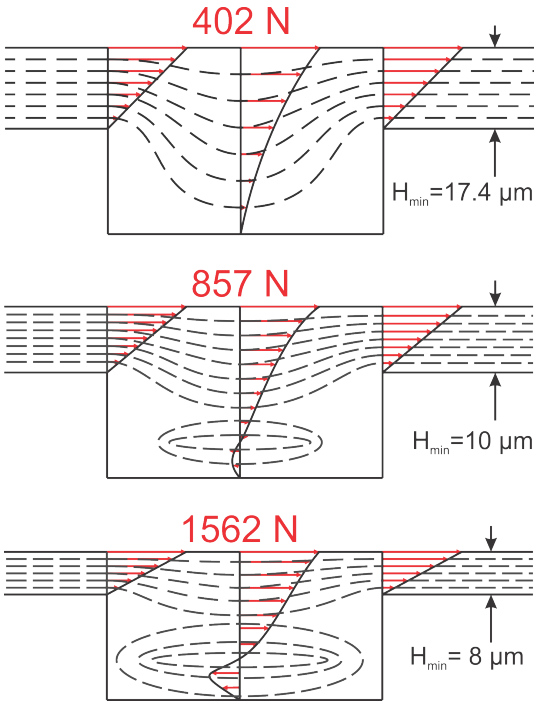

FIGURE 4.21 – Velocity streamlines inside a dimple for different loads of the bearing

Concluding, the cavitation near the trailing edge of the pad due to thermal deformation, allows for a better mixing at the thermal boundary layer at high loads. Additionally, the dimples, due to their low convection values, act as a kind of insulation for low Reynolds number values. Adding those two phenomena, the temperature increase and decrease can be explained.

As result of the above observation, in terms of modelling, the texturing evaluation should not be done by the Reynolds equation because of the importance of the inertia forces on the convection heat flux.

4.3.2 Comparison between parallel surface textured and untextured slider

The use of textures on bearings has been introduced in order to increase the load carrying capacity and reduce the friction losses. Such designs are very expensive to manufacture. In very low load applications like mechanical seals, AST decrease the friction significantly, but in medium and high load applications their advantages seem to disappear. Moreover, significant optimisation is needed for each application, because for different operating conditions the optimal AST parameters vary considerably. In the opposite side, the plain parallel surface thrust bearing is the simplest geometry that can be manufactured, the most inexpensive configuration in terms of design and manufacturing cost and is experimentally proven that it can support considerable load.

In order to identify the advantages and drawbacks of those two designs, a comparison of the textured and untextured parallel surface slider with the TEHD modelling approach in a range of loads has been conducted and presented in Fig. 4.22.

The initial observations are that both designs have considerable advantages over the other. The untextured slider exhibits better performance characteristics in the studied range, in terms of H_{min} and temperature. Meaning that an untextured thrust slider can run in safer operating conditions for given load. On the other hand, the textured slider displays lower values of maximum pressure and considerably lower friction losses, driving to lower wear and more economical operation. Although, the use of lubricant with lower viscosity at the untextured bearing would reduce the friction losses, while operating in lower values of H_{min}, making the advantages of the texture less pronounce. Moreover, due to the larger load carrying capacity of the untextured slider, a comparable design for the same application would have smaller dimensions resulting to more comparable friction losses.

For a better understanding of the differences of the two designs, one similarly loaded instance of each design has been selected and presented in Fig. 4.23.

On the untextured slider, due to the thermal deformation that occurs on the pad, a wedge geometry is generated as it is depicted in Fig. 4.24. A large converging area is generated, from the leading edge until aft of the mid of the slider where the H_{min} is located, which helps the generation of the load carrying capacity of the parallel surface slider. From the longitudinal position of the H_{min} to the trailing edge, a diverging region is generated. On the diverging region, a cavitation zone is present as it can be seen in Fig. 4.23. The converging and diverging regions can be observed also on the textured slider, although the pressure profile is quite different. The pressure increase is smoother until the end of the textured area. The converging effect produced by the thermal deformation is mitigated from the dimples. The film thickness over the converging geometry inside the dimples is very large; therefore, it does not contribute to the pressure build-up.

Furthermore, there is a smaller cavitation region on the textured slider, because the position of the maximum pressure is closer to the trailing edge. On the transversal direction both designs have a larger deformation on the inner and outer sides, due to the high-pressure zone in the middle of the slider. The thermal expansion of the slider is partially mitigated from the mechanical deformation near the mid-plane area, where the pressure is larger.

One of the main observations for the operating of the parallel surface sliders is the way the feeding oil enters the high-pressure zone and reduces the temperature of the bearing. In a taper-land or pocket bearing configurations, the oil inlet from the oil feeding groove allows fresh lubricant in the pad region, reducing the average temperature. In a parallel surface slider, where the oil inlet is considerably smaller,

oil supply at the inlet surface is restricted to the hot oil curried from the previous pad by the rotor. As it can be observed in Fig. 4.24E), cold lubricant enters the pad region almost only from the inner opening at the low-pressure region (cavitation region) close to the trailing edge. Thus, a low-pressure zone is essential for the effective cooling of a parallel surface thrust slider. Comparing the parallel surface textured and untextured configurations, the larger cavitation zones of the untextured slider allows considerably more cold lubricant to enter the pad region, resulting to considerably lower maximum temperature values (see Fig. 4.22).

Summarising, the AST on parallel surface thrust bearings can reduce friction losses compared with the untextured one if the same bearing dimensions and lubricant are utilised. The pressure build-up mechanism of the parallel surface thrust bearing (thermal deformation) is mitigated on the textured slider due to the imposed by the dimples larger mean film thickness on the generated wedge; thus, generating pressure mainly from the step effect of each dimple. The textures expand the high-pressure region, driving to lower maximum pressure for a given load, and confining the cavitation to a small area near the trailing edge. In some sector pad thrust bearing applications, cavitation can occur also inside the outer row of dimples near the leading edge. Furthermore, the textured bearing exhibits considerably higher temperatures than the untextured one, for the reason that the textures partially insulate the convection heat exchange between the fluid and the pad, and because the cavitation region is smaller than in an untextured bearing; thus, allowing a smaller amount of cold lubricant to enter from the oil feeding surface near the low pressure zone.

Finally, before selecting AST for a new design that operates at specific loads over 0.3 MPa, one should consider the higher manufacturing cost, the higher operational temperatures, and lower load carrying capacity of the textured bearing in comparison with the simple untextured one.

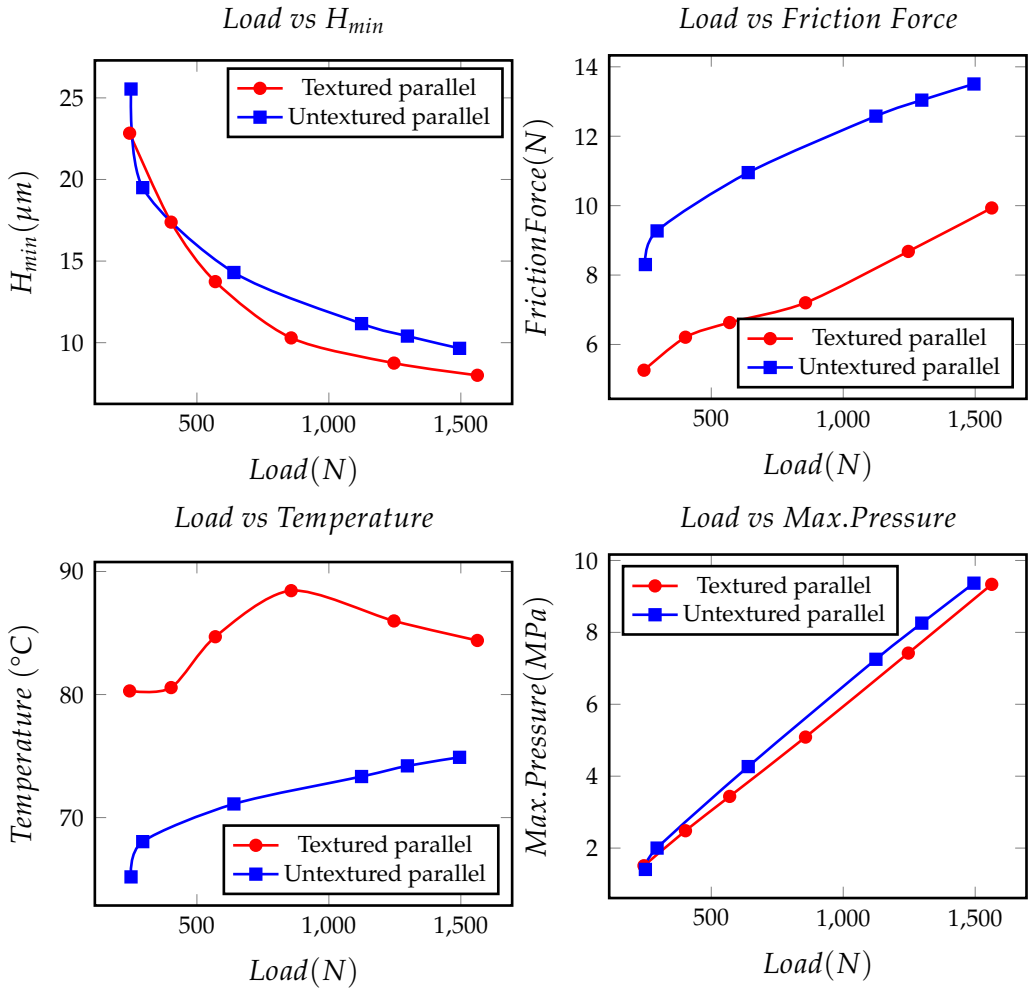

FIGURE 4.22 – Performance characteristics comparison between the textured and untextured parallel surface slider, evaluated with the TEHD model.

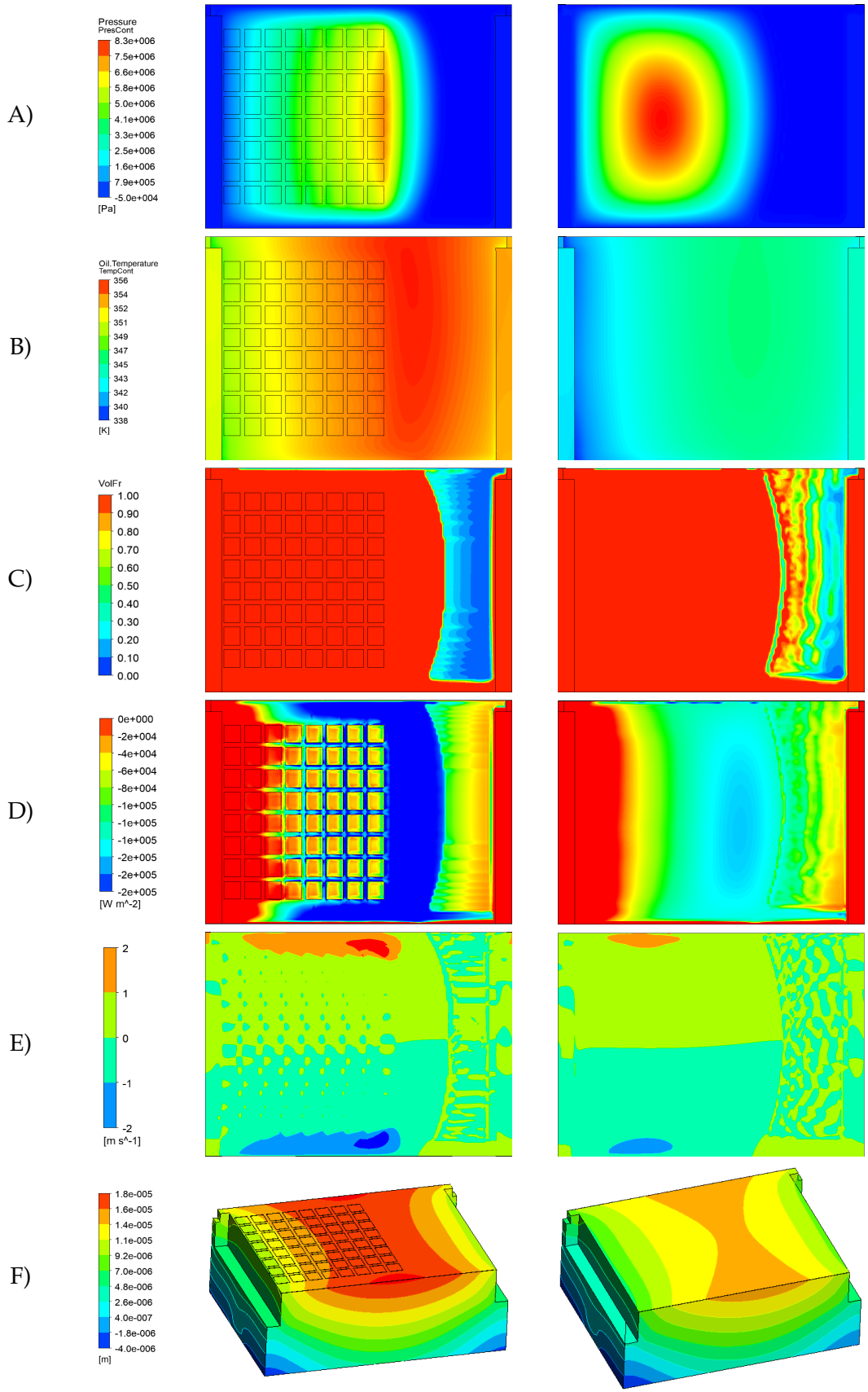

FIGURE 4.23 – Comparison of the textured and untextured parallel surface slider at a load close to 1250 N A) Pressure profile, B) Temperature profile, C) Lubricant volume fraction profile, D) Heat flux, with the TEHD approach, E) Oil velocity in y direction, F) Mesh displacement on the Z direction.

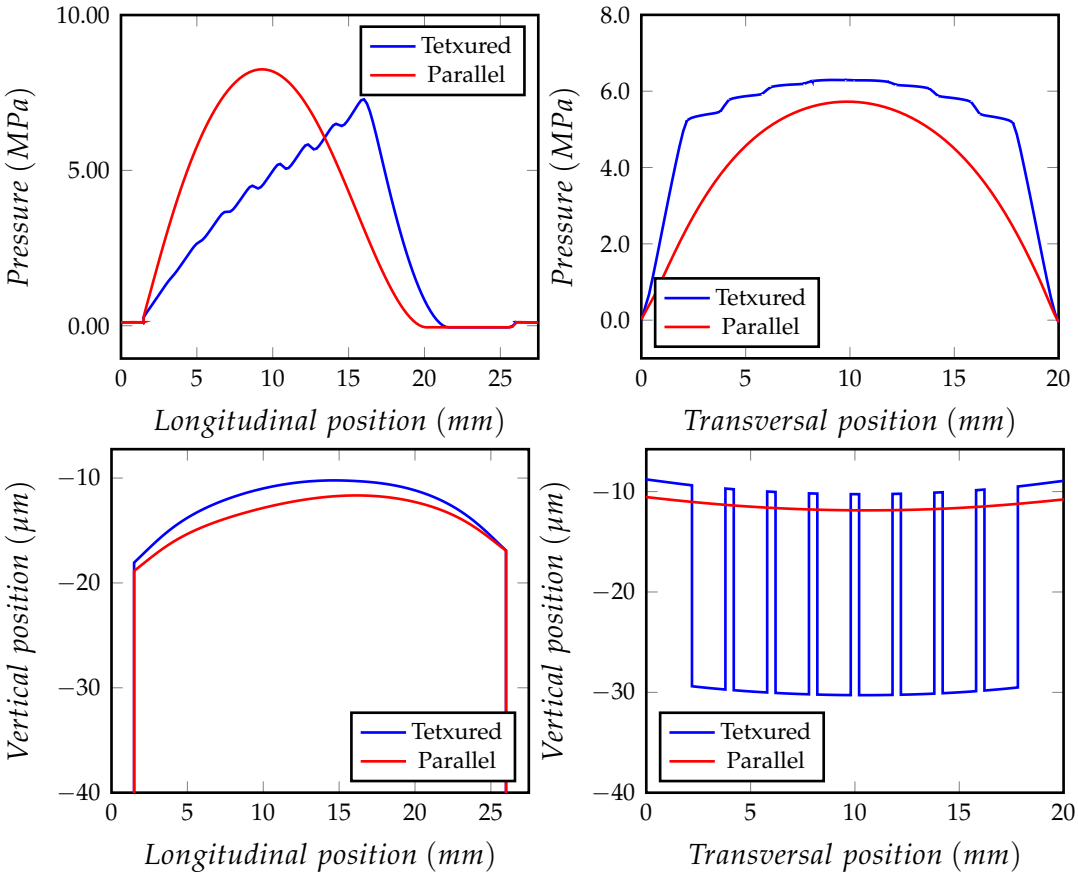

FIGURE 4.24 – Texture and untextured parallel surface slider pressure and film profile comparison.

4.4 Coatings

Metallic and polymer coatings are present in almost all contemporary bearing applications. White metal coatings (Babbitt) have been widely used, but since the 70's polymer coatings have progressively replaced them in some applications. Since the early years, the polymer coatings have been improved considerably, with the use of matrix materials. The new polymer coatings are composite materials with better mechanical properties, wear resistance, and creeping properties. Because of their great importance in the industry, an initial study has been performed to evaluate their effect in the performance of the parallel surface thrust bearing. Their main difference from the metals used for bearing manufacturing are their large thermal expansion coefficients, and their thermal insulating properties. Both of which will affect the main pressure build-up mechanism of the parallel surface thrust bearing.

Three types of coatings have been studied, namely the Babbitt, the PTFE, and the PEEK. Because of their high thermal expansion coefficients evaluation of the TEHD model has been extremely time consuming. The need of a relaxation factor with values lower than 0.05 for the successive over-relaxation method has been vital for the mesh displacements not to produce negative volume elements. Moreover, very small differences of the initial H_{min} values, in the order of magnitude of 0.5 μm can produce load increases of 600% and final film thickness differences of 10 μm. This made very difficult the identification of the initial H_{min} values that correspond to the desirable load range. Furthermore, the problem increases as the load increase, and the resulting high temperatures make the solution unstable.

For the above reasons, only one instance of each coating is presented. The main objective of this section is to evaluate the effect of the coatings on the pressure build-up mechanism of the parallel surface thrust bearing, and how the different coating parameters differentiate the bearing performances. Due to the lack of computational result, and no reference experimental data, only qualitative observations can be made, and no conclusive answers will be given.

All presented results have been plotted in their own colouring scales in Fig. 4.25, because direct comparison is not possible due to different operating conditions. The figures are presented in order to identify the difference in pressure and temperature distributions between the different coatings.

The three coated cases with the reference bronze case are presented in Table 4.4. The Full TEHD model has been utilised for all presented evaluations. The thickness for all coatings is 1 mm and the geometry is presented in Fig. 2.11.

TABLE 4.4 – Performance parameters for the selected coated cases.

Parameter	Bronze	Babbitt	PTFE	PEEK
Load $[N]$	285	206	180	122
H_{min} $[\mu m]$	12	11.34	18.76	15.44
Friction Torque $[N \cdot m]$	0.368	0.247	0.227	0.198
Max. Temperature $[°C]$	82.5	96.8	83.0	96.1
Max. Pressure $[MPa]$	1.86	1.38	0.992	0.741

The main differences observed in all four models are the following. The width of the maximum pressure region is smaller for materials with higher value of the thermal expansion coefficient, with PTFE having the narrower high-pressure zone. Moreover, the high temperature zone for all instances is located at the outer side near the trailing edge, but the spanwize extend for the polymer coatings is considerably

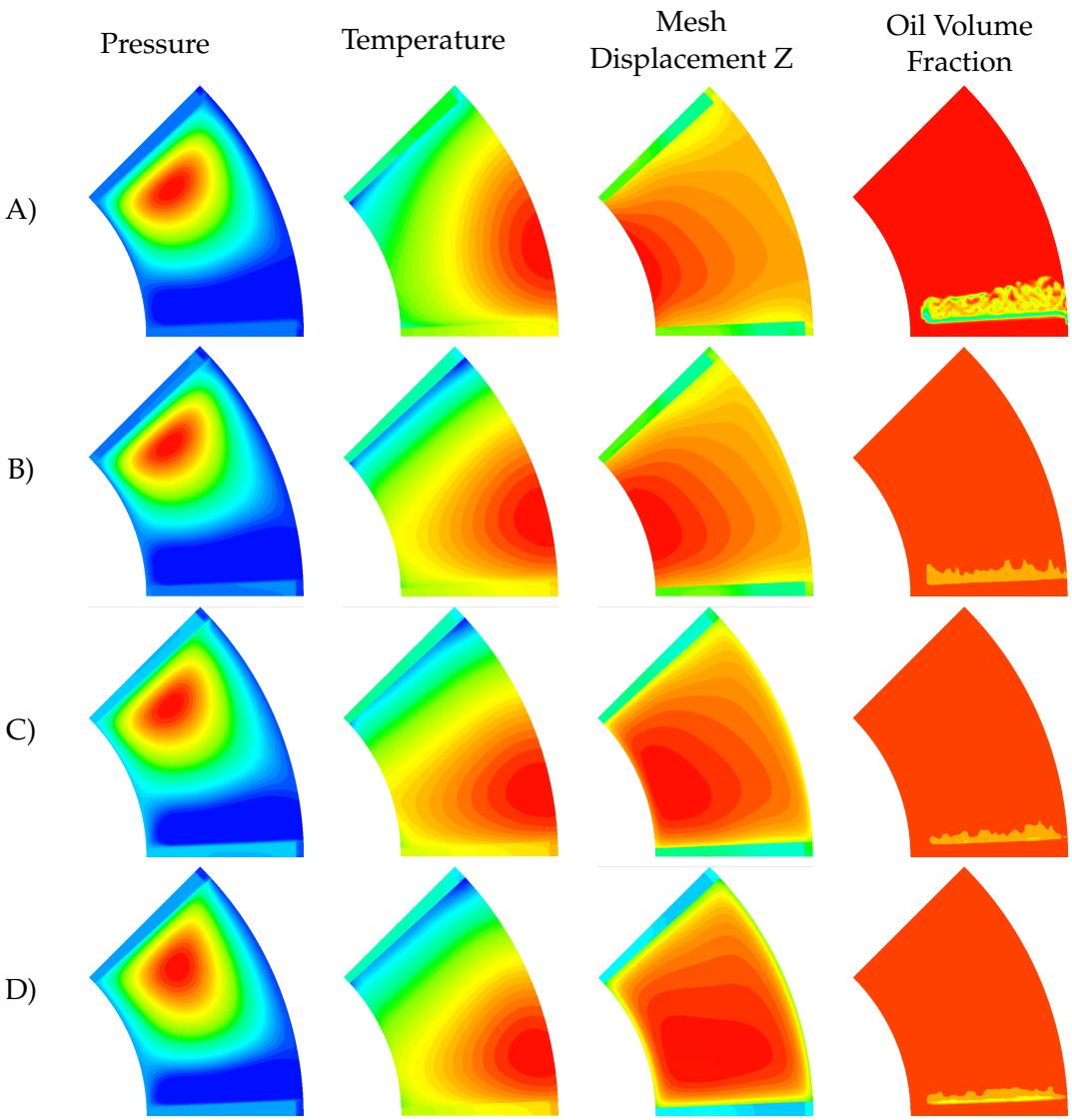

FIGURE 4.25 – Pressure, temperature, mesh deformation at the Z axis, and oil volume fraction distributions for the A) Bronze, B) Babbitt, C) PEEK, and D) PTFE models.

larger than the bronze. The pad deformation of the Babbitt and PEEK is very close to the shape of the bronze bearing, but on the PTFE coating the deformation exhibits a more uniform behaviour in the spanwize direction. Finally, the bronze bearing is the only instance that cavitation occurs.

More analysis is needed in order to identify the effect of coatings on the pressure build-up mechanism, and on the thermal deformation. As mentioned above, this was not possible in the scope of the present Thesis due to the extremely high computational cost.

The future work on the coating analysis that is planned, is divided in two parts. The first is to evaluate the bearing performance in a range of operating conditions for different coating thickness values. The second part is a parametric study for a bi-coated bearing, as it is presented in Fig. 2.11.

4.5 Conclusions

In the present chapter, four different types of contemporary designs have been studied. Each design presented exhibited different behaviour in the studied range. Thus, a different computational approach is suggested for those configurations.

The tapered-land bearing has been evaluated with the THD and TEHD models. Both models manage to evaluate the bearing performance with a very good correlation to the experimental results, with a small underestimation of the pressure at the 70%-50% point for both models, and an overestimation on the temperature for the THD model. In general, the THD modelling approach is recommended for this design, because of the small benefits of the TEHD over its computational cost. Although if a more precise evaluation is needed, especially in terms of temperature distribution, the TEHD modelling approach is suggested, but the need to model the rotor deformations is considered unnecessary.

For the pocket bearing, almost identical results with the tapered-land have been acquired. Very good correlation with both models has been observed, with a small overestimation of temperature for the THD model, and an overestimation of the pressure at the 70%-50% point by both models. The main difference from the tapered-land is that is better accuracy is needed for the performance characteristics evaluation than that managed by the THD model, a TEHD model is proposed that takes into account also the rotor mechanical and thermal deformations. The reason for that is the shape of the pad deformation and temperature distribution.

The textured bearing studied in the present work, represents a slider geometry due to the sector pad geometry complexity and increased computational cost. To evaluate the performance of AST on the parallel surface slider three models have been introduced, the isothermal, the THD, and the TEHD. Isothermal modelling cannot correctly evaluate the performance characteristics of the textured slide, and the THD model diverges from the TEHD model in moderate to high loads. The TEHD modelling showed that the texture cavities function as thermal insulators, and do not allow the heat flux from the lubricant to the pad for a range of H_{min} values, driving to a steep increase of the temperature as the load increases. When the H_{min} reaches a threshold value, a recirculation zone is created inside the cavity that allows the convection heat flux, and from this point on the temperature decreases as the H_{min} decreases, until a value of load is reached, where the heat generation is larger than the heat flux inside the cavities and the temperature increases as the load increases. This drives to the conclusion that new designs for texture depth need to consider the H_{min} operational magnitude. Finally, for the correct evaluation of the performance of the textured parallel surface slider TEHD modelling is strongly suggested.

Comparing the textured slider with an untextured parallel surface slider, the following can be stated. The AST manages to reduce the friction force in comparison with the untextured bearing. The pressure build-up mechanism of the parallel surface thrust bearing (thermal deformation) is mitigated on the textured slider, because of the larger average film thickness on the generated wedge. The high-pressure region is extended by the textures; thus, cavitation is limited near the trailing edge. Moreover, the textured bearing exhibits higher values of temperature, because of the insulating properties the cavities have. Finally, before selecting AST for a new design that operates at specific loads over 0.3 MPa, one should consider the higher manufacturing cost, the higher operational temperatures, and lower load carrying capacity of the textured bearing in comparison with the simple untextured parallel one.

Furthermore, three different coatings have been modelled, but not conclusive results have been established. The main reason for the lack of computational results has been the remarkably high computational cost of the TEHD modelling for materials with high thermal expansion coefficient and low stiffness. In order to evaluate the performance characteristics of a coated parallel surface thrust bearing TEHD modelling is the only option because the main pressure build-up mechanism is the thermal deformation of the pad and rotor geometry.

Chapter 5

Conclusions

5.1 Thesis Summary

In the present Thesis the effects of thermal deformations on the performance of fixed-pad thrust bearings operating under high values of load and temperature has been investigated. First, a detailed literature review has been performed. In the first part of the review, an investigation of the pressure build-up mechanism of the parallel thrust bearing has been reported. The capability of such bearing to support significant amounts of thrust load, observed experimentally in several published studies, is in contradiction with the classic lubrication theory. Thus, many theories have been published, in an effort to understand and explain this behaviour. The principal theories reported in the literature attribute pressure build-up of the parallel thrust bearing to (i) the thermal wedge in the lubricant domain, generated as the result of the thermal expansion of the lubricant as it flows from bearing inflow to bearing outflow, (ii) the viscosity wedge, generated as the result of temperature/viscosity difference in the crossflow direction of the lubricant, (iii) the macro-roughness of the bearing pad surface, leading to the presence of converging and diverging regions generated by the machining of the parallel bearing surface, (iv) the ram pressure, generated at the leading bearing edge due to the abrupt geometry change in the lubricant domain, (v) the thermal deformation of the pad geometry, which generates a converging wedge at the inflow region of the bearing, and (vi) the leading edge chamfer effect, acting as a tapered-land bearing at lubricant inflow. In the course of this Thesis, a detailed investigation of most of the above theories has been performed.

Further, the scientific literature concerning artificial surface texturing for tribology applications has been extensively reviewed, mainly due to the observed inaccuracies between the experimental measurements and the computational results corresponding to a textured parallel thrust bearings that have been recently reported. A more detailed analysis, taking also into account the pressure build-up mechanism of the parallel bearing has been deemed necessary, in order to be able to correlate the corresponding experimental and computational data.

Due to their vast usage in the industry during the last decades, polymer coatings are an important contemporary design characteristic of commercially available bearings. The usage of such coatings allows greater operational temperature, lower wear, and even good performance characteristics in the mixed lubrication regime. Their main advantage is the friction reduction in start-up conditions, eliminating the need for hydrostatic features in highly loaded bearings for the start-up procedure. Their main drawbacks are mechanical properties such as viscoelastic creep and their thermal insulating properties. Additionally, their large thermal expansion coefficient values and low values of Young's modulus, could alter the performance

of a parallel thrust bearing because the thermal and mechanical deformation profiles are taking part to the pressure build-up mechanism. In recent years, many new composite material designs have replaced the old polymer coatings, improving their performance. The performance of parallel bearings with polymer coated pads has not been addressed in the literature, therefore it has been considered of great importance to study the case of polymer coating on the performance of parallel thrust bearings, and quantify the effects on the pressure build-up mechanism.

Taking into account the literature review, a detailed modelling of the mechanical and thermal deformations of thrust bearings is required in order to correlate better the computations with the experiments, and, in consequence, to better understand the physical phenomena. Moreover, the need for an accurate approximation of operating temperature is considered of great importance, for the thermal deformations to be evaluated correctly. For that reason, modelling the groove region of the bearing is mandatory. The cooling effect of the feeding oil on the pad domain is important, but the most prominent effect that needs to be calculated in detail is the hot oil carryover. The hot lubricant that exits the pad is carried from the rotor to the next pad. If the groove geometry is not modelled, a mixing model is needed for approximating the temperature at the leading edge, something that will decrease the accuracy of the results, affecting the accuracy of the calculated temperature distribution in the lubricant film. Furthermore, the Reynolds equation cannot evaluate the recirculation zone generated in the groove region, and also the inertia leading edge ram pressure effect; thus, the Navier-Stokes equations have been utilised.

Concluding, based on the previous analysis, a CFD model has been generated, accounting for the groove geometry, thermal properties of the lubricant domain, and thermal and mechanical deformations for the solid domains. This model has been named through the Thesis as the "Full TEHD model". Variations of this model have been also generated, for identification of the effect of individual lubricant or solid properties, and for decreasing the computational complexity, in cases where it was not required.

The present Thesis has been divided in two parts. The first part has addressed the subject of identification of the pressure build-up mechanism in parallel thrust bearings, whereas the second part has been concerned with evaluation of the effect of mechanical and thermal deformations on the performance of contemporary bearing designs. The main findings are presented in the paragraphs below.

5.1.1 Pressure build-up mechanism

The experimentally observed specific load for parallel thrust bearings lies in the range of 1.5 MPa or higher. In order to quantify the contribution of each of the proposed pressure build-up theories to the experimentally observed pressure, isothermal, THD, and TEHD models of the bearing have been generated and used.

First, the isothermal model has been used to quantify the effects of hydrostatic lift, leading edge ram pressure, and cavitation on parallel bearing performance. Regarding hydrostatic lift, an isothermal model which excludes rotor motion has been generated. Based on the obtained results, the magnitude of pressure due to hydrostatic lift is of the order of 0.1 MPa, much lower than the bearing pressure, when hydrodynamic effects are taken into consideration. Therefore the effect of hydrostatic lift can be considered as insignificant. Second, the leading edge ram pressure effect has been identified. The load carrying capacity, due to this effect, increases with decreasing film thickness, until a threshold value, and then exhibits a decreasing trend. In the latter case, large negative pressure zones have been observed, which

are not realistic in the lubricant domain; thus, cavitation modelling has been considered as an important extension of the bearing model. Different simulations have been performed for two values of oil viscosity, namely those corresponding to oil temperature of 40°C and 90°C. In the former case (high value of viscosity), inclusion of cavitation modelling leads to increase of the computed values of load carrying capacity; for low oil viscosity, cavitation is not present in the lubricant domain, therefore cavitation modelling does not affect the obtained results of load carrying capacity. Based on the results, the maximum magnitude of the ram pressure effect is also considered insignificant.

In the second stage of the analysis, THD models have been introduced, with different lubricant properties, for isolating each of the pressure build-up theories. For evaluating the effect of the thermal wedge, a THD model with temperature dependent density and constant viscosity, has been generated, and the results have been compared with those of an isothermal model with the same constant viscosity. An increase of pressure after the leading edge has been observed. The reason for that pressure increase is attributed to the thermal wedge effect. The thermal wedge effect is of the order of magnitude of 0.08 MPa of specific load, insignificant in comparison with the 1.5 MPa of the observed specific load.

Furthermore, a THD model with temperature dependent viscosity and constant density has been developed, and the obtained results have been compared again with those of the THD model of the previous paragraph. The results of the new model exhibited lower load carrying capacity, but a high pressure region has been generated near the trailing edge of the pad. This pressure increase has been identified in all THD models with temperature dependent viscosity. This increase can be attributed to the viscosity wedge effect. The only difference with the literature, is that in the presented evaluation the pad geometry cannot be considered having constant temperature as it is considered in the literature, neither the rotor having a linearly increasing temperature. In the numerical evaluations, the rotor has almost constant temperature (as a rotating solid only very small fluctuations of temperature can be observed at a constant radius), and the temperature of the pad near the trailing edge due to the feeding oil groove, is colder than the mid pad area. Thus, the viscosity wedge is generated due to the high shear stress region before the trailing edge near the pad upper surface. Yet, again the magnitude of the viscosity wedge is not only insignificant, but also lower than the thermal wedge, the ram pressure effect, and the hydrostatic lift for 0.1 MPa feeding oil pressure.

The pressure build-up mechanisms that account for lubricant properties do no, altogether, manage to generate enough load as that observed in the experiments. Therefore, a THD model that accounts for the mechanical deformations on the pad domain has been introduced. The mechanical deformations generate a small converging geometry near the leading edge, but with an extremely small magnitude, not capable to increase the load carrying capacity considerably.

The next phenomenon for pressure generation, proposed by the literature, is associated with the thermal deformations of the pad geometry. To this end, a TEHD model is generated, that accounts for thermal and mechanical deformations for the pad domain, with a temperature dependent viscosity and constant density (named as "Simple TEHD"). Evaluating the bearing performance with this model resulted to specific loads over 1.5 MPa for values of H_{min} larger than 10 μm. This suggests that the main pressure build-up mechanism of the parallel thrust bearing are the thermal deformations of the pad geometry.

In order to compare the computational results with experimental data from the literature, two more advanced TEHD models have been generated. The first one

is an extension of the Simple TEHD model, that accounts also for temperature dependent density, thermal conductivity, and heat capacity (named "Full TEHD"). The second is the extension of the Full TEHD model, that accounts also for the mechanical and thermal deformation of the rotor domain.

The results of the Simple and Full TEHD models both exhibit a very good correlation with the experimental results. The Full TEHD model is slightly closer than the Simple TEHD model, in terms of friction torque and temperature. Moreover, due to the diverging geometry generated near the trailing edge area, cavitation occurs, diminishing the viscosity wedge effect. A final extension of the Full TEHD model has been performed, by additionally considering the deformations of the rotor; the results of this model exhibited excellent correlation with the experimental results, leading to the conclusion that the thermal and mechanical deformations of the rotor, even if they are not the primary pressure build-up mechanism, play a more significant role than the thermal wedge, viscosity wedge and ram pressure effect.

Finally, the effect of imperfections of the individual pads should be taken into account while comparing experimental and computational results. It is also strongly believed, that the fixation of the pad geometry might be of importance on the performance of the parallel bearing.

In conclusion, based on the analysis of the results, the main reason that a parallel thrust bearing can support load is the thermal deformation of the pad geometry. The addition of the rotor deformation on the calculations adds to the accuracy of the results. The more accurately the temperature distribution is calculated on the lubricant domain, the better the approximation of the performance of the parallel bearing. Thus, both thermal and structural boundary conditions are of utmost importance.

5.1.2 Contemporary designs

An evaluation of four different contemporary bearing designs has been conducted. The first two are commonly used designs, namely the tapered-land and the pocked bearings. The third one is the parallel thrust bearing with artificial surface texturing. At the end of the chapter, an initial analysis of the effects of coatings, that are widely used in industrial applications, on the performance of the parallel thrust bearing has been presented. For all the designs, suggestions for the best computational approach has been made, considering the accuracy and the computational cost.

Regarding the tapered-land bearing, both THD and TEHD models managed to evaluate bearing performance characteristics with a very good correlation with the experimental results. The TEHD managed to estimate slightly better the temperature distribution on the bearing. Also the deformations of the pad generated a larger convergence in the tapered part. So, it is suggested, for new designs where the taper convergence is optimised, to take into account the inclination increase due to thermal deformations. In general, the THD approach is suggested for modelling this type of bearing, except for temperature sensitive applications, where TEHD modelling will offer an additional advantage.

Regarding the pocket bearing, both THD and TEHD models exhibit the same behaviour, as that of the tapered-land bearing. The only observed difference is the shape of the deformation of the pad. In the pocket design, the maximum deformation occurs at the outer side of the pad near the trailing edge. Based on the results, it is proposed that, if the accuracy of THD modelling for pocket bearings is not sufficient (even if the approximation of the experimental data is fair), TEHD modelling

with deformable both the rotor and the pad would be the preferred modelling approach. The reason is that the rotor deformations will partially change the final lubricant film near the H_{min} location, especially in the radial direction.

Regarding bearings with artificial surface texturing, a textured thrust slider bearing with 8 by 8 orthogonal dimples (in the longitudinal and transverse directions, respectively) has been studied by means of isothermal, THD and TEHD modelling. The main conclusions drawn from the results, point to the need of TEHD modelling for thrust bearings with textures that operate from moderate to high loads. The texture cavities operate as insulators not allowing convection for a range of H_{min} over texture depth values. This ratio in addition with the local Reynolds number, determine the generation of a recirculating zone inside the dimples. If the speed of the recirculating zone is low near the bottom of the dimple, the heat flux minimises. This drives to the conclusion, that the operational H_{min} range needs to be taken into account in order to determine the texture depth. For that to be possible, TEHD modelling is definitely required.

A comparison of the textured and untextured parallel slider identified some key operational differences. First, the textured slider exhibited lower values of friction. This can probably be attributed to the considerably higher operational temperatures. Furthermore, the pressure build-up mechanism of the parallel thrust bearing is less pronounced in the case of a textured slider. The larger film thickness inside the dimples does not allow the converging geometry generated by the thermal deformation to increase pressure. Thus, the textured slider only generates pressure from the localized step effect of the textures. A larger high pressure zone is present in the textured bearing, something that aids in restricting the cavitation zone near the trailing zone, where the diverging geometry is generated. Finally, the untextured parallel thrust bearing operates at higher values of H_{min}, which gives an advantage over the operational safety of the bearing.

Before selecting artificial surface texturing for new designs that operate at specific loads over 0.3 MPa, one should consider the higher manufacturing cost, the higher operational temperatures, and lower load carrying capacity of the textured bearing in comparison with the simple untextured parallel one.

Finally, three different coatings have been modelled, but no conclusive results could be established. The main reason for the lack of computational results has been the remarkably high computational cost of the TEHD modelling for materials with high thermal expansion coefficient. In order to evaluate the performance characteristics of a coated parallel thrust bearing, a TEHD modelling is the only option, because the main pressure build-up mechanism is the thermal deformation of the pad and rotor geometry.

5.2 Future Directions

Evaluating the results of the present Thesis, a more clear view for the next research steps in the scientific domain of the present Thesis has been formed.

As mentioned above, the structural boundary conditions may affect the performance of the parallel thrust bearing, and this should be investigated further.

The very limited analysis of the coated bearings identifies the importance of analysing their effect on the pressure build-up mechanism for the parallel bearing. Moreover, the study of a bearing with dual coating is believed that can make the simple parallel design more competitive in comparison to more complex contemporary bearing types.

A longer and more structured analysis of the artificial surface texturing is needed, in terms of TEHD evaluations, for a range of different design parameters, such as texture shape depth, density, etc.

Finally, the most important progress would be a time dependent modelling approach for the parallel thrust bearing, in order to understand the film generation at start-up, and how each mechanism contributes during the progression of the phenomenon.

5.3 Final Remarks

Many different physical phenomena take place in the parallel thrust bearing, in order for load carrying capacity to be generated. The most pronounced one is the effect of the thermal deformation, which generates a converging wedge that can support a considerable load.

To evaluate the performance of such a bearing, a 3D TEHD CFD model is required, and the groove geometry must be modelled. The temperature evaluation and boundary conditions are of utmost importance. Attention must be given to the structural boundary condition, because preliminary investigation suggested that different location and/or number of fixation points can give different deformation profiles.

The imperfection of individual sector pads can introduce different loading conditions on the thrust bearing. Thus measuring a single pad probably would not describe the real working conditions of the whole bearing.

The tapered-land and pocket configurations do not need the expensive TEHD modelling approach.

Textured bearings, especially moderately or highly loaded ones, need to be studied taking into account the thermal deformation of the pad geometry.

Finally, the effect of coatings on parallel thrust bearings needs to be investigated. A hybrid two coating design might enhance considerably the parallel thrust bearings performance.

Bibliography

[1] B. Tower. "First report on friction experiments". In: *Proceedings of the institution of mechanical engineers* 34.1 (1883), pp. 632–659. DOI: 10.1243/PIME_PROC_1883_034_028_02.

[2] M. He and J. Byrne. "Fundamentals of Fluid Film Thrust Bearing Operation and Modeling". In: *Asia turbomachinery & pump symposium*. 2018.

[3] K. Holmberg and A. Erdemir. "Influence of tribology on global energy consumption, costs and emissions". In: *Friction* 5.3 (2017), pp. 263–284. DOI: 10.1007/s40544-017-0183-5.

[4] O. Reynolds. "On the Theory of Lubrication and Its Application to Mr . Beauchamp Tower ' s Experiments , Including an Experimental Determination of the Viscosity of Olive Oil". In: *Philosphical Transactions of the Royal Society of London* 177.May (1886), pp. 157–234. DOI: 10.1098/rstl.1886.0005.

[5] A. Fogg. "Fluid Film Lubrication of Parallel Thrust Surfaces". In: *Proceedings of the Institution of Mechanical Engineers* 155.1 (1946), pp. 49–67. DOI: 10.1243/PIME_PROC_1946_155_011_02.

[6] M.E. Salama. "The Effect of Macro-Roughness on the Performance of Parallel Thrust Bearings". In: *Proceedings of the Institution of Mechanical Engineers* 163.1 (1950), pp. 149–161. DOI: 10.1243/pime_proc_1950_163_019_02.

[7] A. Cameron and W.L. Wood. "Parallel surface thrust bearing". In: *ASLE Transactions* 1.2 (1958), pp. 254–258. DOI: 10.1080/05698195808972338.

[8] A. Cameron. "The viscosity wedge". In: *ASLE Transactions* 1.2 (1958), pp. 248–253. DOI: 10.1080/05698195808972337.

[9] W. Lewicki. "Theory of hydrodynamic lubrication in parallel sliding". In: *The Engineer* 200 (1955), pp. 939–941. DOI: 10.1016/0043-1648(58)90581-7.

[10] C.H.T. Pan. "Calculation of Pressure, Shear, and Flow in Lubricating Films for High Speed Bearings". In: *Journal of Lubrication Technology* 96.1 (Jan. 1974), pp. 80–94. DOI: 10.1115/1.3451919.

[11] N. Tipei. "Flow and Pressure Head at the Inlet of Narrow Passages, Without Upstream Free Surface". In: *Journal of Lubrication Technology* 104.2 (Apr. 1982), pp. 196–202. DOI: 10.1115/1.3253180.

[12] D.D. Heckelman and C.M. Ettles. "Viscous and inertial pressure effects at the inlet to a bearing film". In: *Tribology Transactions* 31.1 (1988), pp. 1–5. DOI: 10.1080/10402008808981791.

[13] S. Taniguchi, T. Makino, K. Takeshita, and T. Ichimura. "A thermohydrbdynamic analysis of large tilting-pad journal bearing in laminar and turbulent flow regimes with mixing". In: *Journal of Tribology* 112.3 (1990), pp. 542–550. ISSN: 15288897. DOI: 10.1115/1.2920291.

[14] D. Dowson and J.D. Hudson. "Thermo-Hydrodynamic Analysis of the Infinite Slider Bearing: Part I, The Plane-Inclined Slider Bearing". In: *Proc IMechE* (1963), pp. 34–44. DOI: 10.1016/0043-1648(63)90302-8.

[15] W.B. Hunter and O.C. Zienkiewicz. "Effect of temperature variations across the lubricant films in the theory of hydrodynamic lubrication." In: *J. Mech. Engng Sci* 2 (1960), p. 52. DOI: 10.1243/JMES_JOUR_1960_002_009_02.

[16] C.M. Ettles and A. Cameron. "Paper 17: The Action of the Parallel-Surface Thrust Bearing". In: *Proceedings of the Institution of Mechanical Engineers, Conference Proceedings* 180.11 (1965), pp. 61–75. DOI: 10.1243/pime_conf_1965_180_320_02.

[17] P.B. Neal. "Film lubrication of plane-faced thrust pads". In: *Proc. Inst. Mech. Engrs, Lubrication and Wear Convention*. Vol. 52. 1963. DOI: 10.1016/0043-1648(63)90293-x.

[18] I.G. Currie, C.A. Brockley, and F.A. Dvorak. "Thermal wedge lubrication of parallel surface thrust bearings". In: *Journal of Fluids Engineering, Transactions of the ASME* 87.4 (1965), pp. 823–830. DOI: 10.1115/1.3650825.

[19] C.M. Ettles. "Hydrodynamic thrust bearing study". PhD thesis. Imperial College, 1965.

[20] C.M. Ettles. "Hot oil carry-over in thrust bearings". In: *Industrial Lubrication and Tribology* 22.8 (1970), p. 209. DOI: 10.1243/PIME_CONF_1969_184_373_02.

[21] V. Zouzoulas and C.I. Papadopoulos. "3-D thermohydrodynamic analysis of textured, grooved, pocketed and hydrophobic pivoted-pad thrust bearings". In: *Tribology International* 110 (2017), pp. 426–440. DOI: 10.1016/j.triboint.2016.10.001.

[22] C.L. Robinson and A. Cameron. "Studies in hydronamic thrust bearings I. Theory considering thermal and elastic distortions". In: *Philosophical Transactions of the Royal Society of London. Series A, Mathematical and Physical Sciences* 278.1283 (1975), pp. 351–366. DOI: 10.1098/rsta.1975.0029.

[23] A.O. Lebeck. "Parallel Sliding Load Support in the Mixed Friction Regime. Part 1—The Experimental Data". In: *Journal of Tribology* 109.1 (Jan. 1987), pp. 189–195. DOI: 10.1115/1.3261317.

[24] A.O. Lebeck. "Parallel Sliding Load Support in the Mixed Friction Regime. Part 2—Evaluation of the Mechanisms". In: *Journal of Tribology* 109.1 (Jan. 1987), pp. 196–205. DOI: 10.1115/1.3261319.

[25] C.M. Ettles. "Transient thermoelastic effects in fluid film bearings". In: *Wear* 79.1 (1982), pp. 53–71. DOI: 10.1016/0043-1648(82)90203-4.

[26] S.M. Rohde and Kong Ping Oh. "A Thermoelastohydrodynamic Analysis of a Finite Slider Bearing". In: *Journal of Lubrication Technology* 97.3 (July 1975), pp. 450–460. DOI: 10.1115/1.3452632.

[27] T.S. Brockett, L.E. Barrett, and P.E. Allaire. "Thermoelastohydrodynamic analysis of fixed geometry thrust bearings including runner deformation". In: *Tribology Transactions* 39.3 (1996), pp. 555–562. DOI: 10.1080/10402009608983566.

[28] Y. El-Saie and R.T. Fenner. "Three-dimensional thermoelastohydrodynamic analysis of pivoted pad thrust bearings Part 1: Treatment of bearing deflections and fluid film flow and heat transfer". In: *Proceedings of the Institution of Mechanical Engineers, Part C: Journal of Mechanical Engineering Science* 202.1 (1988), pp. 39–50. DOI: 10.1243/PIME_PROC_1988_202_084_02.

[29] Y. El-Saie and R.T. Fenner. "Three-dimensional thermoelastohydrodynamic analysis of pivoted pad thrust bearings Part 2: Application of theory and comparison with experiments". In: *Proceedings of the Institution of Mechanical Engineers, Part C: Journal of Mechanical Engineering Science* 202.1 (1988), pp. 51–62. DOI: 10.1243/PIME_PROC_1988_202_085_02.

[30] P. Monmousseau, M. Fillon, and J. Frene. "Transient Thermoelastohydrodynamic Study of Tilting-Pad Journal Bearings Under Dynamic Loading". In: *Journal of Engineering for Gas Turbines and Power* 120.2 (Apr. 1998), pp. 405–409. DOI: 10.1115/1.2818137.

[31] B.R. Kucinschi, K.J. DeWitt, and M.D. Pascovici. "Thermoelastohydrodynamic (TEHD) analysis of a grooved thrust washer". In: *Journal of Tribology* 126.2 (2004), pp. 267–274. DOI: 10.1115/1.1645298.

[32] X. Jiang, J. Wang, and J. Fang. "Thermal elastohydrodynamic lubrication analysis of tilting pad thrust bearings". In: *Proceedings of the Institution of Mechanical Engineers, Part J: Journal of Engineering Tribology* 225.2 (2011), pp. 51–57. DOI: 10.1177/2041305X10394408.

[33] H. Tang, Y. Ren, and J. Xiang. "A novel model for predicting thermoelastohydrodynamic lubrication characteristics of slipper pair in axial piston pump". In: *International Journal of Mechanical Sciences* 124-125 (2017), pp. 109–121. DOI: 10.1016/j.ijmecsci.2017.03.010.

[34] M. Hartinger, M.L. Dumont, S. Ioannides, D. Gosman, and H. Spikes. "CFD modeling of a thermal and shear-thinning elastohydrodynamic line contact". In: *Journal of Tribology* 130.4 (2008), pp. 1–16. DOI: 10.1115/1.2958077.

[35] L. Zhai, Yongyao L., X. Liu, F. Chen, Y. Xiao, and Z. Wang. "Numerical simulations for the fluid-thermal-structural interaction lubrication in a tilting pad thrust bearing". In: *Engineering Computations (Swansea, Wales)* 34.4 (2017), pp. 1149–1165. DOI: 10.1108/EC-08-2015-0209.

[36] X. Deng, C. Watson, M. He, R. Fittro, and H. Wood. "Comparison of experimental, thermoelastohydrodynamic (TEHD) and thermal, non-deforming computational fluid dynamics (CFD) results for thrust bearings: Part II". In: *ASME International Mechanical Engineering Congress and Exposition, Proceedings (IMECE)* 7 (2018), pp. 1–10. DOI: 10.1115/IMECE201887798.

[37] X. Liang, X. Yan, W. Ouyang, R. Wood, and Z. Liu. "Thermo-Elasto-Hydrodynamic analysis and optimization of rubber-supported water-lubricated thrust bearings with polymer coated pads". In: *Tribology International* 138.March (2019), pp. 365–379. DOI: 10.1016/j.triboint.2019.06.012.

[38] C.I. Papadopoulos, E. Efstathiou, P. Nikolakopoulos, and L. Kaiktsis. "Geometry Optimization of Textured Three-Dimensional Micro- Thrust Bearings". In: *Journal of Tribology* 133.4 (Oct. 2011). DOI: 10.1115/1.4004990.

[39] V.G. Marian, D. Gabriel, G. Knoll, and S. Filippone. "Theoretical and Experimental Analysis of a Laser Textured Thrust Bearing". In: *Tribology Letters* 44.3 (Sept. 2011), p. 335. DOI: 10.1007/s11249-011-9857-8.

[40] R.B. Siripuram and L.S. Stephens. "Effect of Deterministic Asperity Geometry on Hydrodynamic Lubrication". In: *Journal of Tribology* 126.3 (June 2004), pp. 527–534. DOI: 10.1115/1.1715104.

[41] A. Shinkarenko, Y. Kligerman, and I. Etsion. "The effect of surface texturing in soft elasto-hydrodynamic lubrication". In: *Tribology International* 42.2 (2009), pp. 284–292. DOI: 10.1016/j.triboint.2008.06.008.

[42] I. Etsion and E. Sher. "Improving fuel efficiency with laser surface textured piston rings". In: *Tribology International* 42 (Apr. 2009), pp. 542–547. DOI: 10.1016/j.triboint.2008.02.015.

[43] W. Grabon, W. Koszela, P. Pawlus, and S. Ochwat. "Improving tribological behaviour of piston ring–cylinder liner frictional pair by liner surface texturing". In: *Tribology International* 61 (2013), pp. 102–108. DOI: 10.1016/j.triboint.2012.11.027.

[44] P. Lu, R.J.K. Wood, M.G. Gee, L. Wang, and W. Pfleging. "The friction reducing effect of square-shaped surface textures under lubricated line-contacts-an experimental study". In: *Lubricants* 4.3 (2016). DOI: 10.3390/lubricants4030026.

[45] V. Brizmer and Y. Kligerman. "A Laser Surface Textured Journal Bearing". In: *Journal of Tribology-transactions of The Asme* 134 (2012), p. 031702. DOI: 10.1115/1.4006511.

[46] S.C. Vlădescu, . Fowell, L. Mattsson, and T. Reddyhoff. "The effects of laser surface texture applied to internal combustion engine journal bearing shells – An experimental study". In: *Tribology International* 134 (2019), pp. 317–327. DOI: 10.1016/j.triboint.2019.02.009.

[47] Hiroyuki Yamada, Hiroo Taura, and Satoru Kaneko. "Static Characteristics of Journal Bearings with Square Dimples". In: *Journal of Tribology* 139.5 (2017), pp. 1–11. ISSN: 15288897. DOI: 10.1115/1.4035778.

[48] M. Fillon. "Is surface texturing really efficient in hydrodynamic sliding bearings ?" In: March. Kaiserslautern: Bearing world, 2018, pp. 6–7.

[49] Izhak Etsion and Gregory Halperin. "A laser surface textured hydrostatic mechanical seal". In: *Sealing Technology* 3 (2003), pp. 6–9. DOI: 10.1016/s1350-4789(03)03018-6.

[50] N. Brunetiere, B. Tournerie, and J. Frene. "TEHD Lubrication of Mechanical Face Seals in Stable Tracking Mode: Part 1—Numerical Model and Experiments ". In: *Journal of Tribology* 125.3 (June 2003), pp. 608–616. DOI: 10.1115/1.1510885.

[51] N. Brunetière and B. Tournerie. "Numerical analysis of a surface-textured mechanical seal operating in mixed lubrication regime". In: *Tribology International* 49 (2012), pp. 80–89. DOI: 10.1016/j.triboint.2012.01.003.

[52] V. Brizmer, Y. Kligerman, and I. Etsion. "A Laser Surface Textured Parallel Thrust Bearing". In: *Tribology Transactions* 46.3 (2003), pp. 397–403. DOI: 10.1080/10402000308982643.

[53] V.G. Marian, M. Kilian, and W. Scholz. "Theoretical and experimental analysis of a partially textured thrust bearing with square dimples". In: *Proceedings of the Institution of Mechanical Engineers, Part J: Journal of Engineering Tribology* 221.7 (2007), pp. 771–778. DOI: 10.1243/13506501JET292.

[54] M. Dobrica and M. Fillon. "Reynolds' model suitability in simulating rayleigh step bearing thermohydrodynamic problems". In: *Tribology Transactions* 48.4 (2005), pp. 522–530. DOI: 10.1080/05698190500385088.

[55] M.B. Dobrica and M. Fillon. "About the validity of Reynolds equation and inertia effects in textured sliders of infinite width". In: *Proceedings of the Institution of Mechanical Engineers, Part J: Journal of Engineering Tribology* 223.1 (2009), pp. 69–78. DOI: 10.1243/13506501JET433.

[56] Y. Feldman, Y. Kligerman, I. Etsion, and S. Haber. "The Validity of the Reynolds Equation in Modeling Hydrostatic Effects in Gas Lubricated Textured Parallel Surfaces". In: *Journal of Tribology* 128.2 (Nov. 2005), pp. 345–350. DOI: 10.1115/1.2148419.

[57] Y. Henry, J. Bouyer, and M. Fillon. "An experimental analysis of the hydrodynamic contribution of textured thrust bearings during steady-state operation: A comparison with the untextured parallel surface configuration". In: *Proceedings of the Institution of Mechanical Engineers, Part J: Journal of Engineering Tribology* 229.4 (2015), pp. 362–375. DOI: 10.1177/1350650114537484.

[58] Y. Henry, J. Bouyer, and M. Fillon. "Experimental analysis of the hydrodynamic effect during start-up of fixed geometry thrust bearings". In: *Tribology International* 120 (2018), pp. 299–308. DOI: 10.1016/j.triboint.2017.12.021.

[59] A. Kovalchenko, O. Ajayi, A. Erdemir, G. Fenske, and I. Etsion. "The effect of laser surface texturing on transitions in lubrication regimes during unidirectional sliding contact". In: *Tribology International* 38.3 (2005). Boundary Lubrication, pp. 219–225. DOI: 10.1016/j.triboint.2004.08.004.

[60] T. Ibatan, M.S. Uddin, and M.A.K. Chowdhury. "Recent development on surface texturing in enhancing tribological performance of bearing sliders". In: *Surface and Coatings Technology* 272 (2015), pp. 102–120. DOI: 10.1016/j.surfcoat.2015.04.017.

[61] L. Bai, Y. Meng, and V. Zhang. "Experimental Study on Transient Behavior of Cavitation Phenomenon in Textured Thrust Bearings". In: *Tribology Letters* 63 (Aug. 2016). DOI: 10.1007/s11249-016-0715-6.

[62] M. Chalkiopoulos, A. Charitopoulos, M. Fillon, and C.I. Papadopoulos. "Effects of thermal and mechanical deformations on textured thrust bearings optimally designed by a THD calculation method". In: *Tribology International* 148 (2020), p. 106303. DOI: 10.1016/j.triboint.2020.106303.

[63] S. Biswas, T. Chander, and D.S. Gole. "Some observations on the surface and subsurface features of failed babbitt pads". In: *Tribology International* 17.2 (1984), pp. 99–105. DOI: 10.1016/0301-679X(84)90051-3.

[64] C.M. Ettles, R.T. Knox, J.H. Ferguson, and D. Horner. "Test results for PTFE-Faced thrust pads, with direct comparison against babbitt-faced pads and correlation with analysis". In: *Journal of Tribology* 125.4 (2003), pp. 814–823. DOI: 10.1115/1.1576427.

[65] A. Schubert and T Brescianini. "Application of a PEEK coated thrust bearing on the occasion of a refurbishment of a large hydro power plant with concurrent load increase." In: In Proceedings of the 10th EDF/Pprime Poitiers Workshop: Condition Monitoring, Performance Improvement and Safe Operation of Bearings, Futuroscope, France, 6–7 October 2011, 2018.

[66] M. Wodtke and M. Wasilczuk. "Evaluation of apparent Young?'s modulus of the composite polymer layers used as sliding surfaces in hydrodynamic thrust bearings". In: *Tribology International* 97 (2016), pp. 244–252. DOI: 10.1016/j.triboint.2016.01.040.

[67] Sergei Glavatskih, Michał Wasilczuk, and Michel Fillon. "Performance peculiarities of PTFE-faced tilting-pad thrust bearings." In: *3rd EDF/LMS Workshop on "Improvement of bearing performance under severe operating conditions"*. Oct. 2004. DOI: 10.13140/2.1.2849.6323.

[68] J.E.L. Simmons, R.T. Knox, and W.O. Moss. "The development of PTFE (polytetrafluoroethylene) faced hydrodynamic thrust bearings for hydrogenerator application in the United Kingdom". In: *Proceedings of the Institution of Mechanical Engineers, Part J: Journal of Engineering Tribology* 212.5 (1998), pp. 345–352. DOI: 10.1243/1350650981542155.

[69] N. Satyanarayana, Sujeet K. Sinha, and Boon Hong Ong. "Tribology of a novel UHMWPE/PFPE dual-film coated onto Si surface". In: *Sensors and Actuators, A: Physical* 128.1 (2006), pp. 98–108. DOI: 10.1016/j.sna.2005.12.042.

[70] S. Jahanmir, A.Z. Hunsberger, and H. Heshmat. "Load capacity and durability of H-DLC coated hydrodynamic thrust bearings". In: *Journal of Tribology* 133.3 (2011). DOI: 10.1115/1.4003997.

[71] P. Lan, J.L. Meyer, B. Vaezian, and A.A. Polycarpou. "Advanced polymeric coatings for tilting pad bearings with application in the oil and gas industry". In: *Wear* 354-355 (2016), pp. 10–20. DOI: 10.1016/j.wear.2016.02.013.

[72] Konstantinos Katsaros, Dimitrios A. Bompos, Pantelis G. Nikolakopoulos, and Stephanos Theodossiades. "Thermal-hydrodynamic behaviour of coated pivoted pad thrust bearings: Comparison between Babbitt, PTFE and DLC". In: *Lubricants* 6.2 (2018). DOI: 10.3390/lubricants6020050.

[73] R. Gheisari, P. Lan, and A.A. Polycarpou. "Tribological Interactions of Advanced Polymeric Coatings". In: *Encyclopedia of Renewable and Sustainable Materials*. Oxford: Elsevier, 2020, pp. 638–647. DOI: 10.1016/B978-0-12-803581-8.10811-2.

[74] Z. Wang and D. Gao. "Comparative investigation on the tribological behavior of reinforced plastic composite under natural seawater lubrication". In: *Materials and Design* 51 (2013), pp. 983–988. DOI: 10.1016/j.matdes.2013.04.017.

[75] M. Fillon and S. B. Glavatskih. "PTFE-faced centre pivot thrust pad bearings: Factors affecting TEHD performance". In: *Tribology International* 41.12 (2008), pp. 1219–1225. DOI: 10.1016/j.triboint.2008.03.011.

[76] A. Charitopoulos, E. Efstathiou, C.I. Papadopoulos, P Nikolakopoulos, and L Kaiktsis. "Effects of manufacturing errors on tribological characteristics of 3-D textured micro- thrust bearings". In: *CIRP Journal of Manufacturing Science and Technology* 6.2 (2013), pp. 128–142. DOI: 10.1016/j.cirpj.2012.12.001.

[77] Y. Henry. "Analyse expérimentale de l'effet de la texturation des patins sur le comportement des butées hydrodynamiques à géométrie fixe". PhD thesis. université de poitiers, 2013, p. 205.

Appendix A

Boundary Conditions

A.1 Slider bearing boundary conditions

TABLE A.1 – Thermal and structural boundary conditions for the slider TEHD model with rigid rotor.

Location	Temperature BC's	Structural BC's
	Stator	
Sides	Periodic conditions	Uy=0
Stator Bottom	HTC: 1000 $W/(m^2K)$, T = 40°C	Ux=0,Uy=0,Uz=0
Stator Inner	HTC: 200 $W/(m^2K)$, T = 40°C	Free
Stator Outer	HTC: 25 $W/(m^2K)$, T = 40°C	Free
Fluid Stator Interface	2-way FSI: Continuity of heat flux and temperature	Free
	Slider	
Sides	Periodic conditions	Fixed
Rotor Outer	HTC: 25 $W/(m^2K)$, T = 20°C	Fixed
Axis Fixation	HTC: 1000 $W/(m^2K)$, T = 20°C	Fixed
Rotor Oil Res.	HTC: 25 $W/(m^2K)$, T = 20°C	Fixed
Fluid Rotor Interface	Continuity of heat flux and temperature, Sliding velocity 22 m/s	Fixed
	Lubricant	
Sides	Periodic conditions	Frictionless support
Fluid Inner	Opening with F.P. 0.1MPa, Temperature 40°C	Ux=0, Uy=0
Fluid Outer	Outlet with static pres. of 0 and Temp. 20°C	Ux=0, Uy=0

*Heat Transfer coefficient (HTC)

**Feeding Pressure (F.P.)

TABLE A.2 – Thermal and structural boundary conditions for the slider THD model.

Location	Temperature BC's	Structural BC's
	Stator	
Sides	Periodic conditions	Fixed
Stator Bottom	HTC: 1000 $W/(m^2K)$, T = 40°C	Fixed
Stator Inner	HTC: 200 $W/(m^2K)$, T = 40°C	Fixed
Stator Outer	HTC: 25 $W/(m^2K)$, T = 40°C	Fixed
Fluid Stator Interface	Continuity of heat flux and temperature	Fixed
	Rotor	
Sides	Periodic conditions	Fixed
Slider Outer	HTC: 25 $W/(m^2K)$, T = 20°C	Fixed
Slider Inner	HTC: 1000 $W/(m^2K)$, T = 20°C	Fixed
Rotor Oil Res.	HTC: 25 $W/(m^2K)$, T = 20°C	Fixed
Fluid Rotor Interface	Continuity of heat flux and temperature, Sliding velocity 22 m/s	Fixed
	Lubricant	
Sides	Periodic conditions	Fixed
Fluid Inner	Opening with F.P. 0.1MPa, Temperature 40°C	Fixed
Fluid Outer	Outlet with static pres. of 0 and Temp. 20°C	Fixed

*Heat Transfer coefficient (HTC)

**Feeding Pressure (F.P.)

TABLE A.3 – Boundary conditions for the slider Isothermal model.

Lubricant		
Sides	Periodic conditions	Fixed
Fluid Inner	Opening with F.P. 0.1MPa	Fixed
Fluid Outer	Outlet with static pressure of 0MPa	Fixed
Fluid Pad Interface	No sliding wall	Fixed
Fluid Rotor Interface	Sliding velocity 22 m/s	Fixed

*Feeding Pressure (F.P.)

A.2 Full eight sector pad thrust bearing boundary conditions

TABLE A.4 – Thermal and structural boundary conditions for the full sector pad TEHD model with rigid rotor.

Location	Temperature BC's	Structural BC's
	Stator	
Pad Bottom	HTC: 1000 $W/(m^2K)$, T = 40°C	Uz=0
Pad Inner	HTC: 200 $W/(m^2K)$, T = 40°C	Free
Pad Outer	HTC: 25 $W/(m^2K)$, T = 40°C	Free
Fluid Stator Interface	2-way FSI: Continuity of heat flux and temperature	Free
	Rotor	
Rotor Outer	HTC: 25 $W/(m^2K)$, T = 20°C	Fixed
Axis Fixation	HTC: 1000 $W/(m^2K)$, T = 20°C	Fixed
Rotor Oil Res.	HTC: 300 $W/(m^2K)$, T = 40	Fixed
Fluid Rotor Interface	Continuity of heat flux and temperature, Rotating velocity 6000 RPM	Fixed
	Lubricant	
Fluid Inner	Opening with F.P. 0.1MPa, Temperature 40°C	Ux=0, Uy=0
Fluid Outer	Outlet with static pres. of 0 and Temp. 20°C	Ux=0, Uy=0

*Heat Transfer coefficient (HTC)

**Feeding Pressure (F.P.)

TABLE A.5 – Thermal and structural boundary conditions for the full sector pad TEHD model with deformable pad and rotor.

Location	Temperature BC's	Structural BC's
	Stator	
Pad Bottom	HTC: 1000 $W/(m^2K)$, T = 40°C	Uz=0
Pad Inner	HTC: 200 $W/(m^2K)$, T = 40°C	Free
Pad Outer	HTC: 25 $W/(m^2K)$, T = 40°C	Free
Fluid Stator Interface	2-way FSI: Continuity of heat flux and temperature	Free
	Rotor	
Rotor Outer	HTC: 25 $W/(m^2K)$, T = 20°C	Fixed
Axis Fixation	HTC: 1000 $W/(m^2K)$, T = 20°C	Fixed
Rotor Oil Res.	HTC: 300 $W/(m^2K)$, T = 40	Free
Fluid Rotor Interface	2-way FSI: Continuity of heat flux and temperature, Rotating velocity 6000 RPM	Free
	Lubricant	
Fluid Inner	Opening with F.P. 0.1MPa, Temperature 40°C	Ux=0, Uy=0
Fluid Outer	Outlet with static pres. of 0 and Temp. 20°C	Ux=0, Uy=0

*Heat Transfer coefficient (HTC)

**Feeding Pressure (F.P.)

Appendix B

Mesh Details

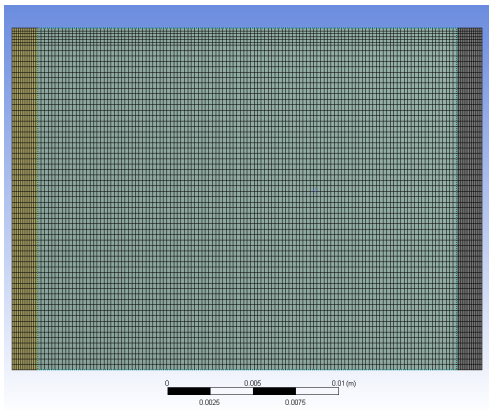

(A) Fluid top view

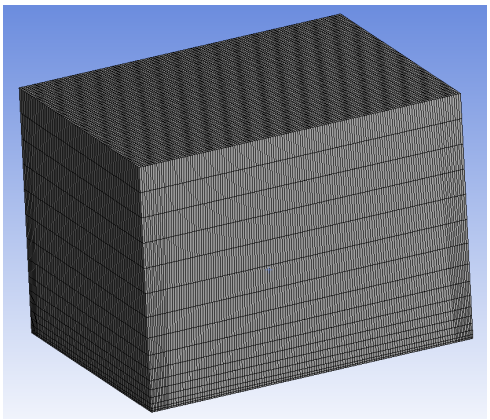

(B) Rotor

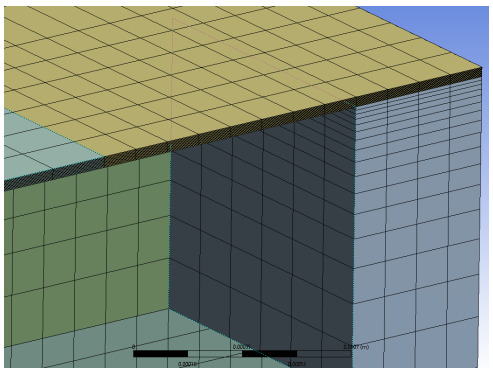

(C) Fluid groove iso-view

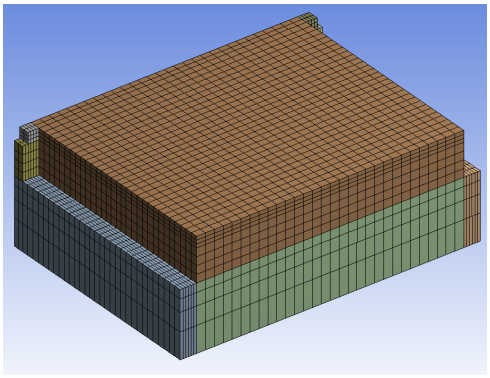

(D) Pad

FIGURE B.1 – Mesh details of the parallel slider model.

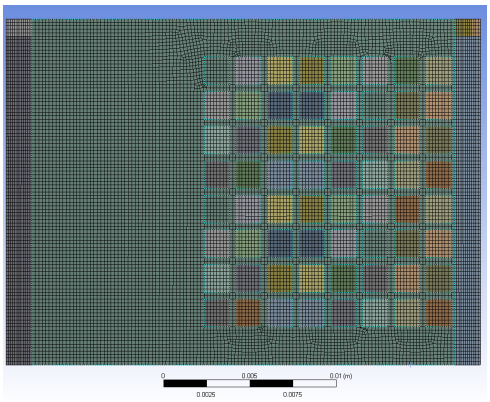

(A) Fluid top view

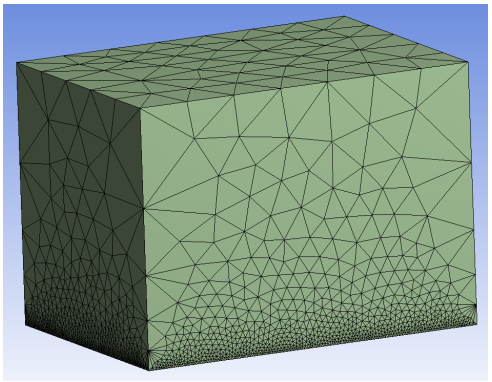

(B) Rotor

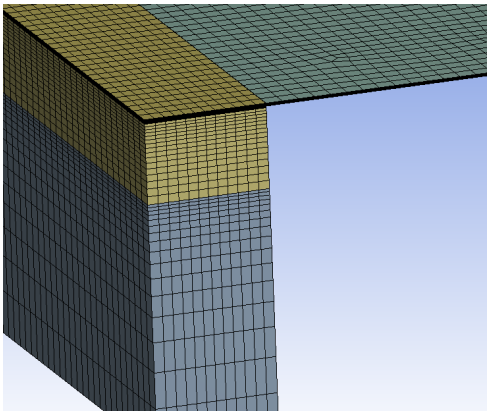

(C) Fluid groove iso-view

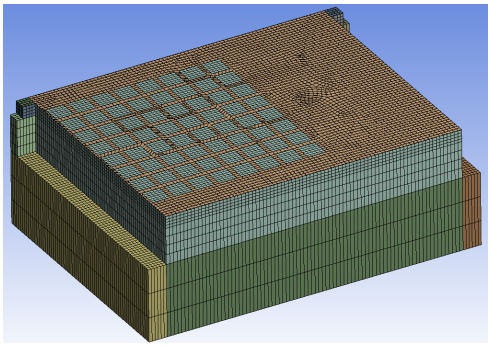

(D) Pad

FIGURE B.2 – Mesh details of the textured parallel slider model.

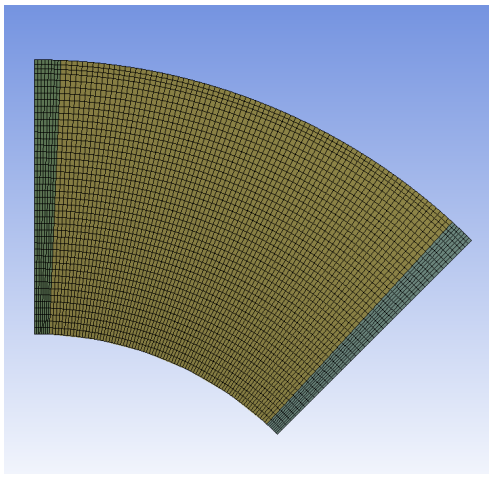

(A) Fluid top view

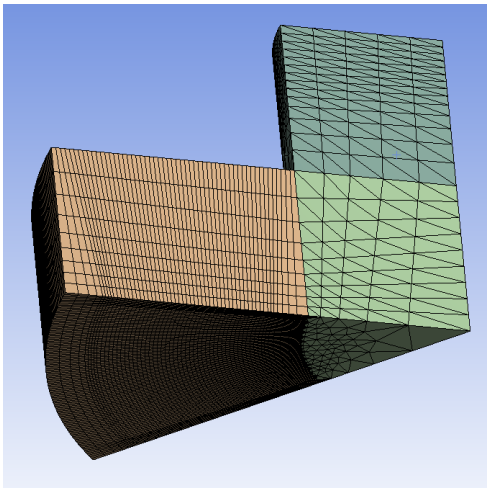

(B) Rotor

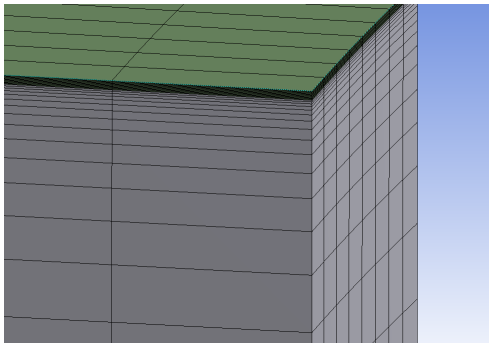

(C) Fluid groove iso-view

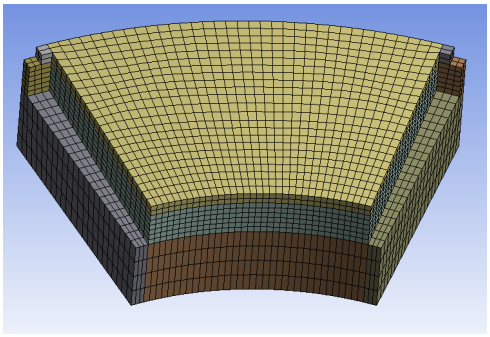

(D) Pad

FIGURE B.3 – Mesh details of the single sector pad parallel model.

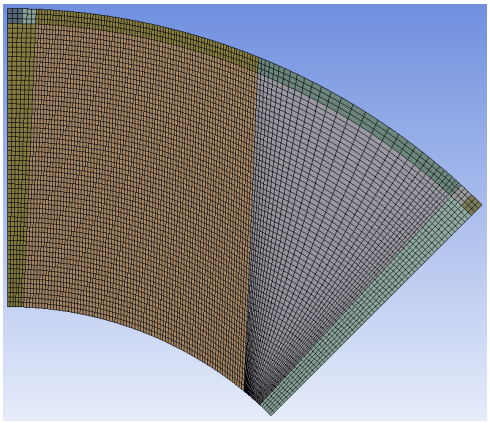

(A) Fluid top view

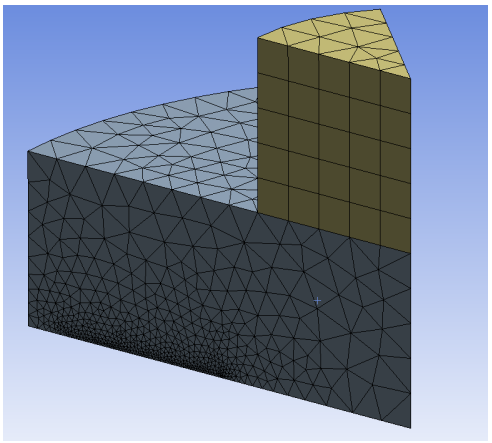

(B) Rotor

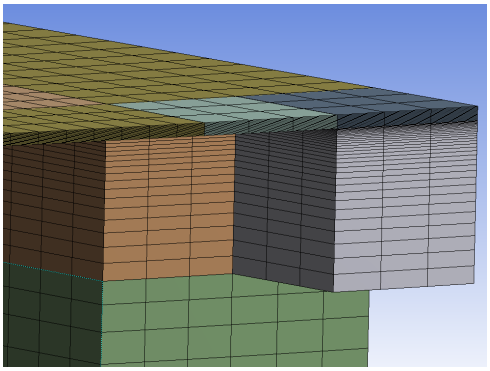

(C) Fluid groove iso-view

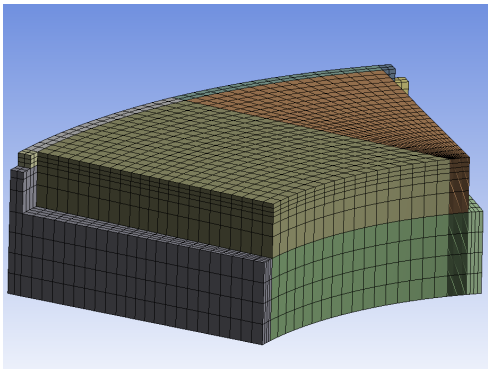

(D) Pad

FIGURE B.4 – Mesh details of the single sector pad tapered-land model.

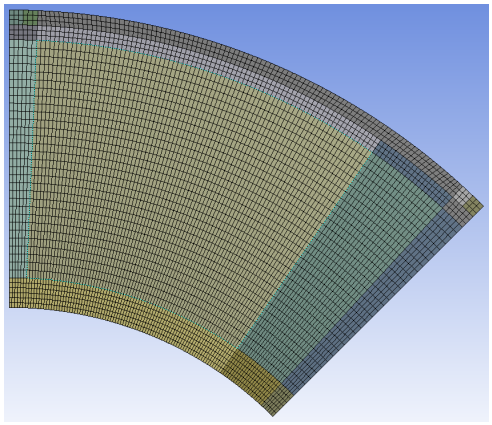

(A) Fluid top view

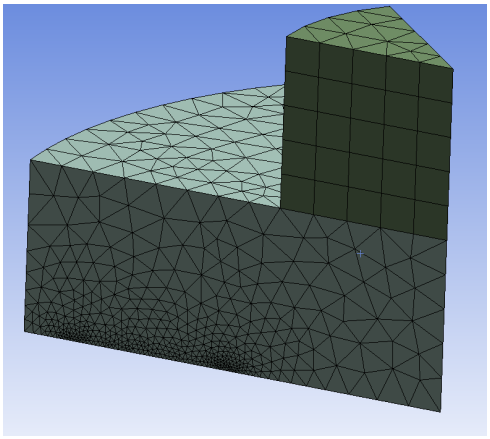

(B) Rotor

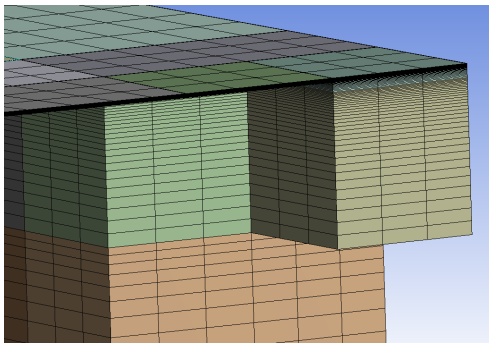

(C) Fluid groove iso-view

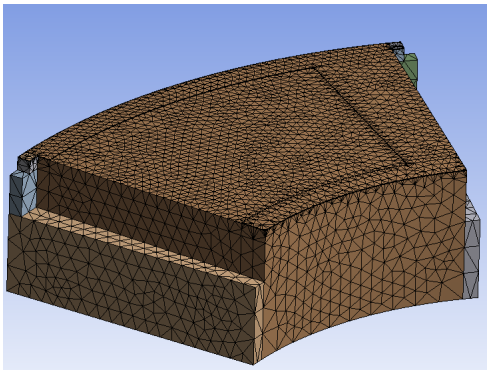

(D) Pad

FIGURE B.5 – Mesh details of the single sector pad pocket model.

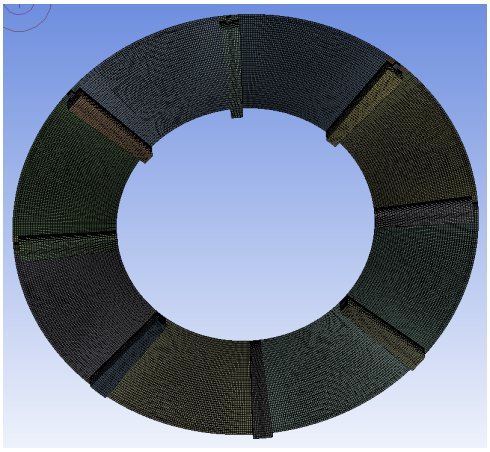

(A) Fluid top view

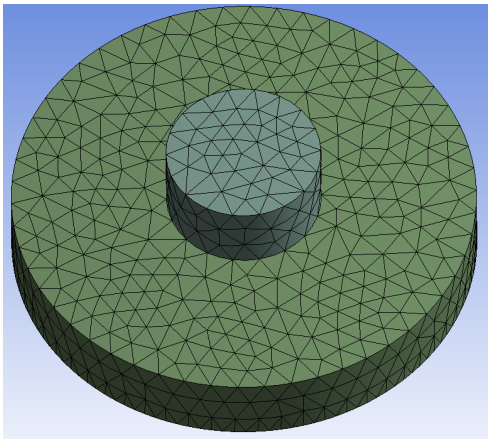

(B) Rotor

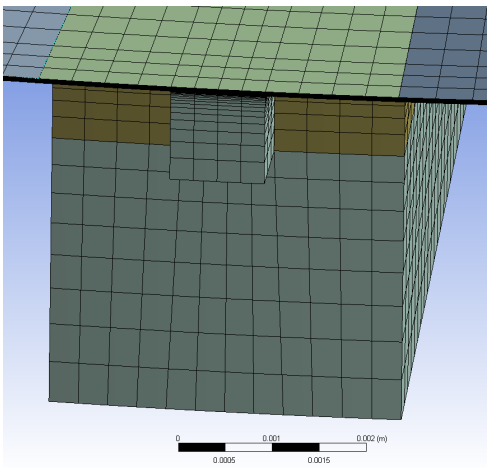

(C) Fluid groove iso-view

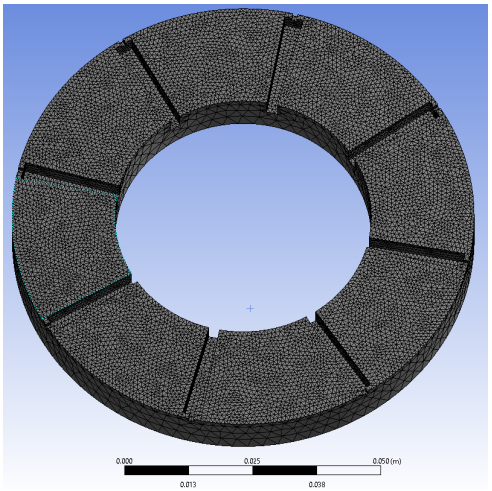

(D) Pad

FIGURE B.6 – Mesh details of the full parallel thrust bearing model.

Appendix C

Résumé étendu

Étude bibliographique

Surmonter les frictions est un des principaux objectifs de la vie quotidienne. On estime que 23% de la consommation totale d'énergie aujourd'hui proviennent de pertes d'énergie dans les contacts tribologiques. Afin de réduire le gaspillage d'énergie total et de concevoir des systèmes mécaniques plus efficaces, la compréhension du mécanisme de friction est la clé. Depuis le début de l'ère industrielle, beaucoup d'efforts ont été faits pour optimiser l'efficacité des conceptions mécaniques. Des modèles analytiques et informatiques ont été générés au fil des ans pour prédire et optimiser les performances de ces conceptions. Au cours des dernières décennies, les capacités de calcul étaient réduites, conduisant ainsi à des simplifications des modèles physiques afin d'acquérir des résultats significatifs avec des ressources de calcul limitées. Cependant, au cours des 20 dernières années, la puissance de calcul disponible a considérablement augmenté, permettant à la communauté scientifique d'utiliser des modèles de calcul plus complexes et plus précis.

La présente étude se concentre sur la modélisation détaillée de la butée à surface parallèles en utilisant une approche de calcul ThermoElastoHydrodynamic (TEHD) basée sur des simulations CFD. Les objectifs de la présente étude sont (a) d'évaluer les mécanismes de génération de pression dans les butées à surfaces parallèles proposées dans la littérature au fil des années, et (b) d'évaluer comment la présente approche de modélisation complexe peut être utilisée pour évaluer les conceptions contemporaines qui ont été réalisées / évaluées à l'aide des méthodes de calcul plus simples.

Butées à faces parallèles

En 1946, Fogg présente les résultats de son expérience avec les butées à faces parallèles. Il a conclu que ces butées peuvent supporter des charges du même ordre de grandeur que les à à patins oscillants. Ces résultats contredisent la théorie classique de la lubrification, du fait de l'absence de zone convergente du film lubrifiant. De nombreuses théories ont été publiées depuis cette période afin d'expliquer ce phénomène. Les théories les plus importantes du mécanisme de montée en pression suggérées dans la littérature sont résumées ci-dessous:

1. L'effet de coin thermique.
2. L'effet de coin de viscosité.
3. L'effet de la macro-rugosité.
4. L'effet de la distorsion thermique.
5. L'effet du saut de pression en entrée du contact.

6. L'effet de la géométrie du chanfrein du bord d'attaque.

La théorie suggérée la plus significative est celle de la distorsion thermique des patins de la butée, mais des effets plus faibles sur la capacité de charge des butées à surfaces parallèles peuvent être attribués à des combinaisons des autres théories.

Texturation de surface artificielle

Dans une autre direction, et dans le sens des efforts importants réalisés ces dernières décennies pour réduire les pertes de puissance dans les systèmes mécaniques, l' influence de la texturation artificielle de surface (AST) dans les contacts tribologiques a été largement étudiée par de nombreux chercheurs. L'AST a été analysée dans une grande variété d'applications telles que les segments de piston, les paliers lisses, les butées et les garnitures mécaniques. De nombreuses formes et tailles de textures différentes ont été étudiées, des simples micro-cavités aux motifs plus complexes tels que les alvéoles rectangulaires, les aspérités positives hexagonales et les alvéoles hémisphériques, résultant en une gamme de conceptions géométriques optimales différentes, même pour de petites modifications des conditions de fonctionnement du système mécanique. Concernant les butées, l'utilisation de la texturation de surface des patins a été appliquée, dans la majorité des études, aux butées à surfaces parallèles.

Revêtements

Depuis l'ère des coussinets en bois lubrifiés à l'eau, la technologie des matériaux des paliers a considérablement évolué. Les Les premiers paliers étudiés par Beauchamp Tower étaient en acier, mais à mesure que la gamme d'applications et la compréhension des contacts tribologiques se sont élargies, de nouveaux matériaux ont été utilisés. Les alliages de cuivre et d'acier présentant de meilleures caractéristiques tribologiques sont les principaux matériaux utilisés aujourd'hui. Néanmoins, les alliages à base de plomb et plus tard, à base d'étain (régule ou métal blanc) ont été systématiquement utilisé comme revêtements sur les coussinets. De tels revêtements sont apparus avec l'utilisation industrielle des paliers,, en raison des avantages qu'ils offrent par rapport aux matériaux courants. Le revêtement Babbitt agit comme une sécurité en cas d'échec de la lubrification. Lorsque la température augmente et que la capacité hydrodynamique du palier n'est pas suffisante pour la charge appliquée, le régule fond et se comporte comme un lubrifiant jusqu'à ce que la machine tournante soit arrêtée en toute sécurité. Cela protège le rotor et l'ensemble du système mécanique, et avec un nouveau revêtement, le palier est à nouveau fonctionnel. Le revêtement mou piège également les particules d'usure, réduisant ainsi l'usure abrasive importante. Néanmoins, les revêtements de métal blanc ne sont pas toujours suffisamment fiables.

Depuis les années 1970, les revêtements de métal blanc ont, dans certains cas, été progressivement remplacés par de nouveaux matériaux tels que les polymères synthétiques. Le premier polymère utilisé était le polytétrafluoroéthylène (PTFE), qui, en raison de sa très faible propriété de frottement statique, diminuait suffisamment le frottement au démarrage permettant ainsi l'élimination de la poche de soulèvement hydrostatique dans les applications à forte charge. Par ailleurs, cela a conduit à une réduction de la taille des paliers pour un profil opérationnel donné, ce qui a entraîné des pertes par frottement plus faibles et des conceptions de paliers moins coûteuses. De plus, la plage de températures de fonctionnement normal du PTFE est

considérablement plus élevée, avec une température de fonctionnement maximale admissible supérieure à 180 °C. Le principal problème de ces revêtements est le fluage de ce matériau. Le PTFE ne peut pas supporter des charges élevées constantes pendant le cycle thermique. De nouveaux matériaux aux propriétés améliorées sont constamment testés pour produire des paliers à grande durée de vie et plus efficaces.

Modélisation théorique et numérique

Géométrie

Pour la génération du modèle des différentes étapes de la thèse, trois configurations géométriques de base ont été utilisées, un patin de glissière, un seul patin d'une butée à huit patins à faces parallèles et une butée à huit patins, sont représentés sur la Fig. C.1. Afin de pouvoir comparer les résultats de calcul avec les données expérimentales, la géométrie des butées est basée sur les données expérimentales publiées, avec une simplification des caractéristiques de rainure et de gouge. Comme on le voit sur la Fig. C.2, les parois de la rainure d'alimentation en huile ont une direction axiale. De plus, la fonction de gouge dans la géométrie de référence a une section triangulaire, mais dans le présent travail, la section de gouge est considérée comme rectangulaire afin de permettre un maillage entièrement hexaédrique dans le domaine du lubrifiant. Les principales caractéristiques géométriques de la butée hydrodynamique sont présentées dans le Tableau C.1.

TABLE C.1 – Principales données géométriques de la butée de référence.

Paramètre	Définition	Valeur	Unités
NOP	Nombre de patins	8	*ul*
$\mathbf{D_{Inner}}$	Diamètre intérieur	50	*mm*
$\mathbf{D_{Outer}}$	Diamètre extérieur	90	*mm*
$\mathbf{L_{GO}}$	Longueur de la gouge	1	*mm*
$\mathbf{D_{GO}}$	Profondeur de la gouge	1	*mm*
$\mathbf{L_{GR}}$	Largeur de rainure	3	*mm*
$\mathbf{D_{GR}}$	Profondeur de rainure	4	*mm*
$\mathbf{D_P}$	Épaisseur du stator	10	*mm*
$\mathbf{D_S}$	Épaisseur du rotor	20	*mm*

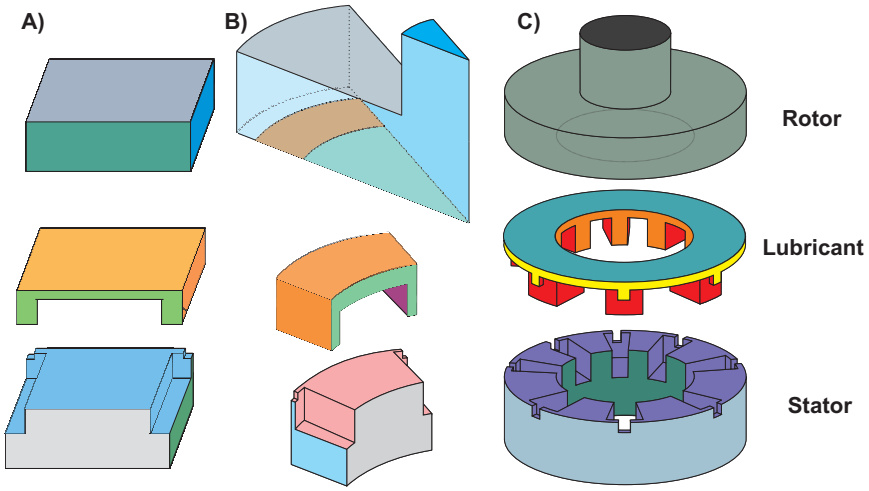

FIGURE C.1 – A) Géométrie du patin de glissière, B) Géométrie d'un seul secteur, C) Géométrie de la butée complète à 8 patins.

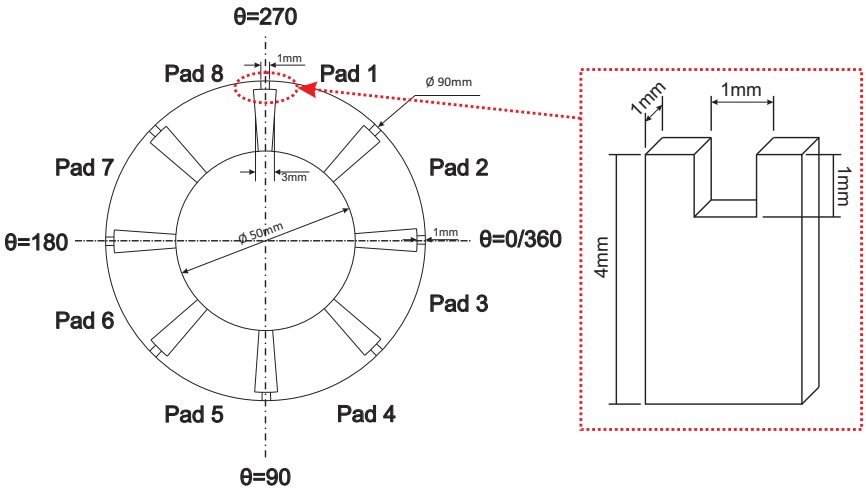

FIGURE C.2 – Vue de dessus de la butée à huit patins et détail d'une goujure.

Maillage

Un maillage typique pour la géométrie limitée à un seul secteur est représenté sur la figure C.3. Pour les modèles à un seul secteur, le nombre d'éléments pour le domaine fluide est de 150.000, pour le rotor 80.000, et pour le patin 12.000. Des études sur l'influence de la taille du maillage et des critères de convergence ont été menées pour tous les modèles introduits dans la présente étude.

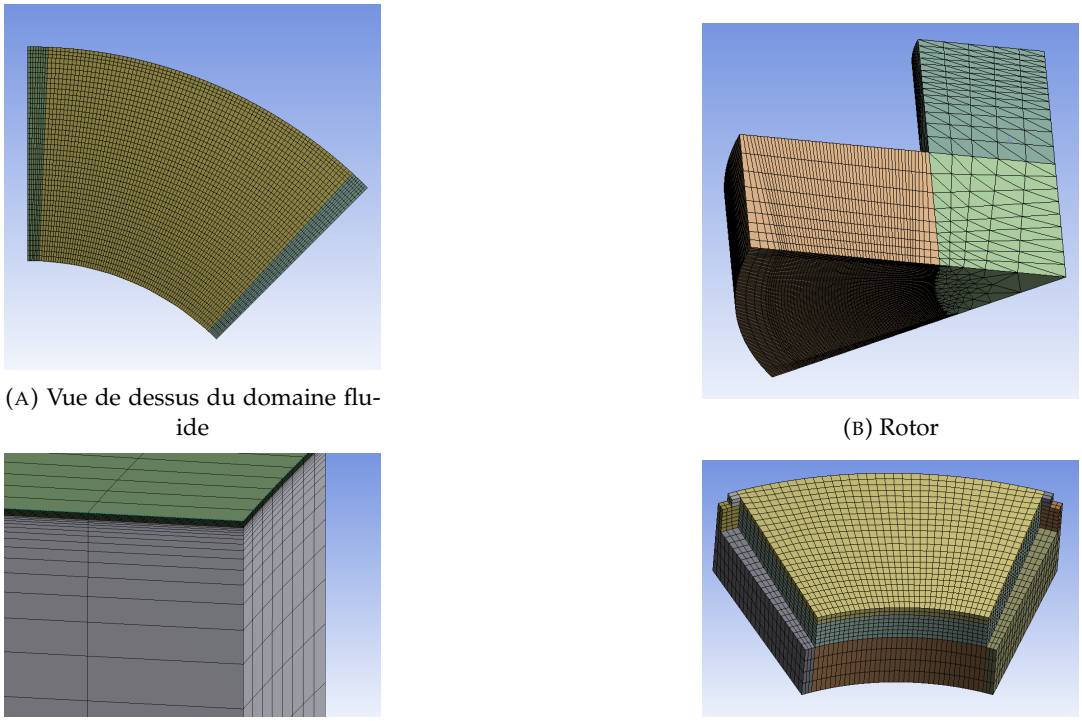

(A) Vue de dessus du domaine fluide

(B) Rotor

(C) Vue iso du fluide dans la rainure

(D) Patin

FIGURE C.3 – Détails du maillage du modèle d'un secteur unique à faces parallèles.

Conditions aux limites

Dans le tableau C.2, les conditions aux limites (BC) pour le modèle TEHD de d'un secteur sont détaillées.

TABLE C.2 – Conditions aux limites thermiques et structurelles pour le modèle TEHD à un seul secteur et un rotor rigide.

Location	Temperature BC's	Structural BC's
	Stator	
Sides	Periodic conditions	Frictionless support
Pad Bottom	HTC: 1000 $W/(m^2K)$, T = 40°C	Uz=0
Pad Inner	HTC: 300 $W/(m^2K)$, T = 40°C	Free
Pad Outer	HTC: 25 $W/(m^2K)$, T = 40°C	Free
Fluid Stator Interface	2-way FSI: Continuity of heat flux and temperature	Free
	Rotor	
Sides	Periodic conditions	Fixed
Rotor Outer	HTC: 25 $W/(m^2K)$, T = 20°C	Fixed
Axis Fixation	HTC: 1000 $W/(m^2K)$, T = 20°C	Fixed
Rotor Oil Res.	HTC: 300 $W/(m^2K)$, T = 40°C	Fixed
Fluid Rotor Interface	Continuity of heat flux and temperature, Rotating velocity 6000 RPM	Fixed
	Lubricant	
Sides	Periodic conditions	Frictionless support
Fluid Inner	Opening with F.P. 0.1MPa, Temperature 40°C	Ux=0, Uy=0
Fluid Outer	Outlet with static pres. of 0 and Temp. 20°C	Ux=0, Uy=0

*Heat Transfer coefficient (HTC)

**Feeding Pressure (F.P.)

Modélisation TEHD

Afin de calculer la géométrie finale du film fluide et du engendrée par les déformations thermiques et mécaniques, un modèle d'interface fluide solide (FSI) à 2 voies a été généré. Un organigramme du calcul du modèle TEHD est décrit à la Fig. C.4. Au début du calcul, après la génération du maillage et des fichiers d'entrée pour les trois domaines et les deux solveurs, l'interface de domaine (FSI) entre le domaine fluide et le plot est cartographiée. La première étape de calcul est l'évaluation de la déformation thermique du stator dans le solveur FE, d'une température froide de 20°C à la température d'huile d'alimentation de 40°C. Ensuite, les emplacements des nœuds d'interface déplacés sont transmis au solveur CFD, et le déplacement de maillage du domaine fluide est appliqué. Le solveur CFD calcule jusqu'à convergence le flux hydrodynamique, la génération de chaleur dans le fluide et le CHT sur le domaine du rotor. Les valeurs de pression et de température du FSI sont transmises au solveur FE et au CHT, et la déformation mécanique et thermique du

stator est réévaluée. Enfin, les deux dernières étapes sont exécutées jusqu'à ce que le déplacement maximum du maillage entre deux calculs consécutifs soit inférieur à $0,01\ \mu m$, et le solveur CFD converge. Lorsque cette procédure itérative est terminée, les caractéristiques tribologiques sont calculées et les valeurs de pression, température et déformation de tous les domaines sont exportées. Le modèle susmentionné est très chargé en calculs. Pour un calcul d'un seul secteur de la butée, avec une unité de calcul de 64 cœurs et de 96 Go de RAM, le temps nécessaire pour converger est d'un peu plus de 3 jours, et pour un patin texturé, le temps nécessaire dépasse 5 jours en raison du maillage plus fin nécessaire pour décrire correctement les cavités de la surface texturée.

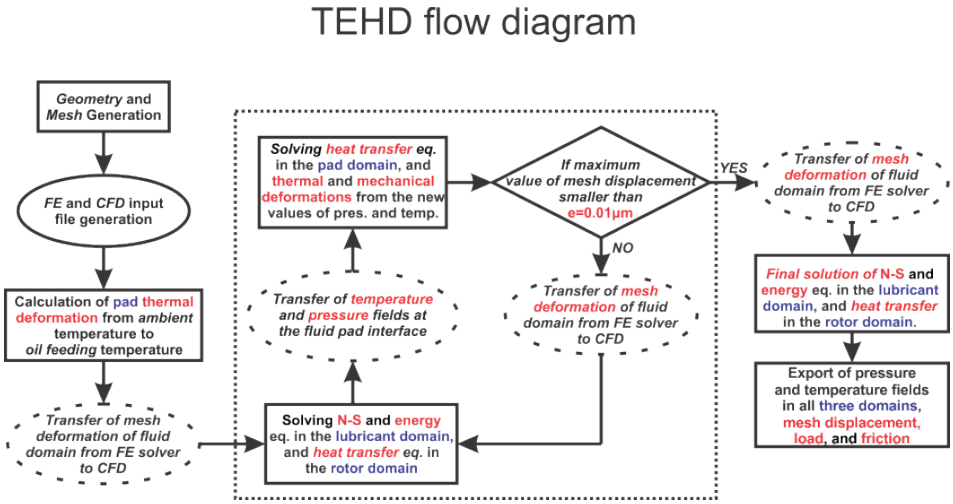

FIGURE C.4 – Organigramme du modèle TEHD.

Étude du phénomène de génération de pression

Dans le présent chapitre, en accord avec la littérature, les mécanismes génération de pression de la butée à faces parallèles ont été évalués. Pour cela, trois approches de modélisation ont été utilisées, afin de dégager des phénomènes spécifiques et de les évaluer séparément.

Avec la modélisation isotherme, trois mécanismes ont été estimés. Tout d'abord, le calcul de la portance hydrostatique, à partir de la pression d'alimentation, a été déterminée par le modèle isotherme sans vitesse de rotation du rotor. L'ampleur en lubrifiant de la portance hydrostatique était insignifiante, mais il était important de soustraire sa valeur de la capacité de charge totale pour l'évaluation des autres effets.

Le deuxième effet d'écoulement qui a été étudié est l'effet du saut de pression à l'entrée du film. En soustrayant la portance hydrostatique des résultats isothermes simples avec rotor rotatif, l'effet du saut de pression a été observé. Avec une charge spécifique maximale de $0,16\ MPa$, son importance en tant que mécanisme de montée en pression est très faible.

De plus, la cavitation a été modélisée avec l'équation de Rayleigh-Plesset. Le modèle isotherme a été évalué avec deux valeurs de viscosité avec et sans cavitation. On observe qu'en raison de la zone de haute pression générée par l'effet de saut de

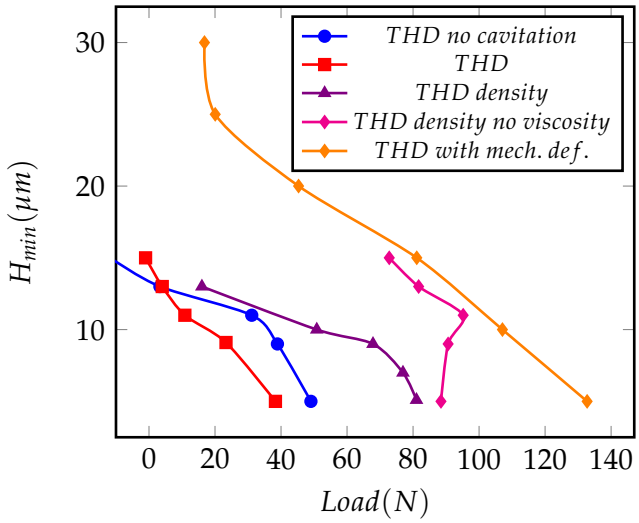

FIGURE C.5 – Résultats THD: évolution de l'épaisseur minimale H_{min} en fonction de la charge.

pression, une fuite latérale se produit à proximité du bord d'attaque. Ainsi, des conditions locales de sous-alimentation d'huile sont présentes dans la section médiane du patin. Pour les faibles valeurs de viscosité, ceci est contré par le flux de lubrifiant plus important provenant de la section située au rayon intérieur. Pour des valeurs de viscosité élevées, ce débit n'est pas suffisant pour alimenter la région médiane en huile, entraînant ainsi une chute de pression. Ceci diminue considérablement la capacité de charge. La modélisation de la cavitation permet alors une description plus précise de ces phénomènes.

Dans une deuxième étape de l'analyse, les mécanismes proposés qui dérivent des propriétés dépendantes de la température du lubrifiant ont été évalués, à l'aide de la modélisation THD (voir Fig. C.5). Un modèle THD prenant en compte la dépendance de la densité avec la température mais imposant une viscosité constante a été créé et les prédictions obtenues ont été comparées aux résultats isothermes déterminés pour la même valeur de viscosité. La montée en pression était plus prononcée dans le modèle THD, conduisant à la conclusion que le coin thermique participe à la capacité de charge de la butée à faces parallèles. Cependant, la pression spécifique générée par le coin thermique est de l'ordre de $0,076\ MPa$, est donc insuffisante pour expliquer les charges observées expérimentalement.

De plus, un modèle THD avec une viscosité dépendante de la température et une densité constante a été généré et évalué, afin d'identifier l'effet de coin de viscosité. Toutes les évaluations THD avec une viscosité dépendante de la température montrent une augmentation de pression près du bord de fuite, comme cela est présenté sur la figure. C.6. Cette augmentation peut être attribuée au gradient de viscosité élevé près de la région de rainure. Le refroidissement de l'huile d'alimentation du patin augmente la viscosité près de l'interface du patin/film fluide, entraînant des forces de cisaillement plus élevées dans cette zone. Cela conduit à une décélération du débit; ainsi, un gradient de pression est généré. Même si l'effet est observable dans tous les modèles mentionnés ci-dessus, son intensité plus petite que celle de l'effet de coin thermique.

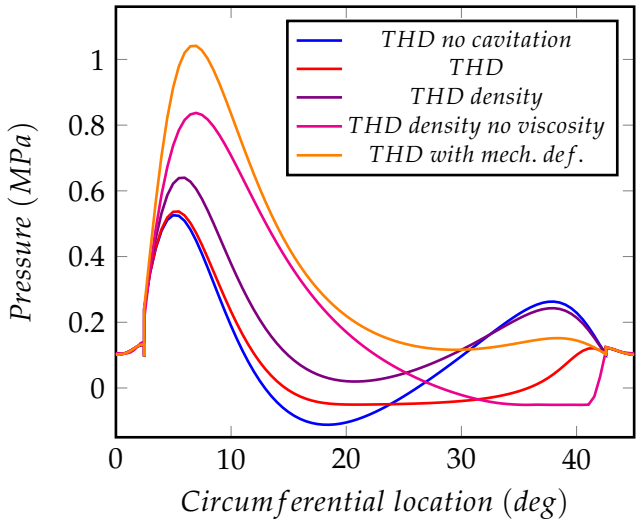

FIGURE C.6 – Résultats THD: comparaison du profil de pression dans le plan médian

Les mécanismes de montée en pression concernant le domaine fluide semblent avoir une faible importance pour la capacité de charge de la butée à surfaces parallèles. Analyser l'influence des propriétés mécaniques et thermiques des domaines solides semble la prochaine étape logique. Tout d'abord, un modèle THD prenant en compte les déformations mécaniques de la géométrie du patin est introduit. Les déformations mécaniques ont généré une petite géométrie convergente. L'amplitude convergente de $0,04\ \mu m$ a réussi à augmenter la pression spécifique des modèles THD précédents de $0,16\ MPa$ supplémentaires.

Progressant sur cette analyse, les déformations thermiques du patin ont été introduites dans le modèle précédent, générant le modèle thermoélastohydrodynamique, nommé TEHD Simple. L'évaluation des performances de la butée avec ce modèle a entraîné des pressions spécifiques supérieures à valeur de $1,5\ MPa$, ce qui suggère que le principal mécanisme de montée en pression de la butée à surfaces parallèles est la géométrie de coin convergente du film lubrifiant générée par les déformations thermiques sur le domaine du patin. De plus, le modèle TEHD Simple a été étendu pour tenir compte de la dépendance de la densité et de la capacité thermique avec la température. Le nouveau de la dépendance modèle s'appelle le modèle TEHD Complet; celui-ci permet d'évaluer la capacité de charge en tenant compte de tous les mécanismes de montée en pression identifiés ainsi qu'une meilleure approximation des températures du domaine. La différence entre les deux modèles est minime. Le TEHD Complet conduit à des valeurs plus faibles du couple de frottement et aux valeurs de température les plus élevées.

La comparaison des résultats issus des deux modèles avec les résultats expérimentaux publiés a démontré une assez bonne corrélation, comme le montre la figure C.7, le TEHD Complet permettant une meilleure prédiction de performances de la butée.

Parce que les déformations thermiques du patin jouent un rôle si important dans la capacité de charge, le modèle TEHD Complet a été étendu pour tenir compte également des déformations thermiques et mécaniques du domaine du rotor. Le nouveau modèle a réussi à établir une corrélation quasi complète avec les mesures

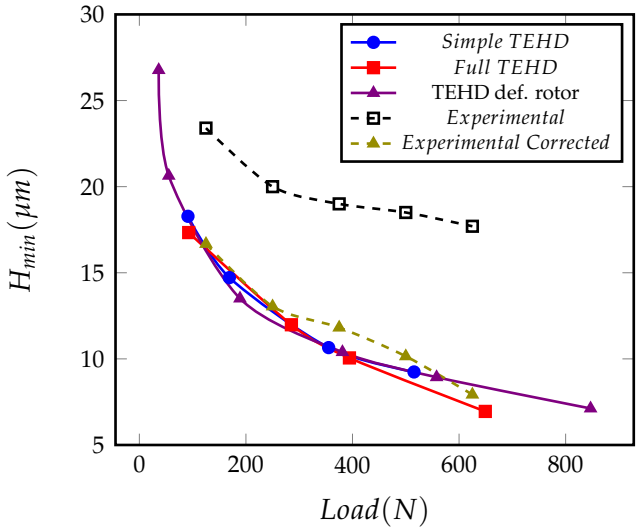

FIGURE C.7 – Résultats TEHD : comparaison avec l'épaisseur minimale H_{min} corrigée, issue de la référence H_{min}.

expérimentales, avec une légère surestimation de la température et une sous- estimation du couple de frottement.

En résumé, après une analyse détaillée de tous les mécanismes possibles de montée en pression pour la butée à faces parallèles, les conclusions de ce chapitre sont que les déformations thermiques et mécaniques du patin et du rotor sont la cause principale de la capacité de charge observée sur ce type de butées.

Afin d'éliminer toute déviation possible du phénomène physique, deux autres points ont été soulevés. Le premier est qu'en raison des imperfections de fabrication de la butée à faces parallèles, des écarts de distribution de pression, de température et d'épaisseur de film se produisent entre tous les patins de la butée. Cela rend certains patins plus chargés que d'autres, et les données mesurées sur la butée d'essais peuvent différer d'un patins à l'autre. Ainsi, une évaluation minutieuse de la géométrie de la butée avant les mesures expérimentales est fortement conseillée, avec la mesure sur tous les patins afin d'acquérir des résultats valides. Le second point est que les contraintes structurelles (fixations du stator sur son support) de la butée à faces parallèles affectent les déformations thermiques, ce qui entraîne une géométrie du film lubrifiant différente pour tous les patins.

Étude des configurations contemporaines

Dans le présent chapitre, quatre types différents de configurations contemporaines ont été étudiés. Chaque cas proposé présente un comportement différent dans la gamme étudiée. Ainsi, une approche de calcul différente est suggérée pour ces configurations.

La butée à plan incliné a été évaluée avec les modèles THD et TEHD. Les deux modèles parviennent à prédire les performances de la butée avec une très bonne corrélation avec les résultats expérimentaux (voir Fig. C.8), malgré une petite sous-estimation de la pression au point 70%-50% pour les deux modèles et une surestimation de la température pour le modèle THD. En général, la modélisation THD est recommandée pour cette conception, en raison des petits avantages liés aux coûts et au temps de calculs par rapport aux simulations numériques en régime TEHD. Pour une évaluation précise, notamment en termes de distribution de température,

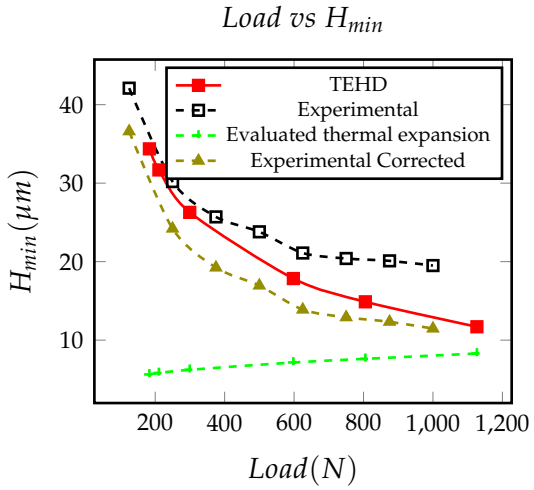

FIGURE C.8 – Palier de butée conique: Correction de H_{min} par rapport à la charge tenant compte de la déformation thermique du patin.

l'approche de modélisation TEHD est suggérée, mais la nécessité de modéliser les déformations du rotor est jugée superflue.

Pour la butée à poche, des résultats presque identiques avec ceux du plan incliné ont été obtenus. Une très bonne corrélation avec les deux modèles a été observée, avec une petite surestimation de la température pour le modèle THD, et une surestimation de la pression au point 70%-50% par les deux modèles (voir Fig. C.9). La principale différence avec le cas du plan incliné est que si une meilleure précision est nécessaire pour l'évaluation des caractéristiques de performance que celle gérée par le modèle THD, un modèle TEHD prenant également en compte les déformations mécaniques et thermiques du rotor est proposé. En effet, la forme geometrique du film lubrifiant est très dépendante des deformations du rotor et des patins.

La butée à patins partiellement texturés étudiée présente, quant à elle, une géométrie complexe du film lubrifiant et du patin en raison de la présence des cavités qui augmente le temps de calcul. Pour évaluer les performances de l'AST sur le patin à faces parallèles, trois modèles ont été introduits, l'isotherme, le THD et le TEHD et la comparaison de leur performances est présentée sur la Fig. C.10. La modélisation isotherme ne peut pas prédire correctement les performance du patin de glissière texturé et le modèle THD diverge du modèle TEHD pour des charges modérées à élevées. La modélisation TEHD a montré que les cavités agissent comme des couches isolantes thermiquement et ne permettent pas le flux de chaleur du lubrifiant vers le patin pour une plage de valeurs de H_{min}; ceci entraîne une forte augmentation de la température à mesure que la charge augmente. Lorsque l'épaisseur minimale H_{min} atteint une valeur seuil, une zone de recirculation est créée à l'intérieur de la cavité. La zone de recirculation permet le flux de chaleur par convection, et à partir de ce seuil, la température diminue au fur et à mesure que le H_{min} diminue. Lorsqu'une certaine valeur de la charge est atteinte et que la génération de chaleur

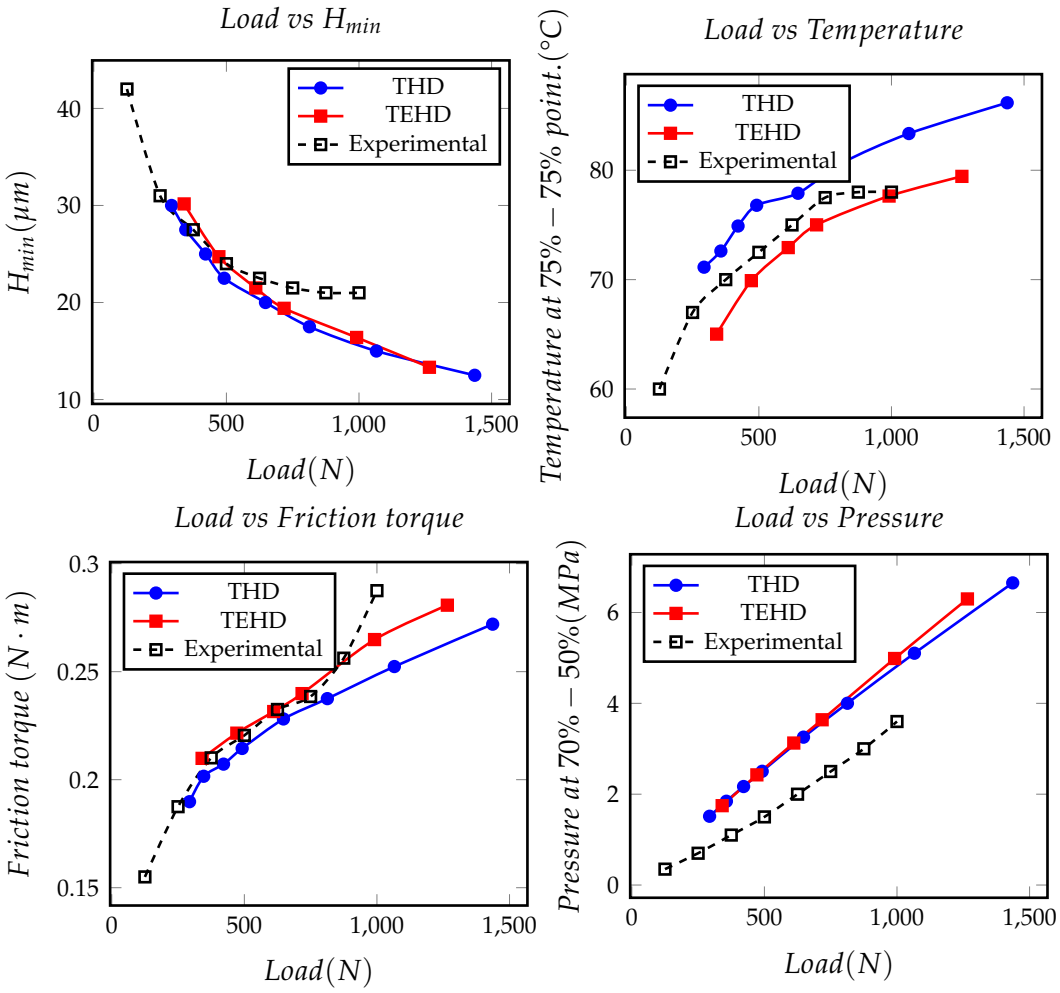

FIGURE C.9 – Butée à plan incliné: influence de la déformation thermique du patin sur l'épaisseur minimale, comparaison avec la valeur expérimentale corrigée Hmin.

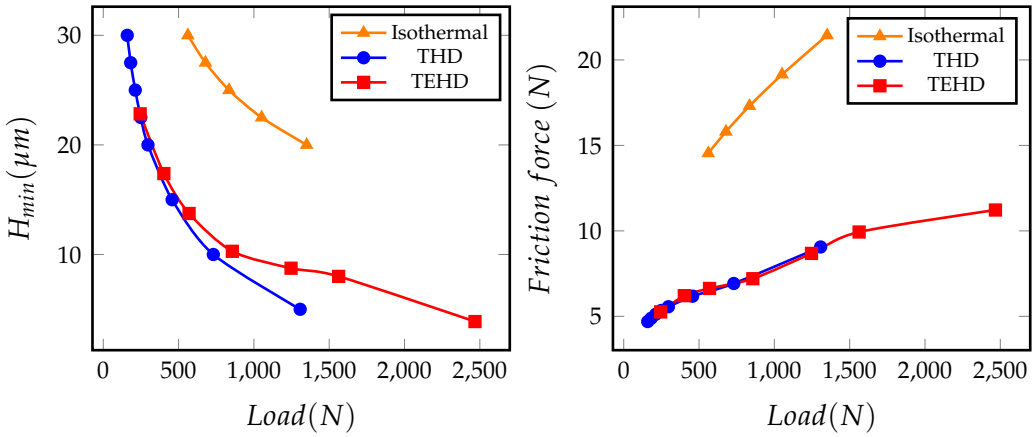

FIGURE C.10 – Comparaison des performances obtenues à l'aide des modèles Isotherme, THD et TEHD pour le patin à surfaces parallèles, partiellement texturé.

est supérieure au flux thermique à l'intérieur des cavités; ainsi, la température augmente à mesure que la charge augmente. Ceci conduit à la conclusion que les nouvelles conceptions des butées texturées doivent tenir compte de la grandeur opérationnelle H_{min} pour définir la profondeur de texture. Enfin, pour l'évaluation correcte des performances de la butée à patins partiellement texturés, la modélisation TEHD est fortement conseillée.

En comparant les patins à faces parallèles partiellement texturé et non texturé (voir Fig. C.11), on peut conclure comme suit. L'AST parvient à réduire la force de frottement par rapport au patin non texturé. Le mécanisme de montée en pression du palier de butée parallèle (déformation thermique) est atténué sur le patin texturé, en raison de l'épaisseur moyenne du film plus grande sur le coin généré. La région de haute pression est prolongée par les textures; ainsi, la cavitation est limitée près du bord de fuite. De plus, le patin texturé présente des valeurs de température plus élevées, du fait des propriétés isolantes des cavités. Enfin, avant de sélectionner AST pour une nouvelle conception de butée qui fonctionne à des charges spécifiques supérieures à $0,3\ MPa$, il faut tenir compte du coût de fabrication plus élevé engendré par la texturation, des températures de fonctionnement plus élevées et de la capacité de charge inférieure de la butée texturée par rapport à la simple butée à faces parallèle non texturée.

De plus, trois revêtements différents ont été modélisés, mais aucun résultat concluant n'a été établi. La principale raison du manque de résultats de calcul est le temps de calcul remarquablement élevé de la modélisation TEHD pour les matériaux à coefficient de dilatation thermique élevé et à faible rigidité. Afin d'évaluer les performances d'une butée à faces parallèles revêtue, la modélisation TEHD est la seule option car le principal mécanisme de montée en pression est la déformation thermique du patin et de la géométrie du rotor.

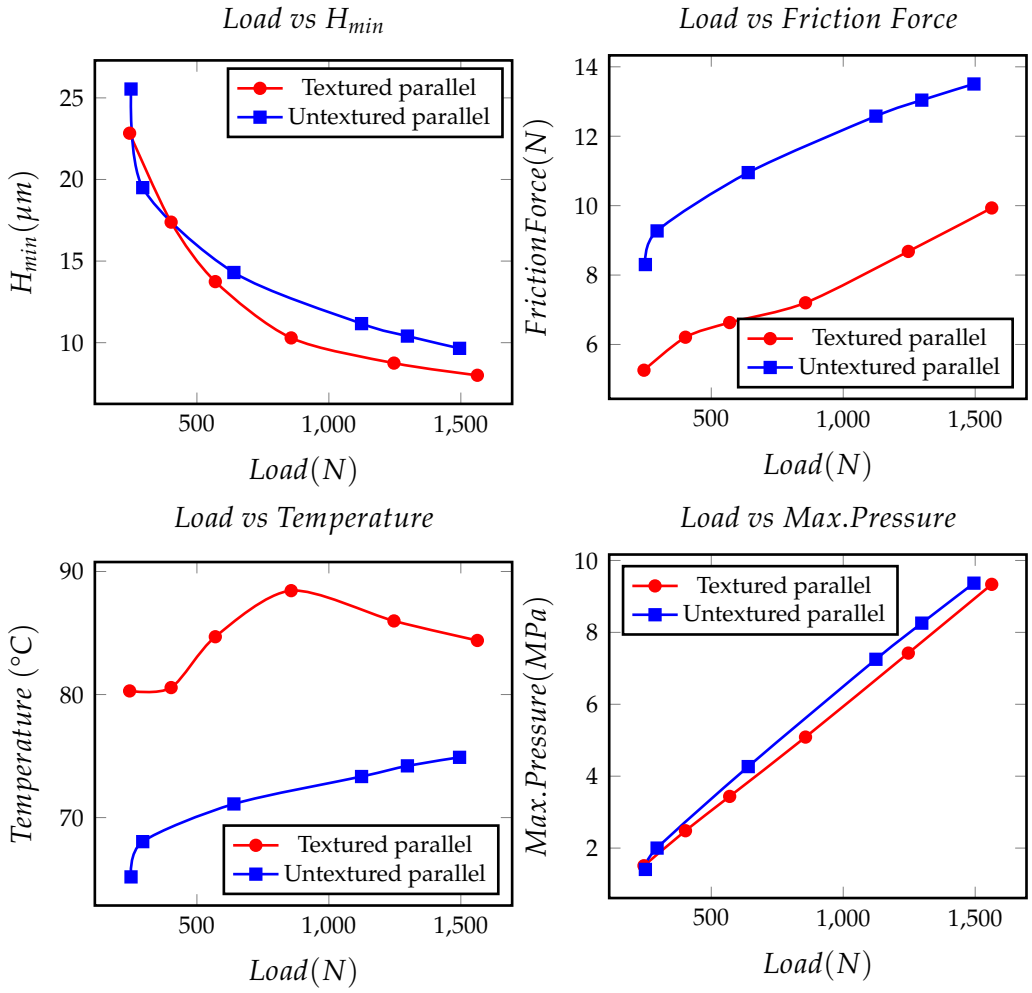

FIGURE C.11 – Comparaison des performances entre le patin à faces parallèle, partiellement texturé et le patin non texturé, avec le modèle TEHD.

Conclusion

De nombreux phénomènes physiques différents se produisent dans la butée à surfaces parallèles afin de générer une capacité de charge. Le plus prononcé est l'effet de la déformation thermique, qui génère un coin convergent pouvant supporter une charge considérable.

Pour évaluer les performances d'une telle butée, un modèle CFD TEHD 3D est nécessaire et la géométrie de la rainure d'alimentation en lubrifiant doit être modélisée. L'évaluation de la température et les conditions aux limites sont de la plus haute importance. Une attention particulière doit être accordée à la condition aux limites structurelles, car une enquête préliminaire a suggéré que différents emplacements et / ou nombres de points de fixation peuvent donner des profils de déformation très différents.

L'imperfection dimensionnelle de chaque patin peut introduire différentes conditions de chargement sur la butée. Ainsi, mesurer un seul patin ne décrirait probablement pas les conditions de travail réelles de l'ensemble du système de guidage axial.

Les configurations de butées à plan incliné et à poche n'ont pas besoin de l'approche de modélisation TEHD coûteuse en temps de calculs.

Les butées à patins partiellement texturés, en particulier ceux moyennement ou fortement chargés, doivent être étudiés en tenant compte de la déformation thermique de la géométrie du patin.

Enfin, l'effet des revêtements sur les butées à surfaces parallèles doit être étudié. Une conception hybride à deux revêtements peut améliorer considérablement les performances des butées à surfaces parallèles.

En analysant les résultats de la présente thèse, on obtient une vision plus claire des prochaines étapes de recherche dans notre domaine scientifique.

Comme mentionné ci-dessus, les conditions aux limites structurelles peuvent affecter les performances de la butée à surfaces parallèles, et cela doit être étudié plus en détails.

L'analyse très limitée des patins revêtus identifie l'importance d'analyser leur effet sur le mécanisme de montée en pression pour la butée à surfaces parallèles. De plus, nous pensons que l'étude d'une butée à double revêtement peut rendre la conception parallèle d'une butée simple à plans parallèles compétitive par rapport aux types de butées contemporaines plus complexes.

Une analyse plus longue et plus structurée de la texturation artificielle de la surface est nécessaire, en termes d'évaluations TEHD, pour une large gamme de paramètres de conception différents, tels que la profondeur et la forme des cavités, la densité, etc.

Enfin, le progrès le plus important serait une approche de modélisation en fonction du temps pour la butée à faces parallèles, afin de comprendre la génération du film au démarrage, et comment chaque mécanisme contribue au cours de la progression du phénomène.

Παράρτημα Δ΄

Εκτενής Περίληψη

Ανασκόπηση της βιβλιογραφίας

Η τριβή είναι παρούσα σε κάθε κίνηση που παρατηρούμε στην καθημερινή μας ζωή. Η μείωση των απωλειών ενέργειας λόγω της παρουσίας δυνάμεων τριβής αποτελεί σημαντικό στόχο σχεδίασης οποιασδήποτε μηχανολογικής κατασκευής. Εκτιμάται ότι το 23% της συνολικής κατανάλωσης ενέργειας προέρχεται από απώλειες ενέργειας στις τριβολογικές επαφές. Στην κατεύθυνση της μείωσης των συνολικών ενεργειακών απωλειών και του σχεδιασμού αποτελεσματικότερων τμημάτων μηχανολογικών συστημάτων, είναι απαραίτητη η κατανόηση του μηχανισμού τριβής. Από την αρχή της βιομηχανικής εποχής, έχουν καταβληθεί πολλές προσπάθειες για τη βελτιστοποίηση της αποτελεσματικότητας των μηχανών. Με την πάροδο των ετών, έχουν δημιουργηθεί αναλυτικά και υπολογιστικά μοντέλα για την πρόβλεψη και τη βελτιστοποίηση της απόδοσης τέτοιων σχεδιάσεων. Μέχρι πρότινος, οι περιορισμοί σε σχέση με την διαθέσιμη ισχύ των υπολογιστικών συστημάτων οδηγούσε σε σημαντικές απλουστεύσεις των φυσικών μοντέλων, προκειμένου να επιτευχθεί ουσιαστικό αποτέλεσμα με περιορισμένους υπολογιστικούς πόρους. Ωστόσο, τα τελευταία 20 χρόνια, η διαθέσιμη υπολογιστική ισχύς έχει αυξηθεί δραματικά, επιτρέποντας στην επιστημονική κοινότητα να χρησιμοποιεί πιο περίπλοκα και ακριβή υπολογιστικά μοντέλα, βελτιώνοντας σημαντικά την ακρίβεια των υπολογισμών και την κατανόηση των σχετικών φαινομένων.

Η παρούσα μελέτη επικεντρώνεται στη λεπτομερή μοντελοποίηση του ωστικού εδράνου παράλληλης επιφανείας, υιοθετώντας μια θερμοελαστοϋδροδυναμική προσέγγιση υπολογισμού (ThermoElastoHydrodynamic TEHD) με χρήση κώδικα υπολογιστικής ρευστομηχανικής (CFD). Οι στόχοι της παρούσας μελέτης είναι (α) η αξιολόγηση των μηχανισμών δημιουργίας πίεσης των παράλληλων ωστικών εδράνων, με βάση τις προτάσεις που έχουν αναφερθεί στη διεθνή βιβλιογραφία και (β) η αξιολόγηση του τρόπου με τον οποίο η προτεινόμενη πολύπλοκη προσέγγιση μοντελοποίησης μπορεί να χρησιμοποιηθεί για την αξιολόγηση σύγχρονων εδράνων που έχουν σχεδιαστεί με χρήση απλούστερων υπολογιστικών μεθόδων.

Παράλληλο ωστικό έδρανο

Το 1946, ο Fogg παρουσίασε τα αποτελέσματα των πειραμάτων του με παράλληλα ωστικά έδρανα. Κατέληξε στο συμπέρασμα ότι το παράλληλο ωστικό έδρανο μπορεί να υποστηρίξει φορτία της ίδιας τάξης μεγέθους με αυτορυθμιζόμενα κεκλιμένα ωστικά έδρανα. Αυτά τα αποτελέσματα έρχονται σε αντίθεση με την κλασική θεωρία λίπανσης, λόγω της απουσίας συγκλίνουσας περιοχής στα παράλληλα έδρανα. Από τότε, έχουν δημοσιευτεί πολλές διαφορετικές θεωρίες, προκειμένου να εξηγηθεί το φαινόμενο αυτό. Οι πιο σημαντικές θεωρίες μηχανισμού δημιουργίας πίεσης που προτείνονται στη βιβλιογραφία συνοψίζονται παρακάτω:

1. Η θεωρία της θερμικής σφήνας.

2. Η θεωρία της σφήνας ιξώδους.
3. Η επίδραση της μακροτραχύτητας των επιφανειών του εδράνου και του ρότορα.
4. Η επίδραση των θερμικών παραμορφώσεων.
5. Η δημιουργία πίεσης στο χείλος εισόδου του εδράνου, λόγω αδρανειακών δυνάμεων και δυνάμεων συνεκτικότητας.
6. Η επίδραση λοξότμησης στο χείλος εισόδου του εδράνου.

Η πλέον επικρατούσα προτεινόμενη θεωρία είναι αυτή της θερμικής παραμόρφωσης του εδράνου, ωστόσο μικρότερες επιδράσεις στην ικανότητα παραλαβής φορτίου των παράλληλων ωστικών εδράνων μπορούν να αποδοθούν σε συνδυασμούς των υπόλοιπων θεωριών.

Τεχνητή επιφανειακή τραχύτητα

Προς την κατεύθυνση των δραστικών προσπαθειών που έχουν γίνει τις τελευταίες δεκαετίες για τη μείωση των απωλειών ισχύος σε μηχανολογικά συστήματα, η χρήση τεχνητής επιφανειακής τραχύτητας (ΤΕΤ) σε τριβολογικές επαφές έχει εξεταστεί εκτενώς από πολλούς ερευνητές. Η ΤΕΤ έχει μελετηθεί σε μια ποικιλία εφαρμογών, όπως ελατήρια εμβόλου, ακτινικά έδρανα, ωστικά έδρανα και στοιχεία στεγανοποίησης. Έχουν μελετηθεί πολλά διαφορετικά σχήματα και μεγέθη τεχνητής τραχύτητας, από απλά μικροκανάλια έως πιο περίπλοκα μοτίβα όπως ορθογωνικές κοιλότητες, εξαγωνικές εξοχές και ημισφαιρικές κοιλότητες, με αποτέλεσμα μια σειρά διαφορετικών βέλτιστων γεωμετρικών σχεδιάσεων, ακόμη και για μικρές αλλαγές στις συνθήκες λειτουργίας του μηχανολογικού συστήματος. Όσον αφορά στα ωστικά έδρανα, η χρήση τεχνητής τραχύτητας στην επιφάνεια του εδράνου έχει εφαρμοστεί, στην πλειονότητα των μελετών, σε παράλληλα ωστικά έδρανα.

Επιστρώσεις

Από την εποχή των ξύλινων εδράνων, η τεχνολογία υλικών των εδράνων έχει προχωρήσει σημαντικά. Στις πρώτες δημοσιεύσεις τα ωστικά έδρανα τριβής ήταν κατασκευασμένα από χάλυβα, αλλά καθώς το εύρος εφαρμογής, και η κατανόηση των τριβολογικών επαφών αυξήθηκε, νέα υλικά άρχισαν να χρησιμοποιούνται. Τα κράματα χαλκού και χάλυβα με καλύτερα τριβολογικά χαρακτηριστικά είναι τα κύρια υλικά που χρησιμοποιούνται σήμερα. Ωστόσο, η χρήση κραμάτων μολύβδου, και αργότερα κραμάτων με βάση τον κασσίτερο (Babbitt) έχουν χρησιμοποιηθεί συστηματικά ως επιστρώσεις σε έδρανα τριβής. Η χρήση τέτοιων επιστρώσεων έχει εισέλθει στη βιομηχανική χρήση σε έδρανα τριβής, λόγω των πλεονεκτημάτων που προσφέρουν σε σύγκριση με τα κοινά υλικά. Η επίστρωση Babbitt δρα ως μια επιπλέον δικλείδα ασφαλείας, εάν παρουσιαστούν προβλήματα λίπανσης. Όταν η θερμοκρασία αυξάνεται και η υδροδυναμική ικανότητα του εδράνου δεν είναι αρκετή για το εφαρμοζόμενο φορτίο, η επίστρωση Babbitt λιώνει τοπικά, και συμπεριφέρεται ως λιπαντικό μέχρι να σταματήσει η λειτουργία του εδράνου. Αυτό προστατεύει τον ρότορα και ολόκληρο το αξονικό σύστημα, και με επισκευή της επίστρωσης του, το έδρανο μπορεί να γίνει ξανά λειτουργικό. Η επίστρωση, επίσης, συγκρατεί σωματίδια φθοράς, μειώνοντας έτσι την εκτεταμένη λειαντική φθορά. Ωστόσο, οι επικαλύψεις Babbitt δεν είναι πάντα επαρκώς αξιόπιστες.

Από τη δεκαετία του 1970, οι επικαλύψεις Babbitt, σε ορισμένες περιπτώσεις, αντικαταστάθηκαν σταδιακά από νέα συνθετικά πολυμερή. Το πρώτο πολυμερές που χρησιμοποιήθηκε ήταν το Πολυτετραφθοροαιθυλένιο (PTFE), το οποίο λόγω της πολύ χαμηλής στατικής τριβής, μειώνει αρκετά την τριβή εκκίνησης, ώστε να είναι δυνατή η εξάλειψη

της ανάγκης δημιουργίας υδροστατικής θήκης ανύψωσης σε εφαρμογές υψηλής φόρτισης. Με τη σειρά του, αυτό οδηγεί σε μείωση του μεγέθους της απαιτούμενης επιφάνειας εδράνου, η οποία οδηγεί σε έδρανα μικρότερων διαστάσεων για δεδομένο προφίλ λειτουργίας. Λόγω του μειωμένου μεγέθους, ελαχιστοποιούνται οι απώλειες τριβής, και οι νέες σχεδιάσεις έχουν μικρότερο κόστος κατασκευής και λειτουργίας. Επιπλέον, το εύρος θερμοκρασίας κανονικής λειτουργίας PTFE είναι σημαντικά υψηλότερο, με τη μέγιστη θερμοκρασία ασφαλούς λειτουργίας να ξεπερνά τους 180°C. Το κύριο πρόβλημα αυτών των επικαλύψεων είναι η περιορισμένη δυνατότητά τους να αντεπεξέρχονται σε φαινόμενα ερπυσμού. Νέα υλικά με βελτιωμένες ιδιότητες εξετάζονται συνεχώς, για την παραγωγή πιο ανθεκτικών και αποδοτικών εδράνων.

Προσέγγιση μοντελοποίησης

Γεωμετρία

Για τα διάφορα στάδια της παρούσας διατριβής χρησιμοποιήθηκαν τρεις βασικές γεωμετρικές διαμορφώσεις για τη δημιουργία μοντέλου, συγκεκριμένα, ένας ευθύγραμμος ωστικός ολισθητήρας, ένα πέλμα από παράλληλο ωστικό έδρανο οκτώ πελμάτων, και ένα πλήρες ωστικό έδρανο οκτώ πελμάτων, όπως απεικονίζονται στο Σχ.Δ΄.1. Για να μπορέσουμε να συγκρίνουμε τα υπολογιστικά αποτελέσματα με πειραματικά δεδομένα, η γεωμετρία των ωστικών εδράνων βασίζεται σε έδρανο που χρησιμοποιήθηκε για την παραγωγή δημοσιευμένων πειραματικών αποτελεσμάτων, με απλοποίηση των χαρακτηριστικών του αυλακιού τροφοδοσίας λιπαντικού. Όπως φαίνεται στο Σχ.Δ΄.2, τα τοιχώματα της αυλάκωσης τροφοδοσίας λαδιού έχουν αξονική διεύθυνση. Επιπλέον, η χαρακτηριστική διαμόρφωση εξόδου του λιπαντικού στη γεωμετρία αναφοράς έχει τριγωνική διατομή, αλλά στην παρούσα εργασία σχεδιάστηκε ως τετράγωνη προκειμένου να επιτρέψει ένα πλήρως εξαεδρικό πλέγμα στην περιοχή λιπαντικού. Οι βασικές παράμετροι σχεδιασμού του ωστικού εδράνου παρουσιάζονται στον Πίνακα Δ΄.1.

Πίνακας Δ΄.1 – Βασικά γεωμετρικά στοιχεία για το ωστικό έδρανο αναφοράς.

Παράμετρος	Περιγρφή	Τιμή	Μονάδες
NOP	Αριθμός τμημάτων	8	*ul*
$\mathbf{D_{Inner}}$	Εσωτερική διάμετρος	50	*mm*
$\mathbf{D_{Outer}}$	Εξωτερική διάμετρος	90	*mm*
$\mathbf{L_{GO}}$	Μήκος διαμόρφωσης εξόδου	1	*mm*
$\mathbf{D_{GO}}$	Βάθος διαμόρφωσης εξόδου	1	*mm*
$\mathbf{L_{GR}}$	Πλάτος αυλάκωσης	3	*mm*
$\mathbf{D_{GR}}$	Βάθος αυλάκωσης	4	*mm*
$\mathbf{D_P}$	Πάχος ρότορα	10	*mm*
$\mathbf{D_S}$	Πάχος πέλματος	20	*mm*

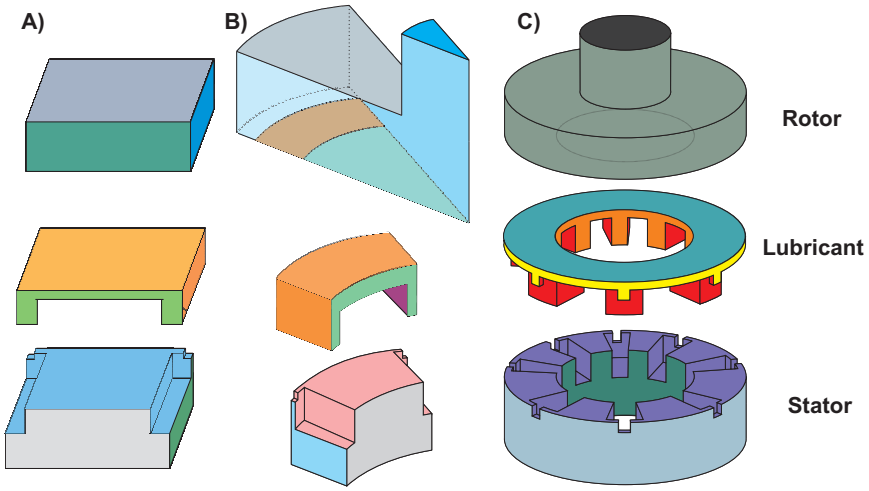

Σχήμα Δ΄.1 – Α) Ευθύγραμμος ωστικός ολισθητήρας, Β) Πέλμα παράλληλου ωστικού εδράνου οκτώ πελμάτων, C) Πλήρες ωστικό έδρανο οκτώ πελμάτων.

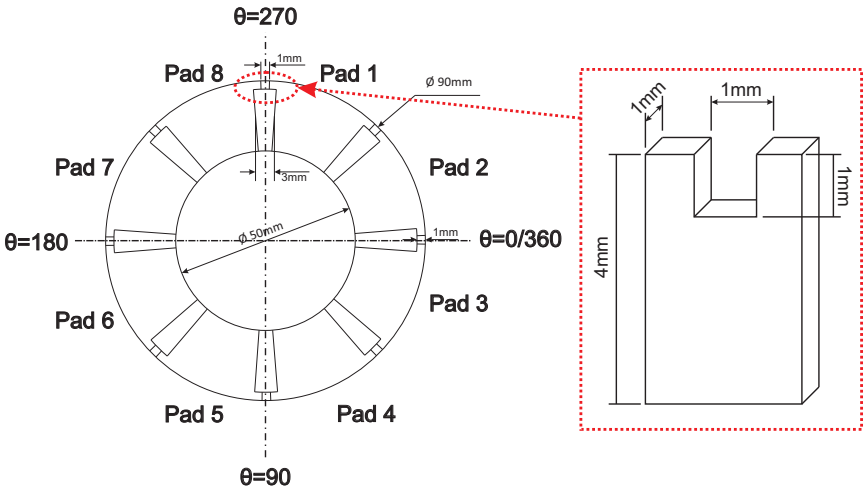

Σχήμα Δ΄.2 – Κάτοψη πλήρους ωστικού εδράνου οκτώ τομέων

Πλέγμα

Ένα τυπικό πλέγμα για τη γεωμετρία τομέα ωστικού εδράνου απεικονίζεται στο Σχ.Δ΄.3. Για τα μοντέλα ενός πέλματος, ο αριθμός στοιχείων για την περιοχή ρευστού είναι 150.000 για τον ρότορα 80.000 και για το πέλμα 12.000. Έχουν διεξαχθεί μελέτες πλέγματος και σύγκλισης για όλα τα διαφορετικά μοντέλα που αναπτύχθηκαν στην παρούσα μελέτη.

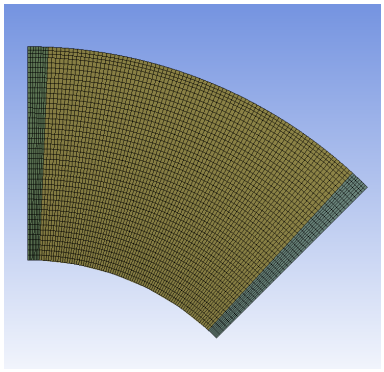

(α΄) Κάτοψη ρευστού

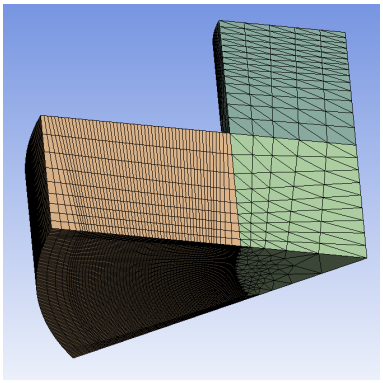

(β΄) Ρότορας

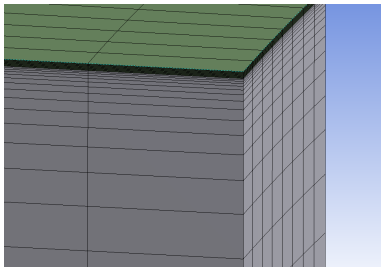

(γ΄) Αυλάκωση τροφοδοσίας λιπαντικού

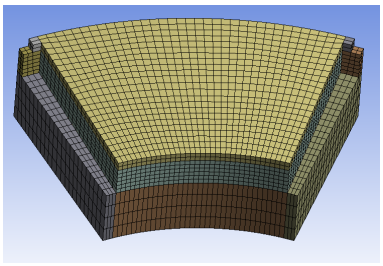

(δ΄) Πέλμα

Σχήμα Δ΄.3 – Λεπτομέρειες πλέγματος για το παράλληλο έδρανο ενός πέλματος.

Οριακές συνθήκες

Στον ακόλουθο πίνακα Δ΄.2 παρουσιάζονται οι οριακές συνθήκες για το μοντέλο TEHD μεμονωμένου πέλματος.

Πίνακας Δ΄.2 – Θερμικές και μηχανικές οριακές συνθήκες για το TEHD μοντέλο μεμονωμένου πέλματος με άκαμπτο ρότορα.

Location	Temperature BC's	Structural BC's
	Stator	
Sides	Periodic conditions	Frictionless support
Pad Bottom	HTC: 1000 $W/(m^2K)$, T = 40°C	Uz=0
Pad Inner	HTC: 300 $W/(m^2K)$, T = 40°C	Free
Pad Outer	HTC: 25 $W/(m^2K)$, T = 40°C	Free
Fluid Stator Interface	2-way FSI: Continuity of heat flux and temperature	Free
	Rotor	
Sides	Periodic conditions	Fixed
Rotor Outer	HTC: 25 $W/(m^2K)$, T = 20°C	Fixed
Axis Fixation	HTC: 1000 $W/(m^2K)$, T = 20°C	Fixed
Rotor Oil Res.	HTC: 300 $W/(m^2K)$, T = 40°C	Fixed
Fluid Rotor Interface	Continuity of heat flux and temperature, Rotating velocity 6000 RPM	Fixed
	Lubricant	
Sides	Periodic conditions	Frictionless support
Fluid Inner	Opening with F.P. 0.1MPa, Temperature 40°C	Ux=0, Uy=0
Fluid Outer	Outlet with static pres. of 0 and Temp. 20°C	Ux=0, Uy=0

*Heat Transfer coefficient (HTC)

**Feeding Pressure (F.P.)

Θερμοελαστοϋδροδυναμική **(TEHD)** προσέγγιση

Προκειμένου να υπολογιστεί η τελική γεωμετρία ρευστού και του πέλματος λόγω θερμικής και μηχανικής παραμόρφωσης, δημιουργήθηκε ένα μοντέλο αμφίδρομης διεπαφής ρευστού-κατασκευής (FSI) Το διάγραμμα ροής υπολογισμών του μοντέλου TEHD παρουσιάζεται στο Σχ.E.4. Στην αρχή των υπολογισμών, αφού δημιουργηθούν τα αρχεία πλέγματος και εισαγωγής για τα τρία υπολογιστικά χωρία και για τους δύο επιλυτές, χαρτογραφείται η διεπαφή τομέων (FSI) μεταξύ της περιοχής του λιπαντικού και του πέλματος. Το πρώτο βήμα υπολογισμού είναι η αξιολόγηση της θερμικής παραμόρφωσης του στάτορα στον επιλυτή πεπερασμένων στοιχείων (FE), από θερμοκρασία 20°C (θερμοκρασία περιβάλλοντος) έως τη θερμοκρασία τροφοδοσίας λαδιού 40°C. Στη συνέχεια, οι μετατοπισμένες θέσεις των κόμβων διασύνδεσης μεταφέρονται στον κώδικα υπολογιστικής ρευστομηχανικής (CFD) και εφαρμόζεται η μετατόπιση πλέγματος της διεπιφάνειας του ρευστού. Ο επιλυτής CFD υπολογίζει μέχρι τη σύγκλιση της υδροδυναμικής ροής, την παραγωγή θερμότητας στο ρευστό και την μεταφορά θερμότητας στην περιοχή του

ρότορα. Οι τιμές πίεσης και θερμοκρασίας της διεπιφάνειας μεταφέρονται στον επιλυτή FE , και η μηχανική και θερμική παραμόρφωση του πέλματος επανεκτιμώνται. Τέλος, τα δύο τελευταία βήματα εκτελούνται επαναληπτικά, έως ότου η μέγιστη μετατόπιση πλέγματος μεταξύ δύο διαδοχικών υπολογισμών είναι μικρότερη από $0,01\ \mu m$ και ο CFD επιλυτής θεωρείται ότι έχει συγκλίνει. Όταν ολοκληρωθεί αυτή η επαναληπτική διαδικασία, υπολογίζονται τα τριβολογικά χαρακτηριστικά και εξάγονται οι τιμές πίεσης, θερμοκρασίας και παραμόρφωσης όλων των υπολογιστικών χωρίων. Το προαναφερθέν μοντέλο είναι υπολογιστικά πολύ απαιτητικό. Για έναν μόνο υπολογισμό ενός πέλματος ωστικού εδράνου, με υπολογιστική μονάδα 64 πυρήνων και 96 GB RAM, ο χρόνος που απαιτείται έως τη σύγκλιση είναι περίπου λίγο περισσότερος από 3 ημέρες, ενώ για ωστικό έδρανο με τεχνητή επιφανειακή τραχύτητα, ο απαιτούμενος χρόνος υπερβαίνει τις 5 ημέρες, λόγω του πυκνότερου πλέγματος που απαιτείται για τον ακριβή υπολογισμό της ροής μέσα στις κοιλότητες.

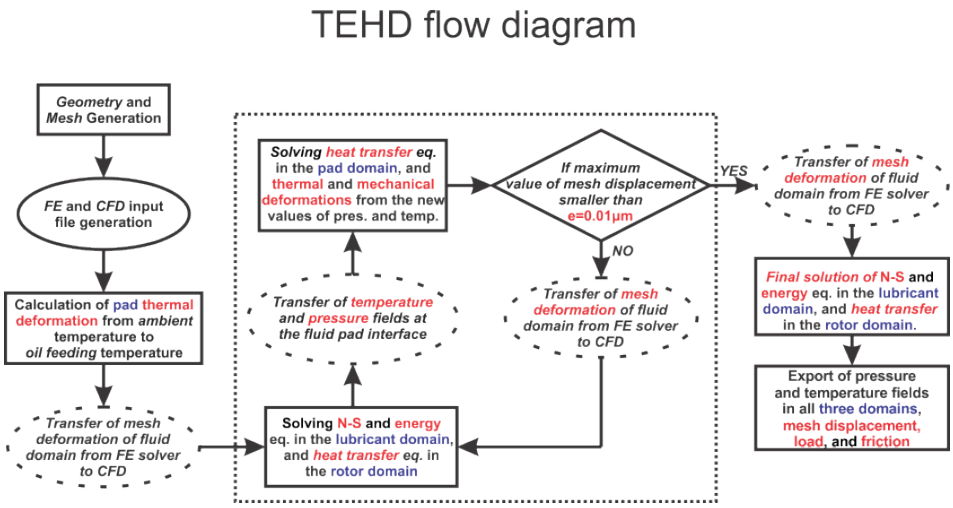

Σχήμα Δ΄.4 – Λογικό διάγραμμα θερμοελαστοϋδροδυναμικού μοντέλου

Διερεύνηση μηχανισμού δημιουργίας πίεσης

Στην συνέχεια αξιολογήθηκαν όλοι οι μηχανισμοί δημιουργίας πίεσης της βιβλιογραφίας του παράλληλου ωστικού εδράνου. Για αυτήν την αξιολόγηση, έχουν χρησιμοποιηθεί τρεις προσεγγίσεις μοντελοποίησης, προκειμένου να συμπεριληφθούν/αγνοηθούν συγκεκριμένα φαινόμενα και να αξιολογηθούν ξεχωριστά.

Με την ισοθερμική μοντελοποίηση, έχουν αξιολογηθεί τρεις μηχανισμοί. Πρώτον, ο υπολογισμός της υδροστατικής ανύψωσης, από την πίεση λαδιού τροφοδοσίας αξιολογήθηκε από το ισοθερμικό μοντέλο, χωρίς επιβολή περιστροφικής ταχύτητας στον ρότορα. Το υπολογισθέν μέγεθος της υδροστατικής ανύψωσης ήταν ασήμαντο, αλλά είναι σημαντικό να αφαιρεθεί η τιμή του από τη συνολική ικανότητα μεταφοράς φορτίου, για την αξιολόγηση της συνεισφοράς των υπόλοιπων μηχανισμών δημιουργίας πίεσης στο έδρανο.

Το δεύτερο φαινόμενο ροής που μελετήθηκε είναι το φαινόμενο πίεσης χείλους εισόδου. Αφαιρώντας την υδροστατική ανύψωση από τα απλά ισοθερμικά αποτελέσματα με περιστρεφόμενο ρότορα, παρατηρήθηκε το φαινόμενο της πίεσης χείλους εισόδου. Τα αποτελέσματα δεικνύουν ότι το μέγιστο ειδικό φορτίο λόγω της ύπαρξης του χείλους στη θέση εισόδου λιπαντικού στο έδρανο είναι της τάξης των $0,16\ MPa$, επομένως η σημασία του ως μηχανισμός δημιουργίας πίεσης είναι πολύ μικρή.

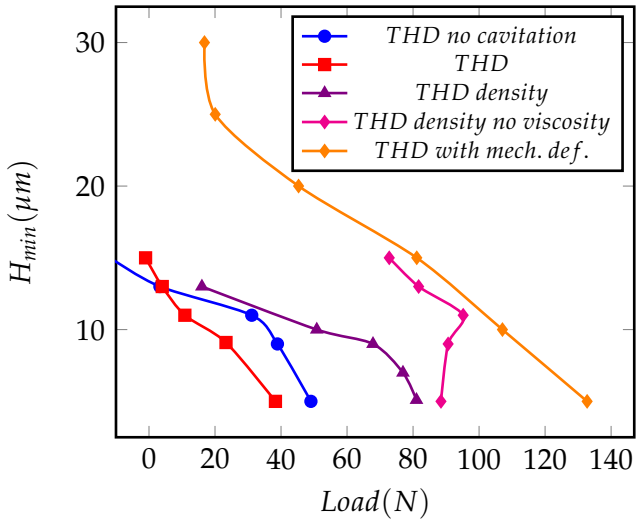

FIGURE D.5 – THD: H_{min} *vs Load*

Επιπλέον, η σπηλαίωση του λιπαντικού έχει μοντελοποιηθεί με την εξίσωση Rayleigh-Plesset. Το ισοθερμικό μοντέλο έχει αξιολογηθεί με δύο τιμές ιξώδους, με και χωρίς σπηλαίωση. Επειδή το φαινόμενο πίεσης χείλους εισόδου αυξάνει την πίεση μόνο κοντά στην περιοχή του χείλους εισόδου, όταν το ιξώδες είναι υψηλό, η πτώση πίεσης από τη ροή Poiseuille από την πίεση λαδιού τροφοδοσίας στην εσωτερική προς την εξωτερική διάμετρο είναι αρκετά μεγάλη, αρκετή για να μειώσει την πίεση σε τιμές χωρίς φυσική σημασία. Αυτό μειώνει σημαντικά το παραλαμβανόμενο φορτίο. Σε χαμηλότερες τιμές ιξώδους, αυτή η πτώση πίεσης δεν είναι αρκετά μεγάλη ώστε να οδηγήσει σε μη ρεαλιστικές τιμές πίεσης. Η μοντελοποίηση της σπηλαίωσης επιτρέπει μια πιο ακριβή περιγραφή αυτών των φαινομένων.

Σε ένα δεύτερο βήμα της ανάλυσης, οι προτεινόμενοι μηχανισμοί που προέρχονται από τις εξαρτώμενες από τη θερμοκρασία ιδιότητες του λιπαντικού έχουν αξιολογηθεί, μέσω της μοντελοποίησης THD (βλ. Σχ.Δ.5). Δημιουργήθηκε ένα μοντέλο THD με εξαρτώμενη από τη θερμοκρασία πυκνότητα και σταθερό ιξώδες και συγκρίθηκε με τα ισοθερμικά αποτελέσματα για την ίδια τιμή ιξώδους. Η δημιουργία υδροδυναμικής πίεσης ήταν πιο έντονη στο μοντέλο THD, οδηγώντας στο συμπέρασμα ότι η θερμική σφήνα συμμετέχει στην ικανότητα μεταφοράς φορτίου του παράλληλου ωστικού εδράνου. Ωστόσο, το ειδικό φορτίο που δημιουργείται από τη θερμική σφήνα είναι περίπου $0,076\ MPa$, και όχι αρκετά μεγάλο ώστε να αντιστοιχεί στα πειραματικά παρατηρούμενα φορτία.

Επιπλέον, δημιουργήθηκε και αξιολογήθηκε μοντέλο THD με λιπαντικό σταθερής πυκνότητας, του οποίου το ιξώδες εξαρτάται από τη θερμοκρασία, προκειμένου να προσδιοριστεί η επίδραση σφήνας ιξώδους. Όλες οι αξιολογήσεις THD με ιξώδες εξαρτώμενο από τη θερμοκρασία εμφανίζουν αύξηση πίεσης κοντά στο χείλος εξόδου, όπως παρουσιάζεται στο Σχ.Δ.6. Αυτή η αύξηση μπορεί να αποδοθεί στην μεγάλη διαφορά ιξώδους κοντά στην περιοχή αυλάκωσης. Η ψύξη από το λάδι τροφοδοσίας κοντά στο χείλος εξόδου, αυξάνει το ιξώδες κοντά στη διεπιφάνεια του υγρού, οδηγώντας σε υψηλότερες διατμητικές δυνάμεις σε αυτήν την περιοχή. Αυτό θα οδηγούσε σε επιβράδυνση της ροής. Έτσι, λόγω διατήρησης μάζας είναι αναγκαία η δημιουργία πίεσης. Ακόμα κι αν το αποτέλεσμα είναι παρατηρήσιμο σε όλα τα προαναφερθέντα μοντέλα, το μέγεθός του είναι ακόμη μικρότερο από το φαινόμενο θερμικής σφήνας.

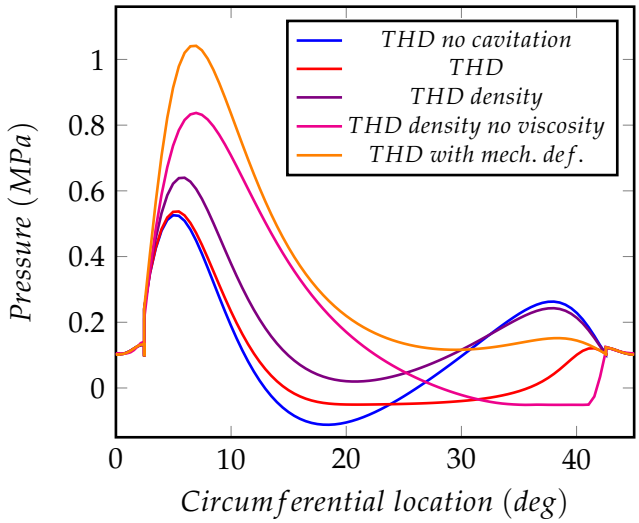

FIGURE D.6 – THD: Σύγκριση προφίλ πίεσης

Οι μηχανισμοί δημιουργίας πίεσης που αφορούν στις ιδιότητες του ρευστού φαίνεται να έχουν μικρή σημασία για τη φέρουσα ικανότητα του παράλληλου ωστικού εδράνου. Η μετάβαση στις μηχανικές και θερμικές ιδιότητες των στερεών περιοχών φαίνεται το επόμενο λογικό βήμα. Πρώτα εισάγεται ένα μοντέλο THD που λαμβάνει υπόψη τις μηχανικές παραμορφώσεις της γεωμετρίας του πέλματος. Οι μηχανικές παραμορφώσεις δημιούργησαν μια μικρή συγκλίνουσα γεωμετρία. Το συγκλίνον εύρος των $0,04\mu m$ κατάφερε να αυξήσει το ειδικό φορτίο από τα προηγούμενα μοντέλα THD επιπλέον $0,16$ MPa. Οι θερμικές παραμορφώσεις του πέλματος έχουν εισαχθεί στο προηγούμενο μοντέλο, δημιουργώντας το μοντέλο Simple TEHD. Η αξιολόγηση της απόδοσης ωστικών εδράνων με αυτό το μοντέλο, οδήγησε σε ειδικές πιέσεις πάνω από το όριο των $1,5$ MPa, υποδηλώνοντας ότι ο κύριος μηχανισμός δημιουργίας πίεσης του παράλληλου ωστικού εδράνου είναι η γεωμετρία συγκλίνουσας σφήνας που δημιουργείται από τις θερμικές παραμορφώσεις στο πέλμα. Επιπλέον, το μοντέλο Simple TEHD έχει επεκταθεί για να ληφθεί υπόψη η θερμοεξαρτούμενη πυκνότητα και η θερμική ικανότητα του λιπαντικού. Το νέο μοντέλο αναφέρεται ως το μοντέλο Full TEHD και είναι σε θέση να αξιολογήσει τη φέρουσα ικανότητα λαμβάνοντας υπόψη όλους τους αναγνωρισμένους μηχανισμούς δημιουργίας υδροδυναμικής πίεσης, καθώς και μια καλύτερη προσέγγιση των θερμοκρασιών του υπολογιστικού χωρίου. Η διαφορά των δύο μοντέλων είναι μικρή. Με χρήση του μοντέλου Full TEHD υπολογίζονται χαμηλότερες τιμές της ροπής τριβής και υψηλότερες τιμές της θερμοκρασίας λειτουργίας. Η σύγκριση και των δύο μοντέλων με δημοσιευμένα πειραματικά αποτελέσματα, έδωσε μια αρκετά καλή συσχέτιση όπως φαίνεται στο Σχ.Δ.7, με το Full TEHD να τα προσεγγίζει καλύτερα.

Επειδή οι θερμικές παραμορφώσεις του πέλματος έχουν μεγάλη επίδραση στη φέρουσα ικανότητα φορτίου, το μοντέλο Full TEHD επεκτάθηκε, ώστε να λαμβάνει υπόψη και τις θερμικές και μηχανικές παραμορφώσεις του ρότορα. Το νέο μοντέλο κατάφερε να συσχετιστεί με τις πειραματικές μετρήσεις σχεδόν πλήρως, με μια ελαφρά υπερεκτίμηση της θερμοκρασίας και μικρή υποεκτίμηση της ροπής τριβής.

Συνοψίζοντας, μετά από λεπτομερή ανάλυση όλων των πιθανών μηχανισμών δημιουργίας πίεσης για το παράλληλο ωστικό έδρανο, τα ευρήματα αυτού του κεφαλαίου είναι ότι οι θερμικές και μηχανικές παραμορφώσεις τόσο του πέλματος όσο και του ρότορα είναι ο κύριος λόγος της παρατηρούμενης φέρουσας ικανότητας φορτίου τέτοιων εδράνων. Προκειμένου να εξαλειφθεί οποιαδήποτε πιθανή απόκλιση από το φυσικό φαινόμενο, έχουν

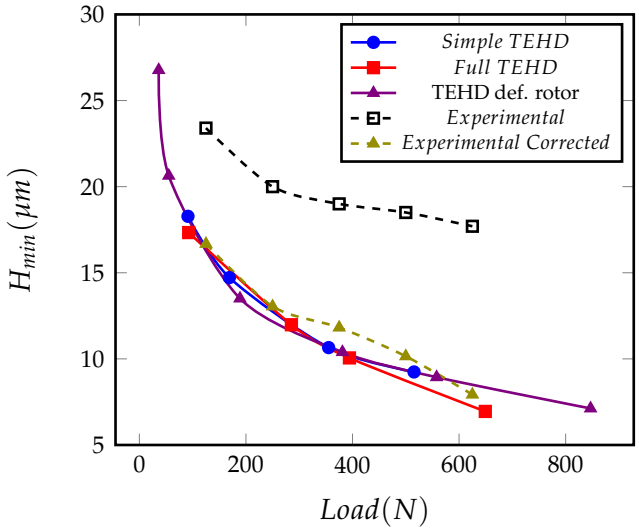

FIGURE D.7 – TEHD: Διόρθωση πειραματικών τιμών H_{min}.

μελετηθεί δύο ακόμη σημεία. Το πρώτο είναι, ότι λόγω κατασκευαστικών ατελειών του παράλληλου εδράνου, δημιουργούνται αποκλίσεις στην κατανομή πίεσης, θερμοκρασίας, και πάχους λιπαντικού μεταξύ των επιμέρους πελμάτων του ωστικού εδράνου. Αυτό καθιστά ορισμένα πέλματα πιο βαριά φορτωμένα από άλλα, και τα δεδομένα που έχουν μετρηθεί πειραματικά ενδέχεται να διαφέρουν από πέλμα σε πέλμα. Επομένως, συνιστάται η προσεκτική αξιολόγηση της γεωμετρίας του εδράνου πριν από τις πειραματικές μετρήσεις και τη μέτρηση περισσότερων από ένα πελμάτων προκειμένου να μετρηθούν έγκυρα τα αποτελέσματα. Το δεύτερο είναι, ότι οι μηχανικοί περιορισμοί (στηρίξεις) του παράλληλου εδράνου επηρεάζουν τις θερμικές παραμορφώσεις, με αποτέλεσμα διαφορετικό προφίλ παραμόρφωσης για τα επιμέρους πέλματα.

Σύγχρονες σχεδιάσεις

Στο παρόν κεφάλαιο, μελετήθηκαν τέσσερις διαφορετικοί τύποι σύγχρονων σχεδιάσεων ωστικών εδράνων. Κάθε σχεδίαση που μελετήθηκε παρουσιάζει διαφορετική συμπεριφορά στο εύρος της μελέτης. Έτσι, προτείνεται μια διαφορετική υπολογιστική προσέγγιση για αυτές τις σχεδιάσεις.

Το ωστικό έδρανο με επικλινή-παράλληλη γεωμετρία έχει αξιολογηθεί με τα μοντέλα THD και TEHD. Και τα δύο μοντέλα καταφέρνουν να αξιολογήσουν την απόδοση του εδράνου με πολύ καλή ακρίβεια, σε σύγκριση με τα πειραματικά αποτελέσματα (βλ. Σχ.Δ.8), με μια μικρή υποεκτίμηση της πίεσης στο σημείο 70%-50% και για τα δύο μοντέλα και υπερεκτίμηση της θερμοκρασίας για το μοντέλο THD. Γενικά, η προσέγγιση μοντέλου THD συνιστάται για αυτόν τον σχεδιασμό, λόγω των μικρών πλεονεκτημάτων του TEHD έναντι του υπολογιστικού κόστους. Εάν η εφαρμογή είναι ευαίσθητη στη θερμοκρασία, προτείνεται προσέγγιση μοντελοποίησης TEHD, αλλά η ανάγκη μοντελοποίησης των παραμορφώσεων του ρότορα θεωρείται περιττή.

Για το ωστικό έδρανο ορθογωνικής κοιλότητας, οι προσομοιώσεις οδηγούν σε συμπεράσματα τα οποία είναι ισοδύναμα με αυτά των εδράνων με επικλινή-παράλληλη γεωμετρία. Συγκεκριμένα, παρατηρήθηκε πολύ καλή συσχέτιση των προσομοιώσεων με τα πειραματικά δεδομένα και για τα δύο μοντέλα, με μικρή υπερεκτίμηση της θερμοκρασίας για το

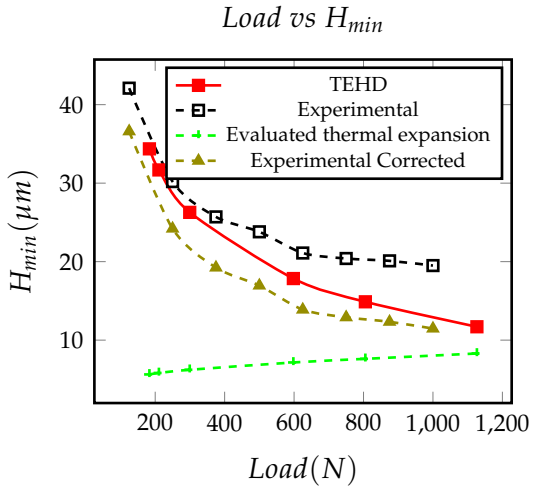

FIGURE D.8 – Επικλινές-παράλληλο:Διόρθωση πειραματικών τιμών H_{min}.

μοντέλο THD και υπερεκτίμηση της πίεσης στο σημείο 70%-50% και από τα δύο μοντέλα (βλέπε Σχ.Δ.9). Η κύρια διαφορά από την επικλινή-παράλληλη γεωμετρία είναι ότι εάν απαιτείται καλύτερη ακρίβεια για την αξιολόγηση των χαρακτηριστικών απόδοσης από εκείνη που διαχειρίζεται το μοντέλο THD, προτείνεται ένα μοντέλο TEHD που λαμβάνει επίσης υπόψη τις μηχανικές και θερμικές παραμορφώσεις του ρότορα. Ο λόγος για αυτό είναι η μορφή της παραμόρφωσης και της κατανομής θερμοκρασίας.

Αντί για ωστικό έδρανο, γεωμετρία ευθύγραμμου ωστικού ολισθητήρα (βλ. Σχ.Δ΄.1Α) επιλέχθηκε για την αξιολόγηση της τεχνητής επιφανειακής τραχύτητας λόγω της πολυπλοκότητας της γεωμετρίας του πέλματος του ωστικού εδράνου και του αυξημένου υπολογιστικού κόστους. Για την αξιολόγηση της απόδοσης της τεχνητής επιφανειακής τραχύτητας στον ευθύγραμμο ωστικό ολισθητήρα παράλληλης επιφανείας έχουν εισαχθεί τρία μοντέλα, το ισοθερμικό, το THD και το TEHD και η σύγκριση απόδοσής τους παρουσιάζεται στο Σχ.Δ.10. Η ισοθερμική μοντελοποίηση δεν μπορεί να αξιολογήσει σωστά τα χαρακτηριστικά απόδοσης της τεχνητής επιφανειακής τραχύτητας και το μοντέλο THD αποκλίνει από το μοντέλο TEHD σε μέτρια έως υψηλά φορτία. Η μοντελοποίηση TEHD έδειξε ότι οι τεχνητές κοιλότητες λειτουργούν ως θερμικοί μονωτές και δεν επιτρέπουν τη ροή θερμότητας από το λιπαντικό στο ευθύγραμμο ωστικό ολισθητήρα για εύρος τιμών H_{min}, οδηγώντας σε απότομη αύξηση της θερμοκρασίας καθώς αυξάνεται το φορτίο . Όταν το H_{min} φτάσει μια οριακή τιμή, δημιουργείται μια ζώνη ανακύκλωσης μέσα στην κοιλότητα η οποία επιτρέπει τη ροή θερμότητας και από αυτό το σημείο και έπειτα η θερμοκρασία μειώνεται καθώς το H_{min} μειώνεται, έως ότου η επιπλέον παραγόμενη θερμότητα είναι μεγαλύτερη από τη ροή θερμότητας μέσω των κοιλοτήτων και η θερμοκρασία αυξάνεται καθώς αυξάνεται το φορτίο. Αυτό οδηγεί στο συμπέρασμα ότι για νέες σχεδιάσεις για το βάθος των κοιλοτήτων πρέπει να λαμβάνουν υπόψη το λειτουργικό πάχος του λιπαντικού. Τέλος, για τη σωστή αξιολόγηση της απόδοσης του ευθύγραμμου ωστικού ολισθητήρα παράλληλης επιφανείας με ΤΕΤ συνιστάται η μοντελοποίηση με TEHD.

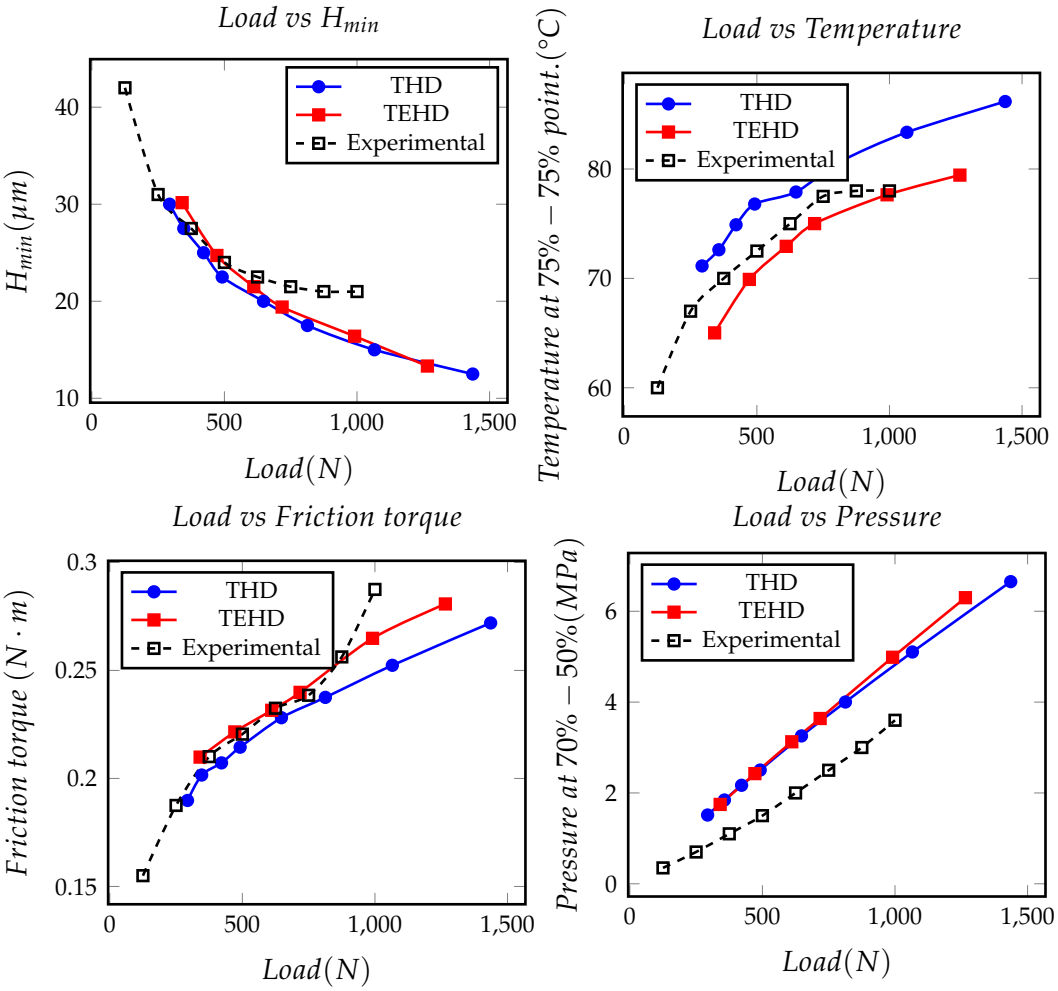

FIGURE D.9 – Έδρανο ορθογωνικής κοιλότητας: Σύγκριση τριβολογικών χαρακτηριστικών για τα μοντέλα THD και TEHD και τα πειραματικά αποτελέσματα.

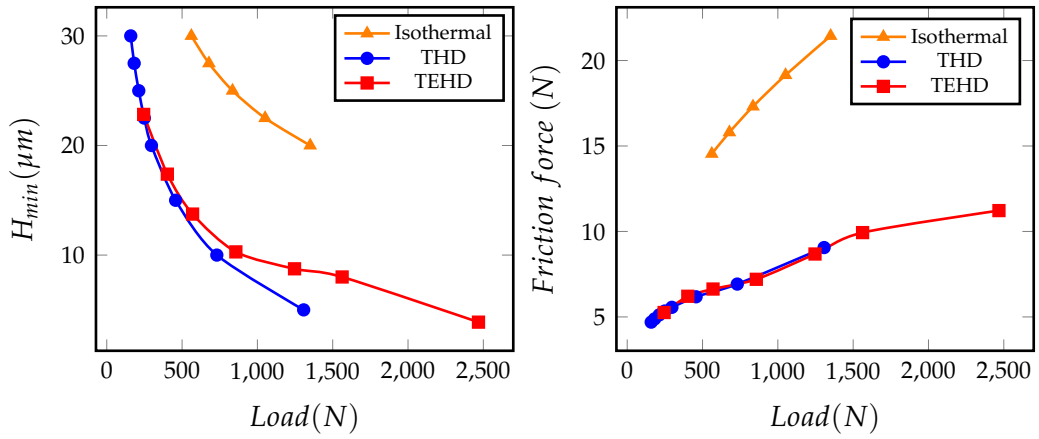

FIGURE D.10 – Έδρανο τεχνητής επιφανειακής τραχύτητας: Σύγκριση τριβολογικών χαρακτηριστικών για τα μοντέλα Isothermal, THD, και TEHD

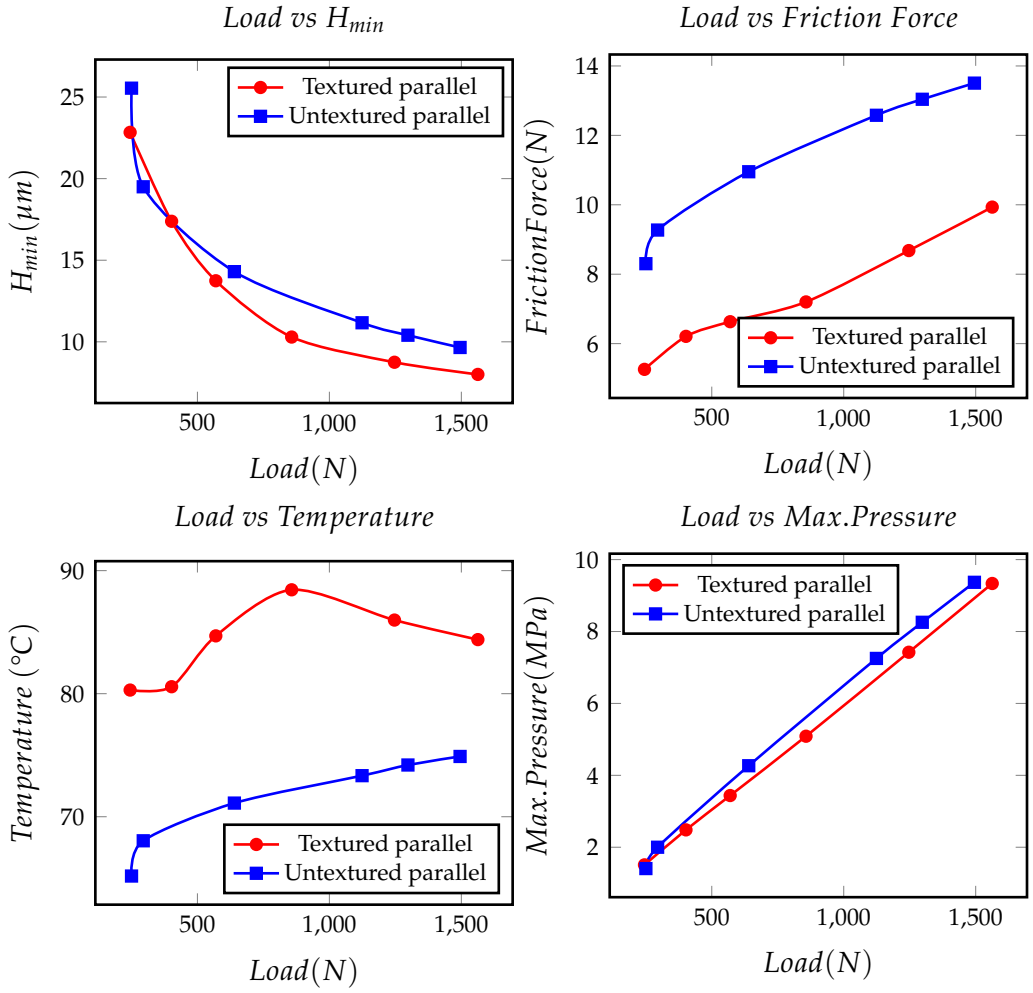

FIGURE D.11 – Σύγκριση χαρακτηριστικών απόδοσης μεταξύ ευθύγραμμου ωστικού ολισθητήρα παράλληλης επιφανείας με και χωρίς TET, τα οποία αξιολογήθηκαν με το μοντέλο Full TEHD.

Συγκρίνοντας τον ευθύγραμμο ωστικό ολισθητήρα παράλληλης επιφανείας με και χωρίς επιφανειακή τεχνητή τραχύτητα (βλ. Σχ.Δ.11), μπορούμε να δηλώσουμε τα ακόλουθα. Η επιφανειακή τεχνητή τραχύτητα μειώνει τη δύναμη τριβής σε σύγκριση με την λεία επιφάνεια. Ο μηχανισμός δημιουργίας πίεσης του παράλληλου ωστικού εδράνου (θερμική παραμόρφωση) μετριάζεται στον ευθύγραμμο ωστικό ολισθητήρα παράλληλης επιφανείας με επιφανειακή τεχνητή τραχύτητα, λόγω του μεγαλύτερου μέσου πάχους φιλμ λιπαντικού στην παραγόμενη σφήνα. Η περιοχή υψηλής πίεσης επεκτείνεται την TET. Έτσι, η σπηλαίωση είναι περιορισμένη κοντά στην περιοχή του πίσω χείλους. Επιπλέον, ο ευθύγραμμος ωστικός ολισθητήρας με TET εμφανίζει υψηλότερες τιμές θερμοκρασίας, λόγω των μονωτικών ιδιοτήτων που έχουν οι κοιλότητες. Τέλος, προτού επιλεχθεί η σχεδίαση μιας νέας TET για έδρανο το οποίο λειτουργεί σε ειδικά φορτία άνω των $0,3\ MPa$, θα πρέπει να ληφθεί υπόψη το υψηλότερο κόστος κατασκευής, οι υψηλότερες θερμοκρασίες λειτουργίας και η χαμηλότερη ικανότητα παραλαβής φορτίου του ωστικού εδράνου με TET σε σύγκριση με το απλό παράλληλο έδρανο.

Επιπλέον, έχουν δημιουργηθεί υπολογιστικά μοντέλα με τρεις διαφορετικές επιστρώσεις, αλλά τα αποτελέσματά τους δεν επαρκούν για την αξιόπιστη εξαγωγή συμπερασμάτων. Ο

κύριος λόγος για την έλλειψη υπολογιστικών αποτελεσμάτων ήταν το εξαιρετικά υψηλό υπολογιστικό κόστος της μοντελοποίησης TEHD για υλικά με υψηλό συντελεστή θερμικής διαστολής και χαμηλή ακαμψία. Προκειμένου να αξιολογηθούν τα χαρακτηριστικά απόδοσης ενός παράλληλου εδράνου με επίστρωση, η χρήση του TEHD μοντέλου είναι απαραίτητη, γιατί ο κύριος μηχανισμός δημιουργίας πίεσης είναι η θερμική παραμόρφωση της γεωμετρίας του πέλματος και του ρότορα.

Συμπεράσματα

Πολλά διαφορετικά φυσικά φαινόμενα παίρνουν μέρος στην παραγωγή πίεσης του παράλληλου ωστικού εδράνου, προκειμένου να δημιουργηθεί ικανότητα μεταφοράς φορτίου. Το πιο έντονο είναι το αποτέλεσμα της θερμικής παραμόρφωσης, η οποία δημιουργεί μια συγκλίνουσα σφήνα που μπορεί να υποστηρίξει ένα σημαντικό φορτίο.

Για να αξιολογηθεί η απόδοση ενός τέτοιου ωστικού εδράνου, απαιτείται ένα μοντέλο 3D TEHD CFD και η γεωμετρία του αυλακιού τροφοδοσίας λιπαντικού πρέπει να μοντελοποιηθεί. Η αξιολόγηση της θερμοκρασίας και οι συνθήκες ορίου είναι υψίστης σημασίας. Πρέπει να δοθεί προσοχή στις μηχανικές οριακές συνθήκες, επειδή προκαταρκτική έρευνα έδειξε ότι διαφορετική θέση και/ή αριθμός σημείων στερέωσης μπορούν να δώσουν διαφορετικά προφίλ παραμόρφωσης.

Η ατέλεια των επιμέρους πελμάτων μπορεί να εισαγάγει διαφορετικές συνθήκες φόρτισης στο ωστικό έδρανο. Έτσι, η μέτρηση ενός μόνο πέλματος ενός ωστικού εδράνου πιθανότατα δεν θα περιγράψει τις πραγματικές συνθήκες λειτουργίας ολόκληρου του εδράνου. Τα ωστικό έδρανα με επικλινή παράλληλη γεωμετρία και ορθογωνικής κοιλότητας δεν χρειάζονται την υπολογιστικά ακριβή προσέγγιση μοντελοποίησης TEHD.

Τα ωστικό έδρανα με TET, πρέπει να μελετώνται λαμβάνοντας υπόψη τη θερμική παραμόρφωση της γεωμετρίας του πέλματος.

Ακόμη, πρέπει να διερευνηθεί η επίδραση των επιστρώσεων στα παράλληλα ωστικά έδρανα. Ένας υβριδικός σχεδιασμός δύο επιστρώσεων μπορεί να βελτιώσει σημαντικά την απόδοση των παράλληλων ωστικών εδράνων.

Appendix E

Extended Abstract

Literature review

Overcoming friction is one of the main objectives of everyday life. It is evaluated that 23% of the total energy consumption today originates from energy losses in tribology contacts. In the direction of reducing the total energy waste and designing more efficient engineering contraptions, the understanding of friction mechanism is the key. Since the beginning of the industrial era, a lot of effort has been made in optimising the efficiency of mechanical designs. Analytical and computational models have been generated through the years, to predict and optimise the performance of such designs. In the past decades, the computational power was scarce, thus driving to simplifications of the physical models in order to acquire meaningful result with limited computational resources. However, in the last 20 years, the available computational power has increased dramatically allowing the scientific and engineering community to utilise more complex and accurate computational models.

The present study focuses on the detailed modelling of the parallel thrust bearing using a CFD-based ThermoElastoHydrodynamic (TEHD) computation approach. The goals of the present study are (a) to evaluate the pressure build-up mechanisms of parallel thrust bearings proposed in the literature over the years, and (b) to evaluate how the present complex modelling approach can be used to assess contemporary designs that have been designed/evaluated by simpler computational methods.

Parallel thrust bearing

In 1946, Fogg presented the results of his experiment with parallel thrust bearings. He concluded that parallel thrust bearings can support loads of the same order of magnitude as tilting pad thrust bearings. These results contradict the classic lubrication theory, due to the absence of a converging zone. Many different theories have been published since then, in order to explain this phenomenon. The most important pressure build-up mechanism theories suggested in the literature are summarised below:

1. The thermal wedge effect.
2. The viscosity wedge effect.
3. The effect of macro-roughness.
4. The effect of thermal distortion.
5. The leading edge ram pressure effect.
6. The effect of leading edge chamfer geometry.

The suggested most prominent theory is that of thermal distortion of the bearing pad, however smaller effects to the load carrying capacity of parallel surface thrust bearings can be attributed to combinations of the other theories/effects.

Artificial surface texturing

In another note, and in the direction of the drastic efforts that have been made the last decades in order to reduce power losses in mechanical systems, the utilisation of artificial surface texturing (AST) on tribological contacts has been extensively examined by many researchers. The AST has been studied in a variety of application such as piston rings, journal bearings, thrust bearings, and mechanical seals. Many different texturing shapes and sizes have been studied, from simple micro-channels to more complex patterns such as rectangular dimples, hexagonal positive asperities, and hemispherical dimples, resulting to a range of different optimal geometrical designs, even for small alteration on the operating conditions of the mechanical system. Regarding thrust bearings, the use of texturing on the pad surface has been applied, in the majority of the studies, to parallel surface thrust bearings.

Coatings

Since the era of wooden, water-lubricated bearings, the material technology of the bearings has advanced considerably. The first studied bearings of Beauchamp Tower were made of steel, but as the range of application and the understanding of the tribological contacts have grown, new materials have been utilised. Copper and steel alloys with better tribological characteristics are the main materials utilised today. Nevertheless, the use of lead and later tin based (Babbitt) alloys have been systematically used as coatings on bearings. The use of such coatings has entered the industrial use in bearings, due to the advantages they offer in comparison with common materials. The Babbitt coating acts as safety if the lubrication fails. When the temperature increases, and the hydrodynamic capacity of the bearing is not enough for the applied load, the Babbitt coating melts and behaves as a lubricant until bearing operation is safely stopped. This protects the rotor and the whole rotational system, and with a re-coating the bearing is functional again. The coating also captures wear particles, thus reducing extensive abrasive wear. Nevertheless, Babbitt coatings are not always adequately reliable.

Since the 1970's, the Babbitt coatings have, in some cases, been gradually replaced by new synthetic polymers. The first polymer used was Polytetrafluoroethylene (PTFE), which due to its very low static friction property, decreased the start-up friction enough to allow the elimination of the hydrostatic lifting pocket in highly loaded applications. In turn, this led to reduction of the size of the required bearing pad area, which led to bearings of smaller principle dimensions for given operational profile, resulting in lower friction losses, and less costly bearing designs. Moreover, PTFE's normal operation temperature range is considerably higher, with a maximum safe operation temperature to be above 180°C. The main problem of those coatings is their creeping properties. PTFE cannot sustain constant high loads while on thermal cycling. New materials with improved properties are constantly being tested to produce more durable and efficient bearings.

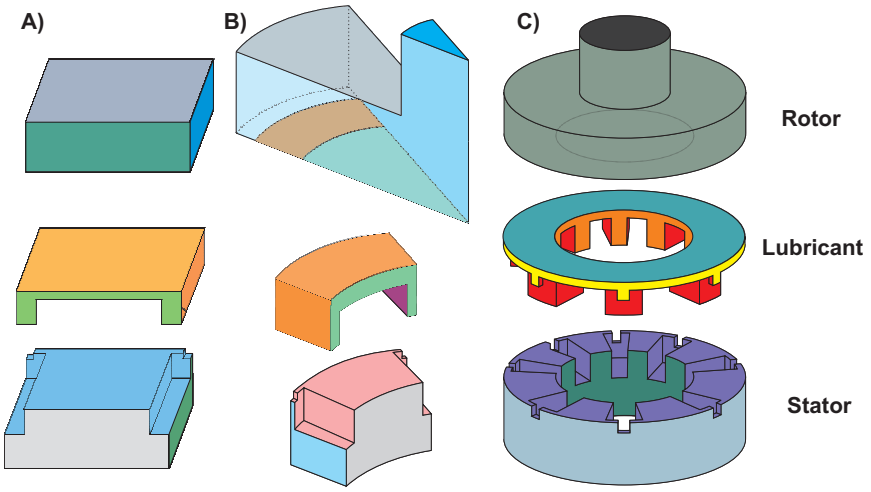

FIGURE E.1 – A) Slider geometry, B) Single sector pad geometry, C) Full thrust bearing geometry.

Modelling approach

Geometry

For the model generation for the different stages of the present Thesis three basic geometrical configurations have been used, a thrust slider, a single sector pad from an eight pad parallel thrust bearing, and a full eight sector pad thrust bearing, are depicted in Fig. E.1. In order to be able to compare the computational results with experimental data, the bearings geometry is based on the bearing utilised by published experimental data, with a simplification on the groove and gouge features. As seen in Fig. E.2 the walls of the oil feeding groove have axial direction. Moreover, the gouge feature in the reference geometry has a triangular section, yet in the present work the gouge section is considered rectangular in order to allow a fully hexahedral mesh in the lubricant domain. The basic design parameters of the sector pad thrust bearing are presented in Table E.1.

TABLE E.1 – Basic geometrical data for the reference thrust bearing.

Parameter	Description	Value	Units
NOP	Number of pads	8	*ul*
$\mathbf{D_{Inner}}$	Pad Inner Diameter	50	*mm*
$\mathbf{D_{Outer}}$	Pad Outer Diameter	90	*mm*
$\mathbf{L_{GO}}$	Gouge Length	1	*mm*
$\mathbf{D_{GO}}$	Gouge Depth	1	*mm*
$\mathbf{L_{GR}}$	Groove Width	3	*mm*
$\mathbf{D_{GR}}$	Groove Depth	4	*mm*
$\mathbf{D_P}$	Stator Thickness	10	*mm*
$\mathbf{D_S}$	Rotor Thickness	20	*mm*

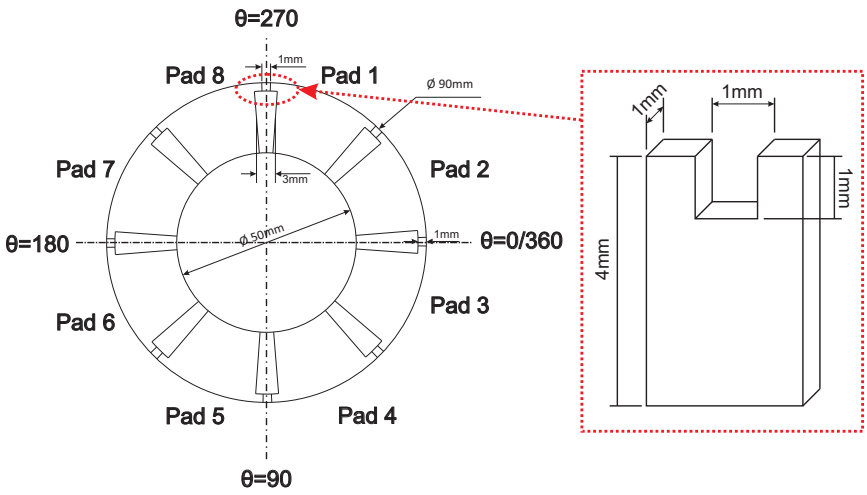

FIGURE E.2 – Eight pad thrust bearing top view

Mesh

A typical mesh for the sector pad geometry is depicted in Fig E.3. For the sector pad models, the number of elements for the fluid domain is 150.000 for the rotor 80.000 and for the pad 12.000. Mesh and convergence studies have been conducted for all the different models introduced in the present study.

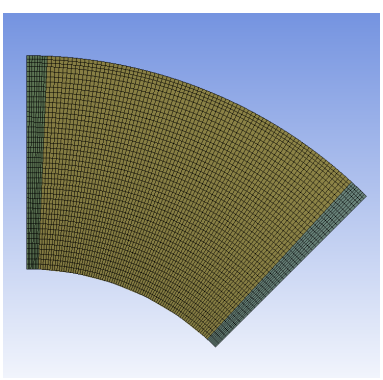

(A) Fluid top view

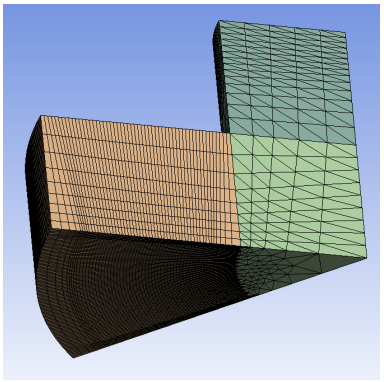

(B) Rotor

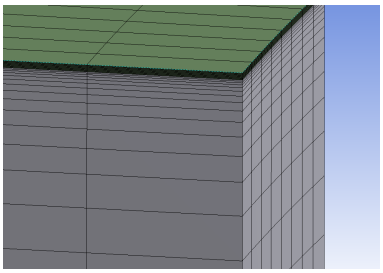

(C) Fluid groove iso-view

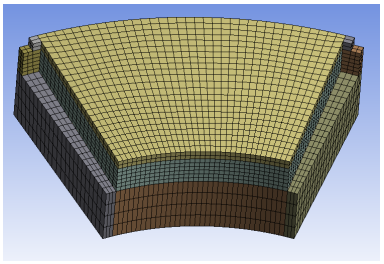

(D) Pad

FIGURE E.3 – Mesh details of the single sector pad parallel model.

Boundary Conditions

In the following Table E.2, the boundary conditions (BCs) for the single sector pad TEHD model are presented.

TABLE E.2 – Thermal and structural boundary conditions for the single sector pad TEHD model with rigid rotor.

Location	Temperature BC's	Structural BC's
	Stator	
Sides	Periodic conditions	Frictionless support
Pad Bottom	HTC: 1000 $W/(m^2K)$, T = 40°C	Uz=0
Pad Inner	HTC: 300 $W/(m^2K)$, T = 40°C	Free
Pad Outer	HTC: 25 $W/(m^2K)$, T = 40°C	Free
Fluid Stator Interface	2-way FSI: Continuity of heat flux and temperature	Free
	Rotor	
Sides	Periodic conditions	Fixed
Rotor Outer	HTC: 25 $W/(m^2K)$, T = 20°C	Fixed
Axis Fixation	HTC: 1000 $W/(m^2K)$, T = 20°C	Fixed
Rotor Oil Res.	HTC: 300 $W/(m^2K)$, T = 40°C	Fixed
Fluid Rotor Interface	Continuity of heat flux and temperature, Rotating velocity 6000 RPM	Fixed
	Lubricant	
Sides	Periodic conditions	Frictionless support
Fluid Inner	Opening with F.P. 0.1MPa, Temperature 40°C	Ux=0, Uy=0
Fluid Outer	Outlet with static pres. of 0 and Temp. 20°C	Ux=0, Uy=0

*Heat Transfer coefficient (HTC)

**Feeding Pressure (F.P.)

TEHD approach

In order to compute the final fluid and pad geometry due to temperature and mechanical deformation, a 2-way fluid solid interface (FSI) model has been generated. A flow chart of the TEHD model calculation can be seen in Fig. E.4. At the beginning of the calculation, after the mesh and input files for the three domains and the two solvers have been generated, the domain interface (FSI) between the fluid domain and the pad, is mapped. The first calculation step is the evaluation of the thermal deformation of the stator in the FE solver, from a cold temperature of 20°C to the feeding oil temperature of 40°C. Then the displaced interface node locations are passed to the CFD solver, and the mesh displacement of the fluid domain is applied. The CFD solver calculates until convergence the hydrodynamic flow, the heat generation in the fluid, and the CHT on the rotor domain. The pressure and temperature values of the FSI is passed to the FE solver and the CHT, and the mechanical and thermal deformation of the stator is re-evaluated. Finally, the last two steps

will be executed until the maximum mesh displacement between two consecutive calculations is less than 0.01 μm, and the CFD solver is converged. When this iterative procedure is completed, the tribological characteristics are calculated, and the pressure, temperature, and deformation values of all the domains are exported. The aforementioned model is computationally very intensive. For a single calculation of a single sector pad thrust bearing, with a 64-core and 96Gb RAM compute unit, the time needed until converging is approximately a little more than 3 days, and for a textured bearing the needed time exceeds the 5 day mark due to the finer mesh needed for the dimple features.

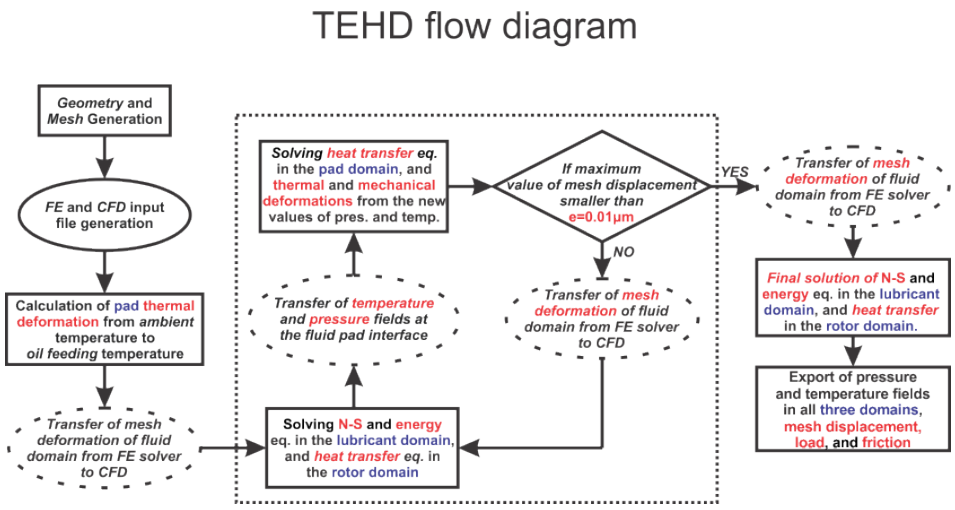

FIGURE E.4 – TEHD model flow chart.

Pressure build-up mechanism investigation

In the present chapter, all supported by the literature pressure build-up mechanisms of the parallel thrust bearing have been evaluated. For this evaluation, three modelling approaches have been utilised, in order to disengage specific phenomena and asses them separately.

With the isothermal modelling, three mechanisms have been assessed. First, the calculation of the hydrostatic lift, from the feeding oil pressure was evaluated by the isothermal model without imposed rotational speed of the rotor. The magnitude of the hydrostatic lift was insignificant, but important to subtract its value from the total load carrying capacity for the evaluation of the other effects.

The second flow effect that has been studied is the ram pressure effect. Subtracting the hydrostatic lift from the simple isothermal results with rotating rotor, the ram pressure effect was observed. With a maximum of $0.16 MPa$ specific load, its significance as pressure build-up mechanism is very small.

Moreover, cavitation has been modelled with the Rayleigh-Plesset equation. The isothermal model has been evaluated with two values of viscosity with and without cavitation. It is observed, that due to the high pressure zone generated by the ram pressure effect, radial leakage occurs near the leading edge region. Thus, local oil starvation conditions are present in the mid-section of the pad. For low values of viscosity this is countered by the flow from the inner surface, where the lubricant is supplied. For high values of viscosity, this flow is not large enough to supply the

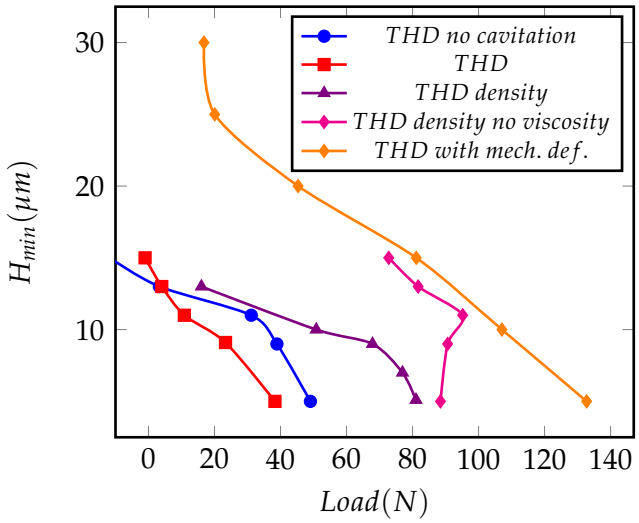

FIGURE E.5 – THD results: H_{min} *vs Load*

mid region with oil, driving to a pressure drop. This decreases considerably the load carrying capacity. The cavitation modelling allows to a more accurate description of those phenomena.

In a second step of the analysis, the proposed mechanisms that derive from temperature dependent properties of the lubricant have been evaluated, in means of THD modelling (see Fig. E.5). A THD model with temperature dependent density and constant viscosity has been generated and compared with the isothermal results for the same viscosity value. The pressure build-up was more pronounced in the THD model, driving to the conclusion that the thermal wedge takes part in the load carrying capacity of the parallel thrust bearing. Yet, the specific pressure generated by the thermal wedge is of the magnitude of $0.076MPa$, not large enough to account for the experimentally observed loads.

Furthermore, a THD model with temperature dependent viscosity and constant density has been generated and evaluated, in order to identify the viscosity wedge effect. All the THD evaluations with temperature dependent viscosity exhibit a pressure increase near the trailing edge, as it is presented in Fig. E.6. This increase can be attributed to the high viscosity gradient near the groove region. The cooling from the feeding oil of the pad, increases the viscosity near the fluid pad interface, driving to higher shear forces in that area. This would drive to a flow deceleration; thus, a pressure gradient is generated. Even if the effect is observable in all the above-mentioned models, its magnitude is even smaller than the thermal wedge effect.

The pressure build-up mechanisms concerning the fluid domain seem to be of small importance to the load carrying capacity of the parallel thrust bearing. Moving to the mechanical and thermal properties of the solid domains seems the next logical step. First a THD model that takes into account the mechanical deformations of the pad geometry is introduced. The mechanical deformations generated a small converging geometry. The converging amplitude of 0.04 μm managed to increase the specific load from the previous THD models an additional 0.16 MPa.

Moving forward, the thermal deformations of the pad have been introduced to the previous model, generating the Simple TEHD model. Evaluating the bearing

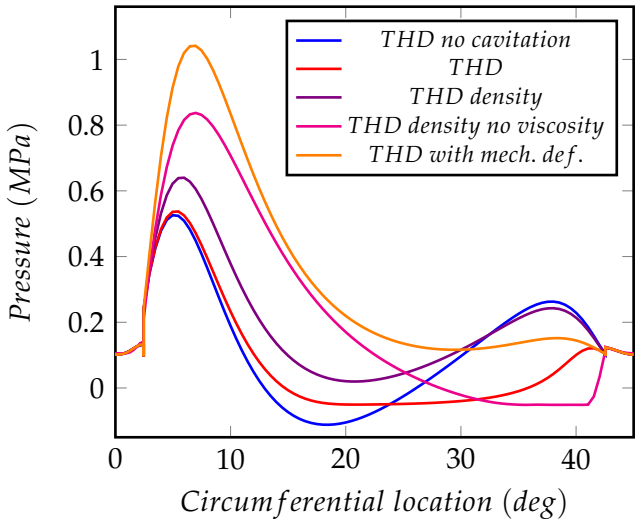

FIGURE E.6 – THD results: Pressure profile comparison

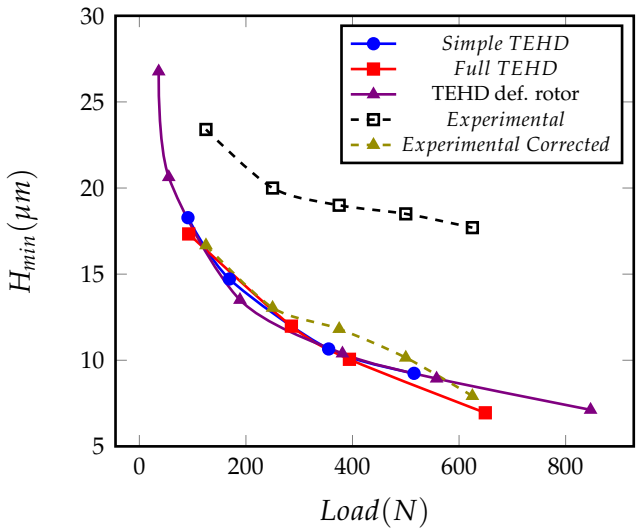

FIGURE E.7 – TEHD results: Experimental H_{min} correction.

performance with this model, resulted in specific pressures over the 1.5 *MPa* limit, suggesting that the main pressure build-up mechanism of the parallel thrust bearing is the converging wedge geometry generated by the thermal deformations on the pad domain. Additionally, the Simple TEHD model has been expanded to account for the temperature dependent density and heat capacity. The new model is referred as the Full TEHD model and being able to evaluate the load carrying capacity taking into account all the identified pressure build-up mechanisms, plus a better approximation of the domain temperatures. The difference of the two models are minimal. The Full TEHD evaluates lower values of friction torque and higher values of temperature.

Comparing both models with published experimental results, gave a fairly good correlation as seen in Fig. E.7, with the Full TEHD being a closer approximation.

The thermal deformations of the pad plays such a big role in the load carrying capacity, the Full TEHD model was extended to account also for the thermal and

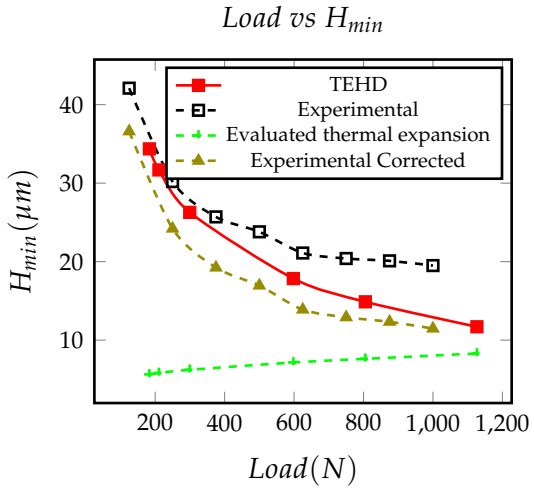

FIGURE E.8 – Tapered-land thrust bearing: Corrected H_{min} vs the Load accounting for the thermal deformation of the pad.

mechanical deformations of the rotor domain. The new model managed to correlate with the experimental measurements almost completely, with a slight overestimation of the temperature and underestimation of the friction torque.

Summarising, after a detailed analysis of all the possible pressure build-up mechanisms for the parallel thrust bearing, the findings of this chapter are that the thermal and mechanical deformations of both the pad and the rotor are the reason of the observed load carrying capacity of such bearings.

In order to eliminate any possible deviation from the physical phenomenon, two more points have been made. The first is, that due to manufacturing imperfections of the parallel bearing, deviation on the pressure, temperature, and film thickness distributions occur between the individual pads of the thrust bearing. This makes some pads more heavily loaded than others, and experimentally measured data might differ from pad to pad. Thus, it is strongly advised a careful evaluation of the bearing geometry before experimental measurements, and the measurement of at least more than one pad in order to acquire valid results. The second is, that it strongly believed that the structural constrains (fixations) of the parallel bearing affect the thermal deformations, resulting in different final shape for the individual pads.

Contemporary designs

In the present chapter, four different types of contemporary designs have been studied. Each design presented exhibited different behaviour in the studied range. Thus, a different computational approach is suggested for those configurations.

The tapered-land thrust bearing has been evaluated with the THD and TEHD models. Both models manage to evaluate the bearing performance with a very good correlation to the experimental results (see Fig. E.8), with a small underestimation of the pressure at the 70%-50% point for both models, and an overestimation on the temperature for the THD model. In general, the THD modelling approach is recommended for this design, because of the small benefits of the TEHD over its computational cost. Although if a precise evaluation is needed, especially in terms of temperature distribution, the TEHD modelling approach is suggested, but the need to model the rotor deformations is considered unnecessary.

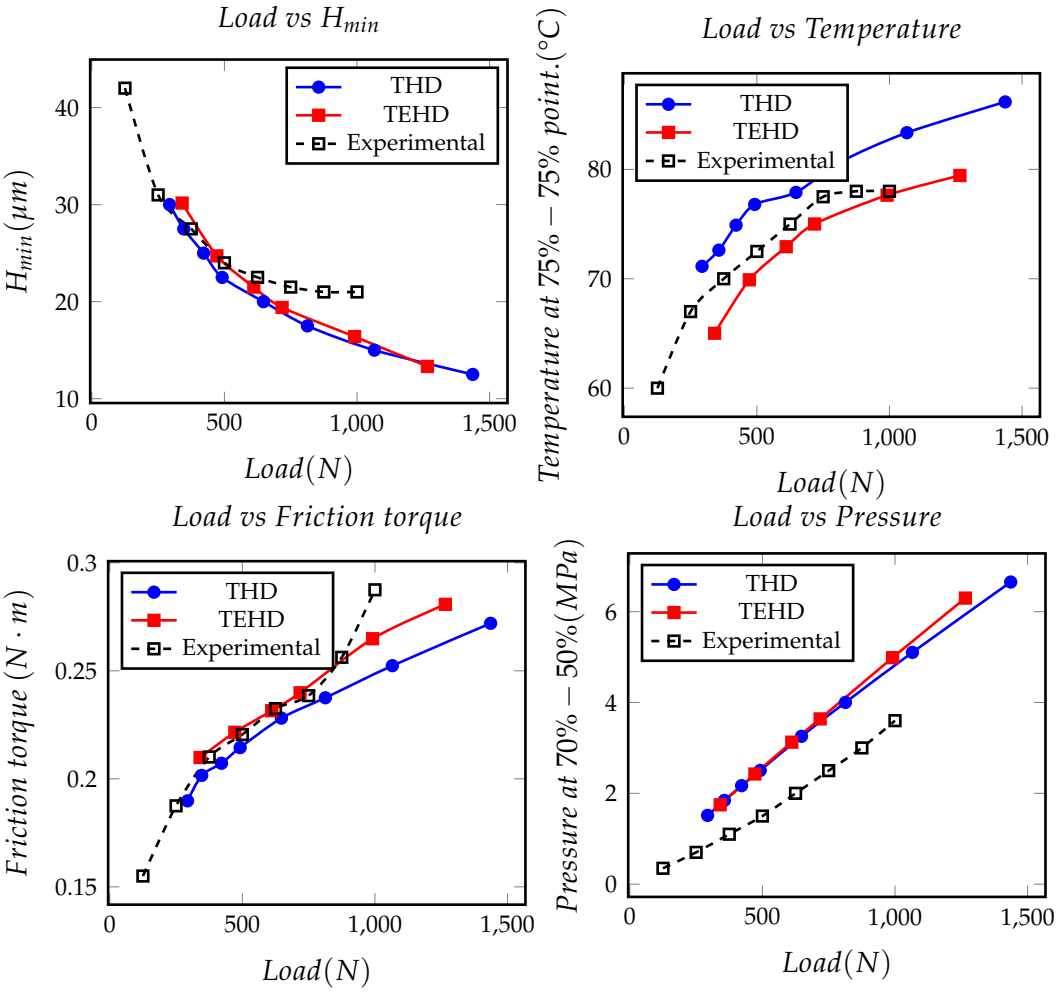

FIGURE E.9 – Pocket thrust bearing: Performance characteristics comparison for the THD, and TEHD models, and experimental results.

For the pocket thrust bearing, almost identical results with the tapered-land have been acquired. Very good correlation with both models has been observed, with a small overestimation of temperature for the THD model, and an overestimation of the pressure at the 70%-50% point by both models (see Fig. E.9). The main difference from the tapered-land is that if better accuracy is needed for the performance characteristics evaluation than that managed by the THD model, a TEHD model is proposed that takes into account also the rotor mechanical and thermal deformations. The reason for that is the shape of the pad deformation and temperature distribution.

The textured bearing studied in the present work, represents a slider geometry due to the sector pad geometry complexity and increases computational cost. To evaluate the performance of AST on the parallel slider three models have been introduced, the isothermal, the THD, and the TEHD and their performance comparison is presented in Fig. E.10. Isothermal modelling cannot correctly evaluate the performance characteristics of the textured slide, and the THD model diverges

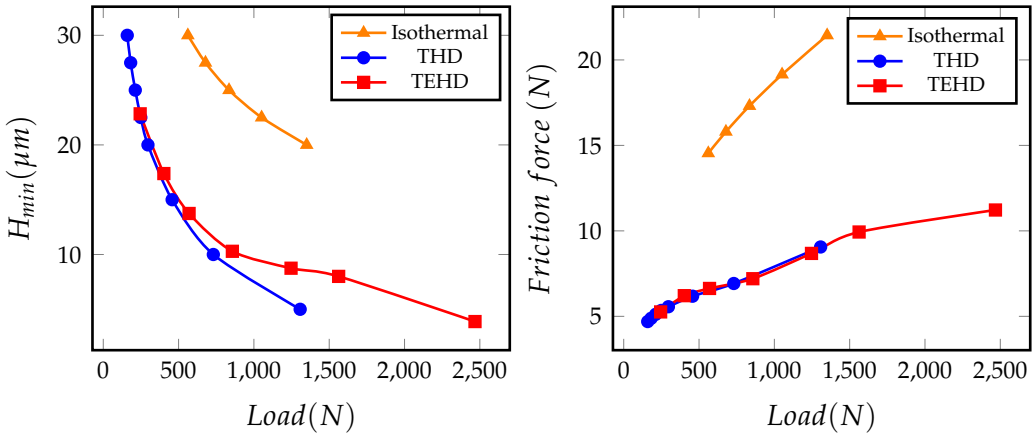

FIGURE E.10 – Performance characteristics comparison for the Isothermal, THD, and TEHD models for the textured parallel surface slider.

from the TEHD model in moderate to high loads. The TEHD modelling showed that the texture cavities function as thermal insulators, and do not allow the heat flux from the lubricant to the pad for a range of H_{min} values, driving to a steep increase of the temperature as the load increases. When the H_{min} reaches a threshold value, a recirculation zone is created inside the cavity. The recirculation zone allows the convection heat flux, and from this point on the temperature decreases as the H_{min} decreases. When a certain value of the load is reached, and the heat generation is larger than the heat flux inside the cavities; thus, the temperature increases as the load increases. This drives to the conclusion that new designs for texture depth need to consider the H_{min} operational magnitude. Finally, for the correct evaluation of the performance of the textured parallel slider TEHD modelling is strongly suggested.

Comparing the textured slider with an untextured parallel slider (see Fig. E.11), the following can be stated. The AST manages to reduce the friction force in comparison with the untextured bearing. The pressure build-up mechanism of the parallel thrust bearing (thermal deformation) is mitigated on the textured slider, because of the larger average film thickness on the generated wedge. The high-pressure region is extended by the textures; thus, cavitation is limited near the trailing edge. Moreover, the textured bearing exhibits higher values of temperature, because of the insulating properties the cavities have. Finally, before selecting AST for a new design that operates at specific loads over 0.3 MPa, one should consider the higher manufacturing cost, the higher operational temperatures, and lower load carrying capacity of the textured bearing in comparison with the simple untextured parallel one.

Furthermore, three different coatings have been modelled, but not conclusive results have been established. The main reason for the lack of computational results has been the remarkably high computational cost of the TEHD modelling for materials with high thermal expansion coefficient and low stiffness. In order to evaluate the performance characteristics of a coated parallel thrust bearing TEHD modelling is the only option because the main pressure build-up mechanism is the thermal deformation of the pad and rotor geometry.

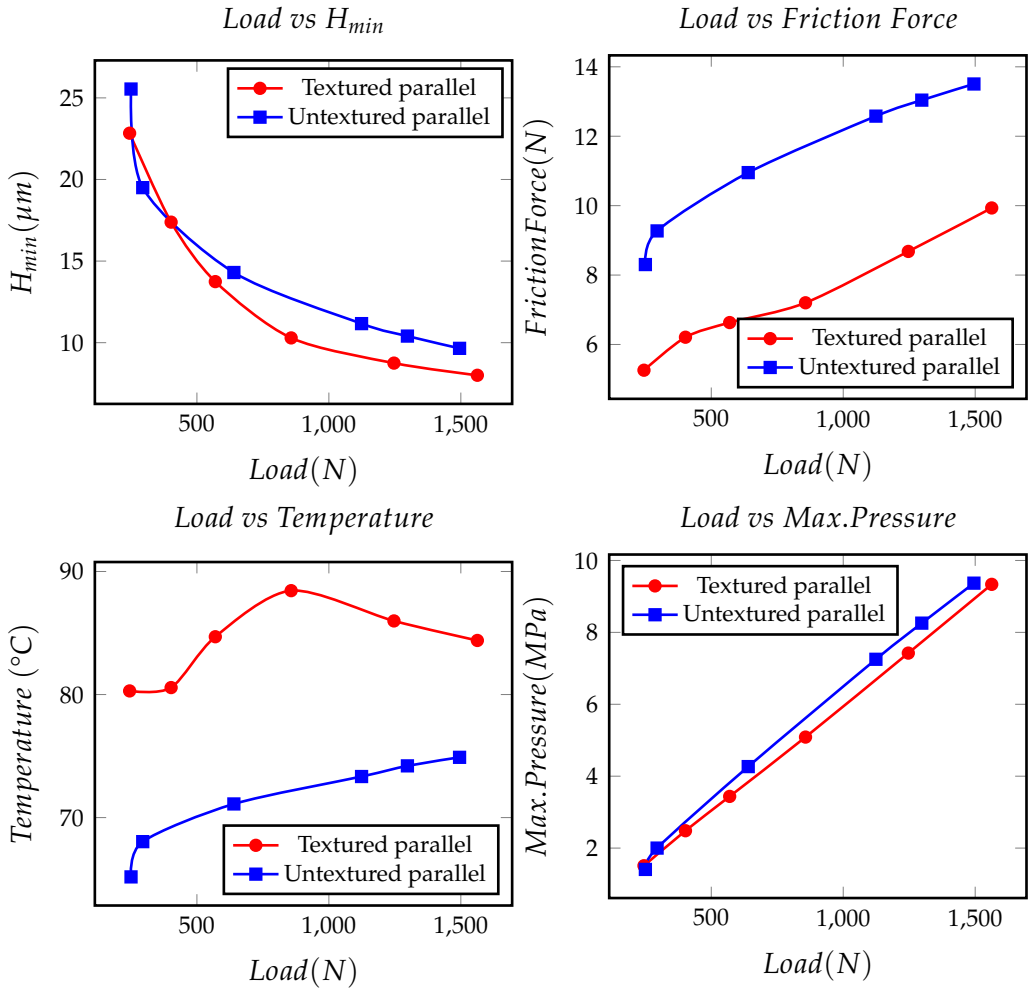

FIGURE E.11 – Performance characteristics comparison between the textured and untextured parallel surface slider, evaluated with the TEHD model.

Conclusion

Many different physical phenomena take place in the parallel surface thrust bearing, in order for load carrying capacity to be generated. The most pronounced one is the effect of the thermal deformation, which generates a converging wedge that can support a considerable load.

To evaluate the performance of such a bearing, a 3D TEHD CFD model is required, and the groove geometry must be modelled. The temperature evaluation and boundary conditions are of utmost importance. Attention must be given to the structural boundary condition, because preliminary investigation suggested that different location and/or number of fixation points can give different deformation profiles.

The imperfection of individual sector pads can introduce different loading conditions on the thrust bearing. Thus, measuring a single pad probably would not describe the real working conditions of the whole bearing.

The tapered-land and pocket thrust bearing configurations do not need the expensive TEHD modelling approach.

Textured bearings, especially moderately or highly loaded ones, need to be studied taking into account the thermal deformation of the pad geometry.

Finally, the effect of coatings on parallel surface thrust bearings needs to be investigated. A hybrid two coating design might enhance considerably the parallel surface thrust bearings performance.

Evaluating the results of the present Thesis, a more clear view for the next research steps in the scientific domain of the present Thesis has been formed.

As mentioned above, the structural boundary conditions may affect the performance of the parallel thrust bearing, and this should be investigated further.

The very limited analysis of the coated bearings identifies the importance of analysing their effect on the pressure build-up mechanism for the parallel surface thrust bearing. Moreover, the study of a bearing with dual coating is believed that can make the simple parallel design more competitive in comparison to more complex contemporary bearing types.

A longer and more structured analysis of the artificial surface texturing is needed, in terms of TEHD evaluations, for a range of different design parameters, such as texture shape depth, density, etc.

Finally, the most important progress would be a time dependent modelling approach for the parallel thrust bearing, in order to understand the film generation at start-up, and how each mechanism contributes during the progression of the phenomenon.